

this document downloaded from

vulcanhammer.info

the website about
Vulcan Iron Works
Inc. and the pile
driving equipment it
manufactured

Visit our companion site
<http://www.vulcanhammer.org>

Terms and Conditions of Use:

All of the information, data and computer software ("information") presented on this web site is for general information only. While every effort will be made to insure its accuracy, this information should not be used or relied on for any specific application without independent, competent professional examination and verification of its accuracy, suitability and applicability by a licensed professional. Anyone making use of this information does so at his or her own risk and assumes any and all liability resulting from such use. The entire risk as to quality or usability of the information contained within is with the reader. In no event will this web page or webmaster be held liable, nor does this web page or its webmaster provide insurance against liability, for any damages including lost profits, lost savings or any other incidental or consequential damages arising from the use or inability to use the information contained within.

This site is not an official site of Prentice-Hall, Pile Buck, or Vulcan Foundation Equipment. All references to sources of software, equipment, parts, service or repairs do not constitute an endorsement.

IMPROVED METHODS FOR FORWARD AND INVERSE SOLUTION OF THE
WAVE EQUATION FOR PILES

By

Don Chester Warrington

James C. Newman, III
Professor of Engineering
(Chairman)

Timothy W. Swafford
Professor of Engineering
(Committee Member)

Boris P. Belinskiy
Professor of Mathematics
(Committee Member)

Joseph Owino
Associate Professor of Engineering
(Committee Member)

IMPROVED METHODS FOR FORWARD AND INVERSE SOLUTION OF THE
WAVE EQUATION FOR PILES

By

Don Chester Warrington

A Dissertation Submitted to the Faculty of the
University of Tennessee at Chattanooga
in Partial Fulfillment of the Requirements
of the Degree of Doctor of Philosophy in Computational Engineering

The University of Tennessee at Chattanooga
Chattanooga, Tennessee

August 2016

Copyright © 2016
Don Chester Warrington
All Rights Reserved

ABSTRACT

This dissertation discusses the development of an improved method for the static and dynamic analysis of driven piles for both forward and inverse solutions. Wave propagation in piles, which is the result of pile head (or toe) impact and the distributed mass and elasticity of the pile, was analyzed in two ways: forward (the hammer is modeled and the pile response and capacity for a certain blow count is estimated) or inverse (the force-time and velocity-or displacement-time history from driving data is used to estimate the pile capacity.) The finite element routine developed was a three dimensional model of the hammer, pile and soil system using the Mohr-Coulomb failure criterion, Newmark's method for the dynamic solution and a modified Newton method for the static solution. Soil properties were aggregated to simplify data entry and analysis. The three-dimensional model allowed for more accurate modeling of the various parts of the system and phenomena that are not well addressed with current one-dimensional methods, including bending effects in the cap and shaft response of tapered piles. Soil layering was flexible and could either follow the grid generation or be manually input. The forward method could either model the hammer explicitly or use a given force-time history, analyzing the pile response. The inverse method used an optimization technique to determine the aggregated soil properties of a given layering scheme. In both cases the static axial capacity of the pile was estimated using the same finite element model as the dynamic method and incrementally loaded. The results were then analyzed using accepted load test interpretation criteria. The model was run in test cases against current methods to verify its features, one of which was based on actual field data using current techniques for both data acquisition and analysis, with reasonable correlation of the results. The routine was standalone and did not require additional code to use.

DEDICATION

This effort is dedicated to three people who went to the other side before its completion.

The first is my mother, Vernell S. Warrington, who passed away in 2000. She expressed an interest in my pursuit of a PhD degree; I am glad her desire could be fulfilled.

The other two are my wife's parents, William and Ruby Foister, who passed away in 1999 and 2014, respectively. The code began to be written in 2013, when Ruby was in the beginning of her last journey; her sickness and death, and my wife's unfailing dedication to her mother's care until the very end, were a large part of our lives during my later coursework and the beginning of this dissertation.

“Seeing, therefore, that there is on every side of us such a throng of witnesses, let us also lay aside everything that hinders us, and the sin that clings about us, and run with patient endurance the race that lies before us, our eyes fixed upon Jesus, the Leader and perfect Example of our faith, who, for the joy that lay before him, endured the cross, heedless of its shame, and now ‘has taken his seat at the right hand’ of the throne of God.” (Heb 12:1-2 TCNT)

ACKNOWLEDGEMENTS

This work would not have come to fruition except for the help of many people, some of which are:

my Committee, whose patience and assistance at many points in the effort is greatly appreciated;

my fellow students at the SimCenter, a very diverse group of people whose help in so many ways was invaluable, and whose maturity in the face of adverse circumstances was an inspiration;

my friends and colleagues at Regent University, whose very helpful suggestions at the critical moment moved the effort forward in a major way;

Mr. Jonathan Tremmier of Pile Hammer Equipment. As was the case with the last degree effort, this one was unfunded. His permission to use Mondello and Killingsworth (2014) and GRLWEAP and his patience during the more intense periods of work were *de facto* financial support for this effort;

my faculty colleagues in the Civil Engineering Department at UTC, whose encouragement meant a great deal, along with Mrs. Saliha Ammour Merabti, my "research assistant" for parts of this study; and

my wife Judy, whose patience and support during her own tragedy was undeserved and whose life reflects the work of our Lord and Savior Jesus Christ.

TABLE OF CONTENTS

ABSTRACT	iv
DEDICATION	v
ACKNOWLEDGEMENTS	vi
LIST OF TABLES	xi
LIST OF FIGURES	xiii
LIST OF SYMBOLS	xix
LIST OF ABBREVIATIONS	xxv
CHAPTER	
I. INTRODUCTION	1
Before the Wave Equation	1
Application of the Wave Equation to Pile Driving	3
Early Attempts at a Solution	3
Smith's Solution	7
Effect of System Parameters	8
Method of Characteristics	9
Use of the Wave Equation in Verification	10
Development of CAPWAP	11
Operation of CAPWAP	13
Other Inverse/Verification Methods	16
Objectives of the Dissertation	17
II. ONE-, TWO-AND THREE-DIMENSIONAL WAVE EQUATION ANALYSES	19
Advantages of One-Dimensional, Finite-Difference Analysis	20
Rationale for Two-Dimensional, Finite-Element Analysis	22
Survey of Two-Dimensional Solutions	24

III.	FORWARD AND INVERSE METHODS FOR DYNAMIC ANALYSIS.	29
	Prerequisites for a Solution	29
	Overview and Application to Pile Dynamics	30
	The Uniqueness Problem	32
IV.	DEVELOPMENT OF A STATIC/DYNAMIC FINITE ELEMENT CODE WITH MOHR-COULOMB PLASTICITY	37
	Code Environment	37
	Analytic Solutions for Static and Dynamic Pile Response to Loading.	38
	Closed Form Solution of the Wave Equation for Piles: Warrington (1997).	38
	Linear Solution for Pile Settlement: Randolph and Wroth (1978) . . .	38
	Rationale for a Plasticity Model.	39
	Elastic and Plastic Response	40
	Failure Theory	44
	Other Issues	46
	Mohr-Coulomb Failure Theory.	46
	Elasto-Plasticity	51
	Finite Element Implementation.	58
	Element Type	59
	Grid Generation	64
	Boundary Conditions and Model Size	66
	Interface Elements for Soil-Pile Interaction.	67
	Effective Stress Computations and Pore Water Pressures	70
	Engineering Properties of Soils	75
	General Considerations	75
	The “xi-eta” Method of Soil Property Aggregation	77
	Modulus of Elasticity	80
	Poisson’s Ratio	84
	Internal Friction Angle	85
	Cohesion	86
	Dry Density.	87
	Specific Gravity of Solids	88
	Static Analysis.	89
	Analytical Static Capacity Estimates	89
	Stepping Scheme for Static Analysis	90
	Static Load Testing Considerations	92
	Dynamic Analysis	97
	Explicit and Implicit Schemes.	97
	Newmark Explicit Stepping Scheme for Dynamic Analysis	104
	Newmark Implicit Stepping Scheme for Dynamic Analysis	105
	Inputs at the Pile Head	106
	Modeling of the Pile Hammer.	108
	Interface Elements for the Hammer and Cap Portion of the Model .	108

	Pile Hammer Model	113
	Parasite Oscillations	114
V.	INVERSE METHOD AND OPTIMIZATION	119
	Overview of the Problem.	119
	Use of Optimization and Signal Matching Techniques.	120
	Overview	120
	Implementation in STADYN	121
	Selection of an Optimization Technique	124
VI.	MODEL TEST CASES	127
	Semi-Infinite Theory Pile Head Force Cases.	129
	Fixed Base.	129
	Dilatancy and Element Squeeze Study	132
	Static Load Test Interpretation.	143
	Modeled Hammer Cases	145
	Fixed End Runs, Cushioned Hammer.	145
	Fixed End Results, Cushionless Hammer	151
	Bearing Graph Study	155
VII.	CASE WITH STATIC LOAD TEST	161
VIII.	COMPARISON WITH GRLWEAP.	171
	GRLWEAP Results	172
	STADYN Results.	176
	Comparison of the Results	180
IX.	OPTIMIZATION RUNS AND CAPWAP COMPARISON	185
	Overview of Field Data	185
	Summary of Results	192
	Details of Standard Two-Layer Case	196
	Other Optimization Cases	207
X.	DISCUSSION	211
	Revisiting the Uniqueness Issue	211
	Rheology.	214
	Numerical Method	217
	Optimization Techniques	218
XI.	CONCLUSION AND RECOMMENDATIONS FOR FURTHER STUDY.	221
	REFERENCES	223

VITA235

LIST OF TABLES

1	Summary of Two-Dimensional Pile Wave Equation Models	25
2	Static Load Results for Various Methods	144
3	Maximum Pile Head Forces for Analytical and Finite Element Models.	148
4	Properties of Vulcan 06 Hammer	162
5	Soil Profile for GRLWEAP Comparison	171
6	Properties of Vulcan 5110 Hammer	173
7	SRD and Blow Count Results from GRLWEAP Calculations	174
8	Static Load Interpretations for GRLWEAP Comparison.	180
9	Overall Results of Mondello and Killingsworth (2014) Comparison.	194

LIST OF FIGURES

1	Velocity-Time History for Pile (after Isaacs (1931))	4
2	Force-Time History of Pile at Pile Middle (after Glanville et.al. (1938))	5
3	One-Dimensional Wave Equation Model With Various Types of Pile Driving Equipment (after Hannigan et.al. (1997))	7
4	Inverse Modeling of Pile Dynamics (after Hannigan et.al. (1997))	12
5	CAPWAP Signal Matching (after Hannigan et.al. (1997))	14
6	Advance of Wavefront in Pile and Soil During Initial Impact (from H�eritier and Paquet (1986))	22
7	Typical Shear Stress-Strain Responses of Soil (from Department of the Army (1986))	41
8	Hyperbolic Soil Model (from Department of the Army (1990))	42
9	Elasto-Plastic Soil Response	43
10	Mohr-Coulomb Failure Theory (after Reid et.al. (2004))	47
11	Mohr-Coulomb Failure Criterion	48
12	Mohr-Coulomb Failure in Three Dimensions (after Owen and Hinton (1980))	50
13	Weighting Functions for Nine-Node Quadrilaterals	61
14	Weighting Function for Four-Node Quadrilaterals	62
15	Natural Coordinates and Quadrature Points for Four-and Nine-Node Quadrilaterals	63
16	Grid Generation for Finite Element Model	65
17	Four-Node Quadrilateral Adapted to Soil Properties	78
18	Modulus of Elasticity as a Function of ξ and η	83

19	Poisson's Ratio as a Function of ξ and η	84
20	Friction Angle as a Function of ξ and η	85
21	Cohesion as a Function of ξ and η	86
22	Dry Density as a Function of ξ and η	87
23	Specific Gravity as a Function of ξ and η	89
24	Davisson's Method of Interpreting Static Load Tests (after Naval Facilities Engineering Command (1986))	95
25	Four-Node Interface Element (format after Zeevaert (1980))	109
26	Pile Hammer Model	113
27	Semi-Infinite Pile Head Force, Displacement-Time Results	129
28	Semi-Infinite Pile Head Force, Stress-Time Results	130
29	Semi-Infinite Pile Head Force, Two-Dimensional Displacement-Time Results	131
30	Semi-Infinite Pile Head Force, Two-Dimensional Stress-Time Results	132
31	CAD Representation of the Pile-Soil Model, Element Squeeze = 3	133
32	Displacement-Time, Element Squeeze = 3	134
33	Stress-Time, Element Squeeze = 3	135
34	Pile Load Test Results	136
35	First Principal Stress Plot for Static Load Test	138
36	First Principal Stress Plot, Pile Head Region	139
37	Third Principal Stress Plot	140
38	y-displacements for Static Test	141
39	Dilatancy-Squeeze Study Using Cohesionless Soil	142
40	Force-and Displacement-Time Relationships, ITR=4	146
41	Force-and Displacement-Time Relationships, ITR=1	147

42	Force-and Displacement-Time Relationships, ITR=0.25	147
43	Pile Stresses, ITR = 4.	149
44	Pile Stresses, ITR = 1.	149
45	Pile Stresses, ITR = 0.25	150
46	Force-and Displacement-Time Relationships, ITR = 4	151
47	Force-and Displacement-Time Relationships, ITR = 1	152
48	Force-and Displacement-Time Relationships, ITR = 0.25	152
49	Pile Stresses, ITR = 4.	154
50	Pile Stresses, ITR = 1.	154
51	Pile Stresses, ITR = 0.25	155
52	Bearing Graph for Air-Steam Hammer	156
53	ξ and η vs. Ultimate Davisson Capacity	157
54	Blow Count vs. Davisson Capacity	158
55	Comparison of STADYN results with Static Load Test Results from Finno (1989).	163
56	First Principal Stresses at Pile Toe, Simulation of Finno (1989)	165
57	y-direction Displacements at Pile Toe, Simulation of Finno (1989)	166
58	x-direction Displacement at Pile Toe, Simulation of Finno (1989)	167
59	y-displacement-time History, Simulation of Finno (1989).	168
60	y-stress-time History, Simulation of Finno (1989).	169
61	Bearing Graph Results for GRLWEAP Comparison	175
62	Force-and Velocity-Time Results for GRLWEAP Comparison	176
63	STADYN Model for GRLWEAP Comparison	177
64	STADYN Force-, Velocity-and Displacement-Time Results for GRLWEAP Comparison.	178
65	STADYN Static Load Results for GRLWEAP Comparison.	179

66	Soil Boring Logs for Nearby Job (from USACE Solicitation W912P8-10-R-0011)	186
67	Unified Soil System Key for Figure 66 (from USACE Solicitation W912P8-10-R0011).	186
68	Force-time and Velocity-time histories for SC-9 Test (from Mondello and Killingsworth (2014))	187
69	Estimated Static Load Test Results (from Mondello and Killingsworth (2014))	188
70	Test Setup for Mondello and Killingsworth (2014)	189
71	Two Shaft Layer Model for Mondello and Killingsworth (2014) Comparison.	193
72	RMS Differences of Mondello and Killingsworth (2014) Comparison.	195
73	Static Load Test Results of Mondello and Killingsworth (2014) Comparison.	195
74	Velocity-Time Histories, Two-Layer Standard Polytope Case	196
75	Optimization History, Two-Layer Standard Polytope Case	197
76	Layer-by-Layer Results, Two-Layer Standard Polytope Case.	199
77	Static Load Test Result, Two-Layer Standard Polytope Case.	200
78	Stress-Time History, Two-Layer Standard Polytope Case	200
79	y-displacement-time History, Two-Layer Standard Polytope Case	201
80	First Principal Stresses, Two-Layer Standard Polytope Case	202
81	First Principal Stresses at Pile Splice, Two-Layer Standard Polytope Case.	203
82	Vertical Displacements, Two-Layer Standard Polytope Case	204
83	Vertical Displacements, Two-Layer Standard Polytope Case, Steel-Wood Interface	205
84	Vertical Displacements, Two-Layer Standard Polytope Case, Pile Toe	206
85	Velocity-Time Histories, Four-Layer Annealed Polytope Case	208

86	Optimization History, Four-Layer Annealed Polytope Case	209
87	Layer-by-Layer Results, Four-Layer Standard and Annealed Polytope Case.	210

LIST OF SYMBOLS

- $AV_{1,2}$, interface integrated constants, m^2
- a_F , failure function vector
- a_Q , plastic function vector
- a_h, b_h , hyperbolic stress-strain coefficients
- a_n , acceleration at beginning and after correction, m/sec^2
- a_0, a_1 , accelerations for Newmark Method (for Equations 92-97)
- $a_{1,2,3}$, failure function subvectors for Equation 33
- a_β , constant for substepping algorithm
- B , strain displacement matrix
- $C_{1,2,3}$, failure function subconstants
- c , cohesion, Pa
- c_a , acoustic speed of soil, m/sec
- c_s , soil shaft damping
- $c_{1,2,3,4,5}$, Newmark coefficients
- $d(x)$, pile strain coefficient
- D_e , elastic constitutive matrix
- D_{ep} , elasto-plastic constitutive matrix
- D_p , plastic constitutive matrix
- d_{head} , elastic pile head displacement under static load, m
- d_{tact} , actual displacement at time t, m
- d_{tcomp} , computed displacement at time t, m
- \tilde{d} , predicted displacement, m
- E , modulus of elasticity, Pa

$E(\varepsilon)$, modulus of elasticity as a function of strain
 E_p , pile modulus of elasticity, Pa
 E_{ti} , tangent modulus of elasticity, Pa
 F , Mohr-Coulomb failure criterion, Pa
 f , force vector
 $f(\xi, \eta)$, soil property derived from dimensionless parameters
 F_o , static pile head axial force, N
 $F_o(t)$, dynamic pile top force, N
 $F_{1,2,3,4,5,6,7,8}$, interface nodal forces, N
 G , shear modulus of elasticity, Pa
 G_s , specific gravity of the soil particles
 G_{mid} , soil shear modulus of elasticity at pile middle, Pa
 G_{toe} , shear modulus of elasticity of soil at pile toe, Pa
 h , height of ram drop, m
 H_n , element shape function
 J'_2 , second deviatoric stress invariant, Pa²
 J'_3 , third deviatoric stress invariant, Pa³
 J_1 , first stress invariant, Pa
 K , stiffness or Jacobian matrix
 K_T , tangent stiffness or Jacobian matrix
 K_{local} , interface element stiffness matrix
 K_o , at-rest lateral earth pressure coefficient
 $K_{1-3,5-7,2-4,6-8}$, interface spring constants, N/m
 k , soil shaft stiffness, N/m²
 k_{loc} , local Jacobian or stiffness matrix
 $k_{s,n}$, coefficient of subgrade reaction, N/m³
 L , pile length or embedded pile length, m
 L_{inter} , interface length, m

L_{min} , minimum length of an element side, m
 L/c , time for wave to travel from pile head to pile toe, sec
 M , mass matrix
 M_{local} , local interface element mass matrix
 m_{loc} , local mass matrix
 $m_{1,2,3,4,5,6,7,8}$, interface element mass, kg
 N , total number of data points or time steps
 n , time or Newton step number
 p , internal force vector
 Q , plasticity potential function, Pa
 q , pressure on element interface, Pa
 q_c , unconfined compression strength of soil, Pa
 R_{allow} , allowable axial capacity or resistance of pile, N
 R_{dil} , dilatancy ratio, ψ / φ
 R_{ult} , ultimate resistance of pile, N
 \mathbb{R}_n , real number set of dimension n
 r , radial coordinate for polar coordinates
 r_{avg} , average interface radial coordinate, m
 r_i , pile inside radius, m
 r_m , magic radius of influence of pile downward deflection in soil, m
 r_o , outside radius of pile, m
 s , effective stress vector
 S_r , computed data values
 s_{blow} , pile set per blow, m
 S_{ier} , diagonalized interface element stiffness matrix
 t , time, seconds
 $t_{implied}$, implied interface element effective thickness, m
 t_{inter} , interface element effective thickness, m

u , pore water pressure, Pa
 $u(x, t)$, displacement as a function of distance and time, m
 V , volume, m^3
 v_{lact} , actual velocity at time t , m/sec
 v_{lcomp} , computed velocity at time t , m/sec
 \tilde{v} , predicted velocity, m/sec
 W_r , weight of ram, N
 $w_{1,2}$, constants for Engineering News Formula
 x , distance, m
 y_r , actual data values
 Z , pile impedance, $N\text{-sec}/m$
 z_w , depth from phreatic surface to point in soil stratum, m
 β , Newmark constant
 β_n , ratio of cohesion to modulus of elasticity
 γ , Newmark constant
 γ_w , unit weight of water, N/m^3
 γ_{dry} , dry unit weight, N/m^3
 γ_{sat} , saturated unit weight, N/m^3
 Δd , change in displacement during time or Newton step, m
 Δd_{rms} , root mean square difference between computed and actual displacement, m
 Δv_{rms} , root mean square difference between computed and actual velocity, m/sec
 Δt , time step, sec.
 ε , strain
 ε_e , elastic strain
 ε_p , plastic strain
 $\varepsilon_{r,z,rz,\theta}$, strains in polar directions
 η , density or consistency, or local coordinate for finite element
 θ , Lode's angle, radians or degrees

λ , elasto-plastic normality or plasticity constant
 λ_p , pile and soil elasticity ratio
 μ_p , pile-soil interaction factor
 ν , Poisson's Ratio
 ν_{CFL} , CFL (Courant-Friedrichs-Lewy) Ratio
 ξ , degree of cohesion or local coordinate for finite element
 ξ_p , pile movement to strain ratio
 ρ , density, kg / m^3
 ρ_p , ratio of the soil shear modulus at pile middle to pile toe
 ρ_{dry} , dry density of the soil, kg / m^3
 ρ_{sat} , saturated density of the soil, kg / m^3
 ρ_{water} , density of water = $980 \text{ kg} / \text{m}^3$
 σ'_z , vertical effective stress, Pa
 $\sigma'_{x,y,z}$, deviator stress in Cartesian directions, Pa
 $\sigma_{1,3}$, principal stresses, Pa
 $\sigma_{x,y,z}$, normal stress in Cartesian directions, Pa
 σ_{yield} , yield strength of material, Pa
 τ , shear stress, Pa
 $\tau_{xy,yz,xz}$, shear stress in Cartesian directions, Pa
 $\hat{\tau}$, integrable time variable
 φ , internal friction angle, degrees or radians
 ψ , dilatancy angle, degrees or radians
 $\psi_{1,2}$, displacement for d'Alembert's Equation, m

LIST OF ABBREVIATIONS

BPF, blows per foot or 300 mm of penetration, $1/_{0.3\text{m}}$

BPM, blows per meter of penetration, $1/_{\text{m}}$

ITR, interface thickness ratio

LMS, least mean squared difference

SRD, soil resistance to driving, N

CHAPTER I

INTRODUCTION

Before the Wave Equation

Driven piles are the oldest form of deep foundations for civil and military structures of all kinds, predating written civilization itself. The main purpose of driven piles, or any deep foundation for that matter, is to transfer loads from a structure situated in soft soils, over water, or both, to a more competent stratum than is available to the structure at its elevation. Until the last fifty years or so piles were configured to transmit primarily axial loads. These kinds of loads remain the predominant loads driven piles transmit, although lateral loads are also important. Anyone who is familiar with pile driving knows that, during installation, the early part of the driving is typically “easy” with the pile advancing several centimeters with each blow. As the pile goes further into the earth, the resistance increases and the advance of the pile with each blow decreases. Although soil strata are anything but uniform and consistent, this is the general trend.

Even without the benefit of analytical tools, there is an intuitive link between the resistance a pile-soil combination to driving and the resistance to the static load it was designed to bear. Beginning in the middle of the nineteenth century, there was an effort to quantify that link. As Chellis (1961) notes, the first attempt at this was the Sanders Formula:

$$R_{allow} = \frac{W_r h}{8s_{blow}} \quad (1)$$

Equation 1, along with most of what came to be called dynamic formulae, were based on Newtonian rigid body mechanics. Sanders attempted to relate this distance a pile advanced per hammer blow to the resistance/capacity of the pile during installation and actual use.

As a matter of clarification, the advance of a pile into the earth can also be defined by its blow count, i.e., the number of blows per unit length of penetration. In its simplest form the relationship is

$$BPM = \frac{1}{s_{blow}} \quad (2)$$

In countries such as the United States where the blow count is measured in feet, the blow count can be readily expressed as blows per 300 mm of penetration, or

$$BPF = \frac{3}{10s_{blow}} \quad (3)$$

Equation 1 introduced the concept of using the installation process itself as a form of load test for a driven pile. For this formula, the problem is that, as $s \rightarrow 0$, $R \rightarrow \infty$, which is obviously unrealistic. Further development lead to the most popular dynamic formula promulgated (in the United States at least,) the Engineering News Formula. Wellington (1893) first published Equation 4 in 1888:

$$R_{allow} = w_1 \frac{W_r h}{s_{blow} + w_2} \quad (4)$$

This equation can be solved for the pile set as

$$s_{blow} = w_1 \frac{W_r h}{R_{allow}} - w_2 \quad (5)$$

Until the 1970's dynamic formulae were the "state of the art" in pile dynamics, even though the proliferation of different formulae and correlation

difficulties (Parola (1970); Likins et. al. (2012)) suggested to many that something was basically wrong with these equations.

Application of the Wave Equation to Pile Driving

Early Attempts at a Solution

Until the end of the nineteenth century virtually all piles were timber piles driven with drop hammers. Between the introduction of Equation 4 and the First World War, steel and precast concrete piles were introduced, and steam driven hammers became more popular (Warrington (2007)). It was those improvements that detonated the first “crisis” for rigid body pile dynamics. During installation, concrete piles began to show extensive damage in the form of cracking, particularly at the mid-point of the piles. Rigid body mechanics were unable to explain these cracks; however, Isaacs (1931) proposed that what was taking place in piles was one-dimensional wave propagation, which in turn was generating tension stresses in piles due to wave reflections from the pile toe. Isaacs also saw that applying wave mechanics to piles could improve the correlation between observed driving parameters and pile capacity. He developed a graphical technique to analyze the time history of impact, as shown in Figure 1.

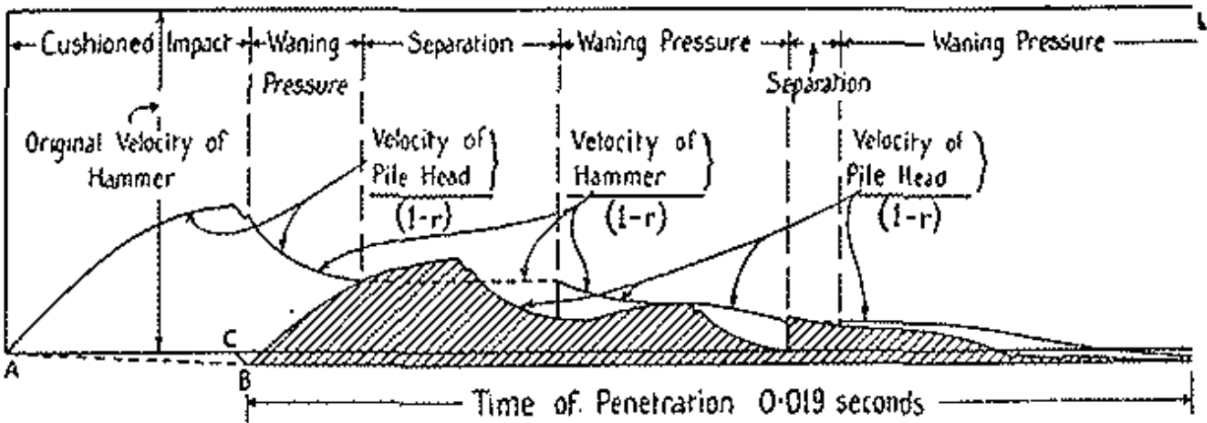


Figure 1 Velocity-Time History for Pile (after Isaacs (1931))

The 1930's saw other advances in wave mechanics for piles, in particular from Glanville et.al. (1938). This research included the first comprehensive program to record the force-time curve of the hammer impact on the pile, as shown in Figure 2. It also saw a heightened awareness of the limitations of dynamic formulae as predictors of pile capacity. Unfortunately applying wave mechanics to pile dynamics was hindered by the complexity of the problem, which included non-linear response of the soil and inextensible interfaces between the hammer, cap and pile.

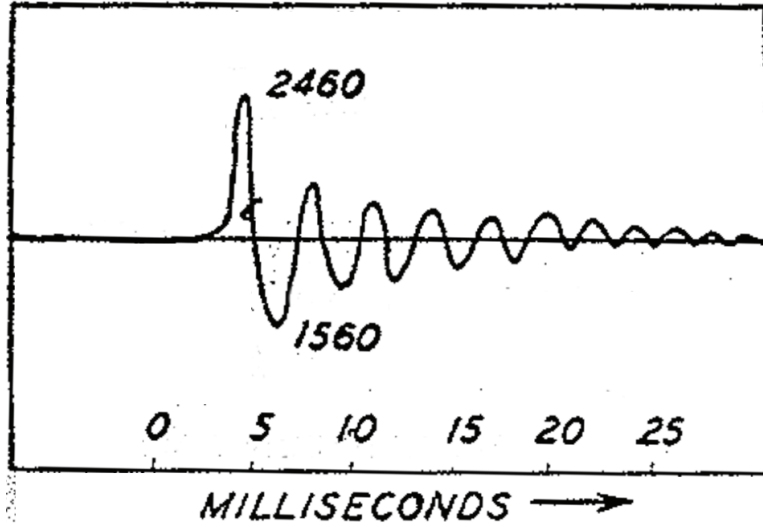


Figure 2 Force-Time History of Pile at Pile Middle (after Glanville et.al. (1938))

Glanville et.al. (1938) also explicitly ascribed the one-dimensional wave equation as the governing equation for driven piles under impact. That equation is

$$\frac{\partial^2}{\partial t^2}u(x, t) = c_a^2 \frac{\partial^2}{\partial x^2}u(x, t) \quad (6)$$

Their solution was based in part on d'Alembert's equation (Sobolev (1964))

$$u(x, t) = \psi_1(x - c_a t) + \psi_2(x + c_a t) \quad (7)$$

Equation 7 appears routinely in the literature relating to the Case Method and CAPWAP (Rausche (1970); Rausche et.al. (1972); Rausche, Goble and Likins (1985)) and in alternative solutions such as Liang (2003). The advent of numerical methods has largely superseded the unaided use of d'Alembert type solutions; the "bookkeeping" necessary to keep up with the upward and downward traveling waves is considerable.

However, the problem with Equation 7 goes deeper than d'Alembert solutions. The most fundamental problem is that Equation 7 assumes no dampening or resistance of any kind along the shaft of the pile. Although many driven piles have exposed portions which do not contact the soil, it is the rare driven pile (or any other type of deep foundation) which lacks shaft resistance of any kind.

One way of incorporating shaft resistance to the problem is to employ the Telegrapher's wave equation (Webster and Pimpton (1966)),

$$c_a^2 \frac{\partial^2}{\partial x^2} u(x, t) = \frac{\partial^2}{\partial t^2} u(x, t) + au(x, t) + 2b \frac{\partial}{\partial t} u(x, t) \quad (8)$$

Obviously, if $a = b = 0$, then Equation 8 reduces to Equation 6.

There are limitations to Equation 8 as well. First, it assumes a uniform cross-section of the pile with no discontinuities. Both of these assumptions are present in the undamped solution as well. Neither of these is necessarily true of any driven pile, and discovery of the latter is the main driving force behind the application of wave propagation theory to pile integrity testing.

Beyond these limitations, the Telegrapher's equation assumes a linear soil response for both elasticity and dampening along the pile shaft. Neither of these (especially the former) can be relied upon on with driven piles, and in reality the whole goal of pile driving is to stress the soil beyond its elastic limit and allow the pile to achieve a permanent set with each blow. This is the inherent weakness of such approaches as Pao and Yu (2011). As was the case with the application of Winkler theory to lateral pile loading and response, the soils simply do not respond to their mobilization in linear ways.

Nevertheless, in spite of these limitations, the Telegrapher's equation is closer to the realities of driven piles than the undamped equation. This is significant in the development of new methods for the dynamic analysis of driven piles.

Smith's Solution

Although World War II delayed progress for more than a decade, these problems were eventually solved by the work of Smith (1960). His computer-solved numerical analysis modeled the soil as an visco-elastic-plastic reaction for both shaft friction and toe resistance, and included special modeling for the pile driver and pile cushion. Some of these features are illustrated in Figure 3.

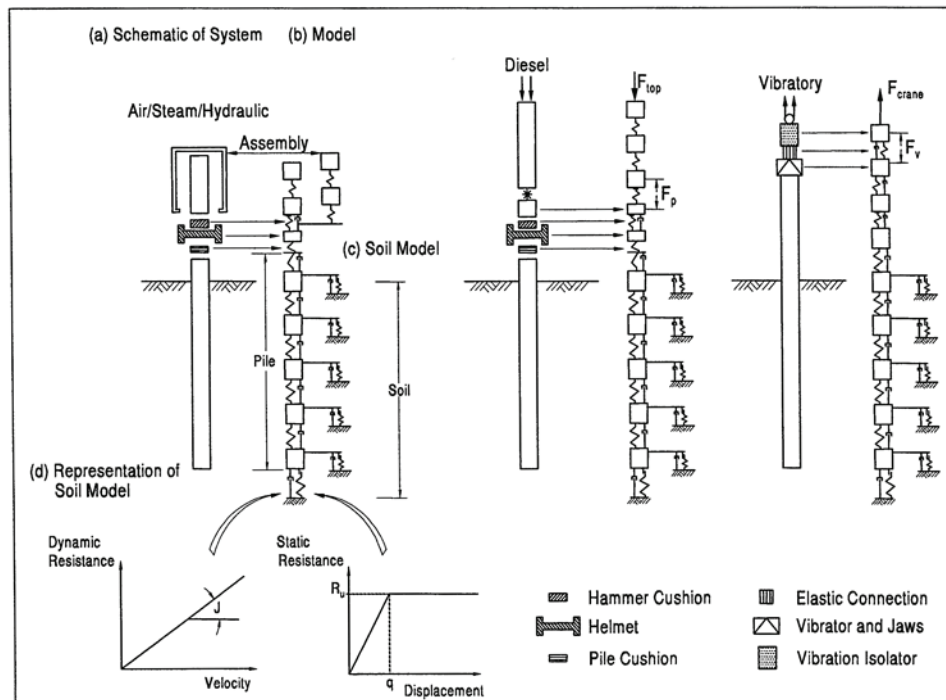


Figure 3 One-Dimensional Wave Equation Model With Various Types of Pile Driving Equipment (after Hannigan et.al. (1997))

The method detailed in Smith (1960) is a modified central-difference technique which sums forces for each mass, which are in turn lumped at the bottom of each pile segment.

The success of Smith's scheme—and those that are based upon it—is such that, when most people in the deep foundations business refer to the “wave equation,” they are referring to a computer program of one kind or another. In the forward method, what the program does is solve a non-linear version of Equation 8 with appropriate modeling of the hammer cushion, driving accessory and pile toe response. The pile itself is discretized into finite segments, which also enables one to vary the soil properties along the shaft in a straightforward way, i.e., to assume that they are constant over the segment but perhaps different from one segment to the next.

Although the limitations of this numerical integration scheme were recognized early (Fischer (1960)), Smith's basic scheme has endured for many years. An immediate result was that his code was further developed by several researchers both to improve usability and to model diesel hammers properly (Hirsch et.al. (1976); Goble and Rausche (1976)). This established the wave equation analysis as the “state of the art” predictive tool for driven piles and piles verified by high-strain dynamic testing, which it remains to this day.

Effect of System Parameters

No numerical model is any better than its input parameters, and the model of Smith (1960) is no exception. With the hammer and pile, the parameters can be established with reasonable accuracy, as these are made of conventional engineered materials and their configuration is generally well known. Turning to the soil parameters, inspection of Figure 3 shows that not only do the values of the soil

damping, quake and resistance need to be known, but also that these can and do vary along the shaft of the pile and at the toe. It makes sense that some parameters will have more effect on the performance of the system than others.

Meseck (1985) examined this problem using WEAP (Goble and Rausche (1976)). Running parametric studies, he concluded that factors such as hammer and cushion configuration and soil dampening were critical, while others such as quake and—most importantly—the distribution of resistance along the shaft and/or the distribution of resistance between shaft and toe were not as critical, as were variations in pile length and elasticity.

These results emphasize the importance of a proper estimate of damping parameters. This is especially important in relating the results of dynamic analysis of any kind to the static performance of the system.

Method of Characteristics

One method employed for the analysis of wave propagation is the method of characteristics. This is described in some detail by Abbott (1966). According to Middendorp and Verbeek (2006), the concept of the method of characteristics was first proposed for driven piles with the soil resistance concentrated at the toe. In the course of the development of the HBG Hydroblok hammer, shaft resistance was added to the model and a practical method of analyzing wave propagation in piles was developed (Voitus van Hamme et.al. (1974)). The method of characteristics is embodied in the TNOWAVE program. The method has both forward and inverse application, and the latter is not restricted to TNOWAVE related applications, being used in CAPWAP-C. Horvath and Killeavy (1988) state that CAPWAP was improved by switching to the method of characteristics from the lumped-mass model.

In its simplest form, the method of characteristics divides up the pile into segments, as is the case with the other numerical methods. The difference comes in that the method of characteristics solves Equation 6 for each segment and time step. Any other resistances or changes along the shaft or toe (soil resistance, change in pile impedance) are represented at the boundaries of each segment. Generally speaking, it is necessary to coordinate the segment length to the time step through the acoustic speed of the pile material. For uniform piles, this is fairly straightforward; where the pile has one or more changes in impedance, time step selection becomes more complicated.

The method of characteristics can thus avoid many of the stability problems inherent in the explicit methods; however, the comments related to Equation 8 apply, to some extent, to the method of characteristics.

Use of the Wave Equation in Verification

The uncertainties inherent in geotechnical engineering have always encouraged the development of field verification methods for virtually any foundation structure. For deep foundations in axial loading, the “reference standard” method is static load testing. This, however, is expensive and time consuming, and this has encouraged the development of alternatives, such as the dynamic formulae. In fact, Equation 4 is the “verification” form of the dynamic formula; given a measured set after a hammer blow, a capacity can be estimated. Isaacs (1931) foresaw the use of the wave equation “inversely,” taking results from pile driving and applying them to wave mechanics to estimate the SRD or ultimate capacity of the pile (and the two are not identical.) One way to do this is to run a wave equation analysis “after the fact” of pile driving, and this is done from time to time (Rausche, Nagy and Webster (2009)). Nevertheless, as is the case with other

fields, the need for a more “direct” solution to what is in reality the inverse problem was recognized early on.

Inverse methods are more computationally costly than their forward counterparts. In the early years of their application, simplifications were made to reduce the computational cost. One common simplification with inverse methods is the concentration of the resistance—static or dynamic—of the pile at the toe. Obviously this goes against both the physical realities of the hammer-pile-soil system. H eritier and Paquet (1986) describe one study used in the development of an inverse method where the pile was set up to minimize shaft friction and to actually concentrate the resistance at the toe. It should also be noted that the CASE Method—the earliest attempt at a “back of the envelope” method of estimating static capacities from dynamic data—makes this assumption, and this is one reason why this method has been problematic in its implementation.

Development of CAPWAP

In reality the concept of using “a Newton-based approach to the dynamic determination of pile capacity” is almost contemporaneous to Smith’s work with the wave equation. According to Goble Rausche and Likins (1975), the idea was first studied by Robert Eiber at the Case Institute of Technology; his master’s thesis on the subject was published in 1958. The project continued during the 1960’s and a more comprehensive solution to the problem was proposed by Rausche (1970). Using theory derived from Saint-Venant and field test correlations, he developed a method that, when further developed, became CAPWAP (Case Pile Wave Analysis Program, Figure 4.) This, with subsequent improvements in both methodology and computer hardware, has become nearly ubiquitous in dynamic testing of driven piles and other deep foundations. It enables, by collecting data from accelerometers and strain gauges at the head of the pile during driving, an estimate of the static

capacity of the pile. The method is well embedded in the recommended methodology by the FHWA and other organizations (Hannigan et.al. (1997); Hannigan et. al. (2006)).

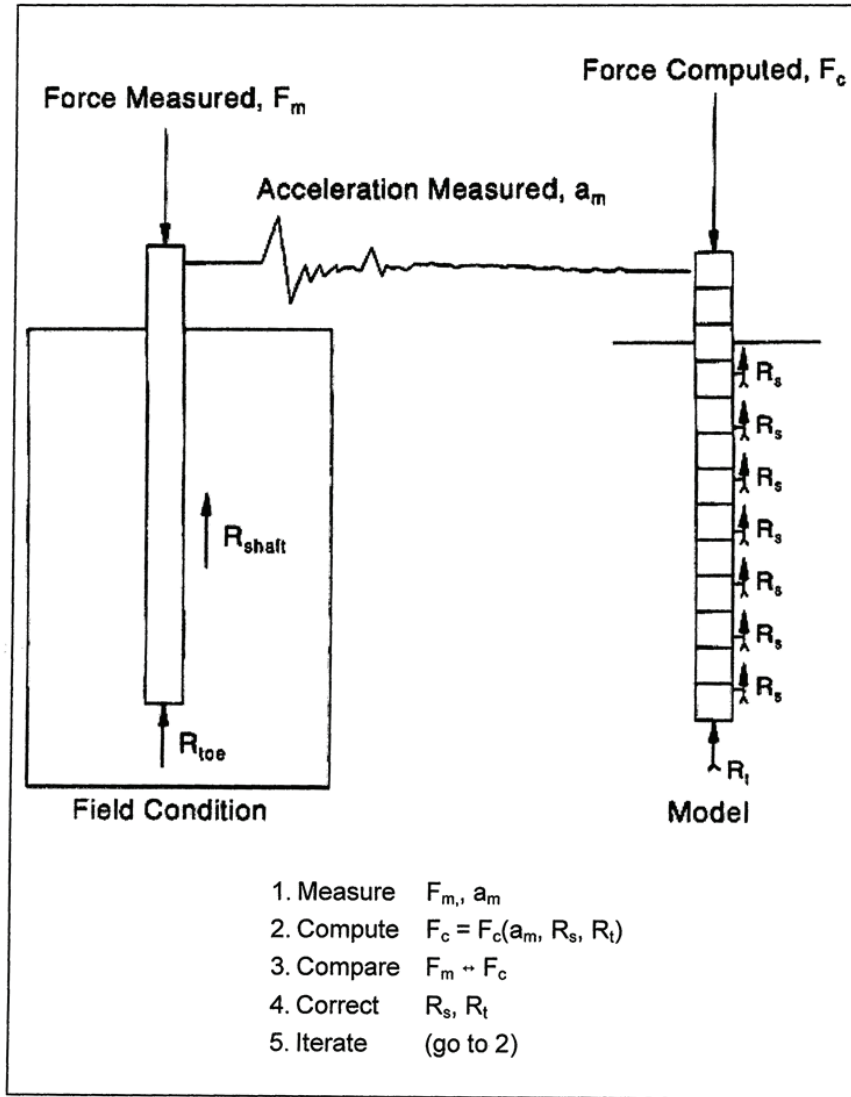


Figure 4 Inverse Modeling of Pile Dynamics (after Hannigan et.al. (1997))

Operation of CAPWAP

As noted the roots of CAPWAP's methodology go back to the beginnings of practical stress-wave analysis in piles, and have been modified by both field experience and the adoption of a numerical model different from the lumped mass method of Smith (1960), namely that of Fischer (1960). The following analysis is based on a recent summary of CAPWAP's methodology, namely that of Rausche et.al. (2010).

CAPWAP is essentially a signal matching routine, as illustrated in Figure 5. The velocity-time history is input into a model whose pile properties are entered based on the pile configuration and whose soil properties are best initial guesses of the actual parameters. A force-time history is returned, and the soil properties are varied until the force-time history returned by the model matches that from the field data.

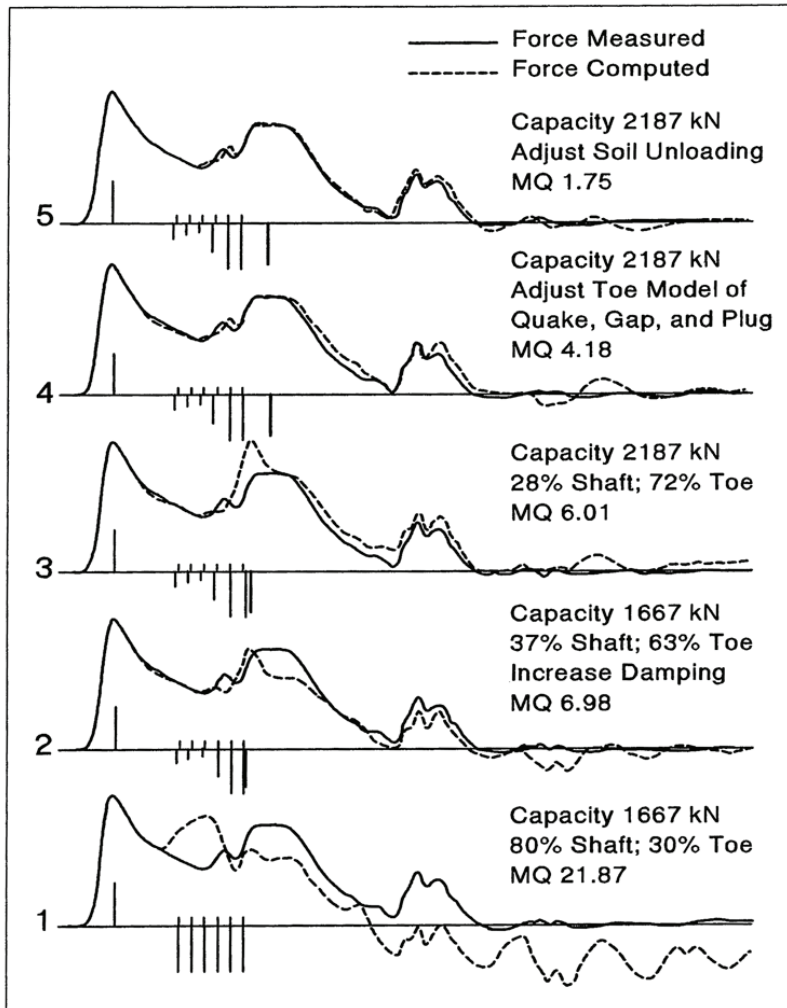


Figure 5 CAPWAP Signal Matching (after Hannigan et.al. (1997))

Rausche et.al. (2010) state that good correlations between CAPWAP results and static load testing can be expected under the following conditions:

1. The time after driving of the static and dynamic tests on the pile itself are comparable, i.e., both procedures are run with the same state of pile set-up;
2. The permanent pile set is at least 2.5 mm, for a comprehensive mobilization of both pile shaft and toe resistance; and

3. The pile is loaded to failure during the static load test and the results evaluated by the Davisson criterion.

With CAPWAP the pile is divided into continuous, uniform segments which have the same travel time t through the segments. As with the conventional wave equation programs, slack in the pile due to splicing, defects in the pile, etc., can be included.

CAPWAP uses a bi-linear, elastic/purely plastic model for the static deflection of the soil. The spring constant of the soil in elastic deformation is determined by the estimated failure load for a given portion of the pile divided by the soil quake, as opposed to elasticity being an input and quake/failure strain being a result as is the case with soil models such as that of Randolph and Simons (1986). In addition to quake values during loading, CAPWAP allows for an unloading which has a different force/displacement characteristic than during loading.

CAPWAP's soil damping model is similar to that used in conventional wave equation programs. As Meseck (1985) showed, the results of a wave equation analysis are very sensitive to the damping values chosen, and this applies to CAPWAP as well. CAPWAP also has an option to model radiation damping, and an option for residual stresses, as is the case with WEAP86 (Goble and Rausche (1986)).

Turning to the signal matching method, CAPWAP defines a "Match Quality" (MQ) which "is quantified by calculating the sum of the absolute values of the differences between calculated and measured quantity (normally wave-up) in four time periods," (Rausche et.al. (2010)) one of which is the time before $2L/c$ and the other three after it. Using the match quality to translate the computed and actual signal correlation to a static load-deflection estimate of the pile is a fairly involved procedure that includes a great deal of data review.

The extensive need for data review during the process makes any objective evaluation of CAPWAP's strengths and weaknesses as a numerical method difficult. With the current state of rheological understanding for both the static and dynamic case and the inherent complexity in the behavior of soils, an entirely “hands-off” type of model is unrealistic to expect. The goal, however, is to perform as much analysis as possible so to give the engineer reasonable choices and courses of action for the situation at hand.

Other Inverse/Verification Methods

It should be noted that CAPWAP is not the only implementation of an inverse method to estimate the capacity of piles from high-strain dynamic testing. Another example of this is the SIMBAT program, originally developed in France (Long (2001)). SIMBAT requires a more elaborate preparation of the pile head than the CAPWAP connection of strain gauges and accelerometers to the pile. Additionally a theodolite is used to track the displacement-time history of the pile head, which provides additional data for analysis (Osman et.al. (2013)). SIMBAT seems to rely more on empirical considerations than CAPWAP, especially with the variation in hammer energy during the test, which in principle at least gives a more comprehensive view of the force-time and force-displacement response of the pile. However, as is the case with the American system, there are limiting assumptions which, depending upon how the current state of the system treats them, may affect the quality of the results significantly.

Another system in use is the TNOWAVE system (Svinkin (2011)), developed in the Netherlands and related to the forward method of the same name. Svinkin (2011) notes accuracy-related differences among all three systems based on soil type.

Objectives of the Dissertation

Pile dynamics, both forward and inverse, was one of the first civil engineering applications to use discrete numerical methods to analyze a non-linear problem. For the most part these methods were developed with much more limited computational capabilities than are available at present. It is reasonable to use these expanded capabilities to take both forward and inverse methods (especially the latter) to a high degree of both precision and accuracy. This dissertation has the following objectives to move this effort forward:

- Development of a forward method that, either using a modeled hammer or predetermined pile head force-time history, will predict the penetration of the pile into the soil. The method should use a pile and soil modeling technique that is a significant advance over the current model.
- Development of an inverse method that, given a pile head force-time history, will determine a soil profile that will return the measured velocity-time history and thus achieve signal-matching, with as little manual intervention as necessary. Although some limited comparisons to actual data will be done, a general correlation with an extensive database is beyond the scope of this dissertation. In order to develop a reasonable model, attention to the theoretical integrity of the model needs to come before its application and verification (or revision or even rejection) in comparison with field data.
- Development of a static model that, using the same model as the dynamic case uses, will determine the static capacity of the pile against accepted criteria for static load tests, or another criterion that the user might desire.

CHAPTER II

ONE-, TWO-AND THREE-DIMENSIONAL WAVE EQUATION ANALYSES

Up until now, all of the solutions described formulate the solution for wave propagation in piles as a one-dimensional problem. This is not physically the case for the following reasons:

1. For true one-dimensional propagation, the center as of the hammer and the center axis of the pile must be the same. As anyone who was watched pile driving knows, this is not always the case.
2. Effects due to pile camber and bending during driving are not considered.
3. The soil mass into which piles are driven can be considered (with some limitations) to be a three-dimensional semi-infinite mass.

The last reason will be considered in this study. All of the models described earlier assume that the pile-soil interaction can be modeled using a one-dimensional type of model.

At the start of this discussion, two things need clarification.

The first is that, in pile dynamics, one-dimensional solutions are usually finite-difference and two-and three-dimensional ones finite element. This is a developmental phenomenon rather than a methodological necessity. It is possible for a finite element method for this class of problems to be based on either 1D or 2D, and in fact Mitwally and Novak (1988) developed a 1D finite element analysis method which used the results of 2D soil modeling to improve the 1D model. Such a model was also used by Danzinger et.al. (1996). Conversely it is possible for two-

and three-dimensional methods to be based on finite difference or even finite volume formulations. Although these (especially the latter) are not unknown in geotechnical engineering, they are not considered in this study.

The second is that the “two-dimensional” analysis under consideration is in fact a simplification of the true three-dimensional analysis, but using axisymmetry to reduce the problem to two dimensions for analytical purposes. Although it is possible, using Fourier Series, to violate the symmetry of the system for lateral displacement purposes (Smith and Griffiths (1988); Potts and Zdravkovic (1999)), this was not considered in this study.

Advantages of One-Dimensional, Finite-Difference Analysis

Although 2D analyses have some advantages over 1D methods, there are at least six reasons why 2D methods have not gained the acceptance of their 1D, finite difference counterparts.

1. Finite difference methods, especially the explicit ones, are easier to set up mathematically. They do not necessarily require use of advanced linear algebra, and the complexities that this introduces into the methodology. This is not only the case with models such as Smith (1960) but also with many other early analysis routines for deep foundations, such as the p-y modeling of lateral loads and t-z modeling of axial loads (Parker and Radhakrishnan (1975)).
2. Many 2D methods have not modeled the hammer/cap/cushion system to any degree. To do so in finite elements is more difficult than it has been using finite differences. Modeling inextensibilities is simpler in explicit, finite difference schemes than those using finite elements.
3. Finite elements have proven even more problematic than their finite-difference counterparts in producing parasite oscillations (Smith and Chow (1982); Deeks

(1992); Warrington (1997)) and other undesired effects in the pile (Randolph and Simons (1986)).

4. Obtaining uniform results for the same input is more difficult with 2D methods than with 1D methods. This is mostly an acceptance issue. Codes and specifications generally “like” an easily reproducible calculation; this is one reason why the wave equation struggled for acceptance vs. the dynamic formulae. The growing use of other 2D and 3D finite element codes for analysis of geotechnical problems should facilitate this acceptance.
5. Rheological issues arising in 2D and 3D implementations are far more complex than with 1D codes (Pinto Grazina and Lourenço (2008)). Geotechnical engineers are well aware of the difficulties in accurately quantifying the response of soils, rocks, and materials in between for relatively simple problems such as bearing capacity and settlement.
6. The wave speed in the pile is much greater than that in the soil. To understand the effects of this, consider the wave propagation schematic shown in Figure 6. The relative slowness of wavefront advance means that relatively little of the soil surrounding the pile is actually mobilized during driving. This makes a one-dimensional analysis more justifiable from the standpoint of the physics of the problem rather than analytical convenience. The last reason may be the most compelling from a physical standpoint. This is subject to variation of the pile material, the nature of the soil and the level to which the soil is strained during the wavefront advance.

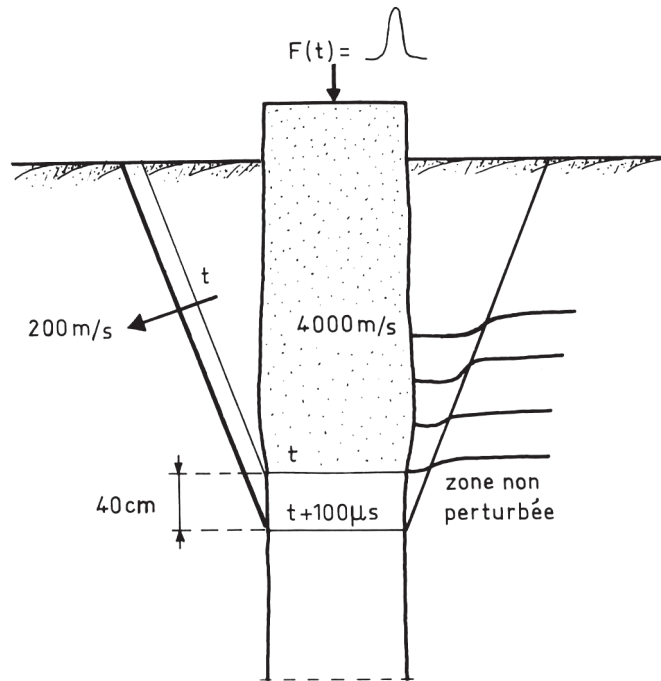


Figure 6 Advance of Wavefront in Pile and Soil During Initial Impact (from H eritier and Paquet (1986))

Rationale for Two-Dimensional, Finite-Element Analysis

In commenting on Smith and Chow (1982), Goble (1983) states that "...the approach has the tremendous advantage of rationality and its use will probably expand." Years later McVay and Kuo (1999) state that "(t)o overcome the problems, a rational model using soil mechanics parameters, such as shear modulus and finite element analysis may provide a better approach to solve the pile driving problems," the application of both of which require a two-dimensional analysis. In spite of the strong points of one-dimensional analysis, a two-dimensional analysis has some significant advantages that make it worth the additional effort:

1. It allows the soil response to be modeled by the properties of the soil itself and not abstractions of these properties in springs and dampers. Over the years several different combinations of spring constant, viscosity and mass modeling have been made for both shaft and toe resistance, in addition to the wide variety of values for the parameters. A two-dimensional analysis gives the opportunity to allow the soil's distributed mass, elasticity and plasticity to model its response.
2. Two-dimensional models can incorporate “far field” effects, i.e., reflections and effects from soil layers that are near the pile but do not actually join to it. This is especially true at the toe; two-dimensional models can also incorporate the effects of thin layers at the toe for both static and dynamic analysis. Two-dimensional models incorporate other phenomena that are impossible with one-dimensional methods. These include beam effects of the driving accessory and induced downdrag in compressive loading (more significant in static than dynamic analysis.)
3. Two-dimensional models can link the basic soil properties (friction, cohesion, elasticity, etc.) with their dynamic response. This has been incorporated into some one-dimensional models (Corté and Lepert (1986); Randolph and Simons (1986)) but ultimately true two- and three-dimensional models are in principle more accurate.
4. For tapered piles, using a 2D analysis eliminates the persistent problem of how to accurately model a tapered surface. Generally soil failure around piles is in shear along the shaft and in compression at the toe; tapered regions incorporate both. Most static capacity methods do not have a straightforward way of taking this into consideration, although Nordlund's Method (Hannigan et. al. (2006)) is a notable exception. For both 1D static and dynamic methods, the pile can be

“step-tapered” analytically and “pile toes” can be distributed along the shaft. With a 2D method the geometry and its interaction with the soil—to say nothing of wave propagation in the pile—can be modeled directly without recourse to workaround such as intermediate pile toes.

These are some of the reasons for developing the two-dimensional axisymmetric model used in this study for both static and dynamic pile loading.

Survey of Two-Dimensional Solutions

Two-dimensional finite-element solutions first appeared in the United Kingdom in the early 1980's, partly because of North Sea offshore oil exploration and the requirements of platform design in that demanding environment, which included platforms installed in deep water. A brief summary of the methods developed since that time is shown in Table 1.

Table 1 Summary of Two-Dimensional Pile Wave Equation Models

Study	Element Type	Integration Scheme	Plasticity	Pile Interface Elements?	Code or Package?	Pore Water?	Typical Pile
Smith and Chow (1982)	8-Node Quad	Implicit Wilson Theta	Mohr-Coulomb	No	Code	No	1.524 m O.D. Steel
To (1985)	8-Node Quad	Implicit Wilson Theta	Mohr-Coulomb	Yes, 6-Node	Code	No	1 m O.D. Steel
Coutinho et.al. (1988)	6-Node Quad	Explicit Central Difference	Mohr-Coulomb	Yes, 6-Node	Code	No	1.422 m O.D. Steel
Nath (1990)	6-Node Quad	Explicit Central Difference	Hypo-elastic Bounding-Surface Plasticity	Yes	Code	No	1 m O.D. Steel
Mabsout and Tassoulas (1994)	8-Node Quad	Implicit Constant Average Acceleration	Mohr-Coulomb	No	Code	No	1 m O.D. Concrete
Masouleh and Fakharian (2008)	Quad	Unknown	Mohr-Coulomb	Yes	FLAC	Yes	300 mm O.D. Concrete
Pinto Grazina and Lourenço (2008)	15-Node Triangle	Implicit Newmark	Mohr-Coulomb	No	Plaxis	No	500 mm O.D. Steel
Serdaroglu (2010)	8-Node Quad	Explicit Newmark	Mohr-Coulomb	Yes	ABAQUS	Yes	1 m O.D. Steel

Some general comments on these methods are as follows:

- Smith and Chow (1982): This was the first attempt at a two-dimensional model of the pile in finite elements. A rectangular grid that was refined nearest to the pile was used. This type of grid is the most commonly one used in this type of analysis. A time-varying force to simulate a hammer impact was applied at the pile head. In addition to modeling the soil three-dimensionally using two-dimensional axisymmetric elements, the pile was modeled in the same manner.
- To (1985): This was a continuation and development of Smith and Chow (1982). The pile hammer was directly modeled at the pile head for the first time, as opposed to simply giving the pile head a force-time relationship. In addition to impact driven piles, vibratory driven piles and surface footings were analyzed

using this code. This study also saw the first use of pile interface elements, based on the concept that the pile-soil interaction is fundamentally different than the interaction of the soil with itself.

- Coutinho et.al. (1988): This was part of a long effort on the part of Petrobras, the Brazilian state oil company, to develop new methods to predict pile drivability using methods more advanced than were available. The model was intended to simulate the driving of large (1422 mm) diameter steel pipe piles 97 m into the earth, which made it the largest pile simulated using 2D to date.
- Nath (1990): Similar in many ways to Coutinho et.al. (1988), it represented an attempt to replicate hyperbolic soil response. Additionally a mapping scheme for the elements was used. The results were compared with actual field data and good agreement was noted, although the sample was understandably small.
- Mabsout and Tassoulas (1994): This study incorporated more complex soil modeling than was previously used, especially more advanced types of failure theory. Both of these were primarily aimed at analyzing clay soils. The advancement of the model, however, ran into computational power limitations.
- Masouleh and Fakharian (2008): The first study to use a software package (in this case FLAC) it was also the first to attempt an inverse solution to the wave equation for piles. Extensive comparison with conventional 1D analyses was done.
- Pinto Grazina and Lourenço (2008): This study actually analyzed wave propagation in piles with both 1D and 2D models. Reasonable agreement was obtained between the two models. The 2D model was the first to get away from the rectangular grid that had been traditional with 2D pile models, in this case using triangular elements with conventional FEA type grid generation.

- Serdaroglu (2010): The primary purpose of this study was not to model for pile performance but to estimate the ground vibrations that result during pile driving. However, an extensive comparison with conventional static capacity estimation methods was also undertaken, with emphasis on the effect of interface elements.

The history of 2D methods is thus one of incremental advances, assisted as with any numerical method by expansion of computer power. What has been lacking has been a comprehensive solution of the wave equation for piles in 2D to match that of 1D methods.

CHAPTER III

FORWARD AND INVERSE METHODS FOR DYNAMIC ANALYSIS

Prerequisites for a Solution

Driven piles are deep foundations that are installed at a high loading rate and used in service at a low loading rate. The latter are frequently characterized as “static loads” but loads with no time change at all are non-existent in civil engineering although “static” methods are used extensively in design. In addition, driven piles are frequently used with loads which are known beforehand to vary in time, such as dynamic loads due to vibrating machinery and seismic loads.

The validity of pile dynamics implies that, in the course of either predicting the performance of a hammer-pile-soil system or measuring the response of the pile-soil system to impact or vibratory excitation, the expected static (or low loading velocity) response of the pile can be extracted from or related to the dynamic data. To accomplish this requires three important prerequisites:

1. The consistency of the engineering properties of soil from static to dynamic conditions, especially those related to the stress-strain response of the soil. The most important aspect of this is that the pile's ultimate capacity and its SRD (soil resistance to driving) are the same, both as a load-deflection comparison and the comparison of an “ultimate” capacity. In practical application the largest discrepancy observed is due to set-up effects in the pile; this is generally dealt with by analyzing the blow in a “restrike” situation after set-up has taken place. However, changes in soil properties from static to dynamic loading (especially

with the modulus of elasticity) cannot be completely discounted. This will be discussed in more detail below.

2. A consistent definition of the static load capacity of the pile. One object of dynamic testing is to replace the necessity of static load testing, and frequently the results of the two have been compared so that the results of dynamic testing can be related to those of static testing. Generally speaking with CAPWAP Davisson's Method is used; however, if another method is common in a different region (and codes can dictate this kind of change) then the dynamic results must be interpreted differently.
3. A physically and mathematically meaningful method of extracting the static response of the pile from the dynamic response obtained during impact or vibration.

Overview and Application to Pile Dynamics

Since this study incorporates both forward and inverse methods for solution of the wave equation for piles, some clarification of what is meant by these terms is necessary.

The simplest way to explain the difference is by using an example. Consider a simple frame structure to which loads are applied. Whether this problem is solved by “classical” methods (energy methods, etc.) or a method such as finite element analysis, a model of the structure is built and the loads applied to determine the deflections and stresses (the latter via the moments and axial forces) of the structure. Such a method is a forward method; the structure is modeled and the loads are applied, and from this, the result is obtained.

Now consider the case of an existing structure where the actual loads on the structure need to be determined. Again the structure is modeled, but then the

results (stress, deflection, etc.) are applied and from that, the loads are determined. Such an analysis employs an inverse method: given the results, the structure is analyzed to obtain the input data. In reality, such an analysis is useful if, for example, the structure is showing distress and it is necessary to determine the magnitude, direction and nature of the loads that might be causing this distress.

Broadly speaking, forward methods are used in design, and inverse methods in verification. Neither of these methods has to be numerical, but for complex systems (and especially non-linear ones) numerical methods are the methods of choice.

Turning to pile dynamics, the wave equation is the forward method used to analyze the driving of piles. The hammer, pile and soil system is modeled and the analysis is performed. Even here, however, the inverse methodology begins to take shape. The “bearing graph” is a method by which a variety of pile resistance profiles is analyzed. The object of this is to relate the performance of the system to a variety of possible results, in this case pile resistances. The uncertainties of both the ground itself and the static capacity methods in use make a rapid transition to inverse analysis a necessity. It is also possible to perform manually determined successive runs of the forward wave equation analysis to obtain an inverse result, as is shown in Rausche, Nagy and Webster (2009).

Use of forward wave equation programs is an imprecise method of determining the SRD of the pile. In most cases signal-matching routines of one kind or another are used, given actual pile head data. While these have been very useful over the years, there have been two persistent issues in pile dynamics that need to be understood completely: the issue of consistency of results and the issue of uniqueness. The first was touched on in the previous section; it is a necessary

condition for pile dynamics to relate to actual strength and service performance. The second has been a long-term issue, especially with inverse methods.

The Uniqueness Problem

As is the case with virtually any engineering problem, pile dynamics involves obtaining a result from a given set of data that is put through a certain process. For a solution to be unique, the process must return a consistent result with a given set of data.

With a forward method, given information about the hammer/pile/soil system, the results (blow counts, stresses, force-time and velocity-time history, etc.) should be the same. With one-dimensional simulation, the simplicity of the models makes uniqueness more attainable, although same simplicity may mask problems other than uniqueness. With the two-dimensional models, for elastic-purely plastic models there is no uniqueness theorem with non-associated flow rules (Isenberg (1972)).

With the inverse methods, uniqueness has been an issue since Rausche et.al. (1972), and specifically the response by Screwvala (1973). In reality his objections are broader than the issue of uniqueness, and the uniqueness of CAPWAP results have been challenged elsewhere (Holeyman (1986); Danzinger et.al. (1996); McVay and Kuo (1999)).

Part of the problem is the non-linear nature of the problem itself. Non-linear solutions are path and stress history dependent; different stress histories will yield different results. In many cases an iterative solution is necessary for non-linear problems; the iteration process itself suggests that the method employed is seeking the most likely solution to the problem as opposed to the only one.

Inverse methods are by necessity iterative; some systematic method of testing a series of solutions is necessary to arrive at the best solution to the problem. How this is done varies, and the method chosen can significantly affect the results. Balthaus (1988), for example, recommends that a subjective method of solution search should be avoided. But this is not the only source of uniqueness difficulties with inverse methods and one-dimensional models; another comes from the basic visco-elastic rheology itself.

The easiest way to see this is to consider the pile head response for a uniform semi-infinite pile subject to a pile head force $F_o(t)$ and governed by Equation 8. The solution to this is (Warrington (1997))

$$u(0, t) = \frac{1}{Z} \int_0^t e^{-b\hat{\tau}} I_0 \left(\sqrt{(b^2 - a)(\hat{\tau}^2)} \right) F_o(t - \hat{\tau}) d\hat{\tau} \quad (9)$$

In this case Z is the pile impedance and I_o is a Bessel function (Bowman (1958)), which appear frequently in analytical solutions of this kind.

Our objective is to determine a and b . The pile head force $F_o(t)$ can be determined from the strain gauges. The pile head displacement can be determined either a) directly through a high-speed theodolite (SIMBAT) or b) through double integration of the accelerometer data (CAPWAP). Z is a property of the pile cross-sectional configuration and material properties.

Even in this relatively simple form, Equation 9 is difficult to solve analytically. For actual force-time curves, the simplest way is to use a root-finding method. Doing that, however, does not avoid the simple fact that there are two unknowns (a and b) and only one equation. It is thus impossible, using data from the pile head, to separate the static and dynamic components of the pile resistance.

To put this rather surprising result into perspective, Equation 8 can be written in a broader form, thus

$$c_a^2 \frac{\partial^2}{\partial x^2} u(x, t) = \frac{\partial^2}{\partial t^2} u(x, t) + a(x) u(x, t) + 2b(x) \frac{\partial}{\partial t} u(x, t) + d(x) \frac{\partial}{\partial x} u(x, t) \quad (10)$$

where two important changes are made. The first is that the functions of elasticity, viscosity, etc., along the shaft can vary with x . This is important because of the things traditionally sought in dynamic testing is the distribution of resistance along the pile shaft, which is in turn based upon the distribution of elasticity and viscosity. The second is that a strain term is added to the equation.

Given proper conditions, it is possible, using data from one boundary of a system governed by Equation 10, to determine the properties of the system. However, with inverse methods such as Gelfand and Levitan (1951), implementations of same such as Ning and Yamamoto (2008) or methods such as boundary control, either $a(x)=0$ or $b(x)=0$. The inclusion of both creates the situation in Equation 9. Rausche et.al. (1972) recognized this problem at the beginning of modern dynamic analysis.

This does not mean that all hope is lost. This problem can be solved if a relationship between $a(x)$ and $b(x)$ can be established, or to be more precise if they are functions of each other. Once this is established Equation 9 becomes one equation in one unknown. What this means is that the portion of the resistance during driving ascribed to the dynamic portion depends upon our assumptions regarding the rheology of the soil and not the inverse methodology at hand. If all other components of the inverse methodology are correct, then the key decision in the process comes with the assignment of soil properties before the reduction of data.

An example if this comes if the soil model of Randolph and Simons (1986) is considered,

$$k = \frac{2\pi G}{\ln\left(\frac{r_m}{r_o}\right)} \quad (11)$$

and

$$c_s = 2\pi r_o \sqrt{G\rho} \quad (12)$$

The variables k and c are the soil stiffness and dampening along the shaft. To transform them to the $a(x)$ and $b(x)$ respectively of Equation 10 requires inclusion of the pile geometry; this is discussed in detail in Warrington (1997). In any case $d(x)=0$.

Examination of Equations 10, 11 and 12 show, however, that the spring and dampening constants are related by the shear modulus G , which in turn is a function of the modulus of elasticity E and Poisson's Ratio. From a standpoint of input parameters, the only difference between the two, other than geometric considerations, is the soil density.

Usually, establishing linear dependence is not a positive development for numerical methods. In this case, however, it is helpful, as it can be shown that $a(x)$ and $b(x)$ are dependent upon each other, at least to some extent. Taking better advantage of this situation would solve one of the oldest problems in pile dynamics.

Having analyzed the effects of linear phenomena on uniqueness, the presence of non-linearity in both the elastic and viscous portions of the resistance must be considered. Equations 10 and 11 both have strong roots in the theory of elasticity; the introduction of non-linearity poses the threat of decoupling the two quantities, either entirely or (more likely) partially. Rausche, Goble and Likins (1985) state

that “...the uniqueness of the CAPWAP resistance distribution is proven under the assumption of an ideal plastic soil behavior.” Eliminating the elasticity of the system, however, makes the soil model inconsistent with those used in the forward methods such as are depicted in Figure 3 (Danzinger et.al. (1996)) and even CAPWAP itself as currently implemented (Rausche et.al. (2010)).

CHAPTER IV

DEVELOPMENT OF A STATIC/DYNAMIC FINITE ELEMENT CODE WITH MOHR-COULOMB PLASTICITY

Selection of a two-or three-dimensional method of analysis presented many challenges in code development.

Code Environment

The computer code for this study was written specifically for the application, and is referred to as STADYN (STAtic-DYNamic.) It was written in FORTRAN 77 using the OpenWATCOM compiler for Windows (which also works under Linux as well.) The program was also compiled and run using gfortran under Linux. Thus two compilers were used alternately, which allowed for a more comprehensive debugging. In general most of the solutions presented in this study were executed using OpenWATCOM because, when properly optimized, it tended to be more efficient and ran more quickly. With either it was possible to compile the program in single or double precision. Which one was necessary depended upon the type of problem being solved; eventually double precision was adopted as standard.

The main physical basis of STADYN came from Smith and Griffiths (1988), with some assistance from Owen and Hinton (1980). Other sources of code for routines of a more general mathematical nature included Carnahan, Luther and Wilkes (1969), Chapra and Canale (1985), King (1984) and Press et. al. (1992). All of these were modified to work as a unit and were, to varying degrees, adapted to the problem at hand.

Analytic Solutions for Static and Dynamic Pile Response to Loading

In development of any finite element code, it is very helpful to have analytic solutions available for simple load and configuration cases. Due to the non-linear nature of the problem, the applicability of analytic solutions is limited; nevertheless, there are two that are employed for comparison purposes to this problem.

Closed Form Solution of the Wave Equation for Piles: Warrington (1997)

Early projects such as Isaacs (1931) and Glanville et.al. (1938) used what amounted to closed form solutions of the wave equation for piles. The limitations of these became quickly evident; however, for the purposes of developing the dynamic code, such a solution is a necessity. The closed form solution of Warrington (1997) gives numerical solutions for simple, linear problems. Using semi-infinite pile theory, it also generates an analytical solution for the hammer impact on the pile (see also Deeks (1992)). For this study a fixed pile toe case was considered, and the “test case” pile/hammer configuration was the same as in the previous study.

Linear Solution for Pile Settlement: Randolph and Wroth (1978)

Analytical solutions for the capacity or settlement of deep foundations into a semi-infinite soil mass are, if anything, more difficult than a closed form solution of the wave equation. For non-plastic analysis probably the best one is that of Randolph and Wroth (1978), which uses Mindlin plate analysis and axisymmetric piles and soil mass. It was possible to use this as a “lower bound” check of pile head load vs. deflection behavior. The implementation of this method in STADYN was based on Randolph (1983).

The method defines a few constants as follows:

$$\lambda_r = \frac{E_p}{G_{toe}} \left(1 - \frac{r_i^2}{r_o^2} \right) \quad (13)$$

$$\xi_r = \ln \left(\frac{5\rho_r (1 - \nu) L}{3r_o} \right) \quad (14)$$

$$\mu_r = \frac{\sqrt{\frac{2}{\xi_r \lambda_r}}}{r_o} \quad (15)$$

$$\rho_r = \frac{G_{mid}}{G_{toe}} \quad (16)$$

$$\eta_r = \frac{\frac{4}{1-\nu} + \frac{2\pi}{\xi_r} \rho_r \frac{\tanh(\mu_r L)}{\mu_r L} \frac{L}{r_o}}{1 + \frac{4}{\pi \lambda_r (1-\nu)} \frac{\tanh(\mu_r L)}{\mu_r L} \frac{L}{r_o}} \quad (17)$$

The pile head displacement can then be computed as follows:

$$d_{head} = \frac{F_0}{G_{toe} r_o \eta_r} \quad (18)$$

Obviously this method assumes a uniform pile cross-sectional area and outside diameter, which limited it to piles of this type. However, for model verification purposes the information from this method can be very useful.

Rationale for a Plasticity Model

As discussed earlier, soils are complex materials in their formation and structure. They are the result of an extended formation period not under the kinds of controlled conditions that characterize most engineering materials. They are also composed of soil particles, water and (when not saturated) air in varying proportions and material arrangements. Consequently modeling these for the

purpose of simulation presents challenges that are not present with many other materials. Compounding the problem further is that soils exist in what is considered a semi-infinite medium, where the response of the soil to both its own weight and external forces take place three-dimensionally.

The complexity of soil rheology has been recognized for many years, and many models of soil behavior have been proposed, analyzed and tested in both laboratory and field conditions (Šuklje (1969)). However, for analytical solutions, implementing these models on a consistent basis has been difficult because of the lack of a suitable framework for analysis. In practice this has led to a schizoid situation where soils are considered to be elastic for some analyses (Boussinesq stresses, Perloff's Method for shallow foundations), non-linear for others (Terzaghi bearing capacity, slope stability) and a separate theory for still other applications (consolidation).

Adoption of the finite-element method enabled all of these states to be considered in one model, which is probably the most important advantage of finite elements in geotechnical engineering.

Elastic and Plastic Response

Part of the complexity of modeling soil response was that their stress-strain properties are, with few exceptions, non-linear, as illustrated in Figure 7.

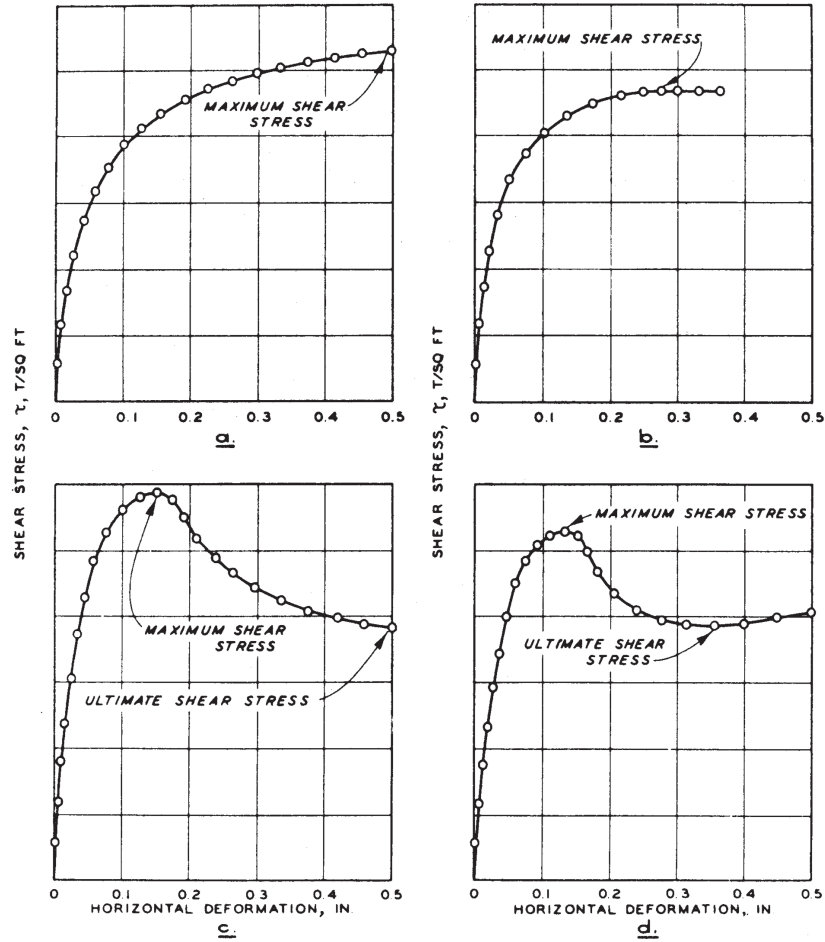


Figure 7 Typical Shear Stress-Strain Responses of Soil (from Department of the Army (1986))

One widely used approach to this problem is to model the soil response hyperbolically, as described in Duncan and Chang (1970). A typical stress-strain relationship of such a model is shown in Figure 8.

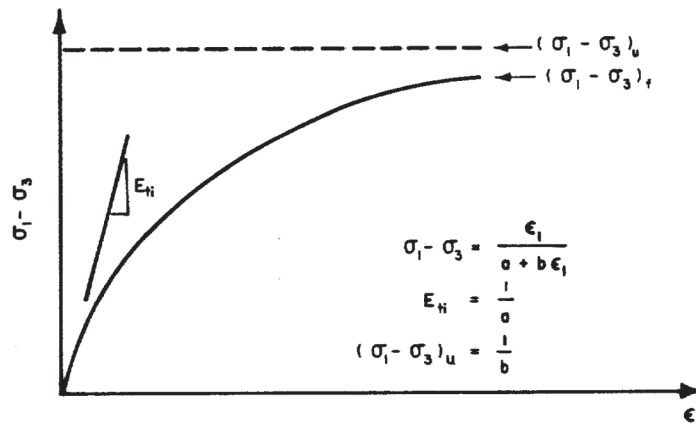


Figure 8 Hyperbolic Soil Model (from Department of the Army (1990))

The problem with implementing such a model is that, to a large degree, all stresses are plastic and have an irrecoverable component that must be modeled properly. This adds to the complexity of the model.

Another model encompasses an elasto-plastic relationship, as shown in Figure 9. The soil is assumed to behave elastically (i.e., in a linear, path-independent fashion) until it reaches the yield stress and strain. From here the stress (and that is broadly defined, with a two-dimensional model it has more than one component) remains constant (purely elasto-plastic,) increases (hardening) or decreases (softening.) Comparison with Figure 7 shows that this is a simplification. Nevertheless it is one that has been used successfully with soils (and other materials) for many years. Its implementation is relatively straightforward, in large measure because there is a definite yield surface beyond which plasticity must be modeled.

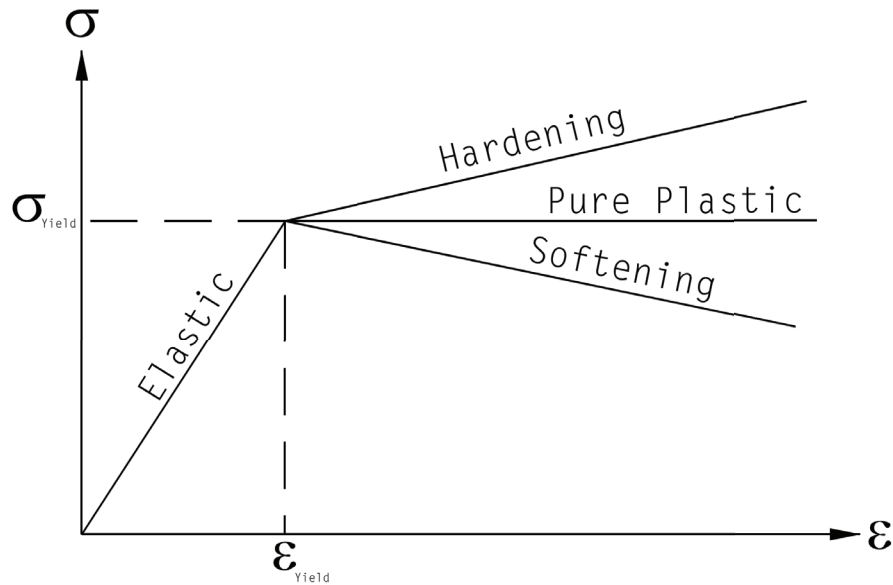


Figure 9 Elasto-Plastic Soil Response

Comparing Figure 9 with Figure 3, it is easy to see that much of the soil modeling used in pile dynamics, statically at least, is a pure elasto-plastic soil model. This includes not only the model of Smith (1960) but the more advanced ones such as Randolph and Simons (1986) and Corté and Lepert (1986) which are developed from axisymmetric models. On the other hand, Nath (1990) uses a hardening model to simulate the response of a hyperbolic model without the non-linear complexities that come with that model.

The choice remaining was thus whether a pure elasto-plastic model, a hardening model, or a softening one would be adopted. The softening model was not considered because there is no theoretical or experimental data to support it in this application. Turning to a hardening model, while it can be used to simulate hyperbolic response, there is likewise little data to determine the degree of hardening that would be appropriate for pile dynamics. Also, the hardening model

can be non-conservative, especially at the toe, and may conceal plunging failure when it occurs.

Based on this and past practice in pile dynamics, in this study a purely elasto-plastic model was adopted, which means that, once the failure criterion was reached, unless the soil reverts to the elastic region with unloading, the stresses remained on the failure surface at a failure stress state. This was done for all static modeling, along with forward and inverse dynamic modeling.

Failure Theory

Having decided on a non-hardening model as shown in Figure 9, it was necessary to consider a failure theory, and thus determine the yield point of the material. Potts and Zdravkovic (1999) divide the failure theories possible for geotechnical finite element codes into two types:

1. Simple models such as Tresca, von Mises, Mohr-Coulomb, Drucker-Prager and Cam Clay.
2. Advanced models such as limited tension, Lade's Double Hardening, the MIT models and Bubble Models such as that of al-Tabbaa and Wood.

Since the application of these to dynamic methods is not common in practice, it made sense to use methods that do not require the evaluation of additional variables not commonly seen on soil boring logs. Based on this and the elasto-plastic discussion, the Mohr-Coulomb failure model was chosen. As Abbo et.al. (2011) point out: "The Mohr-Coulomb yield criterion provides a relatively simple model for simulating the plastic behavior of soil. Other more sophisticated constitutive models for predicting the behavior of soil have been developed over the past three decades, however the complexity of these models, as well as the additional testing required to determine the various soil parameters involved, minimizes their utility

for practicing geotechnical engineers. The Mohr–Coulomb yield function is also of importance to finite element researchers and practitioners as it forms the basis of many analytical solutions. These analytical solutions serve as crucial benchmarks for validating numerical algorithms and software.” This observation is supported by McCarron (2013).

The Mohr-Coulomb model also can be applied to a variety of soils. This is important as piles are driven into a wide range of soil types, cohesive and cohesionless alike.

In adopting this model, however, a few things need to be kept in mind:

1. Except for purely cohesive soils, a purely associated flow rule is to be avoided for soil materials in the model. Such a rule is acceptable for many engineering materials but does not realistically model the dilation of soils, especially cohesionless ones. The downside to this is that the elasto-plastic constitutive matrix is non-symmetric, which, strictly speaking, will result in a non-symmetric stiffness matrix, increasing the cost of the problem solution. These are issues that will be dealt with in the course of the analysis.
2. Effective stress must be modeled, as the overburden acting on the frictional resistance of the soil is the principal source of soil strength for purely cohesionless soils.
3. Matching the actual soil behavior with that predicted by the finite element code, even with a highly developed soil model, can be very problematic, as Reid et.al. (2004) and Townsend et. al. (2001) demonstrated.

Other Issues

One important issue with traditional wave-equation methods with piling is the nature and implementation of damping along both the shaft and the toe of the pile. Several different variations of damping modeling have been used, and, as is seen in Mukherjee and Nagarajub (2013), a wide variety of damping coefficients have been employed. However, most of the dampening around piles during driving is energy radiation into the semi-infinite soil mass. As a result the distributed mass in the model will serve as the modeling of the dampening in conjunction with the distributed elasticity/plasticity of the soil. Since the object of this study is not to model vibrations induced by pile driving the addition of velocity-dependent dampening to the model would primarily introduce complications into the simulation without necessarily adding to the accuracy of the model.

Another thing that should be noted here is that many issues with finite element codes in other geotechnical applications are absent here. These include excavation considerations, unlevel soil surfaces, and effects due to remolding of the soil. The absence of these allowed some simplification of STADYN.

Mohr-Coulomb Failure Theory

The following is a brief summary of the application of this theory to the problem at hand. It is not meant to be a comprehensive treatment of the subject. Much of it is drawn from Nayak and Zienkiewicz (1972) and Owen and Hinton (1980).

According to this theory, failure occurs when the combined stresses find themselves outside of the failure envelope defined by the equation

$$\tau = c + \sigma \sin\phi \quad (19)$$

This is illustrated in Figure 10.

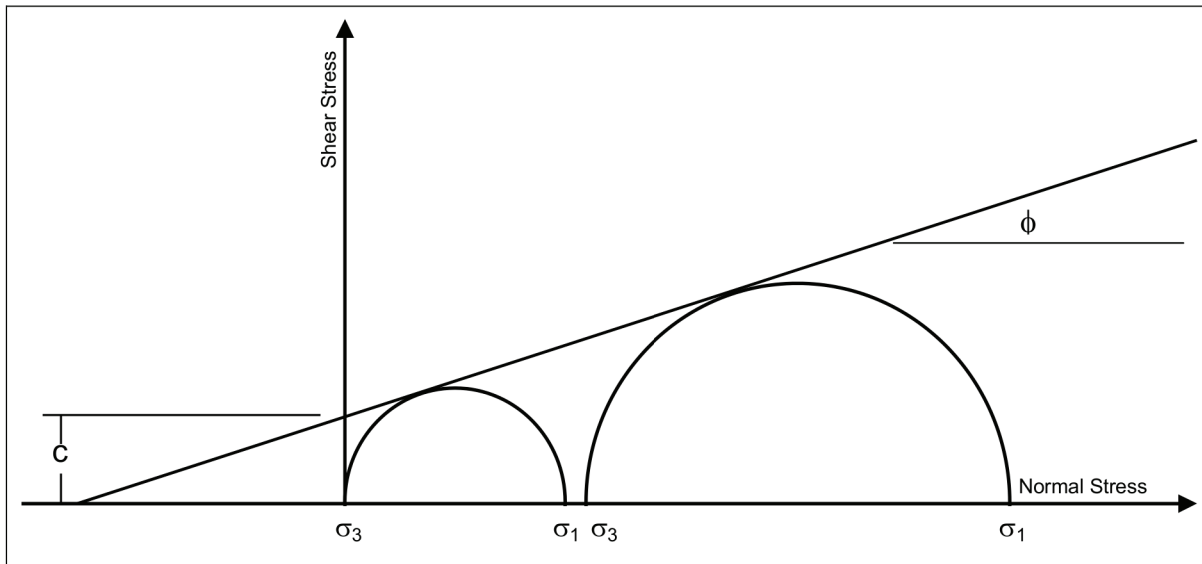


Figure 10 Mohr-Coulomb Failure Theory (after Reid et.al. (2004))

It should be noted that both Equation 19 and Figure 10 are based on the typical geotechnical sign convention of positive compression. For this study, STADYN was written so that the compression is negative, in which case Equation 19 becomes

$$\tau = c - \sigma \sin \phi \quad (20)$$

and the graph is the mirror image of Figure 10 about the shear stress (τ) axis.

Failure takes place when Mohr's Circle for the stress state either intersects or goes above the failure line. The state of intersection, in terms of the principal stresses, is expressed by Verruijt and van Bars (2007) as

$$\sigma_1 - \sigma_3 - 2c \cos(\phi) + \sin(\phi) (\sigma_1 + \sigma_3) = 0 \quad (21)$$

For many applications, such as triaxial testing, this is sufficient, as the goal is to determine parameters c and ϕ from the tests. But what if it is necessary to analyze stress states other than those on the failure line, as is certainly the case with finite elements? For these cases the failure criterion can be defined as

$$\sigma_1 - \sigma_3 - 2c \cos(\phi) + \sin(\phi) (\sigma_1 + \sigma_3) = F \quad (22)$$

This is illustrated in Figure 11.

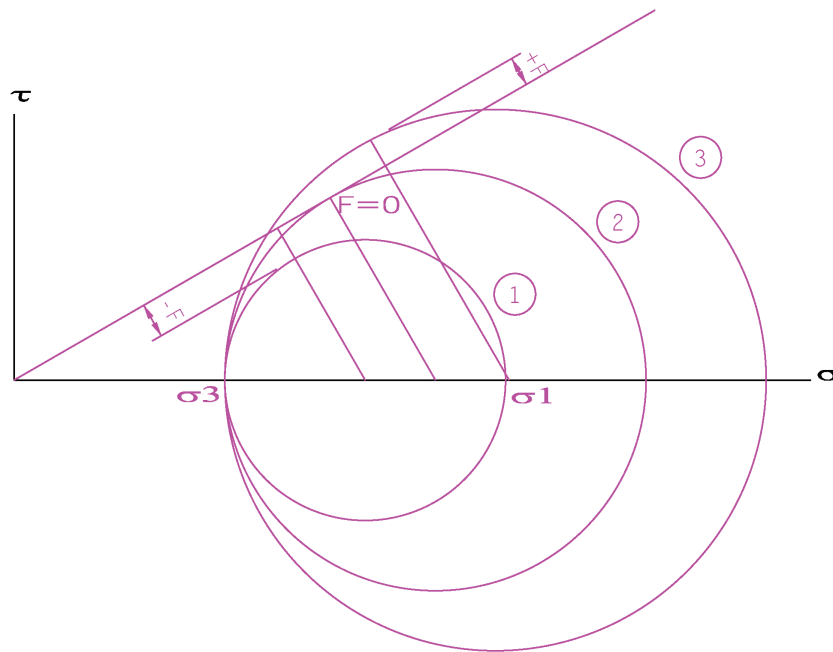


Figure 11 Mohr-Coulomb Failure Criterion

There are three possibilities for the right hand side:

1. $F < 0$, failure has not been achieved.

2. $F=0$, failure has been achieved.
3. $F>0$, the stress state is beyond failure.

How the model responds to each of these states depends upon how the response is modeled. In any case, once $F=0$, the effects of further stress are irrecoverable.

For use in finite element code, it is frequently more convenient to express these using invariants. For the case of plane strain/axisymmetry in this problem (and the general case for problems of this kind) it is assumed that

$$\tau_{yz} = \tau_{xz} = 0 \quad (23)$$

and the first invariant is

$$J_1 = \sigma_x + \sigma_y + \sigma_z \quad (24)$$

The deviator stresses are defined as

$$\begin{aligned} \sigma'_x &= \sigma_x - \frac{J_1}{3} \\ \sigma'_y &= \sigma_y - \frac{J_1}{3} \\ \sigma'_z &= \sigma_z - \frac{J_1}{3} \end{aligned} \quad (25)$$

The second and third deviatoric invariants are

$$\begin{aligned} J'_2 &= \frac{\sigma'^2_x + \sigma'^2_y + \sigma'^2_z}{2} + \tau_{xy}^2 \\ J'_3 &= \sigma'_z (\sigma'^2_z - J'_2) \end{aligned} \quad (26)$$

With all of this, Equation 22 can be restated thus:

$$\sqrt{J'_2} \left(\cos\theta - \frac{\sin\theta \sin\phi}{\sqrt{3}} \right) - c \cos(\phi) + \frac{J_1}{3} \sin(\phi) = F \quad (27)$$

where

$$\theta = -\frac{1}{3} \arcsin \left(\frac{3\sqrt{3}}{2} \frac{J'_3}{J_2'^{\frac{3}{2}}} \right) \quad (28)$$

The Mohr-Coulomb failure criterion is frequently depicted using a three-dimensional representation on the principal stress axes as is shown (along with the Drucker-Prager criterion) in Figure 12. On the left is the failure surface in true three-dimensional representation, and on the right is same in the octahedral plane. The significance of Lode's Angle can also be clearly seen.

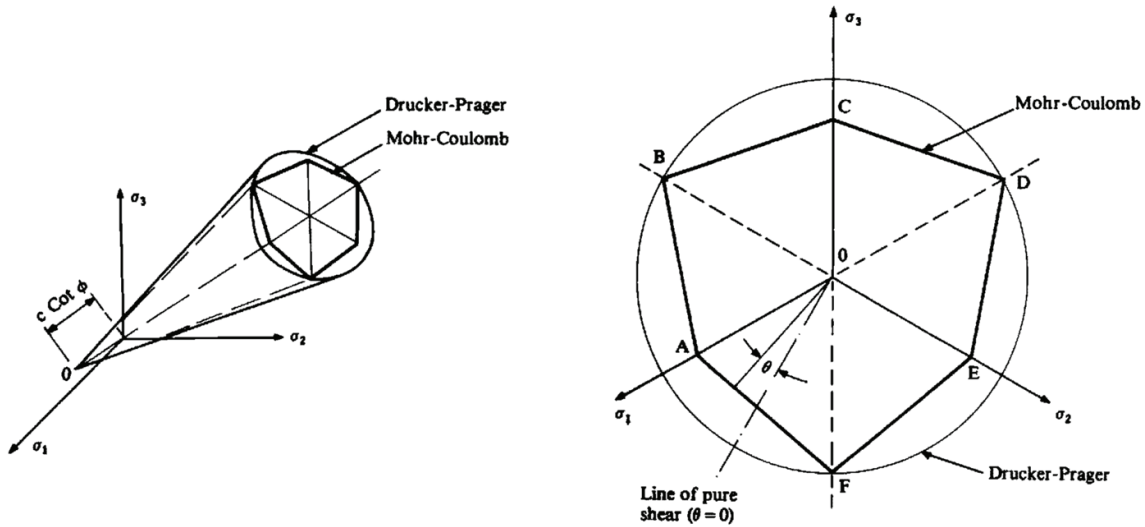


Figure 12 Mohr-Coulomb Failure in Three Dimensions (after Owen and Hinton (1980))

Inspection of Equation 27 shows that the failure function F is not the result of a unique combination of stresses. Additional information is available in the plastic potential function, which in turn is a function of the dilatancy of the material.

The simplest way of determining this is by substituting the dilatancy angle ψ for the friction angle φ in Equation 27 (Griffiths and Willson (1986)), or

$$\sqrt{J_2'} \left(\cos\theta - \frac{\sin\theta\sin\psi}{\sqrt{3}} \right) - c \cos(\psi) + \frac{J_1}{3} \sin(\psi) = Q \quad (29)$$

Elasto-Plasticity

With the Mohr-Coulomb failure criterion defined, the elasto-plastic constitutive matrix can be developed. As stated earlier, pure plasticity is assumed, i.e., once failure is reached $F = 0$ and the stresses can “rearrange” themselves to remain at the failure surface but cannot move from it unless the strains are reduced to the point where the stress state is within the failure surface and $F \leq 0$.

To do this, both Equations 27 and 29 are differentiated. Considering that

$$\sigma = \begin{bmatrix} \sigma_x \\ \sigma_y \\ \tau_{xy} \\ \sigma_z \end{bmatrix} \quad (30)$$

for the two-dimensional model, then

$$\frac{\partial F}{\partial \sigma} = a_F = C_1 a_1 + C_2 a_2 + C_3 a_3 \quad (31)$$

where

$$\begin{aligned}
C_1 &= \frac{\sin\phi}{3} \\
C_2 &= \cos\theta \left[(1 + \tan\theta \tan 3\theta) + \frac{\sin\phi (\tan 3\theta - \tan\theta)}{\sqrt{3}} \right] \\
C_3 &= \frac{\sqrt{3}\sin\theta + \cos\theta \sin\phi}{2J'_2 \cos 3\theta}
\end{aligned} \tag{32}$$

and

$$\begin{aligned}
a_1 &= \begin{bmatrix} 1 \\ 1 \\ 0 \\ 1 \end{bmatrix} \\
a_2 &= \frac{1}{2\sqrt{J'_2}} \begin{bmatrix} \sigma'_x \\ \sigma'_y \\ 2\tau_{xy} \\ \sigma'_z \end{bmatrix} \\
a_3 &= \begin{bmatrix} \sigma'_y \sigma'_z + \frac{J'_2}{3} \\ \sigma'_x \sigma'_z + \frac{J'_2}{3} \\ -2\sigma'_z \tau_{xy} \\ \sigma'_y \sigma'_x - \tau_{xy}^2 + \frac{J'_2}{3} \end{bmatrix}
\end{aligned} \tag{33}$$

Inspection of Equation 32 will show that C_2 and C_3 are undefined for values of $\theta = 30^\circ$. This is the well-known “corner” problem that has occupied the literature for many years, as summarized by Abbo et.al. (2011). For this study the “corner cutting” of Owen and Hinton (1980) is used, and

$$\begin{aligned}
C_1 &= \frac{\sin\phi}{3} \\
C_2 &= \frac{1}{2} \left[\sqrt{3} - \frac{\sin\phi}{\sqrt{3}} \right], \theta \approx \pm 30^\circ \\
C_3 &= 0
\end{aligned} \tag{34}$$

Although the accuracy of this “corner cutting” can be improved with methods such as those of Abbo et.al. (2011), they come at more computational expense.

In like fashion for the plastic potential function,

$$\frac{\partial Q}{\partial \sigma} = a_Q = C_4 a_1 + C_5 a_2 + C_6 a_3 \tag{35}$$

where

$$\begin{aligned}
C_4 &= \frac{\sin\psi}{3} \\
C_5 &= \cos\theta \left[(1 + \tan\theta \tan 3\theta) + \frac{\sin\psi (\tan 3\theta - \tan\theta)}{\sqrt{3}} \right] \\
C_6 &= \frac{\sqrt{3} \sin\theta + \cos\theta \sin\psi}{2J_2 \cos 3\theta}
\end{aligned} \tag{36}$$

and by extension

$$\begin{aligned}
C_4 &= \frac{\sin\psi}{3} \\
C_5 &= \frac{1}{2} \left[\sqrt{3} - \frac{\sin\psi}{\sqrt{3}} \right], \theta \approx \pm 30^\circ \\
C_6 &= 0
\end{aligned} \tag{37}$$

and the vectors a_1, a_2, a_3 are the same as with Equation 31.

Now the elasto-plastic constitutive matrix can be considered. For any strain increment partially or totally beyond the yield surface, that strain increment will contain both elastic and plastic portions (Griffiths and Willson (1986)), or

$$d\epsilon = d\epsilon^e + d\epsilon^p \quad (38)$$

Strain increments occur normal to the plastic potential surface, thus

$$d\epsilon^p = \lambda a_Q \quad (39)$$

For elastic materials, the incremental stress-strain relationship is simply

$$d\sigma = D^e d\epsilon^e \quad (40)$$

where, for plane strain and axisymmetric problems (Owen and Hinton (1980)),

$$D^e = \frac{E(1-\nu)}{(1+\nu)(1-2\nu)} \begin{bmatrix} 1 & \frac{\nu}{1-\nu} & 0 & \frac{\nu}{1-\nu} \\ \frac{\nu}{1-\nu} & 1 & 0 & \frac{\nu}{1-\nu} \\ 0 & 0 & \frac{1-2\nu}{2(1-\nu)} & 0 \\ \frac{\nu}{1-\nu} & \frac{\nu}{1-\nu} & 0 & 1 \end{bmatrix} \quad (41)$$

and, for axisymmetric problems only,

$$\epsilon^e = \begin{bmatrix} \epsilon_r \\ \epsilon_z \\ \epsilon_{rz} \\ \epsilon_\theta \end{bmatrix} \quad (42)$$

For a perfectly elasto-plastic material, i.e., one without hardening or softening, stress changes will take place only during elastic action. Thus in these cases Equations 38, 39 and 40 can be rearranged to yield

$$d\sigma = D^e (d\epsilon - \lambda a_Q) \quad (43)$$

Since stresses on the failure surface can “rearrange” themselves without leaving same surface,

$$a_F^t d\sigma = 0 \quad (44)$$

Combining and rearranging Equations 38 through 44 yields the following relationships:

$$\lambda = \frac{a_F^t D^e d\epsilon}{a_F^t D^e a_Q} \quad (45)$$

$$d\sigma = \left(D^e - \frac{D^e a_Q a_F^t D^e}{a_F^t D^e a_Q} \right) d\epsilon \quad (46)$$

or

$$d\sigma = (D^e - D^p) d\epsilon \quad (47)$$

where

$$D^p = \frac{D^e a_Q a_F^t D^e}{a_F^t D^e a_Q} \quad (48)$$

and finally

$$D^{ep} = D^e - D^p \quad (49)$$

from which

$$d\sigma = D^{ep} d\epsilon = (D^e - D^p) d\epsilon \quad (50)$$

The first thing to note about Equation 49 is that, if same is used to reconstruct a tangent stiffness matrix K_T in a true Newton stepping scheme, K_T will not be symmetric if φ is not equal to ψ . For many engineering materials, and especially those where both of these quantities are zero, this is not an issue; the flow rule is associated, D_{ep} is symmetric and K_T will be also. “Regular” engineering

materials are used for the hammer and pile components of the system, but interest in plastic deformation of these components is of limited interest to most geotechnical engineers. It is also not an issue with purely cohesive soils. For situations with cohesionless soils, this is not the case; generally φ is much greater than ψ and a non-associated flow rule is necessary. This aspect will be important in many decisions regarding the structure and types of schemes used in the model.

Turning to the inclusion of plasticity itself, it is certainly possible to compute the plastic stresses from Equation 49, and possible to explicitly derive Equation 48 (Griffiths and Willson (1986)). However, it is not always optimal to do so, either from the standpoint of a workable algorithm or from a computational efficiency standpoint. To compute the final stress state in a load or time step where failure takes place, some type of iteration or multiple steps are required. Potts and Zdravkovic (1999) state that there are two basic types of algorithms to accomplish this: substepping (such as Sloan (1987)) and return (Ortiz and Simo (1986)). For this study a return algorithm was chosen, and implemented as follows:

1. For a load or time step, the estimated incremental strain was computed.
2. The estimated incremental stress was computed, based on the assumption that the strains were still in the elastic region.
3. The resulting incremental stresses were added to the stresses at the beginning of the step. If these were elastic, then plasticity was not considered and the incremental stresses were added to the original ones. If they were not, then the plasticity routine was invoked.
4. The plasticity routine began by computing a_F , a_Q , F , θ and a_β , the last given by the equation

$$a_\beta = \frac{1}{a_F^t D^e a_Q} \quad (51)$$

5. The plasticity constant λ was determined by a modification to Equation 45, namely

$$\lambda = F a_\beta \quad (52)$$

6. The incremental strains in the return step were computed by the equation (see Equation 43)

$$d\epsilon_r = \lambda a_Q \quad (53)$$

7. The return incremental stresses were thus

$$d\sigma_r = D^e d\epsilon_r \quad (54)$$

8. Both of these were subtracted from the current estimated strain and stress, thus

$$\begin{aligned} d\epsilon_{ep}^{n+1} &= d\epsilon_{ep}^n - d\epsilon_r \\ d\sigma_{ep}^{n+1} &= d\sigma_{ep}^n - d\sigma_r \end{aligned} \quad (55)$$

9. The current stress state was checked against the previous stress state. If the norm of the vector difference of the two stress states was within the convergence tolerance, the iteration was stopped and the computed elasto-plastic stresses and strains were accepted. If not, the cycle was repeated.

Potts and Zdravkovic (1999) criticize the return algorithms because they obtain a result based on information and computations in illegal stress space. However, overall the experience in this study is that the return algorithm worked well, with most of the convergence to the new failure surface stress state taking place in the first iteration and the rest refinement steps. A fair way of differentiating between the two is that, with substepping, one starts with the

existing stress state and works one's way to the failure surface, while the return algorithm starts by overshooting the failure surface and then coming back to it. The goal in both cases is to return to the failure surface, and in principle the result should be the same. Another way of differentiating between the two is that substepping is, with its avoidance of illegal stresses, more of an engineering type of approach to the problem, while the return algorithm is a more strictly mathematical method of arriving at a solution.

One factor that differentiated the cases examined by Potts and Zdravkovic (1999) from this study was that their examples used Cam Clay soil modeling. Returning to the relative simplicity of Mohr-Coulomb without hardening or softening made the location of the failure surface considerably simpler.

Finite Element Implementation

Finite element analysis of geotechnical engineering problems is well established in theory and in practice. The most common method to implement finite elements for solid mechanics is the Bubnov-Galerkin method, which uses a weak formulation of the governing equation for each element. This is the method employed for this study; Hughes (2000) discusses the theory behind this in detail, along with the element implementation for the elements described below.

For each element two local matrices are developed. The first is the Jacobian, or stiffness matrix, which models the distributed elasticity and plasticity of the system. For two dimensional, quadrilateral elements, the stiffness matrix for each element is developed using the equation

$$k_{loc} = \int \int_A B^t D B dy dx \quad (56)$$

The constitutive matrix D , both elastic and plastic, has been discussed in detail. For the purposes of this study geometric nonlinearity was not considered, and so the B matrices were solely dependent upon the original geometry of the element.

For dynamic problems, there is also the mass matrix as well, developed using the equation

$$m_{loc} = \rho \int_A \int N^t N dy dx \quad (57)$$

Except for the interface elements, all of the integration to form the local mass and stiffness matrices is done using Gauss quadrature. Once these are developed, they are added to assemble the global stiffness and mass matrices, using a global steering vector which links the local nodal system to the global one.

Element Type

It is interesting to note that, for all of the variety of elements available in two dimensions, eight-node serendipity quadrilaterals have predominated from To (1985) to Serdaroglu (2010). Many reasons for this have been given, from suitability in modeling collapse loads (Smith and Griffiths (1988)) to common use in commercial codes.

For this study, it was considered best to adopt a true Lagrangian element with full quadrature to match that of the element. To decrease the computational cost, reduced integration is commonly used in codes such as LS-DYNA, but it also leads to the “hourglassing” problem (Cook, Malkus and Plesha (1989)), which was a major issue with Reid et.al. (2004). Selecting a Lagrangian element was a more

involved process than originally anticipated, and three element types were tried before a “final” one was selected.

The first element considered was a six-node triangular element with three Gauss points for full integration. This element proved satisfactory in the early stages of development. With a generally orthogonal grid, the rectangles were simply divided into two right triangles and the resulting grid generation was relatively straightforward. The elements performed reasonably for both the static and implicit elastic dynamic (pile only) runs, in spite of their high aspect ratio in the pile. The problem came in when the explicit dynamic runs were developed. The main weakness of six-node triangles from a dynamic standpoint is their mass lumping. The most common type of mass lumping produces zero masses at the vertices (Fried and Malkus (1975)), and other mass lumping schemes produced unsatisfactory results.

Faced with this problem, it was a straightforward matter to convert the model to the nine-node quadrilateral; the nodes were the same, two right triangles became one quadrilateral, and the number of Gauss points for full integration increases to nine per element. For this element the weighting functions are shown in Figure 13.

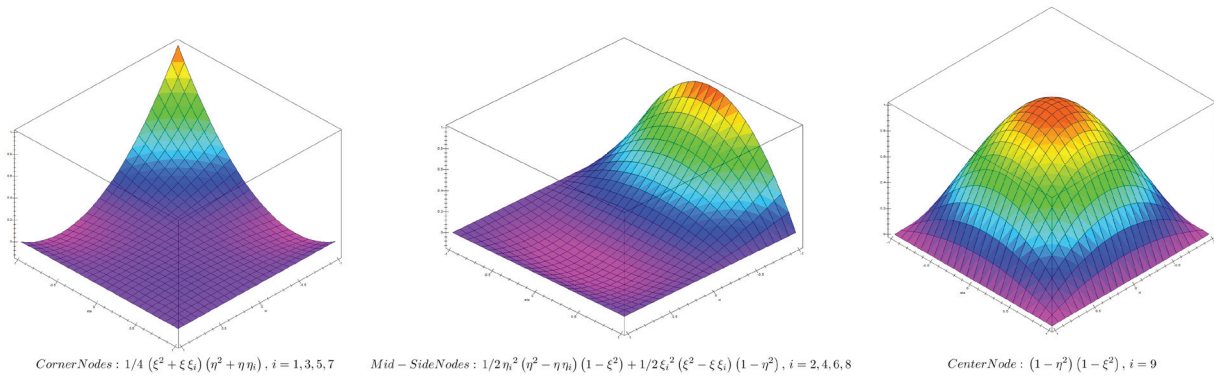


Figure 13 Weighting Functions for Nine-Node Quadrilaterals

Probably the greatest advantage of using this element is that it mass lumps consistently, independent of method, as shown in Zienkiewicz and Taylor (2000a). When mass lumping is required, the global consistent mass matrix is formed and then multiplied by the unit vector to yield a lumped “vector” which, when the values are placed on the diagonal, becomes a lumped mass matrix that is readily inverted.

With the static analysis the nine-node quadrilateral was very successful, as was the case with the elastic dynamic pile-only runs. When plasticity was included, the results became unsatisfactory. As Cook, Malkus and Plesha (1989) note, “(i)n wave propagation problems, discontinuities of strain propagate throughout the model. Lower-order displacement elements are more adept at modeling these discontinuities than are higher-order elements, which tend to produce more numerical noise.” This certainly was the experience with the model developed. Higher order elements also tend to propagate these errors more rapidly to the boundary, which in turn makes that formulation more critical to the success of the model.

This suggested the four-node quadrilateral with four quadrature points. Isenberg (1972) also used these elements. The weighting function is shown in Figure 14.

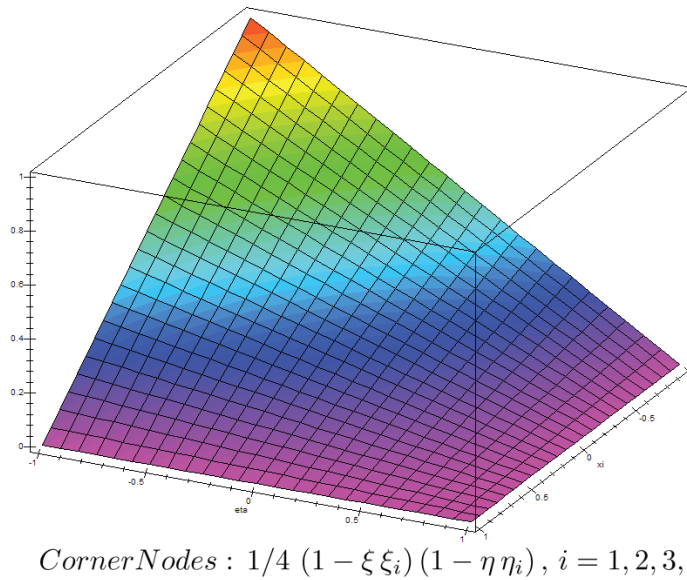


Figure 14 Weighting Function for Four-Node Quadrilaterals

A comparison of the locations and number of Gauss integration points—along with the natural coordinates used—is shown in Figure 15.

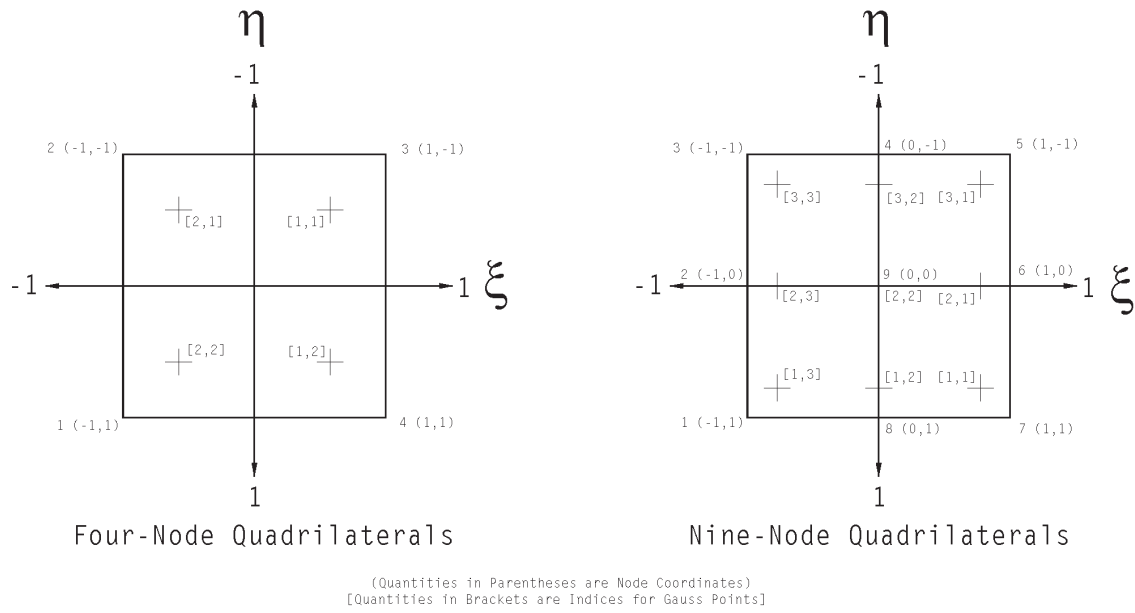


Figure 15 Natural Coordinates and Quadrature Points for Four-and Nine-Node Quadrilaterals

The four-node quadrilateral is also a Lagrangian element, and mass lumping was done the same way as it was for the nine-node quadrilaterals.

For cases without interfaces, the problem of spurious numerical results was significantly reduced with a four-node quadrilateral element. Using this element combines the advantage of a simpler element (lower bandwidth, fewer nodes, fewer quadrature points, etc.) while at the same time allowing for full integration. The only drawback to the element is that it is slightly stiffer, but this can be compensated for by using more elements.

Grid Generation

Compared with many finite element applications, grid generation was relatively straightforward, as the geometry was regular. However, because of the variations in material and configuration, there were a few challenges to be overcome.

In order to generate the rectangular grid convenient to the use of quadrilaterals, a region system was devised. Each region was defined by its geometry, the number of rows and columns of elements, the other regions it interfaced with, its material(s), the part of the system it is in (hammer, pile or soil) and other important parameters. To generate the grid within a region, the nodes and elements were defined using a natural coordinate system; then, a linear transformation was applied to map the natural coordinates into the physical region. A major advantage of this is that the regions, although quadrilateral, do not have to be orthogonal; this proves very useful when piles of non-uniform diameter (tapered piles) are modeled.

The “obvious” way to divide the regions is with regular rows and columns of nodes and elements. However, from Smith and Chow (1982) onward, the normal practice with rectangular grids has been to more closely space them as they approach the pile surface, both along the shaft and at the pile toe. To accomplish this the model allowed the grid to be “squeezed” in the following way:

1. The grid was defined with zero at one side of the region and unity at the other. This was done in both directions.
2. This “natural” coordinate system was then taken to a specific power in the direction the elements were to be squeezed. The program allowed elements to be squeezed at the left and top sides of the regions.

3. The squeezed coordinates were then mapped to the actual geometry of the region. The squeezing was also transferred to the adjacent elements to maintain a regular grid system.

Two examples of this are shown in Figure 16, concentrating on the region around the pile toe. On the left is a second order power squeeze to both the pile shaft and toe; on the right is a third order power squeeze to the shaft and toe. The pile is in red on the left (center axis) side of the grid.

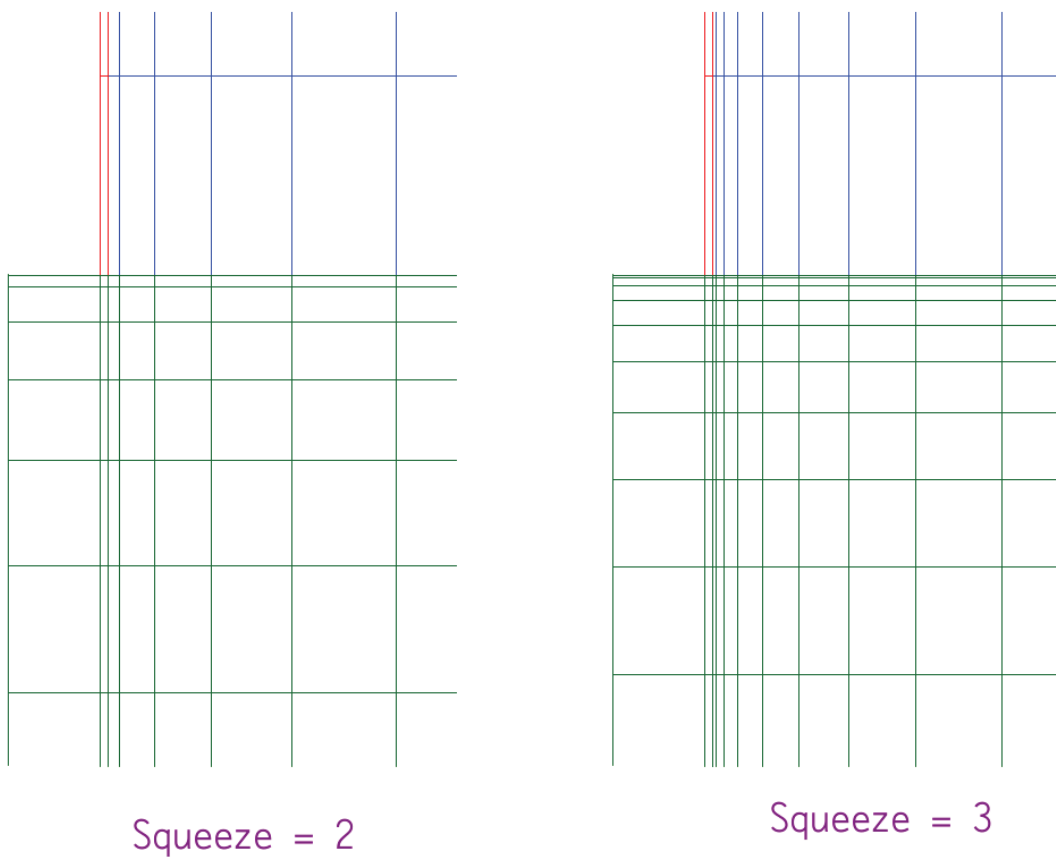


Figure 16 Grid Generation for Finite Element Model

Using the geometry of the nodes and elements, STADYN generated an IGES file, which colored the element boundaries according to the portion of the system and the soil layer for the element. The IGES file was then imported into the DesignCad program and the drawing was output in Adobe Acrobat, which made it possible to manipulate it graphically. Although this mating of finite element analysis with computer aided drawing was primitive, it was effective in that any irregularities in the geometry could be seen and dimensionally checked.

Once the grid was generated, a reordering of the degrees of freedom was performed, using a routine based on Cuthill and McKee (1969). This resulted in more than halving the required matrix size, even with the skyline Cholesky arrangement of the stiffness matrix. Because of this it is employed for both routines that require the use of a stiffness matrix (static, implicit dynamic) and those which do not (explicit dynamic.)

Boundary Conditions and Model Size

The need to model a “semi-infinite” soil mass is a necessity with many geotechnical problems. One approach has been to use special boundary conditions that absorb the waves emanating from the central pile, as was used in To (1985) and Mabsout and Tassoulas (1994). This allows for a reduced model size, since the reflections of the waves are undesirable.

Another approach (Nath (1990)) is to construct a model large enough so that the effects of pile loading, static or dynamic, do not reach the boundaries, or interact with them in a meaningful way. Such a model must be by necessity large. However, the continuous growth of available computer power makes a larger model more viable and simplifies the construction of the global stiffness matrix. The situation is ameliorated by the fact that, as the plasticity is concentrated around the pile, most

of the model remains elastic, and thus the time to analyze it is significantly reduced. This approach, which is based on the time taken for the stress wave to reach the boundary of the soil, was the one adopted for this study.

Related to the boundary condition selection was that of model size. The main objective in setting the model size for a problem such as this and with the boundary conditions used here was so that the stress waves in the soil would not reach the boundary during the time of the analysis. In the early stages of model development, the model was sized based upon the acoustic speed of water (for saturated soils). However, for soils themselves, the distance required to keep the stress wave in the soils from reaching the boundary is considerably less than this. On the other hand, when a significant reduction in model size was attempted, far field effects began to show and significant variations in the results were observed.

To bring this problem to resolution, a survey of the previous 2D efforts was done. The major outlier in this is Serdaroglu (2010), but this is because his objective was to model ground vibrations, which require a considerably larger model.

Based on this (and admittedly some of the proportions were measured or extrapolated) the decision was made to set the soil model up so that the right boundary was one pile length away from the pile and the bottom of the model one pile length away from the toe. Unless otherwise noted, this is the proportion that was adopted for grid generation of the model.

Interface Elements for Soil-Pile Interaction

If soil-pile interaction is the “stickiest wicket” of the whole problem of the wave equation for piles (and static loading, for that matter) the issue of interface elements is right at the center of the discussion. It is a good example of a phenomenon that is all too common with geotechnical engineering: no matter which

approach was chosen, the difficulties associated with that approach created as many problems as the approach solved.

Interaction between a geotechnical structure (pile, retaining wall, footing, etc.) and its surrounding soil is of one or two natures: compression or shear, as any such interface is inextensible. Compression is fairly easy to handle; the elements simply come up against each other and interact. One major issue here is the avoidance of tension, which can be handled either by the basic elasto-plastic soil model or by an interface element. With shear the problem is a little different, because once the shear strength of the soil-structure bond is exceeded there is relative movement of soil and structure, which violates a basic nodal assumption of a Galerkin finite element scheme such as the one in use here and in most geotechnical models.

Driven piles, both statically and dynamically, have both kinds of interface with the soils. The whole object of pile driving is to effect relative movement of the pile with the soil; thus, the breaking of the pile-soil bond is inevitable. To a lesser extent this is true in static testing, even that which is not done to plunging failure, as the partial mobilization of the resistance implies that the plastic limit of that portion has been exceeded and that relative movement has taken place.

Potts and Zdravkovic (1999) note that there are four solutions to this problem:

1. Use of thin continuum elements with the same types of constitutive laws as the soil.
2. Linkage elements, where opposite nodes are connected by discrete springs.

3. Special interface elements of either zero or very small thickness with special constitutive properties, such as described in To (1985). He additionally uses interface elements to model the inextensibilities of the hammer system as well.
4. Hybrid elements where soil and structure are linked via constraint equations.

They spend some time discussing their own interface element. Interface elements also play a large role in Serdaroglu (2010), who did an extensive comparison of the static capacity of the pile from the finite element model with static capacity formulae. His study shows that the ultimate capacity of the pile (in his case, plunging failure) that is returned by the finite element model is strongly influenced (governed may not be too strong of a word) by the coefficient of friction he has chosen for the interface elements, relative both to different coefficients and models without interface elements. He concludes that "...modeling of the soil pile interface is critical to accurately compute the shaft capacity of a pile."

Or is it? Having developed an interface element model, Potts and Zdravkovic (2001) analyze this model and conclude that "...a better alternative is probably not to use interface elements at all?" So what is to be done?

Part of the problem is that not all interface elements are the same. Some mostly model Coulombic friction, others include properties such as elastic and bulk moduli of soils. So, there is not always an exact comparison taking place.

Beyond that, Potts and Zdravkovic (2001) and Serdaroglu (2010) both show that the core properties of the interface element to a large extent drive the static shaft resistance of the pile. In the forward method, whatever properties are chosen, with or without interface elements or elements along the pile surface with different properties than the main body of the soil will determine the SRD. In the inverse method, however, any limiting assumptions made about the surface properties of

the soil will determine the SRD *a priori*, which defeats the entire purpose of the inverse method.

A further complicating factor, as pointed out by Potts and Zdravkovic (2001), is the issue of dilatancy. For the case where $\varphi = \psi$, the soil will dilate indefinitely without reaching a critical state condition. In response to this they varied the dilatancy of interface elements and the parent soil itself between $\psi = 0$ and $\psi = \varphi$. Although the interface elements still dominate the shaft capacity, when $\psi = 0$ their results are much improved, and that improvement continues when $\psi = 0$ for the parent soil as well.

Given these considerations, interface elements that are different in properties from the surrounding soils were not used. Using very thin elements at the soil interface, however, were used, and the effect of dilatancy was considered, and these two parameters were tested in the model.

Effective Stress Computations and Pore Water Pressures

Another issue of importance with geotechnical finite element codes is that of the effective stresses of the soils. This aspect of soil mechanics separates geotechnical finite element analysis from other solid mechanics almost as much as either the non-associative plasticity or replicating the three-phase nature of the medium. It became one of the major challenges of the development of this model.

If one constructs a finite element mesh using soils with typical properties of modulus of elasticity, Poisson's Ratio and density, and applies gravity loading to the mesh, the first thing that will happen is that the mesh will "collapse," possibly experiencing strains up to 5%. The reason for this is that actual soils, with a stress history, have already been "prestressed" by gravity and compacted by the deposition process. This is the case both for normally and pre-consolidated soils;

the latter simply have a higher internal stress due to previous external pressure. This magnitude of deflection will create serious difficulties in the analysis of pile movement, be it static or dynamic. If gravity is not applied, with cohesionless soils premature failure will take place, as all of the strength of the soil is derived from overburden pressures on the soil skeleton.

Although routines to deal with the problem are included in many geotechnical codes (such as CRISP; see Woods and Rahim (2008)) complete solutions to the problem are rare in the literature. The solution used in this routine is based on Naylor et. al. (1981) with some important modifications.

In this model the soils were prestressed in this fashion:

1. The location of every Gauss point in the mesh was determined. For this purpose only the vertical axis is significant.
2. The soils were layered as desired. Because most piling is driven into a layered stratum, the properties were varied with depth. Each stratum could have its own density, modulus of elasticity, Poisson's Ratio, friction angle and cohesion. For this study soil layers were horizontally uniform.
3. The effective stress for each Gauss point was determined. This was done in the same way as one would do it in elementary soil mechanics (see Hannigan et. al. (2006)) considering the overburden above the point in question and the fact that the Gauss point was at an interior point in the layer.
4. The resulting vertical stresses were entered as the initial stresses for the soil Gauss points only. The stresses and strains were kept track of separately from the primary variables on a Gauss point basis.
5. The two horizontal (radial and circumferential for our axisymmetric model) stresses were computed and entered into the Gauss point stress data.

6. Local force vectors were computed based on the effective stresses, using Equation 58. These were then assembled into a global force vector to “counteract” the effect of the stresses. This became the initial internal force vector for the system.

$$s = \int B^t \sigma dV \quad (58)$$

7. Now that the stresses were “embedded” in the system, it was necessary to keep this effective stress global force vector active and constant, adding it to the internal force vector every step.

Determining the vertical effective stresses s_z is a fairly straightforward process, although the “bookwork” of the layers requires some care. The resulting horizontal stresses within the soil mass are another matter altogether. As Verruijt and van Bars (2007) point out, these horizontal stresses are very uncertain, and without either extensive testing, a good understanding of the stress history of the soil, or both they can be computed in a number of ways.

The first thing that can be noted is that, before disturbance, the three stresses in the soil can be considered to be the principal stresses with no shear in the soil. This can be expressed as

$$\begin{aligned} \sigma_z &= \sigma_1 \\ \sigma_r &= \sigma_2 \\ \sigma_\theta &= \sigma_3 \end{aligned} \quad (59)$$

The two horizontal stresses can be assumed equal, thus

$$\sigma_r = \sigma_\theta = \sigma_3 \quad (60)$$

Using the relationships of Equations 59 and 60, the relationship between the horizontal and vertical stresses can be defined as

$$\sigma_3 = K_o \sigma_1 \quad (61)$$

The central problem is thus to define K_o for the effective stresses. Given the constitutive modeling of the soil during static loading or impact, Naylor et. al. (1981) recommended to use the theory of elasticity, in which case

$$K_o = \frac{\nu}{1 - \nu} \quad (62)$$

Soil, however, is not a truly elastic material, and in any case its formation is generally complex. A more realistic (if theoretically weaker) expression for this relationship for at-rest earth pressures is Jaky's Equation for normally consolidated soils, or

$$K_o = 1 - \sin\phi \quad (63)$$

For this model, this is what was adopted for the horizontal earth pressures that result from effective stresses. It is used in the Plaxis finite element code (Townsend et. al. (2001)). It was also possible to use the pre-consolidated form of this equation for soils that require it, although this was not included in this model. Using Equation 63 rather than Equation 62 allows $K_o=1$ to apply to cohesive soils in general and soft cohesive soils in particular. Although this could be accomplished by setting $\nu = 1/2$ in Equation (62), doing so created serious difficulties with D_e (see Equation 41.)

Complicating matters further was the inclusion of hydrostatic pore water pressure. Piles are more often than not driven into saturated soils. The relationship between total stresses and effective stresses is given by the equation

$$\sigma'_z = \sigma_z - u \quad (64)$$

With the vertical stresses, this was straightforward. The hydrostatic stresses are computed by the equation

$$u = \gamma_w z_w \quad (65)$$

and then applied to Equation 64. For the horizontal stresses, following Verruijt and van Bars (2007),

$$\sigma_r = \sigma_\theta = K_o \sigma'_z + u \quad (66)$$

STADYN limits its modeling of pore water pressures to hydrostatic conditions without capillary rise. This is reasonably satisfactory for most cohesionless soils; however, it does not take into consideration excess pore water pressures that are generated during driving into low permeability, cohesive soils. The result of this is pile set-up, where the SRD up until the end of driving is lower than the ultimate capacity of the pile, sometimes by a factor of 2-5. A discussion of pile set-up can be found in Hannigan et. al. (2006). Including set-up effects in a pile dynamics algorithm is a highly desirable goal; in principle it could eliminate the need for pile restrikes. However, there are three main reasons why it was not included in this study.

The first is that, although the rise in pore water pressures is the most important factor in pile set-up, it is not the only one. Clay soils are also subject to thixotropy which can influence their behavior under impact and vibratory loads (Gumenskii and Komarov (1961)).

The second is that the rise in pore water is caused by the “low” permeability in the soils. Schümann and Grabe (2011), for example, model this in finite elements, and some of the previous models with piles did so. However—and this particularly applies to the inverse method—the wide variations in permeability, and the

difficulties in accurately quantifying it, add another variable which could drive the solution to unrealistic results.

The third is that the rise in pore water pressures is also influenced by the number, frequency and intensity of blows that precede the blow under study. It would require multiple blows to properly analyze which certainly can be done but which increase the overall computational cost of the analysis.

These reasons not only led to the exclusion of elevated pore water pressures in this model; they also insure that restrikes will continue to be performed in pile dynamics for the foreseeable future.

Engineering Properties of Soils

General Considerations

As is evident from Figure 3, most pile dynamic modeling consists of defining properties such as soil spring constant, quake, and damping. Although some 1D solutions include common soil properties (Corté and Lepert (1986); Randolph and Simons (1986)), with a 2D finite element implementation, the direct consideration of these properties is unavoidable.

Given the foregoing discussion on elasto-plastic theory and effective stress implementation, the following soil properties are essential to know for each soil element in the model:

- Modulus of Elasticity E
- Poisson's Ratio ν
- Dry Density of Soil ρ
- Cohesion c

- Yield Strength of Soil s_{yield} . This is in reality

$$\sigma_{yield} = q_c = 2c \quad (67)$$

- Internal Friction Angle of Soil φ
- Dilatancy Angle of Soil ψ . This was discussed earlier; it is either set to zero or is a function of φ .
- Acoustic Speed of Soil or Other Material c_a , which is determined by

$$c_a = \sqrt{\frac{E}{\rho}} \quad (68)$$

- Specific Gravity of the soil particles, G_s .

For the purposes of this study, there were six (6) independent soil property variables to consider. In the forward method, each of these properties was assigned to each layer, taking into consideration whether the layer is under the water table (saturated) or not. These can be obtained either directly from laboratory tests or from field test correlations (Townsend et. al. (2001)).

A more complicated issue was the inverse method. Here all six independent properties had to be determined for each layer from the dynamic data. (One assumption made in this study is that the water table level is known, generally the case with soil borings.) Since virtually every soil into which piles are driven is layered and the differences in soil properties can vary widely from one layer to the next, ultimately the number of unknowns that must be solved for was six times the number of layers. Clearly the number of variables would become very large very quickly.

Ideally the layering that should be used would be the horizontal divisions in the pile and soil shaft layers, which only made the proliferation of variables worse.

One way of addressing this issue is to use the soil's known stratigraphy to mark out layers which actually correspond to geological reality, and in doing so reduce the layer numbers. STADYN allowed for this expedient.

The layer issue addressed, the next evident question was this: since some of the soil properties were shown to be dependent on others in some way, was it possible to show other dependencies and thus reduce the number of independent variables? The answer was a qualified “yes” and a method of doing so follows.

The “xi-eta” Method of Soil Property Aggregation

The wide variety of soil properties, coupled with varying geological histories and the presence or absence of water, make geological rheology one of the major challenges of civil engineering. Having said that, there are many commonalities in the properties of soil that allow the use of simplifications to estimate soil properties. The best known of these are the “typical” density (cohesionless soils) and consistency (cohesive soils) that are widely disseminated in the literature and used frequently in practice. These are especially important with deep foundations, as the extraction of undisturbed samples necessary for tests such as consolidation or triaxial tests becomes more problematic with increasing depth.

The method used in this study—which is entitled the “xi-eta” method, for reasons which will become evident—is not meant to be comprehensive or applicable to all soils. It is designed to be applied to a wide variety of soils that are found in the earth. It represents a first attempt at reducing the size and complexity of the problem, especially the inverse problem, although the forward problem can benefit from this also, given that “typical” values are frequently used in actual practice.

In the broadest terms soil properties can be said to vary in two important ways:

- In terms of degree of cohesion, which were designated by the dimensionless variable ξ . Deep foundation practice tends to classify soils as one or the other, but the reality is that there is a continuum from very cohesionless soils (gravels, clean sands) to very cohesive soils (clays). An inspection of a gradation chart of a well-graded silty sand or sandy silt illustrates this.
- In terms of density or consistency, which were designated by the dimensionless variable η . For cohesionless soils there are soils that range from very loose to dense, a range that affects both the density of the soil and the internal friction angle. For cohesive soils there are soils which range from very soft to hard, a range that affects both the density of the soil and the cohesion/unconfined compression strength/yield strength.

To graphically understand these concepts, consider the four-node quadrilateral “element” in natural coordinates as shown in Figure 17.

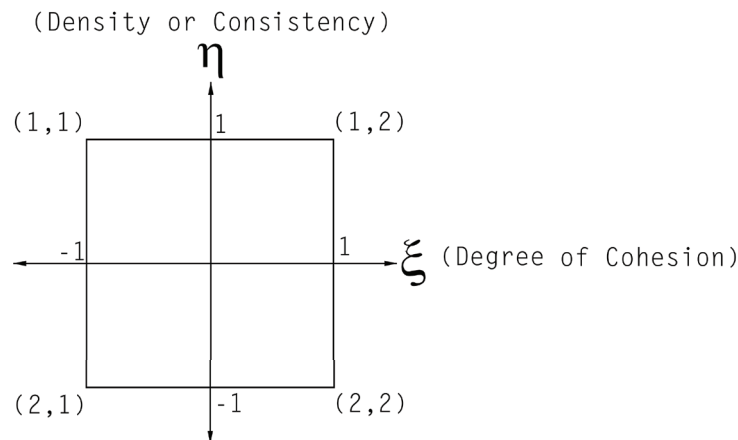


Figure 17 Four-Node Quadrilateral Adapted to Soil Properties

As is the case with the four-node quadrilateral elements that were used in this study, the natural coordinates of this system were defined on the ξ and η axes.

Given that the basic dimensionless values vary from -1 to 1, these variables relate to actual soil properties in this way:

- A soil with a $\xi = -1$ was completely cohesionless, thus $c = 0$; one with $\xi = 1$ was completely cohesive with $\varphi = 0$.
- A soil with $\eta = -1$ was very loose or very soft; a soil with $\eta = 1$ was very dense or hard.

The values at the corners with entries as shown were then defined in a simple 2×2 matrix. Each of the five soil parameters could thus be defined for general purposes as a function of two variables, or $f(\xi, \eta)$. Using the standard shape functions for this element and the corner values as shown, the value of any of the variables could be expressed as

$$\begin{aligned}
 f(\xi, \eta) = & \frac{1}{4} (1 - \xi) (1 + \eta) f_{1,1}(\xi, \eta) + \\
 & \frac{1}{4} (1 + \xi) (1 + \eta) f_{1,2}(\xi, \eta) + \\
 & \frac{1}{4} (1 - \xi) (1 - \eta) f_{2,1}(\xi, \eta) + \\
 & \frac{1}{4} (1 + \xi) (1 - \eta) f_{2,2}(\xi, \eta)
 \end{aligned} \tag{69}$$

Equation 69 shows that, if the corner values were known for each property and a value of ξ and η were given, the actual properties for the soil could be determined. Conversely, if the soil properties were known values of ξ and η could be computed, if the actual soil properties did not stray from the “standard” values. (One way of addressing this issue would be to define corner properties based on local experience.)

In this way the number of independent variables was reduced from six (6) to two (2) times the number of layers, which is both a considerable reduction and a potential benefit to the inverse problem. It is worth noting that pile dynamics

aggregates the soil properties into the classic quake/resistance/damping framework; this simplification is not as novel in concept as it may appear.

One thing that Figure 17 “implies” is that values of ξ and η cannot exist outside of the quadrilateral. Obviously Equation (69) returns values when $|\xi| > 1$ or $|\eta| > 1$. Whether these values have any validity depends upon the soil property under considerations.

Generally speaking, soil properties that are solely a function of ξ must stay within bounds, i.e., $|\xi| = 1$.

The following sections deal with the way in which the various properties are mapped into the “xi-eta” framework, which in turn depends upon the nature of the properties themselves.

Modulus of Elasticity

The use of an elasto-plastic model is a simplification; the ramifications of that simplification need to be well understood. Of all of the soil properties relevant to this study, the soil modulus of elasticity poses some of the “knottiest” problems in geotechnical finite element simulation.

To begin the discussion, consider a “less radical” simplification of the soil model, namely the hyperbolic soil model as shown in Figure 8. Taking the derivative of the deviator stress-strain curve yields

$$\frac{d(\sigma_1 - \sigma_3)}{d\epsilon_1} = E(\epsilon) = (a_h + b_h\epsilon_1)^{-1} - \frac{b_h\epsilon}{(a_h + b_h\epsilon_1)^2} \quad (70)$$

This relationship is neither constant nor linear. It shows that, for $\epsilon_1 = 0$, $E(\epsilon_1) = 1/a_h$, and the modulus of elasticity decreases until, as $\epsilon_1 \rightarrow \infty$, $E(\epsilon_1) \rightarrow 0$. Therefore the maximum elastic modulus of a soil is at zero stress and strain and decreases

until complete plastic yield is experienced. This general trend of the elastic modulus is demonstrated experimentally in studies such as Builes et.al. (2008), and a complete discussion of this issue relative to shear moduli and testing techniques can be found in Massarsch (1983). Equation 70 only considers the hyperbolic simplification; other factors such as the stress history of the soil should be taken into consideration.

Since the slope of the curve decreases with increasing strain, the modulus of elasticity is likewise continuously changing with strain. Small-strain applications, such as are found in geophysical methods, “experience” a higher modulus of elasticity than large-strain applications such as pile dynamics. Because of Equation 68, this affects the acoustic speed of the soil. This carries over into the static modeling of the pile-soil system because, for the whole analogy between dynamic stresses and strains in piles and soils and static strains in piles and soils to be meaningful, not only do the static and dynamic moduli of elasticity need to be the same, the stress and strain level in both must also essentially be the same. This is why the mobilization degree of shaft and toe resistance is crucial to proper dynamic testing. Without that correspondence the whole validity of pile dynamics as a method of estimating static capacity begins to come unraveled. Conversely, the similarity of those two stress-strain levels is a large reason why pile dynamics, with the large dynamic stresses it causes, is viable at all.

Having said that, as discussed earlier in a qualitative way, the object of elasto-plastic modeling is to superimpose a model such as shown in Figure 9 on a soil that behaves more as shown in Figure 8. That process affects the quantification of the modulus of elasticity.

Another approach is to include a hardening cap (Townsend et. al. (2001)). This tends to force the model to “act more hyperbolically” than without the cap.

Under these conditions it makes sense to use a tangent modulus (the E_{ti} shown in Figure 8). With a purely elasto-plastic approach, a “secant modulus,” where the elastic stress-strain line is a chord across the actual soil behavior is more appropriate.

These considerations indicate that the standard elastic moduli used with this program should be on the “soft” side. Since it is sometimes difficult to determine how standard elastic moduli were determined, establishing either standard values for the “xi-eta” approach or values for a specific case can be challenging.

The values for modulus of elasticity were subject to wide research, including sources such as Samtani and Nowatski (2006), Winterkorn and Fang (1975) and some of the previous 2D studies. For cohesionless soils probably the best values were found in Reid et.al. (2004); although the application was different, the method used in testing had a strain rate that was closer to that experienced in driven piles than is normal with direct shear testing.

All of this considered, the elastic values for the corners are in Equation 71 and the plot is in Figure 18.

$$\begin{aligned} E(-1, -1) &= 10 \text{ MPa} \\ E(-1, 1) &= 50 \text{ MPa} \\ E(1, -1) &= 3.75 \text{ MPa} \\ E(1, 1) &= 75 \text{ MPa} \end{aligned} \tag{71}$$

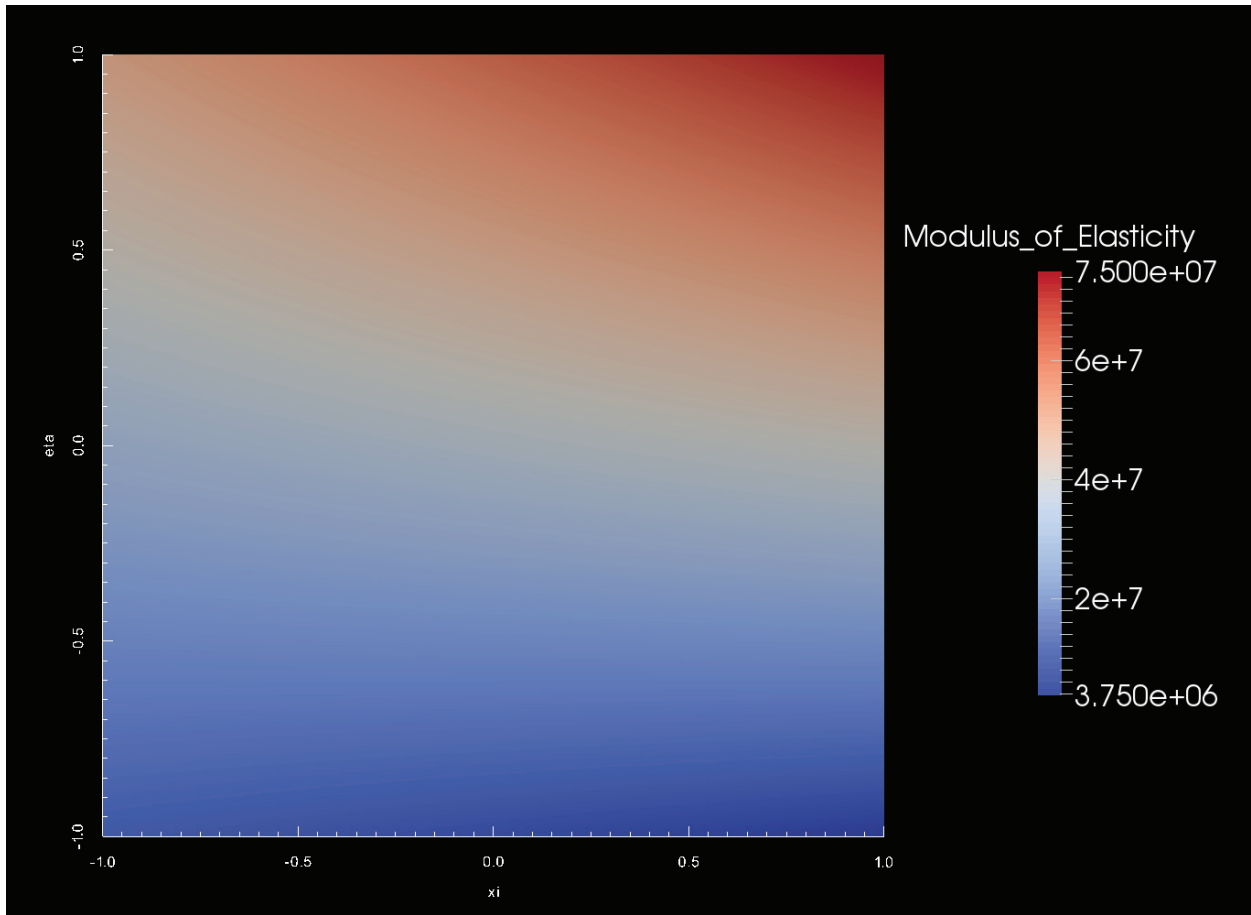


Figure 18 Modulus of Elasticity as a Function of ξ and η

Values of E could be computed if either $|\xi| > 1$ or $|\eta| > 1$ from Equation 69; however, the program had a lower bound of E so that it is not zero, negative or very small positive. Although it is tempting with the complexities of the elastic modulus to dismiss the whole elastic concept with soils, as Powrie (2014) observes, “...elastic calculations, combined with judiciously selected elastic parameters, can often lead to reasonable estimates of the soil settlements associated with foundations and other near surface loads.”

Poisson's Ratio

This was independent of η . For this study $\nu(-1, \eta) = 1$ and $\nu(1, \eta) = 9/20$. The lower bound was primarily per Reid et.al. (2004). The upper bound was to prevent problems with Equation 41; a value in this range is justified by Equation 63. The program was set up so that the minimum value is enforced if $\xi < 1$ and the maximum value enforced if $\xi > 1$. There are no restrictions for any value of η . A plot of this is shown in Figure 19.

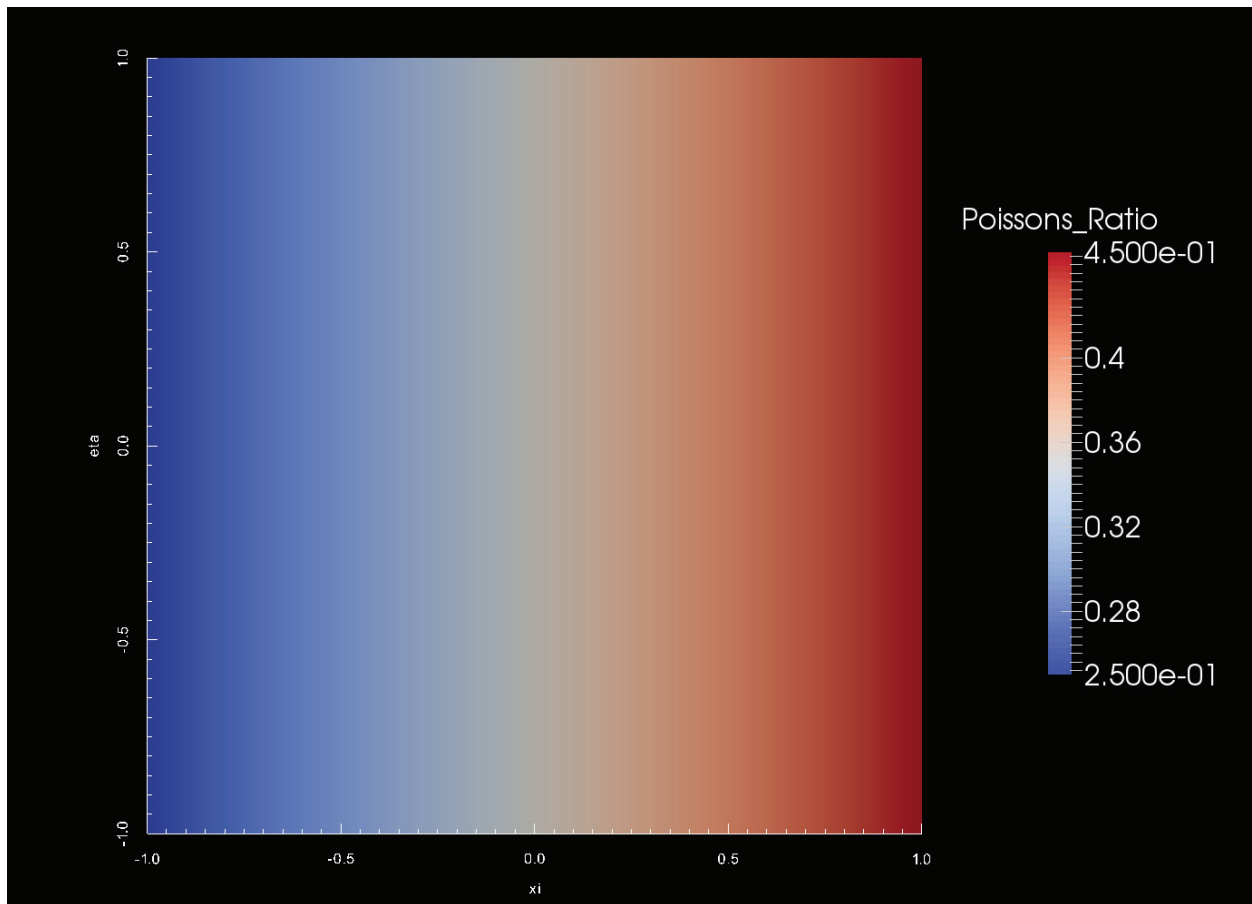


Figure 19 Poisson's Ratio as a Function of ξ and η

Internal Friction Angle

While the friction angle f is always zero for purely cohesionless soils with $\xi=1$ (thus $\varphi(1, \eta)=0$), it obviously varies with the density and thus η . The survey resulted in setting $\varphi(-1, -1)=27.3^\circ$ and $\varphi(-1, 1)=42^\circ$. The results are plotted in Figure 20. In any case for all values of ξ and η , $\varphi \geq 0$.

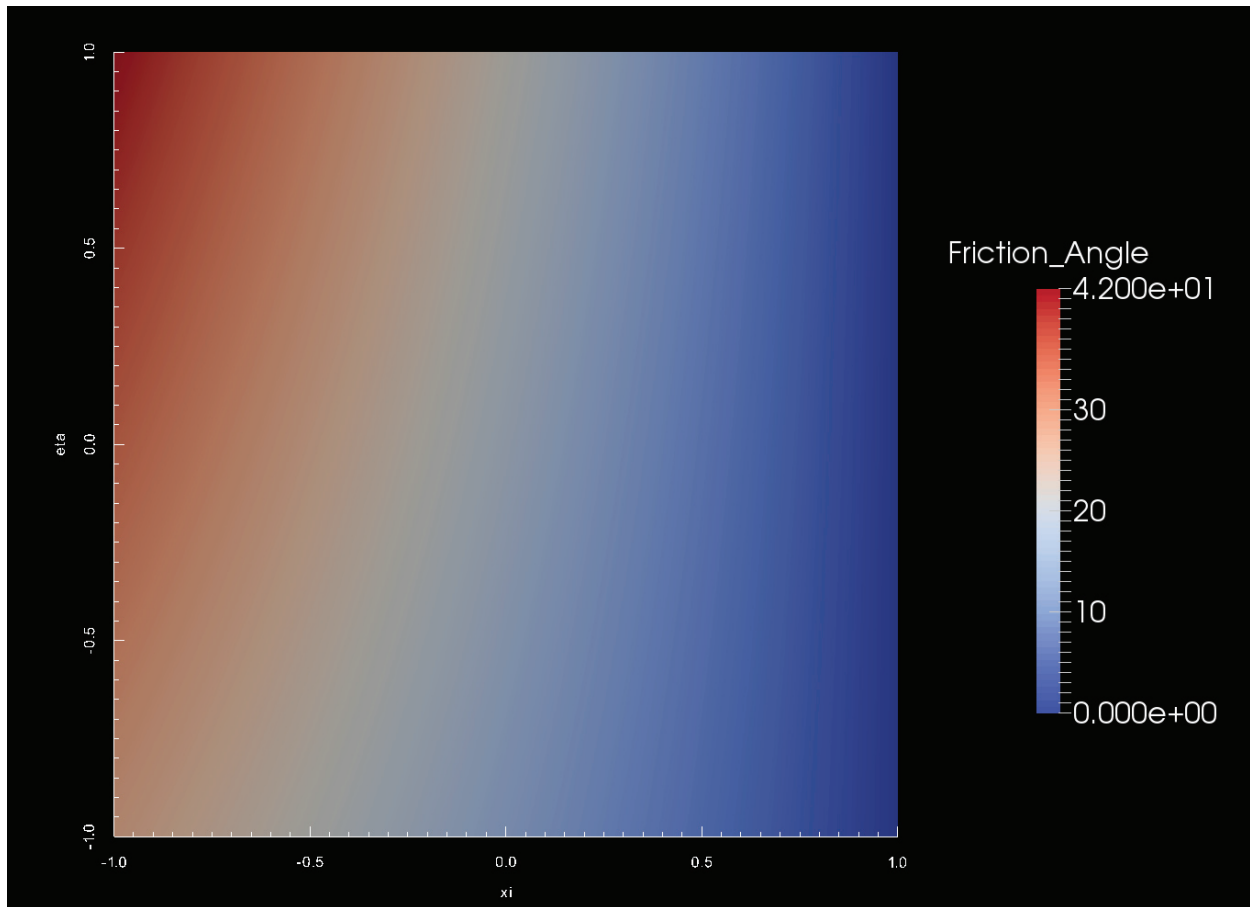


Figure 20 Friction Angle as a Function of ξ and η .

Cohesion

This was almost the mirror image of the friction angle, with $c(-1, \eta) = 0$ for purely cohesionless soils. On the opposite side of the quadrilateral, Das (1985) states that the cohesion and modulus of elasticity relate as follows:

$$E = \beta_r c \quad (72)$$

He gives a variety of values for β_r , but in general $500 < \beta_r < 1500$. Winterkorn and Fang (1975) set β_r at $250 < \beta_r < 500$. For this study $\beta_r = 375$, which is more of a result of the survey than a pre-posed parameter. Based on this, $c(1, -1) = 20$ kPa and $c(1, 1) = 200$ kPa. The results are plotted in Figure 21.

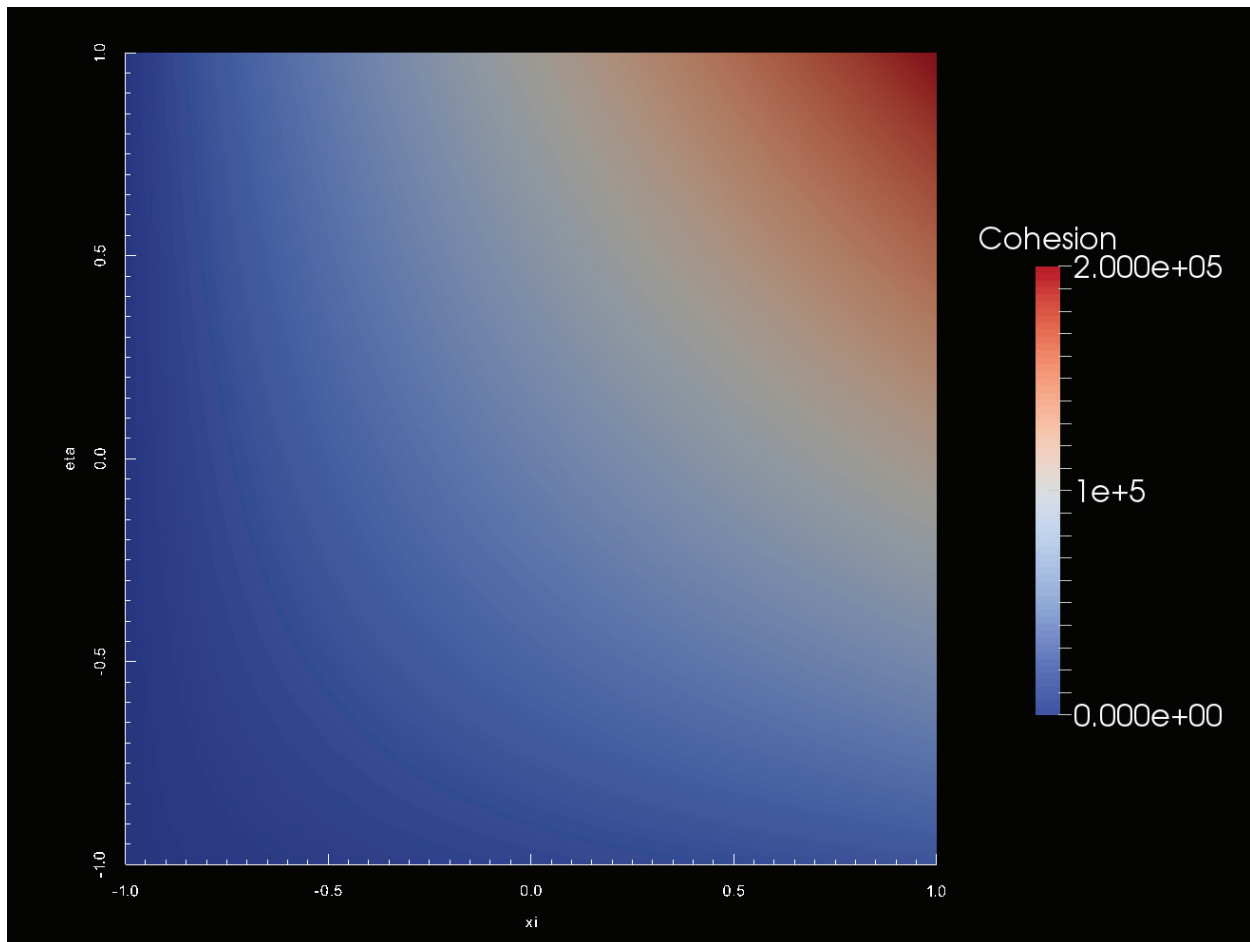


Figure 21 Cohesion as a Function of ξ and η

Cohesion was never allowed to fall below zero for any ξ or η .

Dry Density

This varied with both ξ and η . The values at the corners are shown in Equation 73, and the plot is shown in Figure 22.

$$\begin{aligned}\rho(-1, -1) &= 1500 \text{ kg/m}^3 \\ \rho(-1, 1) &= 2000 \text{ kg/m}^3\end{aligned}\tag{73}$$

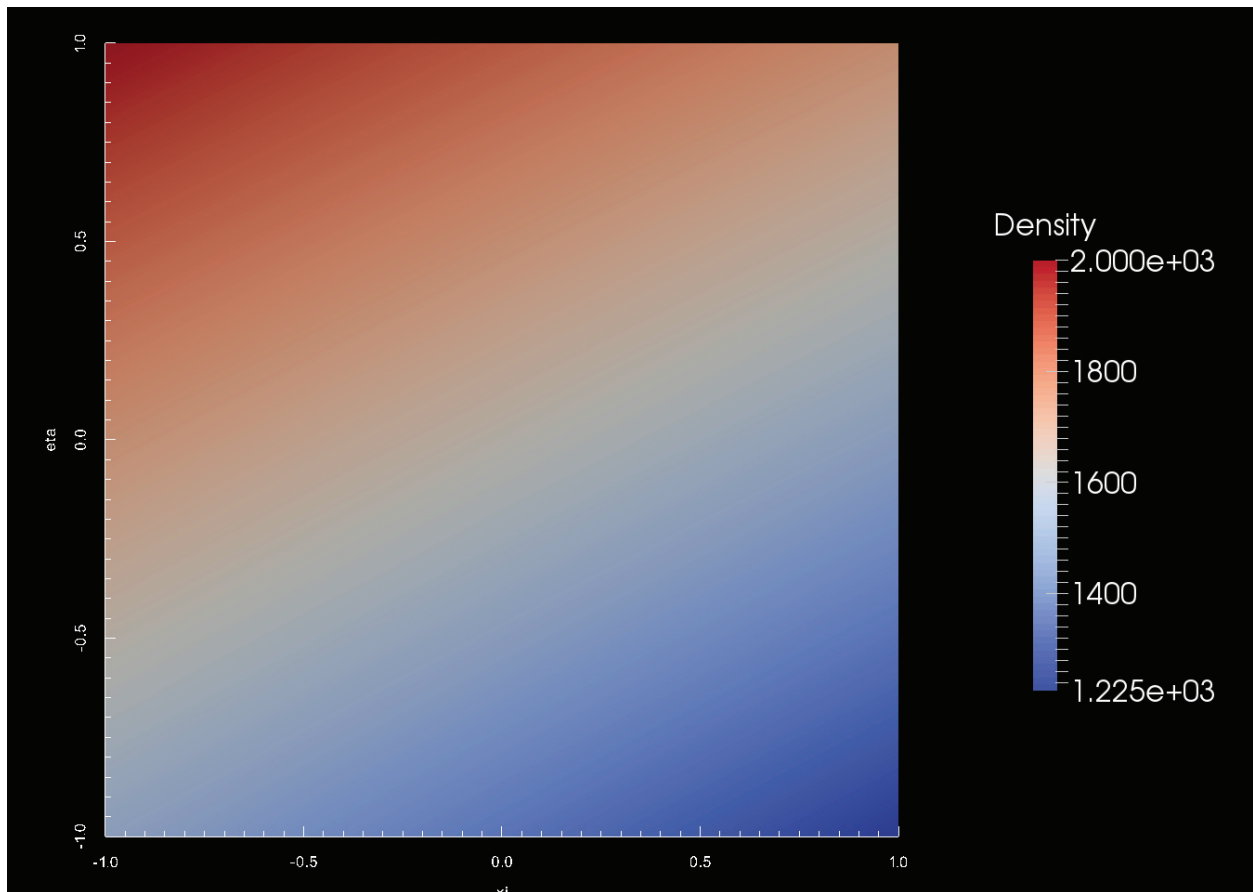


Figure 22 Dry Density as a Function of ξ and η

For layers under the water table, the pores were basically “filled up with water” and the saturated density becomes

$$\rho_{sat} = \left(1 + \frac{\rho_{water}}{\rho_{dry}} - G_s^{-1} \right) \rho_{dry} \quad (74)$$

for all values of ξ and η . The effects of phenomena such as capillary action were not included in this study.

Specific Gravity of Solids

As was the case with Poisson’s Ratio, the specific gravity of soils mostly varies with ξ , and for this model it is assumed to be independent of η . Using values from Reid et.al. (2004), $G_s(-1, \eta)=2.65$ and $G_s(1, \eta)=2.78$. Values were not permitted to go outside of this range. This quantity was essential for the proper computation of Equation 74, although the variation is minimal. A graphical representation of this is shown in Figure 23.

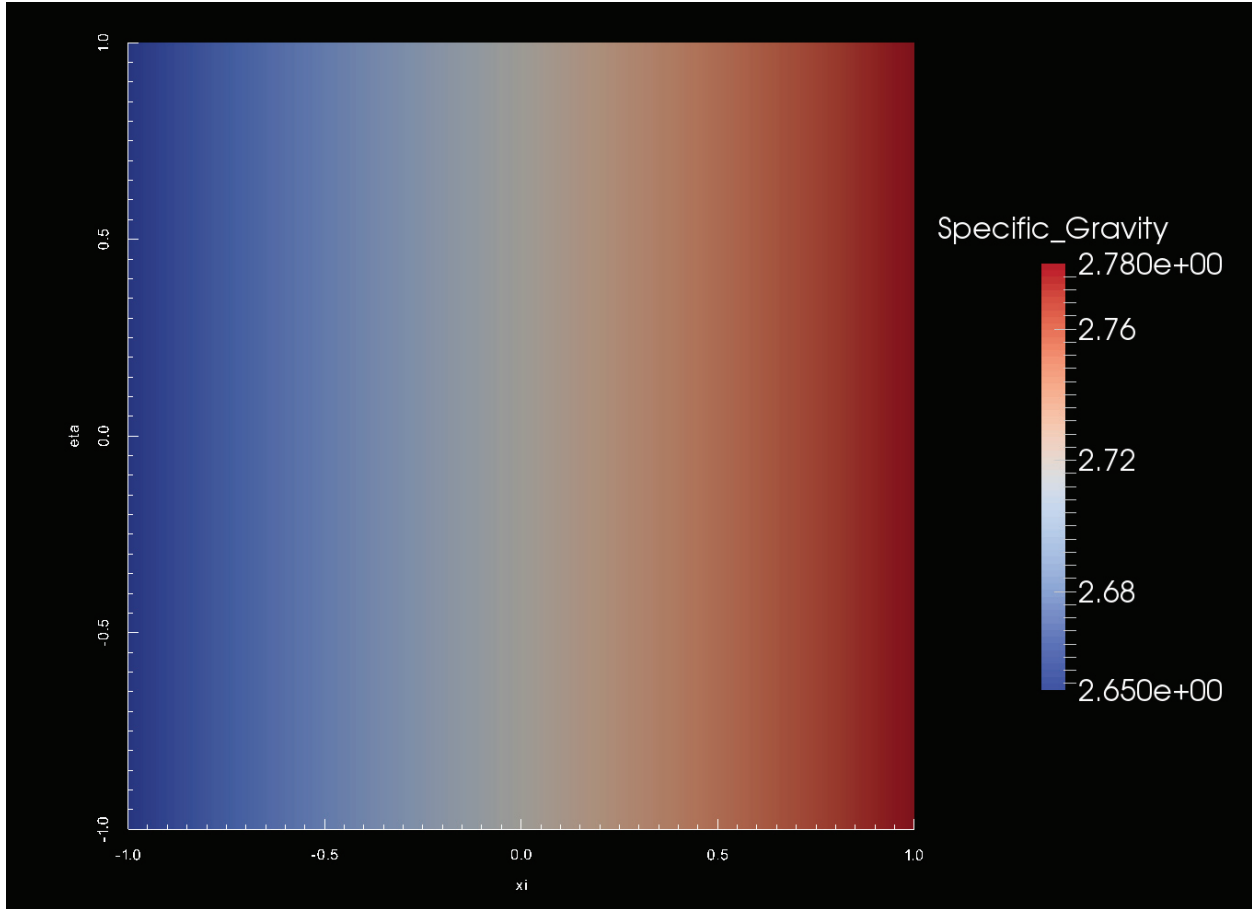


Figure 23 Specific Gravity as a Function of ξ and η .

Static Analysis

Analytical Static Capacity Estimates

Before discussing STADYN’s methodology for estimating static capacity in the context of the load-deflection characteristics of the pile, some mention should be made of current “closed form” methodologies in the estimation of pile capacity.

The development of static methods to estimate the ultimate or unfactored bearing capacity of piles and other deep foundations has occupied the geotechnical literature for a long time. There has been a proliferation of formulae and methods to

estimate the ultimate static capacity of piles (Finno (1989)), with a variety of results for different types of piles in different applications. It is tempting to use these as an analytical comparison with finite element results, as Serdaroglu (2010) does. As will be seen below, the concepts inherent in the finite element analysis of pile response to axial load—to say nothing of other t-z methods—and those of static methods are widely different, and divergent results are to be expected.

Because one-dimensional methods such as the classic wave equation for piles and CAPWAP use the results of static methods for their analysis, such methods will appear below. The use of Meyerhof's Method is simply to establish a far upper bound for loading purposes, not to give an estimate of static capacity.

Stepping Scheme for Static Analysis

Returning to STADYN's own model, it was necessary to formulate a method of performing both static and dynamic analysis. Since this was a problem of pile dynamics, the dynamic analysis is self-evident. Static analysis enabled the routine to estimate the static capacity of the pile, as was previously discussed.

To perform a truly static analysis of the pile, as is the case with actual static load testing it is necessary to apply a stepwise increasing force at the pile head. With physical testing, the load is applied in such a way that time-dependent effects are ideally not present in the load-displacement curve of the pile head. In the model the dynamic component (principally distributed mass) is not modeled; only the elasto-plastic stiffness of the system was modeled.

For each load step Newton's Method was employed to model the system, solving the equation

$$K\Delta d = f - p + s \quad (75)$$

The procedure was as follows:

1. The right hand side of Equation 75 was nulled.
2. The external forces on the system were computed, in this case the downward forces at the pile head. “Forces” is accurate because the pressure of the load testing “apparatus” is assumed to be uniform; it is then distributed proportionally to the pile head nodes. This was substituted into Equation 75 as the vector f .
3. The internal force vector for all of the nodes was computed, considering the effects of plasticity. This was substituted into Equation 75 as the vector p .
4. The compensating loads for effective stress were substituted into Equation 75 as the vector s . The Gauss point stresses induced by effective stresses were added at the beginning of the analysis.
5. Equation 75 was solved for Δd by back substitution. The stiffness matrix K was reduced after its initial formulation and not changed during the loading sequence. Strictly speaking, in Newton’s Method the stiffness matrix must be altered each time a Newton step is run. This occasions the reassembly and reduction of K each step, which is both a costly operation and, with non-linear and non-associative materials, results in a non-symmetric K . There are a number of ways to deal with this, including quasi-Newton methods (Healy, Pecknold and Dodds (1992)), by producing a symmetric stiffness matrix which is “close” to the non-symmetric stiffness matrix for the purpose of Newton convergence, or by not altering the stiffness matrix at all from its initial, elastic formation. It is the last option that is used in this program; the downside of this is a relatively large number of Newton steps, especially for loads beyond Davisson’s criterion. This two-step direct solution used Cholesky factorization. Potts and Zdravkovic (1999) state that iterative methods such as conjugate

gradient are less efficient than banded solvers (Sewell (1985)) due to non-linearity considerations. In fact, a reduction/back substitution method is their preferred method for problems such as this. Given the number of nodes and elements in the system, this is reasonable.

6. The resulting Δd was added to the displacement vector d .
7. The Euclidean norm of Δd was compared to the tolerance. If the result was less than the tolerance, Newton stepping was stopped, the load increased, and the process begun again. If not, the internal force vector was updated with the current displacements d and another Newton step was performed with the same pile head load.

In order to anticipate a maximum possible load given the soil conditions, an adaptation of Meyerhof's SPT method (Hannigan et.al. (1997)) was used to develop an upper bound for load stepping. In theory, the number of steps was irrelevant. In practice, step size had a significant effect on the results of the model, as will be seen.

Static Load Testing Considerations

Once a static model is built and run, it was necessary to interpret the results.

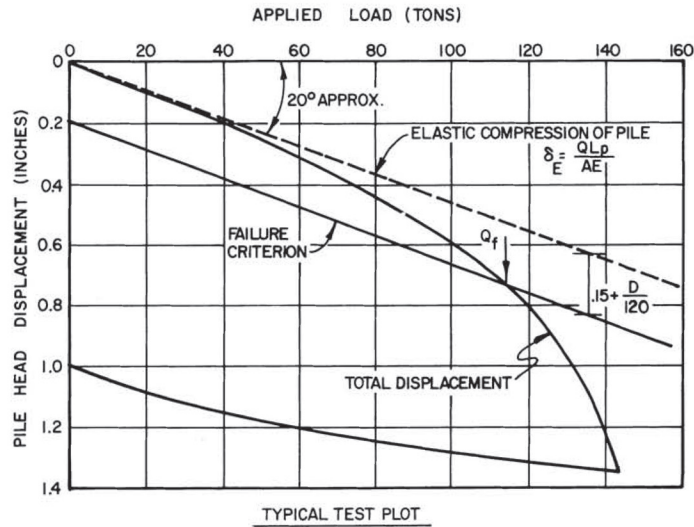
Traditionally geotechnical analysis and design has been divided into two parts: design for strength and design for service. The division is well embedded in practice, from the pedagogy in basic geotechnical courses to the implementation of LRFD (Federal Highway Administration (2001)). A good example of this is the design of shallow foundations, which is commonly divided into two aspects: bearing capacity (strength) for shear failure on a surface, and settlement (service) by excessive movement of the structure under load, be that movement total (all of the structure at once) or differential (parts of the structure more than others.) If

a purely elasto-plastic soil response is considered, the settlement movement takes place in the elastic portion of the soil response and the bearing capacity failure takes place during the plastic portion of the soil response. Analysis to strength failure is not uncommon in geotechnical finite element analysis (Griffiths and Lane (1999)).

This approach suffers from several shortcomings:

1. Much of the settlement in soils is not, strictly speaking, due to elastic deflection, although the theory of elasticity is often applied to describe the phenomenon (Verruijt and van Bars (2007)). The most obvious example of this is consolidation, which itself is divided into primary and secondary consolidation.
2. With driven piles and other deep foundations, the situation is further blurred by the interaction between the soil, the shaft and the toe. In general, the shaft interface is a frictional one, and so the failure interface is that of the pile surface itself, although deflections in the soils can produce effects such as downdrag. The whole concept of bearing capacity failure at the toe, enshrined in many static formulas, has been justifiably criticized (Fellenius (2011)). The pile toes are so deep and the effects of overburden are so pronounced that development of a clear-cut failure surface is difficult if not impossible.
3. Deep foundations seldom experience plunging failure loads in service, except in the case of gross misunderstanding of the stratigraphy by the designer. This is intentional, but it shifts the primary question in design from “What load will produce plunging failure?” to “How much deflection is produced by a certain load?” and “Is this deflection excessive for the structure the deep foundation supports?” With this paradigm shift, the whole concept of a single “ultimate load” for a deep foundation loses much of its relevance, a fact that is not given full consideration by many current design concepts.

Complicating the issue further with deep foundations is the nature of both load testing and the interpretation of the results. There is more than one loading sequence allowed for statically testing a pile, even within the ASTM D1143 standard (Kyfor et. al. (1992)). Although ideally any proper static load testing sequence should produce the same results, in reality the nature of the stratigraphy, the presence or absence of ground water, and other factors will make variations inevitable. Once the pile head load-deflection curve is obtained, there are many ways to determine the “ultimate” capacity of the pile. The most common method used in the United States is Davisson’s Method, which is outlined in Figure 24.



1. Calculate elastic compression of pile (δ_E) when considered as a free column by:

$$\delta_E = \frac{QL_p}{AE}$$

Q = test load, lbs
 L_p = pile length, in. (for end-bearing pile)
 A = cross-sectional area of pile material, sq in
 E = Young's Modulus for pile material, psi
2. Determine scales of plot such that slope of pile elastic compression line is approximately 20°.
3. Plot pile head total displacement vs. applied load.
4. Failure load is defined as that load which produces a displacement of the pile head equal to:

$$S_f = \delta_E + (.15 + \frac{D}{120})$$

S_f = displacement at failure, in.
 D = pile diameter, in.
5. Plot failure criterion as described in (4), represented as a straight line, parallel to line of pile elastic compression. Intersection of failure criterion with observed load deflection curve defines failure load, Q_f .
6. Where observed load displacement curve does not intersect failure criterion, the maximum test load should be taken as the failure load.
7. Apply factor of safety of at least 2.0 to failure load to determine allowable load.

Figure 24 Davisson's Method of Interpreting Static Load Tests (after Naval Facilities Engineering Command (1986))

Davisson's Method, being an "offset yield" method, does not require that the pile be tested to plunging failure. It is also relatively straightforward to interpret, although if done graphically it can be very sensitive to plotting errors.

Other methods do in fact either require some degree of plunging failure or attempt to anticipate it in their methodology. Given the different approaches to static load interpretation, which are represented in different codes, it makes sense to incorporate more than one interpretation criterion in the static routine. Unfortunately many methods were developed for hand processing of load-deflection curves, and their implementation with numerically generated results is not always clear.

That being the case, in this study five different methods are used to interpret static load tests. Information on these can be found in Kyfor et. al. (1992) and Fellenius (2014). They are as follows:

1. Davisson's Method, described in Figure 24. For all methods the load-deflection curve is considered as a piecewise linear interpolation of the data points; Davisson's ultimate load is determined where the two lines (Davisson's Line and the piecewise interpolated line) intersect.
2. Brinch-Hansen's 80% Method, where the ultimate load is where 80% of that load takes place at 25% of the ultimate deflection. Although methods have been developed to mathematically approximate the load-deflection curve (and thus make the determination more accurate,) in this case actual data points were used to determine the load at which the criterion was met.
3. Brinch-Hansen's 90% Method, where the ultimate load is where 90% of that load takes place at 50% of the ultimate deflection. Analysis procedures are similar to the 80% Method.
4. Maximum Curvature Method. As piecewise linear interpolation is used, the point at which the slopes of the two lines connected to it have the greatest difference is the point of maximum curvature.

5. Slope-Tangent Method. In this method the intersection of two lines is considered. One is the first piecewise line whose slope exceeds $142.7 \times 10^{-9} \text{ m/N}$. The other is the initial slope of the load-deflection curve. Since this can be difficult to determine accurately, Davisson's Line was moved upwards so that it intersected the origin.

Given the variety methods used, wide variations in the results are reasonable to expect and in fact take place (Kyfor et. al. (1992)). For methods other than Davisson's, linear interpolation to determine slopes and ultimate points was avoided. This forced more data points to be taken than the plasticity methodology actually required, but illustrates an advantage of computer generated load-deflection results over field data: the former has greater flexibility in determining the load step. The end result is that the static axial capacity (ultimate, allowable or factored) from static load tests is not univocal.

Dynamic Analysis

Now that the methodology—and the shortcomings—of static methods have been discussed, the dynamic implementation of the model can be described.

Explicit and Implicit Schemes

The scheme presented in Smith (1955) is an “explicit” scheme. So what does this mean? It is a little easier to explain this in terms of finite difference methods with uniform spatial and temporal differences. As an example of this, the “one-way” (semi-infinite) undamped wave equation, as shown by Warrington (1997), will be used. It is given by the expression

$$\frac{\partial}{\partial t} u(x, t) = -c_a \frac{\partial}{\partial x} u(x, t) \quad (76)$$

Use of this equation also allows the development of numerical schemes without the complications of either the second derivatives or dampening/elastic terms. LeVeque (1992) refers to this as the time-dependent Cauchy problem, and the following treatment of the solution is based on his presentation.

Because this is a dynamic (time-varying) phenomenon, time as well as distance must be discretized. This is done through what are referred to as “time-marching” schemes of one kind or another. For one-dimensional analyses of pile dynamics, the whole process is relatively simple compared to two-or three-dimensional problems in such fields as fluid dynamics or solid mechanics. The time step chosen depends upon both the nature of the system and the numerical integration scheme.

When the Explicit or Backward Euler scheme is applied to Equation 76, the result is

$$\frac{u(x, t)_i^{n+1} - u(x, t)_i^n}{\Delta t} = -c_a \frac{u(x, t)_{i+1}^n - u(x, t)_{i-1}^n}{2\Delta x} \quad (77)$$

The time discretization can be seen on the left-hand side, and the spatial discretization can be seen on the right. Schemes such as this can be (and usually are) derived for ordinary or partial differential equations using Taylor series expansions, which would include consideration of higher order terms.

In this case n , $n + 1$ are not powers but represent the point in time where the system is “marching,” n being the current time step and $n + 1$ being the next one. The subscript i is the data point; the point $i + 1$ is the data point “in front of” the one under consideration and $i - 1$ is the one behind it.

Knowing the conditions of the current point in time n , Equation 77 can be explicitly solved for the value of $u(x, t)$ for the next time step, thus the designation explicit:

$$u(x, t)_i^{n+1} = u(x, t)_i^n - \frac{c_a \Delta t}{2 \Delta x} (u(x, t)_{i+1}^n - u(x, t)_{i-1}^n) \quad (78)$$

At this point the Courant-Friedrichs-Lewy (CFL) number is defined,

$$\nu_{CFL} = \frac{c_a \Delta t}{\Delta x} \quad (79)$$

and substituting Equation 79 into 78,

$$u(x, t)_i^{n+1} = u(x, t)_i^n - \frac{\nu_{CFL}}{2} (u(x, t)_{i+1}^n - u(x, t)_{i-1}^n) \quad (80)$$

The consistency of Equations 76 and 77 (and thus Equation 80) is easy to see. Unfortunately, although the method is certainly consistent, in order for the scheme to converge it must, by the Lax Equivalence Theorem for linear equations, be stable. Unfortunately, it can be shown that Equation 80 is unstable for any value of ν_{CFL} .

A more satisfactory result takes place when an “upwind” scheme is used.

Equation 76 is thus expressed discretely in the following way:

$$\frac{u(x, t)_i^{n+1} - u(x, t)_i^n}{\Delta t} = -c_a \frac{u(x, t)_i^n - u(x, t)_{i-1}^n}{\Delta x} \quad (81)$$

Equation 81 can be solved to

$$u(x, t)_i^{n+1} = u(x, t)_i^n - \nu_{CFL} (u(x, t)_i^n - u(x, t)_{i-1}^n) \quad (82)$$

It can be shown that this scheme is conditionally stable, the condition being that

$$\nu_{CFL} \leq 1 \quad (83)$$

It is interesting to note that, in some ways, the scheme used by Smith (1955) is similar to Equation 82. Upwind schemes, as the name implies, are most effective

when the wave propagation is unidirectional, which is not the case with driven piles.

As seen here, explicit schemes are widely variable in their performance. However, Lomax et. al. (2003) note that none of the explicit schemes are “A-stable,” which means that “it is unconditionally stable for all ODE’s (ordinary differential equations) that are stable.” This not only includes schemes such as explicit Euler but also predictor-corrector methods such as the well-known Runge-Kutta techniques, one of which was employed by Bossard and Corté (1983). This means that all explicit schemes have limitations on their time steps to insure stability, unless of course, like the original explicit Euler scheme, they are unconditionally unstable, in which case there is no time step that will insure stability.

There are also “implicit” schemes as well. Starting again with Equation 76, the Implicit Euler scheme can be written as follows:

$$\frac{u(x, t)_i^{n+1} - u(x, t)_i^n}{\Delta t} = -c_a \frac{u(x, t)_{i+1}^{n+1} - u(x, t)_{i-1}^{n+1}}{2\Delta x} \quad (84)$$

which can be rearranged (the CFL number being defined by Equation 79) to become

$$u(x, t)_i^{n+1} = u(x, t)_i^n - \frac{\nu_{CFL}}{2} (u(x, t)_{i+1}^{n+1} - u(x, t)_{i-1}^{n+1}) \quad (85)$$

Note that the desired quantity $u(x, t)_i^{n+1}$ cannot be solved for from terms in time n , thus the designation implicit. In simple terms, explicit schemes predict the future by computing the next step from present data, and implicit schemes compute the next step from both present and future data. It can be shown that Equation 85 is stable for any value of ν_{CFL} , i.e. it is unconditionally or “A” stable. There is no limit on the time step except that peaks in the results may be missed with an excessively high time step. Not all implicit schemes are unconditionally stable, but most in

practical use are, and incur a higher computational cost that accompanies their use relative to explicit schemes.

Both implicit and explicit schemes exist for finite element analysis as well as finite difference, and many of the same stability considerations apply to both. So it is necessary to consider both in approaching the problem of pile dynamics.

Implicit schemes are not unknown in wave propagation analysis in piles; one (Wilson's Theta Method) was used by Smith and Chow (1982) and To (1985). Although in principle implicit methods should be advantageous because they allow longer time steps (and thus fewer computational steps,) in reality there is a trade-off between the number of computational steps, the cost for each step, and time accuracy. With an implicit method it is necessary (directly or indirectly) to invert the entire stiffness and mass matrices (or some combination) and perform complete matrix multiplications.

With an explicit method, this is unnecessary; the computations can be done using local stiffness matrices only, and the mass matrix can be lumped (diagonalized,) which makes its inversion trivial. Additionally, in principle the CFL criterion for maximum time step requires extraction of the eigenvalues from the stiffness and mass matrices. This is a tedious procedure, even from the standpoint of linear algebra. A more expeditious method is to combine the geometry of the elements with the acoustic speed of the material and limit the time step to the shortest time required for the stress wave to traverse an element at its "shortest" distance (Cook, Malkus and Plesha (1989)). Mathematically this can be expressed as

$$\nu_{CFL} = \frac{c_a \Delta t}{L_{min}} \leq 1 \quad (86)$$

The value for L_{min} is taken to be the shortest side length of the element; that length is then multiplied by the maximum CFL criterion and then divided by the

acoustic speed of the element material to determine the time step that element “recommends” to the model. The smallest time step found in the model becomes the time step for the system. Because the determination of L_{min} is inexact and due to other factors, Cook, Malkus and Plesha (1989) recommend that v_{CFL} should be set between 0.95-0.98. Another explanation of minimum time steps for such methods is given in Hughes (2000).

How the computational cost comparison works out depends upon the nature of the model. While Smith and Chow (1982) and To (1985) come down on the side of implicit methods, Randolph and Simons (1986) find explicit methods advantageous. Although an implicit scheme was included in STADYN, ultimately an explicit scheme was chosen for the dynamic analysis of this study based on a more compelling consideration: the non-linearity of the problem.

Consider the elasto-plastic model as depicted in Figure 9. At low values of strain, elasticity applies and the relationship between stress and strain is determined by the slope of the line, the modulus of elasticity. In the elasto-plastic models considered, the reality is that the relationship between stress and strain is always linear; the key difference between the elastic and plastic regions is that, upon entrance into the plastic region, there are irrecoverable strains which take place. Cook, Malkus and Plesha (1989) observe that, in the plastic region, there is a plastic modulus, which is less than the elastic modulus and, in the case of softening materials, actually negative. They also observe that, in this region, the acoustic speed is lower than that in the elastic region, according to Equation 68. This is a similar phenomenon to that of the variations in elastic modulus and acoustic speed based on strain, which complicated the determination of the applicable soil properties.

With a purely elasto-plastic model, the plastic modulus is zero, and thus the acoustic speed is also zero. This effectively decouples the mass from the elasticity in the purely plastic region. This result is more pronounced as the time (and thus the distance) step is increased; the model tends to “skip over” the elastic region and the inertial effects in that region. Thus with larger time steps inertial effects are significantly reduced, and their ability to resist pile movement is likewise reduced.

This phenomenon was actually encountered during the development of the model. As long as an elastic test case was being performed, the implicit method performed well, obtaining results very close to the analytical solution and virtually invariant with changes in time step. When plasticity was introduced, the time step had a great deal of effect on the performance of the model. This type of result is not unique to this study; it also appears in McNamara (1974).

This phenomenon significantly reduces the potential utility of implicit methods. Unless time steps determined by very small elements in the hammer are much less than the time steps determined by the rest of the system, the back substitution and Newton stepping required by implicit methods make them uneconomical compared to explicit methods. Since the non-linear physics of the problem restrict the time step to time steps in the same range as the CFL requirement for explicit schemes, the additional cost of implicit schemes is questionable at best. Thus an explicit scheme was used for all of the dynamic analysis in this study.

One possible alternative to this binary decision would have been to use a mixed formulation with both in the same routine (Hughes and Liu (1978)), but this was not used in this study due to the continued need for matrix inversion with small time steps.

Newmark Explicit Stepping Scheme for Dynamic Analysis

With dynamic analysis, the obvious choice for an integration scheme was Newmark's (Newmark and Rosenbleuth (1971)). The explicit method used was adapted from Hughes (2000), taking plasticity into consideration.

For both explicit and implicit methods, the Newmark coefficients are defined as

$$c_1 = \frac{\Delta t^2}{2} (1 - 2\beta) \quad (87)$$

$$c_2 = \Delta t \gamma \quad (88)$$

$$c_3 = \Delta t (1 - \gamma) \quad (89)$$

$$c_4 = \Delta t^2 \beta \quad (90)$$

$$c_5 = \Delta t \quad (91)$$

In both cases the Newmark constant $\gamma = 1/2$. For the explicit case the Newmark constant $\beta = 0$.

To set up the explicit method, the time step Δt was computed by the procedure noted earlier, except that, in solving Equation 86, $\nu_{CFL} = 3/4$, based on experience with the model. After this, the stiffness and consistent mass matrices are developed. For an explicit method, the stiffness matrix is, strictly speaking, unnecessary, but since the two matrices are generated together using the same shape functions it is more convenient to do them both. The consistent mass matrix is then lumped into a diagonal matrix.

Having computed the effects of effective stress, the time stepping can begin. The Newmark method is a predictor-corrector method; considering time 0 as the beginning of the time step and time 1 as the end, the predictor equations are

$$\begin{aligned}\tilde{d}_1 &= d_0 + c_5 v_0 + c_1 a_0 \\ \tilde{v}_1 &= v_0 + c_3 a_0\end{aligned}\tag{92}$$

The recursion relationship is similar to Equation 75 and is

$$Ma_1 = f - p + s\tag{93}$$

To solve for the acceleration vector, the external force, internal force and effective stress vectors are computed in the same fashion as they are with static loading (the internal force vector uses the results of Equation 92) and then the inverted lumped mass matrix is multiplied by the right hand side to produce a_1 . The corrector equations are

$$\begin{aligned}d_1 &= \tilde{d}_1 \\ v_1 &= \tilde{v}_1 + c_2 a_1\end{aligned}\tag{94}$$

Because the time steps are so small, it is certainly possible but generally unnecessary to Newton step with explicit methods, so the next time step is proceeded to directly with the time 1 of the previous step becoming time 0 of the next one.

Newmark Implicit Stepping Scheme for Dynamic Analysis

In some ways, the implicit method combines the explicit method's dynamic predictor-corrector methodology with the static method's Newton stepping. Because $\beta = 1/4$, unconditional stability with any time step is obtained, which in principle can save a great deal of computational effort. The effects of plasticity, however, affect this significantly.

The method used comes from Owen and Hinton (1980). The stiffness and consistent mass matrices are assembled; however, the stiffness matrix is reduced

for back substitution and the mass matrix remains consistent. Using the Newmark coefficients in Equations 87-91, for each time step the predictor relationship is

$$\tilde{d}_1 = d_0 + c_5 v_0 + c_1 a_0 \quad (95)$$

$$\hat{v}_1 = v_0 + c_3 a_0$$

$$a_1 = 0$$

$$d_1 = \tilde{d}_1$$

$$v_1 = \hat{v}_1$$

The recursion relationship is

$$\left(K + \frac{M}{c_4} \right) \Delta d = f - p + s - M a_1 \quad (96)$$

As before, this is solved using values from Equation 95 and the result is inserted into the corrector equation

$$d_1 = d_1 + \Delta d \quad (97)$$

$$a_1 = \frac{d_1 - \tilde{d}_1}{c_4}$$

$$v_1 = \hat{v}_1 + c_2 a_1$$

The result for Δd is then checked for convergence. If convergence had not been achieved, then Equation 96 was solved again. As noted earlier, this routine was not used in the actual analysis.

Inputs at the Pile Head

From a physical standpoint, what actually drives the pile is the force generated by the hammer upon impact. There are two ways of modeling this in this routine.

The first was to explicitly model the pile hammer, hammer cushion, driving accessory and pile cushion. Not all of these components will be a part of every hammer system.

The second was to input an external time-varying force f into the recursion relationships (Equations 93 and 96.) Assuming a uniform pressure q on the pile head, the force was distributed among the pile head nodes and then directly applied using the recursion relationships. This done, the response of the model could be recorded.

Although an assumed or field force-time relationship can be used for single runs, the most important application of assumed force-time and velocity-time histories is the inverse method. In these cases, since force-time and velocity-time histories are known, the explicit modeling of the hammer is unnecessary. Although it is possible to “match” the hammer with the data (Dolwin and Poskitt (1982)), to do so requires that the hammer system being modeled be the same as the one used to drive the pile, and given the variations in hammer configuration this can be difficult. A more common matching problem is to match the soil properties with the data, which will be discussed below.

If the force-time data are matched in time with each time step of the model, it can be used directly. For many cases this is not possible; thus, an interpolation technique is necessary. The interpolation technique used in this model is a cubic spline as implemented by King (1984). This technique produced force-time and velocity-time results with the optimum combination of smoothness and accuracy. This minimized spurious artifacts in the data that degrade accuracy and introduce numerical noise into the system.

Modeling of the Pile Hammer

The description of the dynamic stepping scheme is an appropriate place to describe the inclusion of the last part of the physical system under investigation: the pile hammer. Pile dynamics is an interdisciplinary field that draws from geotechnical engineering, engineering mechanics, computational engineering and equipment design and simulation, and no where is this more evident than in the modeling of the pile hammer.

The variations in hammer construction and operation principle are numerous (Warrington (2007)). Their modeling has been a major part of the development of successful wave equation analysis, especially the inclusion of diesel hammers (Goble and Rausche (1976)). In order to focus the efforts on the research at hand, the types of hammers were restricted as follows:

1. All the hammers analyzed were external combustion hammers (Hannigan et. al. (2006)), although with the extensible interface developed addition of the combustion pressures is not a difficult task.
2. Hammers with hammer cushions and simple cross-sections were included.
3. Hammers without cushions can be modeled. This includes the “standard” ram-cap configuration and a “direct-drive” anvil type of configuration.

Interface Elements for the Hammer and Cap Portion of the Model

Earlier the use of special interface elements for the pile-soil interface was ruled out for this study. With the inextensible interfaces between the driving accessory and the pile head and those between the ram and the driving accessory (with or without hammer cushion) some kind of interface element was unavoidable.

Studies in the past that used interface elements, such as To (1985), were forced to mate the eight-node serendipity elements with six-node interface elements, as the latter had no depth. One additional advantage of using four-node quadrilaterals is that the interface elements are likewise four-node, which means that the stiffness and mass matrix assembly procedures are uniform. Although Isenberg (1972) developed interface elements for use with four-node quadrilaterals, for this study these elements were developed using the method of Zeevaert (1980). Consider the interface element shown in Figure 25.

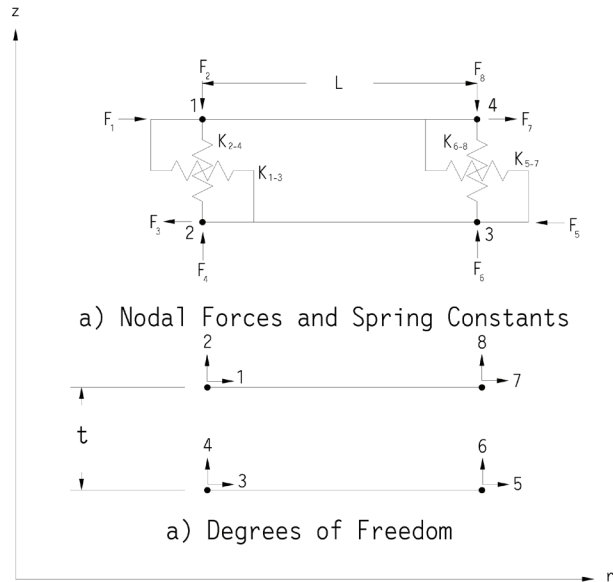


Figure 25 Four-Node Interface Element (format after Zeevaert (1980))

The analysis can be simplified from a general development with the following assumptions:

1. The interface elements in the hammer were always horizontal, thus there is no angle from the horizontal axis.

2. The development was only for axisymmetric elements.

Using the same local coordinate system employed for both the four-node quadrilateral elements themselves and the xi-eta soil property system, the nodal forces were

$$F_i = \int_{-1}^1 2\pi r q H_n dr \quad (98)$$

Using the appropriate shape functions applied to the appropriate nodes, the interface nodal forces were

$$F_{1,2,3,4} = q \times AV_1 \quad (99)$$

$$F_{5,6,7,8} = q \times AV_2$$

where the subscripts of F were local degrees of freedom and the integrated constants are

$$AV_1 = \frac{L_{inter}}{2} \left(r_{avg} - \frac{L_{inter}}{6} \right) \quad (100)$$

$$AV_2 = \frac{L_{inter}}{2} \left(r_{avg} + \frac{L_{inter}}{6} \right)$$

where

$$L_{inter} = r_7 - r_1 = r_5 - r_3 \quad (101)$$

and

$$r_{avg} = \frac{r_7 + r_1}{2} = \frac{r_5 + r_3}{2} \quad (102)$$

At this point, there were two ways the spring constants could be determined. Zeevaert (1980) uses the interface elements in the semi-infinite soil mass, so he uses the coefficient of subgrade reaction, thus

$$\begin{aligned} K_{1-3,5-7} &= k_s \times AV_1 \\ K_{2-4,6-8} &= k_n \times AV_2 \end{aligned} \quad (103)$$

Although in theory the shear and normal spring constants are the same, in reality the shear constants were not very relevant physically for the interfaces under study. To reduce any spurious oscillations due to these, they were softened by assuming $k_s = \frac{k_n}{10}$.

The coefficient of subgrade reaction was dependent on the material properties of the semi-infinite mass and the geometry of the pressure-bearing member. Using Boussinesq theory with an applied ring load (Verruijt and van Bars (2007)), the coefficient of subgrade reaction for an interface with a given material is

$$k_n = \frac{E}{2L(1 - \nu^2)} \quad (104)$$

This was the initial approach for uncushioned interfaces such as the driving accessory-pile interface with steel piling.

With a hammer cushion, however, there is a body with elasticity and thickness. For elements with a known thickness, the “coefficient of subgrade reaction” can be computed using

$$k_n = \frac{E}{t_{inter}} \quad (105)$$

The approach of Equation 104 assumes that the elements had no thickness. However, as can be seen in Desai et.al. (1984), all interface elements had some kind

of thickness, expressed or implied. Equating Equations 104 and 105 yielded this implied thickness as

$$t_{implied} = 2L(1 - \nu^2) \quad (106)$$

Variation of this implied thickness became important in the control of parasite oscillations.

The spring constants that appear in Equation 103 suggested the construction of a diagonal local stiffness matrix

$$S_{ier} = \begin{bmatrix} K_{1-3} & 0 & 0 & 0 \\ 0 & K_{2-4} & 0 & 0 \\ 0 & 0 & K_{5-7} & 0 \\ 0 & 0 & 0 & K_{6-8} \end{bmatrix} \quad (107)$$

However, the primary variable is displacement; the spring constants were based on the difference in displacements between two degrees of freedom. To convert from one to another required a transformation matrix, thus

$$B = \begin{bmatrix} -1 & 0 & 1 & 0 & 0 & 0 & 0 & 0 \\ 0 & -1 & 0 & 1 & 0 & 0 & 0 & 0 \\ 0 & 0 & 0 & 0 & 1 & 0 & -1 & 0 \\ 0 & 0 & 0 & 0 & 0 & 1 & 0 & -1 \end{bmatrix} \quad (108)$$

The local stiffness matrix for an interface element could be computed as follows:

$$K_{local} = B^t S_{ier} B \quad (109)$$

which could then be used in the same way as all the other local stiffness matrices. The local stiffness matrix thus developed was symmetric and has no zeroes on the diagonal.

During time stepping, when the vertical forces acting on the interface element put the element in tension, they were zeroed out, as are the corresponding horizontal forces. In this way, the element is inextensible.

One place where inextensible elements could be useful is at the pile toe. For this study, since all of the static testing was in compression and all of the dynamic impact was downward, this was not employed. Had either or both of these conditions been included, then toe inextensibility would have to be included.

Pile Hammer Model

An example of a pile hammer model is shown in Figure 26.

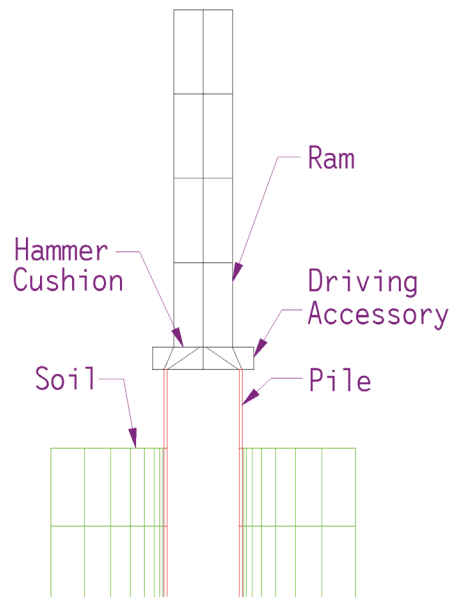


Figure 26 Pile Hammer Model

The interface between the pile and the driving accessory was an inextensible interface as previously described. Although a hammer cushion is shown, that interface could also be a “steel on steel” impact interface as well. The ram had a uniform cross-section, although the program could be modified for non-uniform cross sections. The hammer cushion thickness was not reflected in the finite element geometry but it was modeled as an inextensible interface. The “half section,” which is how the system is modeled using symmetry, has been mirrored for clarity.

The ram was given an initial velocity based on its actual or equivalent stroke and a mechanical efficiency. Effects due to gravity were not included in this model, as they would further complicate the situation with the effective stresses.

The modeling of the driving accessory made it possible to model beam effects in the cap. When the diameter of the cushion/impact point is much smaller than the inside diameter of the pile (assuming the latter is hollow) and the cap is relatively thin, plate effects can become significant. These are not considered at all in the one-dimensional model unless the cap stiffness includes beam effects; the model shown here is obviously more detailed and reduces the number of assumptions. The cap geometry was kept simple for ease of program operation and to prevent further reduction of the time step due to small elements; it certainly could be modeled in more detail if the situation calls for it.

Parasite Oscillations

One place where the limitations of dynamic numerical integration schemes manifest themselves is a phenomenon noted by Bossard and Corté (1983): “parasite oscillations” where the numerical model exhibits high-frequency vibrations that largely do not correspond to physical reality. They are the result of the confluence of

two factors, one coming from the nature of the loading and the other the nature of numerical integration in general and the Newmark numerical integration scheme in particular.

Absent from Equation 7 are the Heaviside step functions (Rausche, Goble and Likins (1985); Warrington (1997)), which denote a sharp discontinuity between what is ahead of the leading edge of the stress-wave (no stress) and behind it (stress.) This means that each blow of the hammer sends what amounts to a shock wave down the pile. These are a challenge to any discretization and numerical integration system. With a given pile head force, this phenomenon is mitigated by the fact that the driving accessory's inertia will soften the rate of increase of the pile head force and stresses. Thus, in the inverse method parasite oscillations, although present, are more easily managed. With the hammer explicitly modeled, the interface between the hammer and the driving accessory or anvil–cushioned or not–has an instantaneous ram point velocity on one side and zero initial velocity on the other. Under these conditions, especially with cushionless impact, parasite oscillations are unavoidable.

Newmark's integration scheme, although the most popular integration scheme in dynamic finite element analysis, is subject to parasite oscillations, especially with secondary variables such as stress, force and velocity. This difficulty is discussed in detail by Deeks (1992).

Probably the most practical approach to dealing with parasite oscillations is to manage them as opposed to requiring their complete elimination. Attempting the latter runs the risk of creating one set of system distortions in order to eliminate another. Having said that, there are three measures that were or can be taken to eliminate these spurious effects:

1. Substituting the four-node quadrilaterals for the higher-order elements, which eliminated much of the general numerical noise of the system, even before the effect of interface elements was included.
2. Adding dampening or other non-linearity (such as a “coefficient of restitution”) to the interfaces, to say nothing of the rest of the model. This is common with the finite-difference methods in use today. All materials have some degree of material dampening in them; however, the relationship between the actual material dampening and the amount added to the numerical models is not clear. This is especially true with the impact interfaces; very little work has been done on studying the nature of these in pile driving.
3. Changing the numerical method to one that includes some type of algorithmic dampening which attenuates high-frequency parasite oscillations. Most of these integration schemes are implicit and the difficulties with using an implicit scheme in this application have already been discussed in detail.

Given the limitations of the system, having switched the type of element, probably the best solution is to include some kind of dampening in the places where spurious oscillations are generated. Up until now, no velocity-dependent dampening coefficients have been included in this system. All dissipative effects have taken place with the Mohr-Coulomb plasticity. To add this—especially with the small number of elements in question—is not difficult, but another approach may be more appropriate for this system: the inclusion of Rayleigh (or more precisely pseudo-Rayleigh) dampening at the interfaces through the inclusion of mass in the interface elements which is associated with the stiffness.

To see how this might work, consider Equation 98 and, instead of the uniform pressure q on the surface, the interface element is a plate with a constant density ρ and a constant thickness t_{inter} . Equation 98 would then be rewritten

$$F_i = \int_{-1}^1 2\pi r \rho t_{inter} H_n dr \quad (110)$$

The masses would then be

$$\begin{aligned} m_{1,2,3,4} &= \rho t \times AV_1 \\ m_{5,6,7,8} &= \rho t \times AV_2 \end{aligned} \quad (111)$$

The shape function based constants are the same for both. Since the directionality of the masses is already determined and the nodal accelerations are absolute and not relative to another node, a diagonal mass matrix can be constructed as follows:

$$M_{local} = \begin{pmatrix} m_1 & 0 & 0 & 0 & 0 & 0 & 0 & 0 \\ 0 & m_2 & 0 & 0 & 0 & 0 & 0 & 0 \\ 0 & 0 & m_3 & 0 & 0 & 0 & 0 & 0 \\ 0 & 0 & 0 & m_4 & 0 & 0 & 0 & 0 \\ 0 & 0 & 0 & 0 & m_5 & 0 & 0 & 0 \\ 0 & 0 & 0 & 0 & 0 & m_6 & 0 & 0 \\ 0 & 0 & 0 & 0 & 0 & 0 & m_7 & 0 \\ 0 & 0 & 0 & 0 & 0 & 0 & 0 & m_8 \end{pmatrix} \quad (112)$$

Although it is possible to use transformation matrices to construct a consistent mass matrix, given that explicit methods are used for dynamic analysis, the effort is not worthwhile.

For hammer and pile cushions, the mass matrix of Equation 112 is physically meaningful; the cushion material has physical mass and this is reflected in the mass matrix for the element. Modeling cushion mass is generally not done with piling wave equation routines, but it certainly appears here. Also, examination of

Equations 105 and 111 shows that element thickness has the opposite effect on stiffness than it does on mass; as t_{inter} increases, the stiffness decreased while the mass increased, which for hammer and pile cushion corresponds with reality.

With other interfaces, the mass is physically artificial, but so is the stiffness as well. The idea of including mass in these types of interfaces is that, if the stiffness must be reduced to smooth parasite oscillations, the mass increases to compensate for the loss of resistance of the interface. How well this works out will be shown below.

CHAPTER V

INVERSE METHOD AND OPTIMIZATION

With the basic configuration of the model confirmed, the inverse problem is now considered. Some of the basic difficulties—uniqueness, non-linearity, and the like—have been discussed in a preliminary way. Now it is necessary to put these to some kind of application, even if that application is very elementary.

Overview of the Problem

Generally speaking, determination of pile capacities and resistances from dynamic tests are taken from pile head data. In the “classic” setup for CAPWAP, for example, strain gauges and accelerometers are mounted at the top of the pile. During the impact time, these measure material strain and acceleration. The former is converted into pile head force by including the elastic modulus and pile head cross-sectional area of the pile; the latter is integrated to velocity. With some methods (such as SIMBAT) a theodolite is mounted at the pile head which measures pile head displacement. Although instrumenting piles at points below the pile head (especially the pile middle and pile toe) has a long history going back to Glanville et.al. (1938), and there are certainly advantages to doing so, this practice is generally restricted to research work. For the majority of actual job-site dynamic pile monitoring only the pile head is instrumented.

Once the data are gathered, there are two basic approaches to for reduction. The first is to take the velocity-time data and successively modify the pile-soil model so that the computed force-time data match that taken from the strain gauges

(Goble (1983)). The second is to do the opposite, to take the force-time curve as a model input and match the computed velocity-time curve with the relationship given by the field data.

This is deceptively simple; pile-soil responses to impact are complex. It is first necessary to model the pile properly, both in terms of segment length (piles can change in both cross-sectional area and material) and material properties. With steel the material properties are fairly consistent; with concrete and especially wood, more variability can be expected. Failure to do so will result in it being impossible to obtain a proper signal match under any conditions.

Use of Optimization and Signal Matching Techniques

Overview

From a purely mathematical standpoint, the existence of multiple input variables (the soil properties at various points along the pile shaft and at the toe) and the possibility of aggregating them into one result (the difference between the computed and actual velocity-time or displacement-time histories) make optimization techniques a natural for the application. However, due to both the nature of the problem and optimization techniques themselves, actually implementing that successfully has many pitfalls which must be navigated carefully.

Gill, Murray and Wright (1981) describe three basic elements to an optimization problem:

1. The objective function, which is the function to be minimized. For this problem, it is the result of the dynamic simulation of the pile under a predetermined

force-time relationship, which is then aggregated into the difference between the computed and actual velocity-time or displacement-time history.

2. The input variables for the objective function, which are in this case the xi-eta soil properties for various segments of the pile shaft and at the pile toe. The use of the xi-eta soil model is largely aimed at use in optimization. By aggregating the soil properties into two relatively simple variables, the objective function is in turn simplified and more precisely defined.
3. The constraints, which are on the input variables. These constraints and the objective function are referred to as the problem function. Problems without constraints on the input variables are, obviously, unconstrained optimizations, and have the most general techniques, although there are ways to constrain the input variables even with these types of techniques.

To arrive at a result, the optimization method inputs initial values for the input variables into the objective function, which returns a result. The optimization technique then adjusts the input variables subject to the constraints (if any) and recomputes the objective function. This process is repeated until the objective function is minimized. It is thus necessary to set up the objective function so that the desired result is a minimum (or maximum.)

Implementation in STADYN

For each optimization step, using the pile geometric and material properties and the xi-eta soil inputs, the stiffness and mass matrices are constructed, as varying the soil properties will change both. Then the dynamic model is run with the force-time history as an input and the computed velocity-time history as an output. This is reversed from CAPWAP; however, the nature of finite element

analysis, with the external forces as a right-hand input and the velocities as an output, make this arrangement more natural to the solution technique.

With the computed velocity-time history in hand, a comparison with the actual data is necessary to achieve the result of the optimization step. There are two ways of accomplishing this. The first is to compare the computed velocity-time history with the actual one, which is interpolated from the data. The second is, using the trapezoidal rule, to integrate the actual data to an actual displacement time history and compare this to the computed displacement-time history. The former method has the advantage of using the data directly, albeit integrated in the field; the latter has the advantage of using a primary variable in the finite element analysis.

Depending upon which comparison is being done, computed and field data are compared to arrive at a least mean squared difference between the two. Manley (1945) defines this as:

$$LMS = \frac{1}{N} \sum_{n=1}^{n=N} (y_r - S_r)^2 \quad (113)$$

One can also take the square root of the sum and produce a Euclidean norm, thus for displacement and velocity,

$$\Delta d_{rms} = \frac{1}{N} \sqrt{\sum_{n=1}^{n=N} (d_{t_{act}} - d_{t_{comp}})^2} \quad (114)$$

$$\Delta v_{rms} = \frac{1}{N} \sqrt{\sum_{n=1}^{n=N} (v_{t_{act}} - v_{t_{comp}})^2} \quad (115)$$

Using a Euclidean norm approach makes the difference function essentially linear. Linearity of difference function is also the case with CAPWAP's Match Quality (Rausche et.al. (2010)). The advantage of this is that the descent in the

early portion of the optimization is not as steep as with a true least-squares approach, which is one method of avoiding selecting a local minimum. The scale factor can also be placed under the square root, although the best way to keep comparison between runs comparable is to retain the same scale factor/number of data points for all the runs optimized.

Once this is computed new values for input variables can be computed and the run repeated until convergence is achieved, i.e., a variation tolerance is achieved. Although unconstrained optimization techniques are used, the input variables themselves are constrained. This was discussed in the description of the soil properties.

In the early portion of the research, an attempt was made to reduce the cost somewhat by stopping the analysis at a point which is at a time $2L/c$ later than the first maximum peak of the velocity-time curve after impact. (For most pile dynamics problems, the first force-time and velocity-time maxima take place simultaneously.) By this time stress waves from all parts of the pile have had a chance to be reflected from various points along the pile shaft and from the pile toe and be modified by both changes in the pile profile (including both material and cross-sectional changes) and modifications due to pile-soil interaction. However, the interaction between pile and soil proved more complex than originally anticipated; there was valuable information in the velocity-time history after the original stopping point and divergence was noted in some runs after that time. Thus, for completeness virtually all of the signal available was included in the analysis.

Also, in the earlier portion of the research, both velocity-and displacement-matching techniques (Equations 114 and 115) were attempted. Although in principle either should be satisfactory, velocity matching produced more consistent results, and thus Equation 115 was used for most of the study.

Selection of an Optimization Technique

With the ability to produce a scalar value to minimize, it is necessary to select an optimization technique. As is the case with many things in geotechnical engineering, this is not as straightforward of a process as it may seem.

An early attempt to use optimization techniques for this problem was Dolwin and Poskitt (1982). They employed a Newton type of optimization, but their objective was a little different from conventional inverse methods for this type of problem in that they attempted to size an optimum hammer for a given pile-soil system. Although they, as is the case here, applied constraints to the variables, the difficulty in optimizing the pile hammer is that pile hammer parameters are not an arbitrary combination of the variables but a limited combination of them for the various hammer sizes, types and driving accessory and cushion combinations. It is easy under these conditions to specify a hammer that does not exist. Although some customization of hammers is common in this industry, even with the largest hammers there is only a fixed number of models to choose from.

Use of a Newton type of optimization is obviously a desirable objective, and to that end the original idea of this project was to use the UNCMIN optimizer (Schnabel, Koontz and Weiss (1985)). In this way the optimizer would be integral to STADYN and not require a separate routine for optimization.

The difficulty with this type of optimization is in the nature of the functions themselves. The objective function, the result of a finite element run, is not a simple one, and there is no guarantee of things such as differentiability, smoothness, etc., of either the functions or its derivatives. The finite difference gradients (and Hessians if necessary) are tedious to generate and may yield undesirable results in the event differentiability is a problem. A more serious problem is that of local minima; it is easy for a routine such as this to find a local minimum when in fact

the global minimum is at another location and for a different set of variable values. This is one reason why grid optimizations are often found in geotechnical routines, but grid optimization is simply too inefficient for this application.

With Newton type unconstrained minimization shown unsatisfactory, other optimization techniques have been used, including genetic algorithms (Balthaus (1988)) and neural networks (Chow et.al. (1995); Shahin, Jaksa and Maier (2001)). Both of these are considerably more complex—and slower—than Newton type methods. Since speed is to be compromised, a simpler approach was finally arrived at for this routine, namely a polytope algorithm (Gill, Murray and Wright (1981)). An overview of direct search methods in general and the polytope method in particular can be found in Lewis, Torczon and Trosset (2000). STADYN's implementation was modified from Press et.al. (1992). In addition to getting around the formal requirements for differentiability, etc., a major advantage of the polytope algorithm is that, at the beginning of the optimization, it is necessary to form the polytope, i.e., a set of initial combinations of the variables, in the number of the number of variables plus one. Selection of starting variables in a broad range of ξ and η values reduces the possibility that a local minimum will be arrived at and increases the possibility of finding the true minimum of the problem function.

Even with the broad starting point the polytope method afforded, some of the results suggested that some further search for a real minimum was in order. To accomplish this annealing was added to the polytope routine using a code modified from Press et.al. (1992). Both unannealed and annealed optimizations were performed.

Once the optimization technique was run and the properties of the soil layer were established, complete dynamic and static analyses (with extensive output) were performed. Because of both typical American load testing practice and the

development of CAPWAP, the Davisson criterion is emphasized in analysis of the static test.

CHAPTER VI

MODEL TEST CASES

STADYN developed, a test case was necessary to verify some of its basic features. The test case was based on that in Warrington (1997). The basic parameters are as follows:

1. Pile. All of the cases incorporated the same pile configuration.
 - (a) 1000 mm O.D. x 40 mm wall thickness steel pipe pile, uniform cross-section.
 - (b) 50 m long.
 - (c) Open ended pile.
 - (d) Pile divided into fifty (50) 1 meter long elements.
2. Soil Cases. Two soil cases were considered:
 - (a) No soil, no shaft resistance, pile fixed at toe. This was primarily to compare the results with an analytical solution.
 - (b) Uniform soil starting 1 m below the pile head. The phreatic surface is 25 m below the soil surface. Soil properties will vary as detailed below.
3. Hammer Cases. Two hammer cases were considered:
 - (a) Hammer as detailed in Warrington (1997), with a 15,000 kg mass ram, 3,000 kg mass driving accessory, single-acting with a 1.5 m stroke and 80% mechanical efficiency. There is an optional micarta and aluminum cushion ($E = 2.413 \text{ GPa}$, $\rho = 1827 \text{ kg/m}^3$) which is 750 mm O.D. (as is the ram) and 435 mm in thickness. The hammer system is shown in Figure 26.

(b) Pile top force-time and velocity-time curve based on semi-infinite pile theory.

The idea behind this is well detailed elsewhere (Warrington (1987); Deeks (1992); Warrington (1997)). The actual equation for the pile head force (the force is set to zero after $t = L/c$) is

$$F_0(t) = 54600930e^{-835.2732t} - 54600930e^{-396.1255t} \cos(401.6697t) + 59695490e^{-396.1255t} \sin(401.6697t) \quad (116)$$

and the velocity is simply this quantity divided by the pile impedance. The hammer used to generate Equation 116 is, of course, the same as detailed above.

Many plots and graphs will be included in the results. The various types in this chapter are as follows:

1. Line Graphs

(a) y-displacement-time graphs at pile head, middle and toe and force-time graphs at the pile head (pile toe displacement does not apply to fixed base runs.)

(b) Stress-time graphs at pile head, middle and toe.

(c) Pile top load-displacement graphs for static runs (do not apply to fixed base runs.)

(d) CAD representations of the system.

2. Two-dimensional Plots

(a) y-displacement-time graphs for length of pile.

(b) y-stress-time graphs for length of pile

(c) Stress plots (σ_x -, σ_y -, σ_z -, σ_I -, σ_3 - and τ_{xy}) at end of a static load test, not all stresses are shown for every case, does not apply to fixed base runs as there is no soil.

There are also plot types that only apply to optimization runs; these will be discussed below.

Semi-Infinite Theory Pile Head Force Cases

All of these cases incorporated the Hammer Case 3(b).

Fixed Base

The analysis started with the fixed base analysis, Soil Case 2(a). The first result was the displacement-time graphs, shown in terms of dimensionless L/c time in Figure 27.

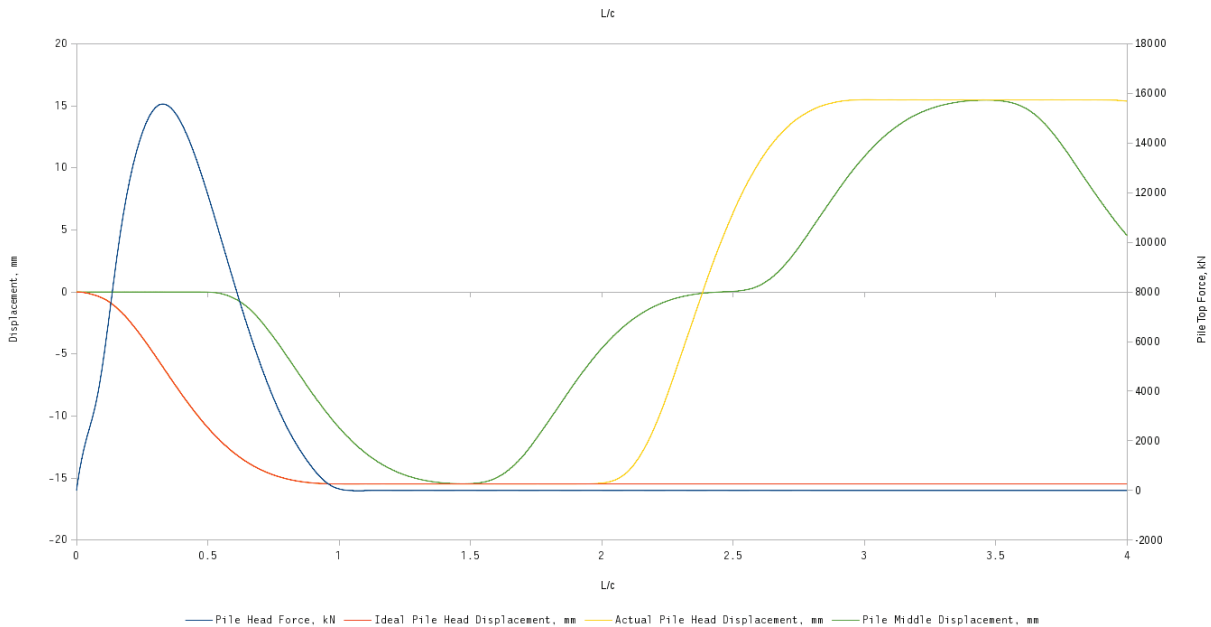


Figure 27 Semi-Infinite Pile Head Force, Displacement-Time Results

The force was an impulse complete by time $2L/c$, which was a constraint in Warrington (1997). The resulting values for actual pile head and middle

displacement values corresponded nearly exactly with those from the analytical solution in Warrington (1997) for a fixed base and no shaft resistance. The ideal pile head displacement was strictly based on semi-infinite pile theory; it and the actual displacement separated at $2L/c$, which is also to be expected, as semi-infinite pile theory does not provide for reflections from the pile. Comparison of pile head and middle displacements with the results of Warrington (1997) shows a nearly exact correlation between the two; the plots are no different.

The stresses—which were actually extrapolated to the same nodes as the displacements—are shown in Figure 28.

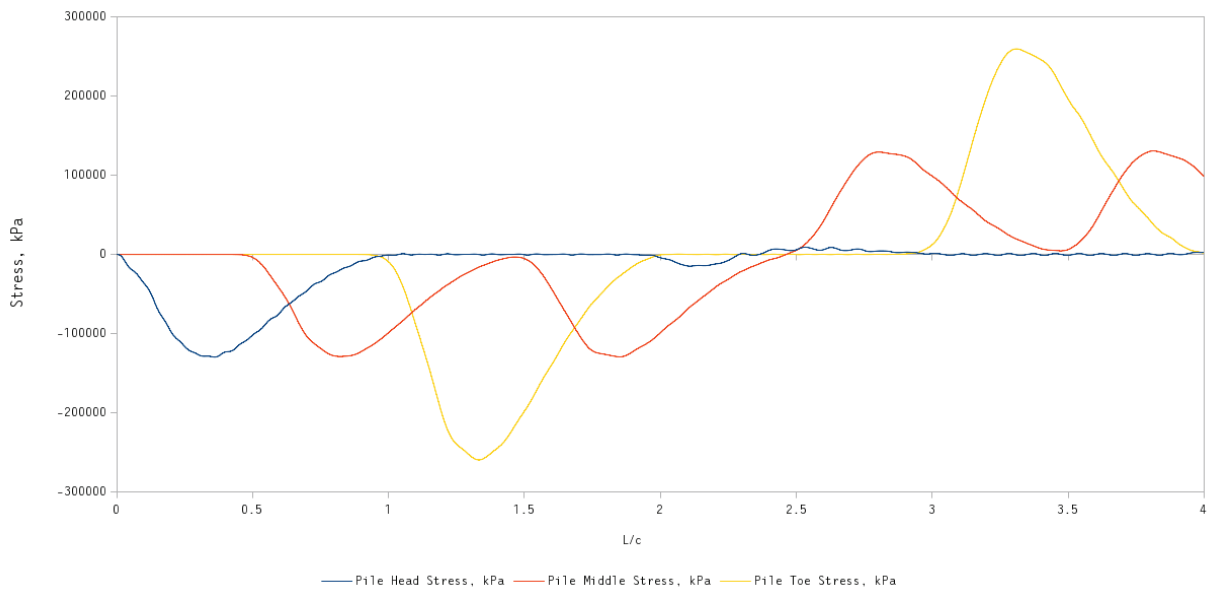


Figure 28 Semi-Infinite Pile Head Force, Stress-Time Results

Although these too tracked closely with Warrington (1997), they showed initial signs of parasite oscillations. This was especially true of the pile head stresses; they should have been zero for time greater than L/c .

Both the displacements and the stresses could be tracked two-dimensionally as well; the displacement-time relationship for the entire pile can be seen in Figure 29.

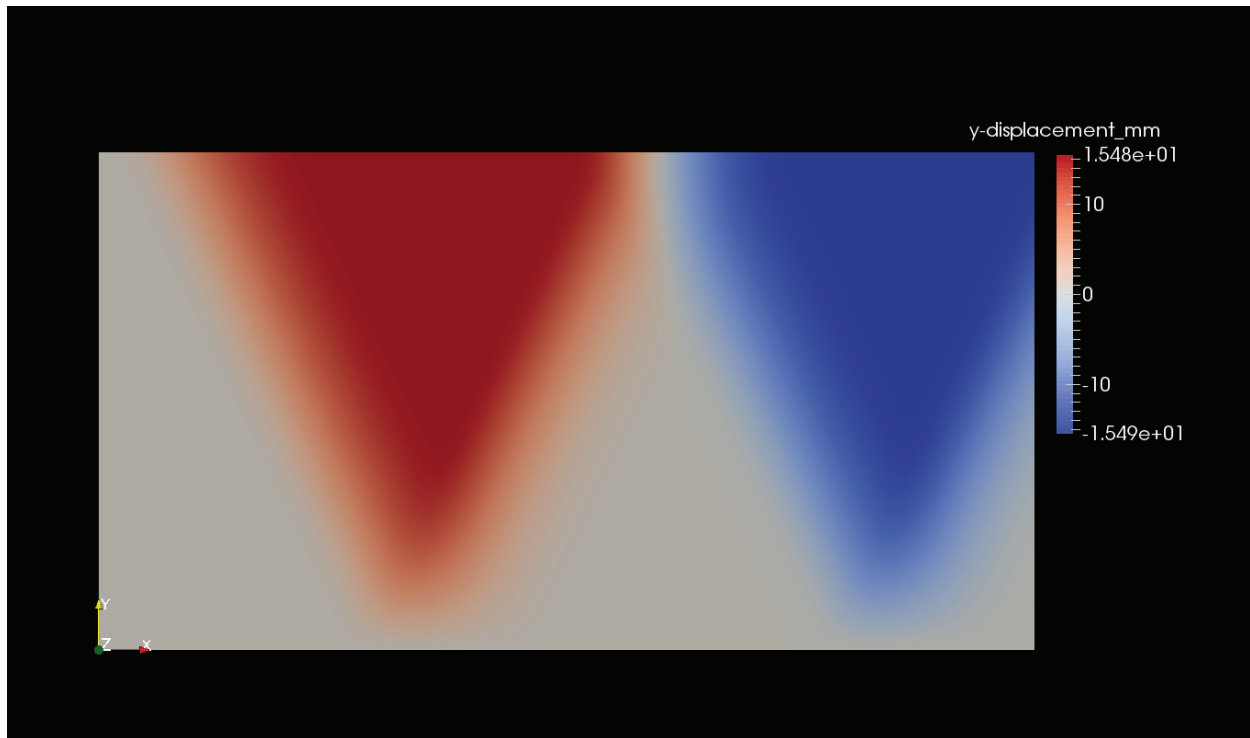


Figure 29 Semi-Infinite Pile Head Force, Two-Dimensional Displacement-Time Results

Using the axis marker in the lower left hand corner, the “x” axis is actually a time axis, proceeding from the starting time to the end of the run, in this case $4L/c$ (as seen also in Figure 27). The “y” axis is the position along the pile; the bottom edge of the graph is at the pile toe and the top edge of the graph is the pile head. The alternating downward (positive) and upward (negative) displacements are to be expected with a stress wave that was reflected off the free end of the pile head. As one approached the fixed pile toe, the displacements decrease to zero.

In a similar way, the pile stresses are shown in Figure 30.

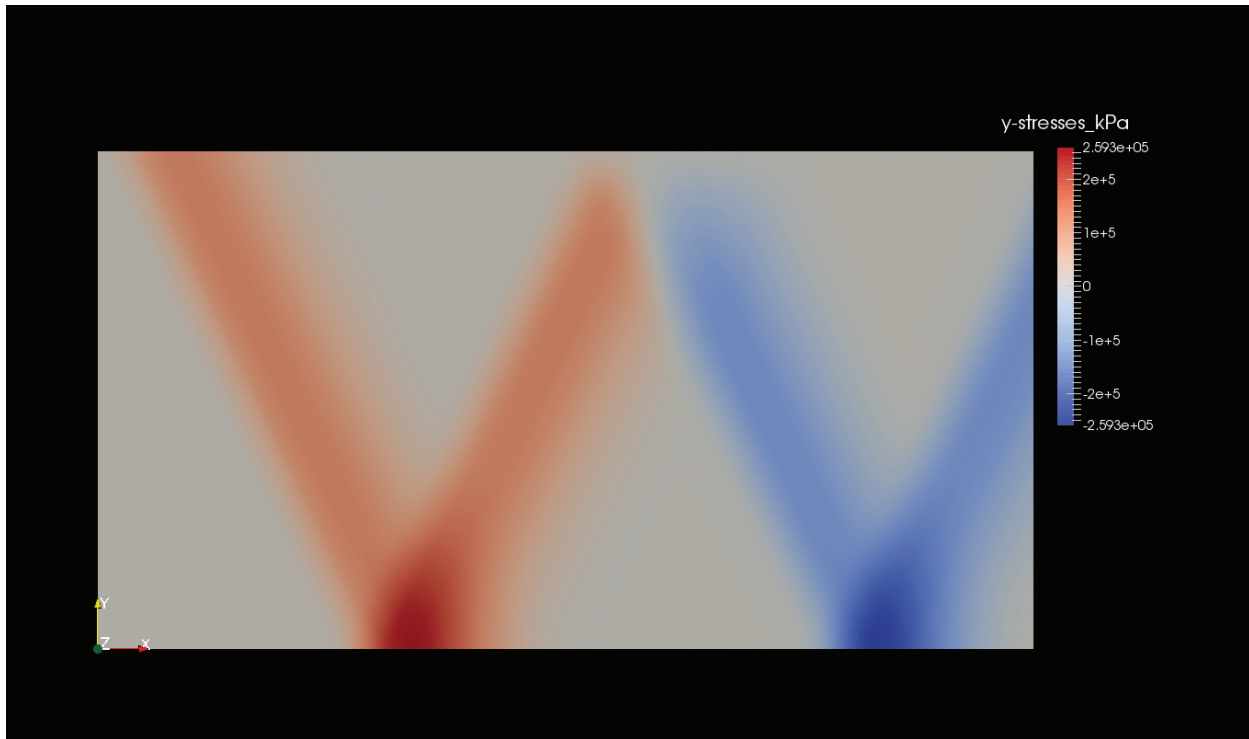


Figure 30 Semi-Infinite Pile Head Force, Two-Dimensional Stress-Time Results

The stress wave comes into the pile compressively in early time, and then was reflected off the pile toe while essentially doubling (and not changing sign) at the fixed end. When the stress wave reached the pile head, the magnitude of the stresses were unchanged but the sign was reversed from compressive to tensile, and the doubling effect was repeated at the pile toe for the tensile stresses.

Dilatancy and Element Squeeze Study

This case used Soil Case 2(b) with $\xi = -1$, $\eta = 0$. The use of a completely cohesionless soil was a maximum test of the finite element code in one respect: it was the most non-associated flow rule encountered in Mohr-Coulomb plasticity.

Both dilitancy and element squeeze are important parameters which relate to the way the soil is modeled and actually responds to the downward movement of the pile, whether that movement be part of a dynamic analysis or the movement associated with a static load test.

To begin the analysis, the CAD file of the model was imported from the IGES file generated by the program, and is shown in Figure 31.

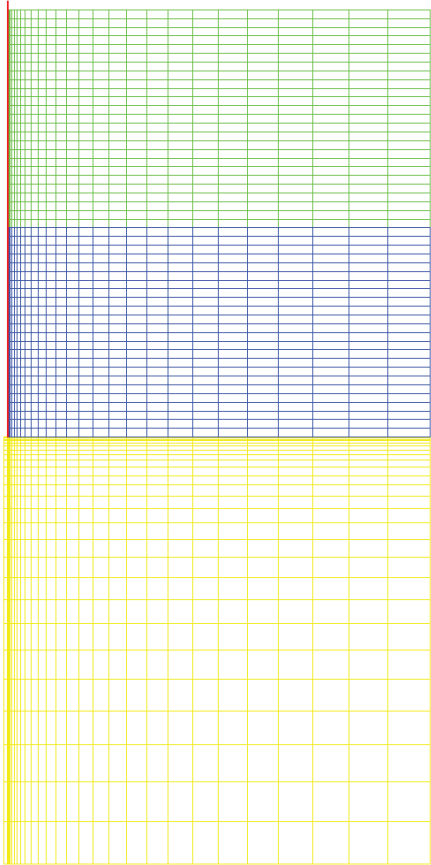


Figure 31 CAD Representation of the Pile-Soil Model, Element Squeeze = 3

The pile is the long, narrow vertical part in the upper left-hand corner of Figure 31. The shaft soil was divided by the phreatic surface and the toe soil

was modeled as a separate layer; both of these can be clearly seen. In addition to inputting the program for these large layers, the program was checked to insure that the results would be the same even if each row of soil elements above the toe were made individual layers (the results were the same.)

A selected displacement-time history at the pile head, middle and toe, along with data for the pile head velocity, is shown in Figure 32 for $\xi = -1$, $\eta = 0$.

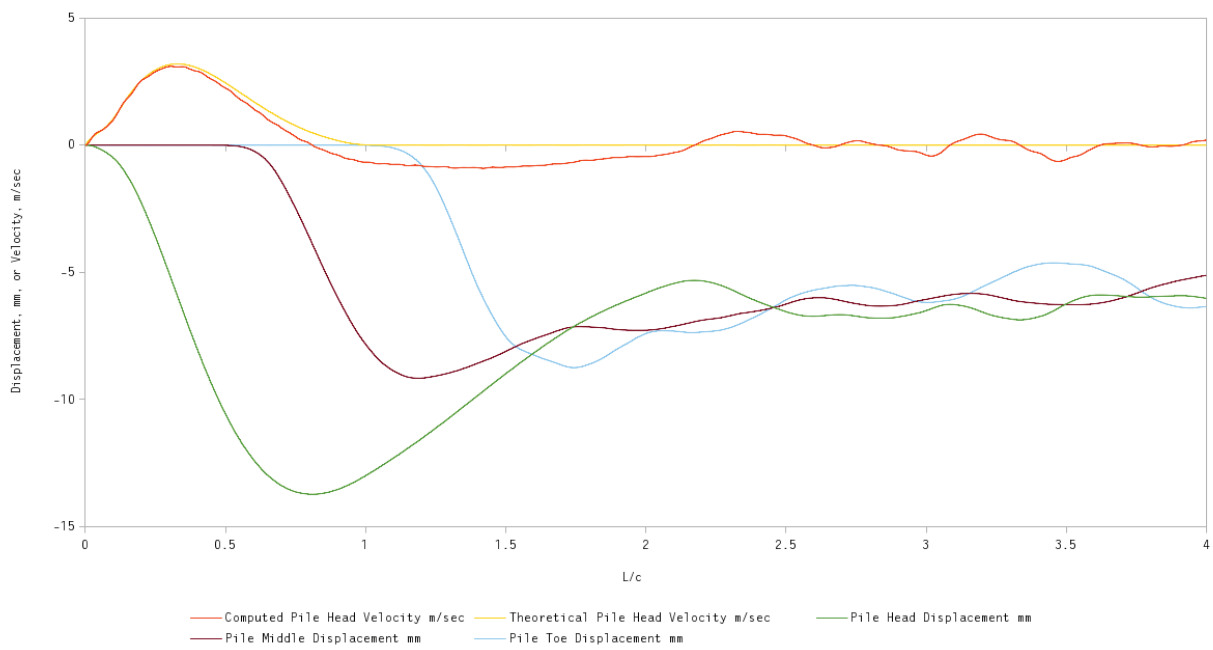


Figure 32 Displacement-Time, Element Squeeze = 3

The classic downward movement and subsequent rebound of a pile can be clearly seen. Also clearly seen is the effect of the delay induced by the length of the pile; the pile middle began deflecting at $L/_{2c}$ and the pile toe at $L/_{c}$. In this case the three points on the pile came to a similar deflection. Eventually the deflections will stop and the pile will come to rest, usually before the next blow. As the study progressed, longer runs were found necessary in order to approach this rest point.

The “theoretical pile head velocity” is the theoretical pile head force from the method of Warrington (1997) divided by the pile head impedance. This type of plot is common with CAPWAP output, as will be shown. The computed pile head velocity is from STADYN; it includes the effects of overall pile movement and rebound. In the very early portion of the impulse, before $L/_{2c}$, the two are very close, and this reflects the reality that the pile head in this region is governed by semi-infinite pile theory. As the pile moves downward, the results can be expected to diverge from this theory, and in fact this is the case.

Switching to the two-dimensional plot, the pile stresses for this case are shown in Figure 33.

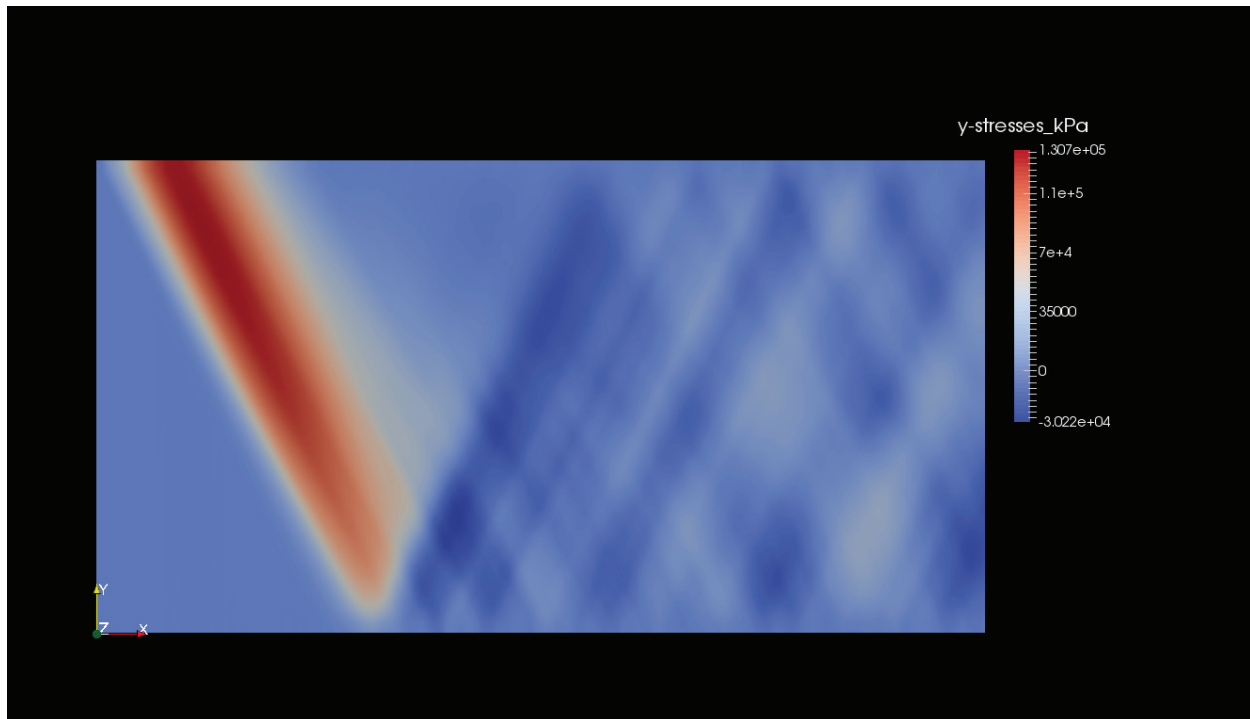


Figure 33 Stress-Time, Element Squeeze = 3

Comparing this with Figure 30 immediately shows the effect of the soil: the stress wave was dissipated into the soil through both plasticity and radiation, and the intermediate reflections of the soil layers can be seen as well. Noteworthy also are the relatively low stresses at the toe of the pile; in this case the toe was acting almost as a free end.

Including the soil also began the calculation of static capacity. The static run was performed after the dynamic one is complete; the pile head results are shown in Figure 34.

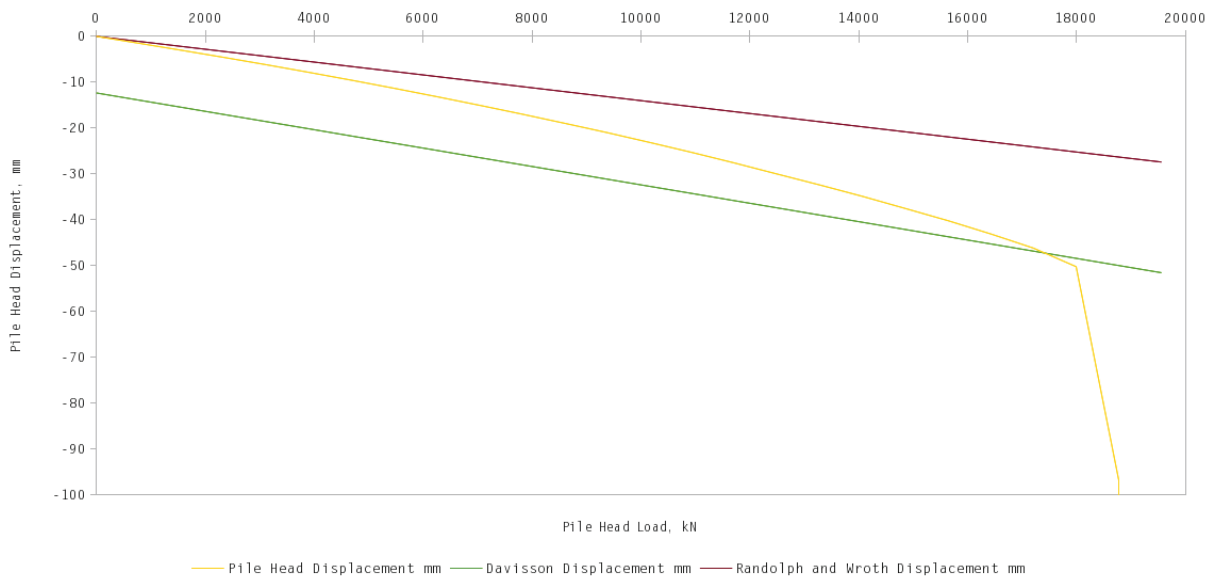


Figure 34 Pile Load Test Results

The following should be noted about this:

1. Three lines were plotted: the actual pile head load-deflection curve, the Davisson displacement line, and the Randolph and Wroth (1978) displacement line.

2. The Davisson failure load took place at the intersection of the Davisson displacement line and the pile head load-deflection curve.
3. The Randolph and Wroth (1978) curve is the “lower bound” (i.e., deflection is greater with plasticity) of the pile head load-deflection curve. This was as one would expect; intersection of the two curves at any point would indicate severe stiffness in the finite element model. It is also interesting to note that the Randolph and Wroth (1978) curve is “flatter” (i.e., stiffer) than its Davisson counterpart. The slope of the Davisson line is the stiffness of the pile with a fixed toe and no shaft resistance. Although the soil is much softer than the pile, the soil “grabs” the pile all along the length, thus reducing the effective length of the pile for elastic purposes, a phenomenon incorporated into semi-empirical methods for settlement such as Vesic (Naval Facilities Engineering Command (1986)).

Stress and displacement graphics—which are standard for this type of two-dimensional finite-element analysis—were also generated. The first presented is the first principal stress plot, shown in Figure 35. The principal stresses are plotted for the first load point after the Davisson load. Frequently after that, point the model collapses, violating the small displacement assumption of the methodology.

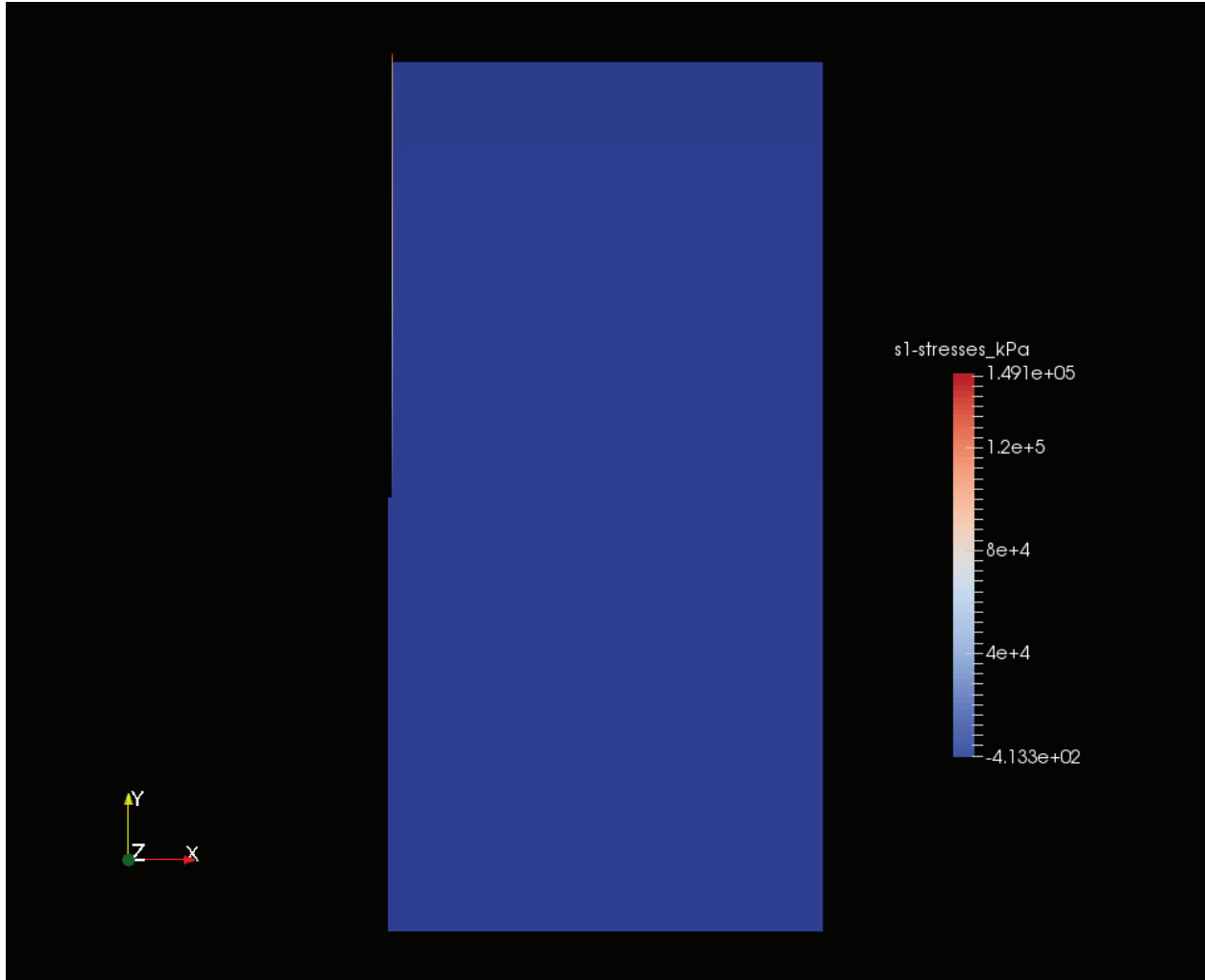


Figure 35 First Principal Stress Plot for Static Load Test

Because the elevated stresses extended little beyond the pile itself, the stress levels shown in the soil do not vary much. This result was anticipated by Potts and Martins (1982). A more interesting result came if the pile head area was focused upon as it is in Figure 36.

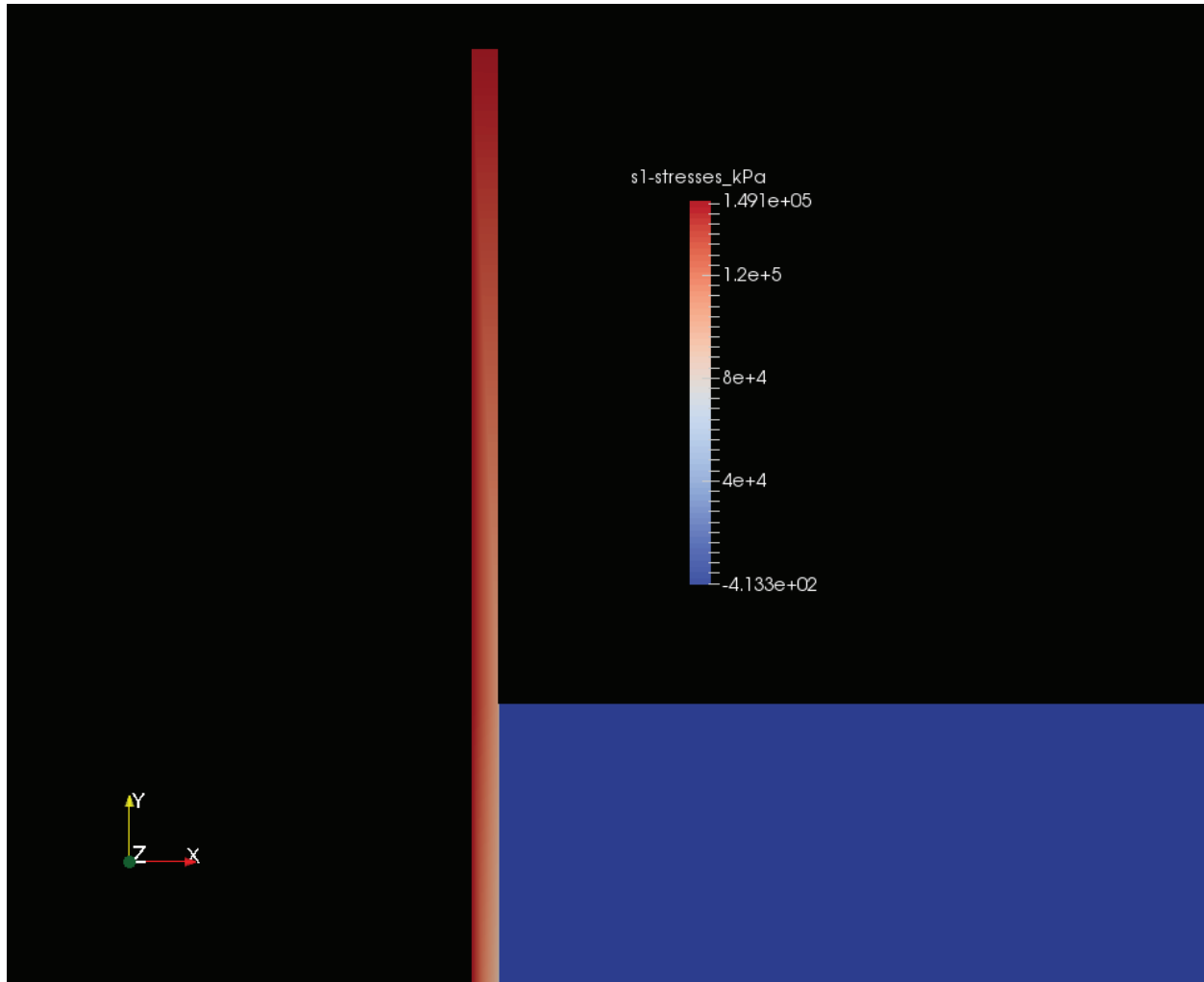


Figure 36 First Principal Stress Plot, Pile Head Region

At the pile head, the stresses were uniform. By the time the pile reaches the mudline, the stresses were not uniform in the cross-sectional area of the pile. The stresses along the outside diameter of the pile matched those of the soil; on the inside diameter, they were much higher. With one-dimensional assumptions (static and dynamic) it is assumed that the cross-section of the pile experiences uniform forces and stresses; this is not always the case.

Another interesting result was the very small affected zone in the soil of the pile movement. The plasticity in the soil is restricted to a region very close to the pile-soil interface.

The third principal stress for the static case is shown in Figure 37.

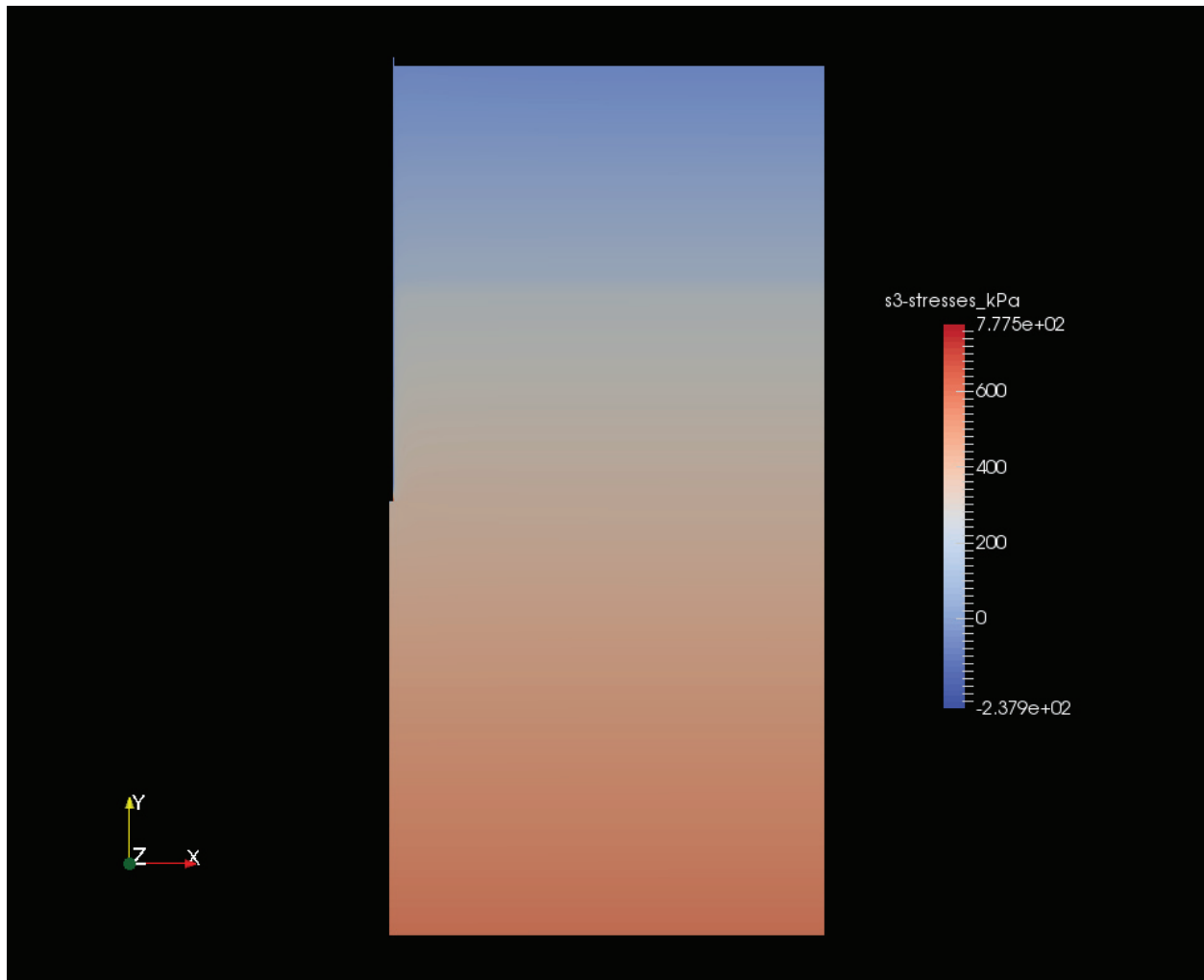


Figure 37 Third Principal Stress Plot

Since the values of σ_3 for the pile were minimal, it is easy to see the increase in effective stress in the model with increasing depth. It is even possible to discern the transition induced by the phreatic surface halfway down the pile.

Displacements in the y-direction are shown in Figure 38.

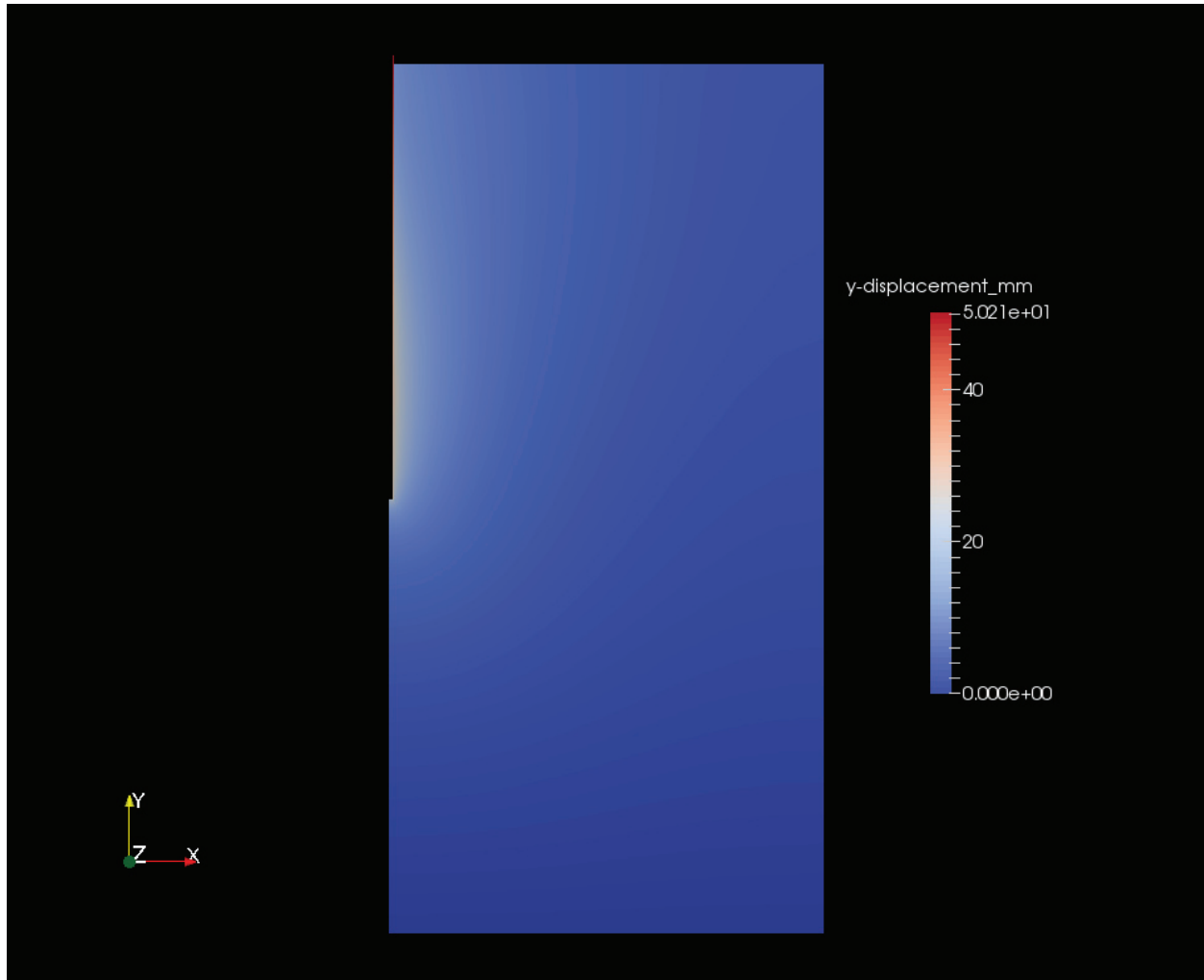


Figure 38 y-displacements for Static Test

The displacements around the pile were the most pronounced, more extensive than the stresses. It is interesting to note that, although the region

affected plastically by the pile (as shown in Figure 36) was relatively small, the progressive effect of the downward shear induced downward displacement in the soil surrounding the pile. Downward displacements such as this are generally associated with pile downdrag, although in most cases of interest the downward deflections were induced by external surcharges and other effects. In this case, the apparent downdrag was induced by the progressive downward loading of the pile itself.

The basic parameters established, a study of the effects of varying dilitancy and shaft element squeeze was undertaken using static analysis. The dilitancy ratio was varied with values of zero, 0.1, 0.2 and 0.3. At the same time the soil squeeze exponent was varied with values of 1, 2, and 3, 1 being evenly spaced element columns between the pile shaft surface and the right edge of the model and 2 and 3 “squeezed” towards the pile, with the elements closer to the pile being progressively narrower than those at the right edge of the model.

The results with Davisson’s criterion are shown in Figure 39.

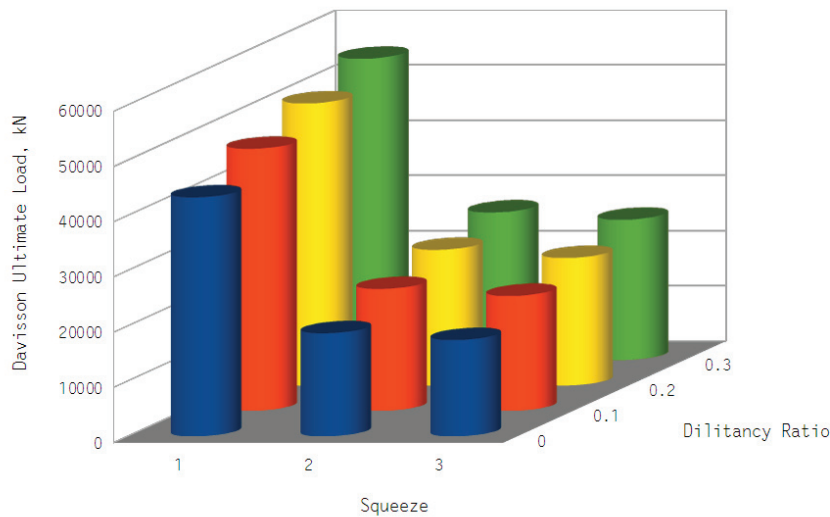


Figure 39 Dilitancy-Squeeze Study Using Cohesionless Soil

With the squeeze, the largest difference came between a squeeze of 1 and 2; going to 3 did not have that much effect. Thus, a squeeze of 3 was used for the rest of the study for both static and dynamic runs. The apparent stability of the results (the 3-squeeze model's soil elements along the pile shaft were 2 mm thick and 1 m long) was consistent with Pande and Sharma (1979).

With dilitancy, progressively increasing the dilitancy ratio (and thus the dilitancy angle) resulted in increasing the resistance of the soil to axial force on the pile head. It did so in a way that did not vary with the element squeeze, although it was understood that the two were not necessarily related.

The quantification of dilitancy in geomechanics is an issue with surprisingly little research, although some work has been done (Bolton (1986)). Standard values for ψ , to say nothing of specific values for various soils, are scarce, and frequently assigned on an ad hoc basis. Although it can be tested for, such tests are not frequent in practice. It can also be estimated from the difference between the maximum and critical friction angle of the soil, although having both of these quantities on hand is not frequent either. Its effect on model response is evident in Figure 39. For the remainder of this study $R_{dil} = 0$.

Static Load Test Interpretation

As before, this case used Soil Case 2(b) with $\xi = -1$, $\eta = 0$. The hammer model is not relevant here. The variations in static load test interpretation methods using the same force-deflection curves is now of interest.

The methods were applied to the results, which were a series of load steps. The load steps varied to a "maximum" load based on Meyerhof's method. This final load was not necessarily meant to be an absolute upper limit as much as it was to

prevent endless looping of the static load routine. This maximum load was divided by the number of steps desired; that quotient was the increase in load at each load step.

In the early stages of model development, there were 40 steps to the maximum Meyerhof load. For Davisson results, this is satisfactory. For other methods, the relatively large load steps resulted in significant inaccuracies in the determination of static loads. This is especially true since linear interpolation was not used for any of these methods except for Davisson’s and the slope-tangent method. Thus, to “catch” the load-deflection relationships of, say, the Brinch-Hansen methods, or the maximum curvature, more load steps were required. Thus the number of maximum load steps was increased to 100.

In Figure 34, static loads up to the Davisson criterion are shown. In reality, this static load analysis was performed for higher loads so that other load testing criteria could be used. The static load test results for the various methods applied to Figure 34 are shown in Table 2.

Table 2 Static Load Results for Various Methods

Interpretation Method	Static Load, kN
Davisson Load	17416
Brinch-Hansen 80% Load	19556
Brinch-Hansen 90% Load	18774
Maximum Curvature Load	18774
Slope-Tangent Load	18602

The result is reasonably consistent for all of the methods, which is not always the case with static load testing (Fellenius (2014)). This is especially remarkable when one considers that Davisson’s Method is based upon limiting the deflections

from soil plastic failure, i.e. finding a “yield” point in the pile. This is a similar concept with offset-yield methods used with other materials. The other methods, to varying degrees, attempt to find a true ultimate failure point. Although the pattern seen above is not consistently replicated with other pile and soil configurations, from an ideal standpoint it is instructive. Both Davisson and the Brinch-Hansen methods are embodied in various building codes, but each is based on a different concept of “ultimate” pile loads.

In other STADYN runs some of the methods yielded inconsistent results or no results at all. This was especially true with the Brinch-Hansen methods. In this study, of the non-Davisson methods the Slope-Tangent method produced the most consistent results.

Modeled Hammer Cases

At this point Hammer Model 2(a) began to be used, as shown in Figure 26. This applies to both cushioned and cushionless hammers, since the thickness of any interface elements was not geometrically represented in the finite element model.

Fixed End Runs, Cushioned Hammer

Using the fixed end model of the pile (Soil Case 2(a)) made it possible to both verify the basic integrity of the model and to check it for variations caused by changes in important parameters. In this case the most important addition to the model was the inextensible interface elements. There are two of these, one between the driving accessory and the pile head and the other between the ram and the driving accessory. With a cushioned hammer, the stiffness of the latter was determined by the stiffness of the cushion material. The former, however, could be varied according to its effective thickness, defined in Equation 106. The implied

thickness in this formula was based on the response of a semi-infinite mass to static loading. The actual thickness used to compute the “subgrade reaction” coefficient in Equation 105 is related to the nominal thickness computed by Equation 106 by the quantity

$$ITR = \frac{t}{t_{implied}} \quad (117)$$

For the cushioned hammer, the only thickness that was being varied is that of the pipe top interface. This thickness determined both the stiffness and the imputed mass of the interface. As ITR increases, the stiffness decreased and the mass increased.

Figures 40, 41 and 42 show the force-time and displacement-time relationships with varying values of ITR. All of the variables are plotted as a function of L/c ; however, the displacements are scaled with the primary (left) y-axis and the pile head forces scaled with the secondary (right) y-axis.

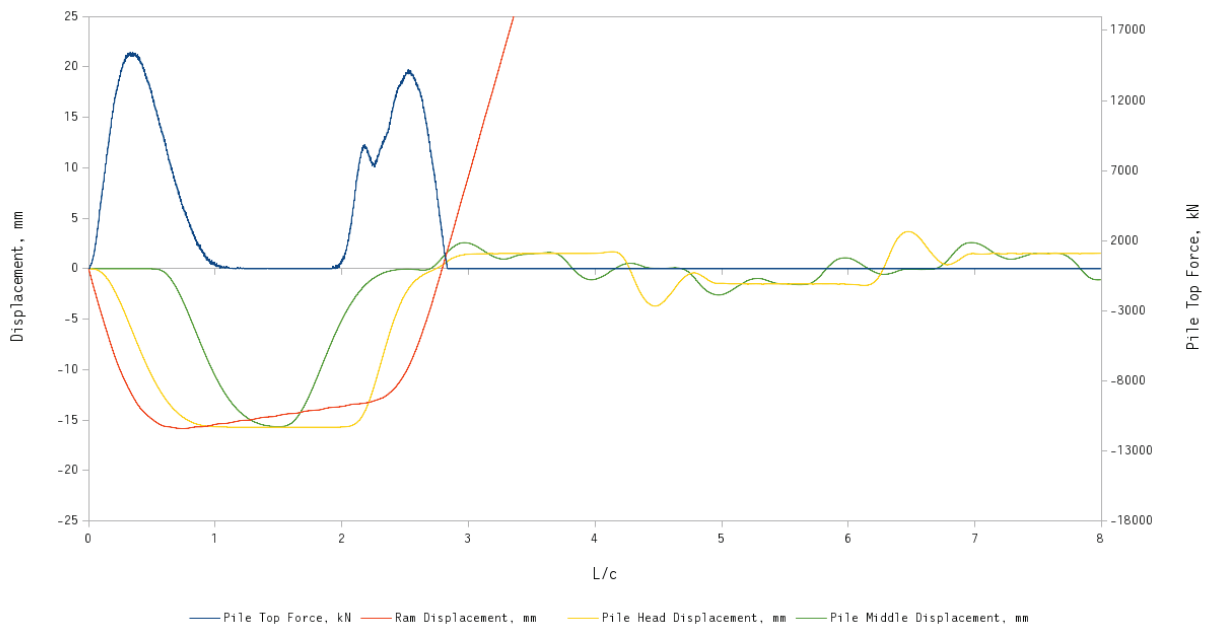


Figure 40 Force-and Displacement-Time Relationships, ITR=4

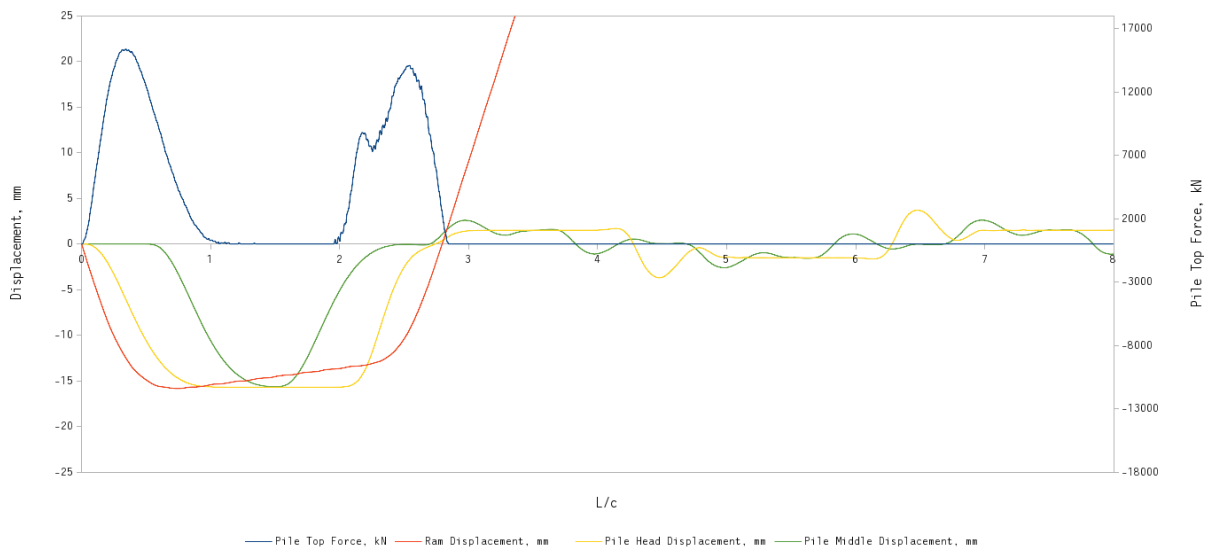


Figure 41 Force-and Displacement-Time Relationships, ITR=1

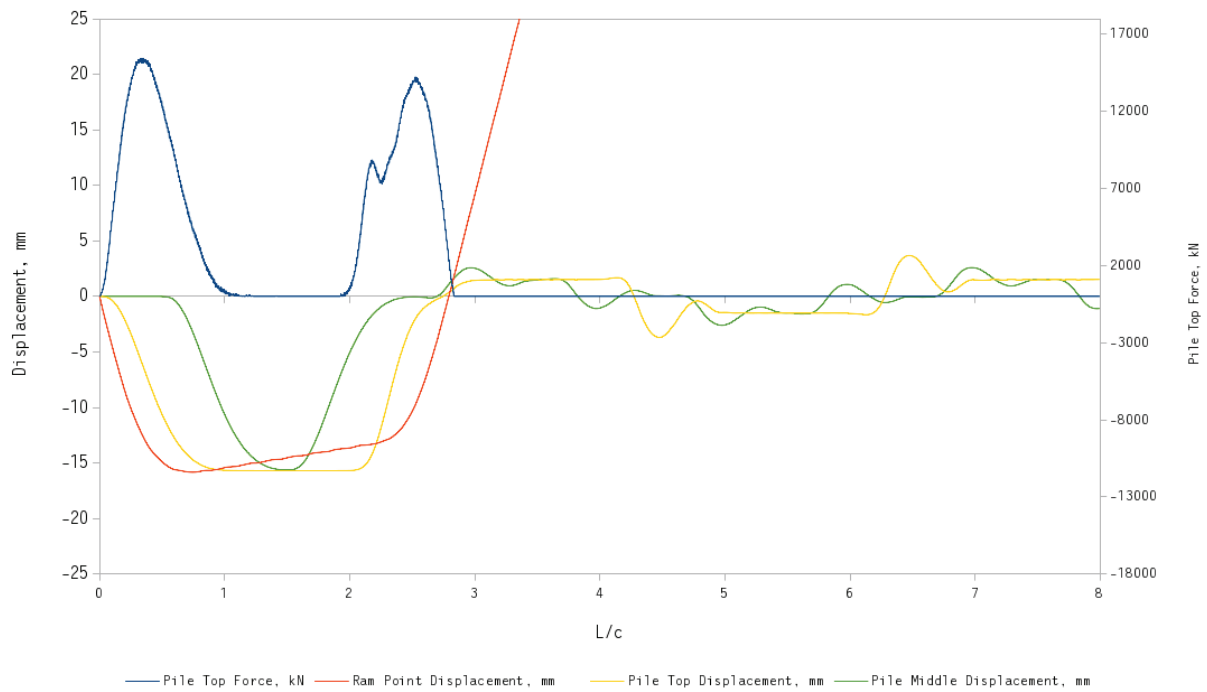


Figure 42 Force-and Displacement-Time Relationships, ITR=0.25

These should be compared with Figure 27, where the force-time curve is determined analytically, as opposed to being a product of the finite element model here. A comparison of the maximum pile head force results for the various models can be seen in Table 3.

Table 3 Maximum Pile Head Forces for Analytical and Finite Element Models

Model	Maximum Pile Head Force, kN
Analytical (Warrington (1997))	15569.72
FEA, ITR = 4	15465.12
FEA, ITR = 1	15369.49
FEA, ITR = 0.25	15465.12

The finite element solution is very close to the analytical solution, at worst 1.3% less. It should be noted that the analytical solution assumed a rigid cap while the finite element solution allows for flexibility in the cap; perfect agreement was not to be expected.

This agreement is also reflected in examination of Figures 40, 41 and 42; there was little difference among the three. In addition to pile head and middle displacements, the displacement of the ram point is also included. It deflected ahead of the pile head in phase, then begins to rebound due to the cushion material. When the stress wave came back to the pile head at $2L/c$, the pile head was again in compression and the rebound pushed the cap, cushion and ram upwards. When the cushion force reached zero, the ram went into a free rise at a constant velocity. In this case the remaining energy in the pile oscillated between pile head and toe; comparison with Figure 27 shows that the energy in the pile was significantly diminished since much of it was used to push the ram upwards.

A similar consistency of results can be seen in the pile stresses as shown in Figures 43, 44 and 45.

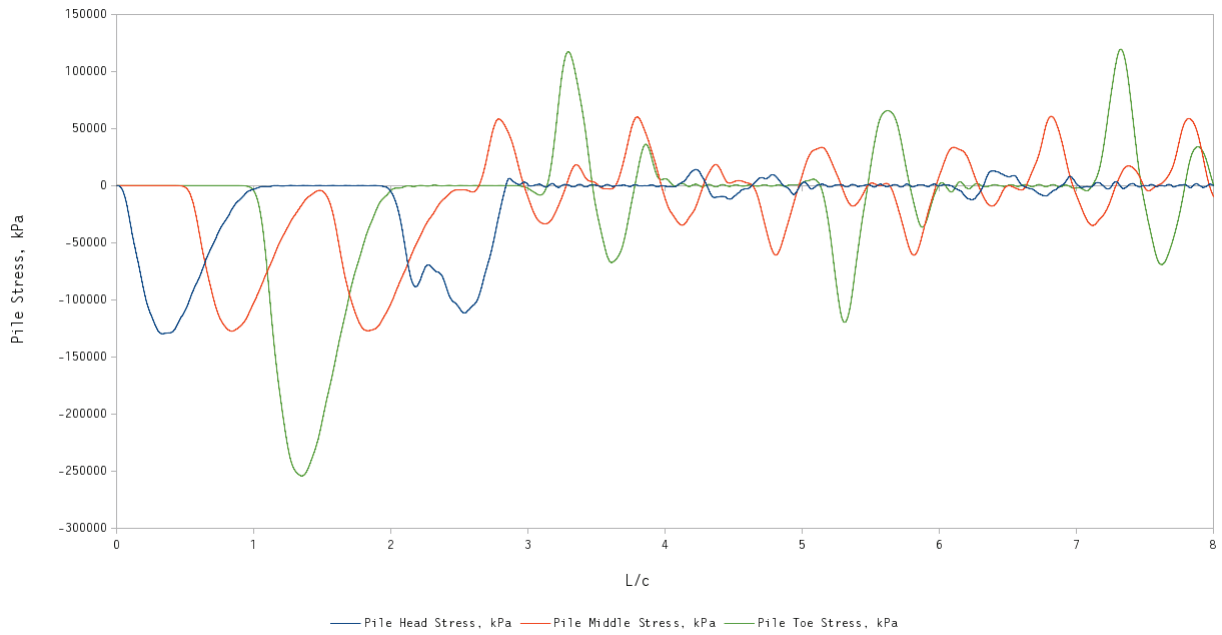


Figure 43 Pile Stresses, ITR = 4

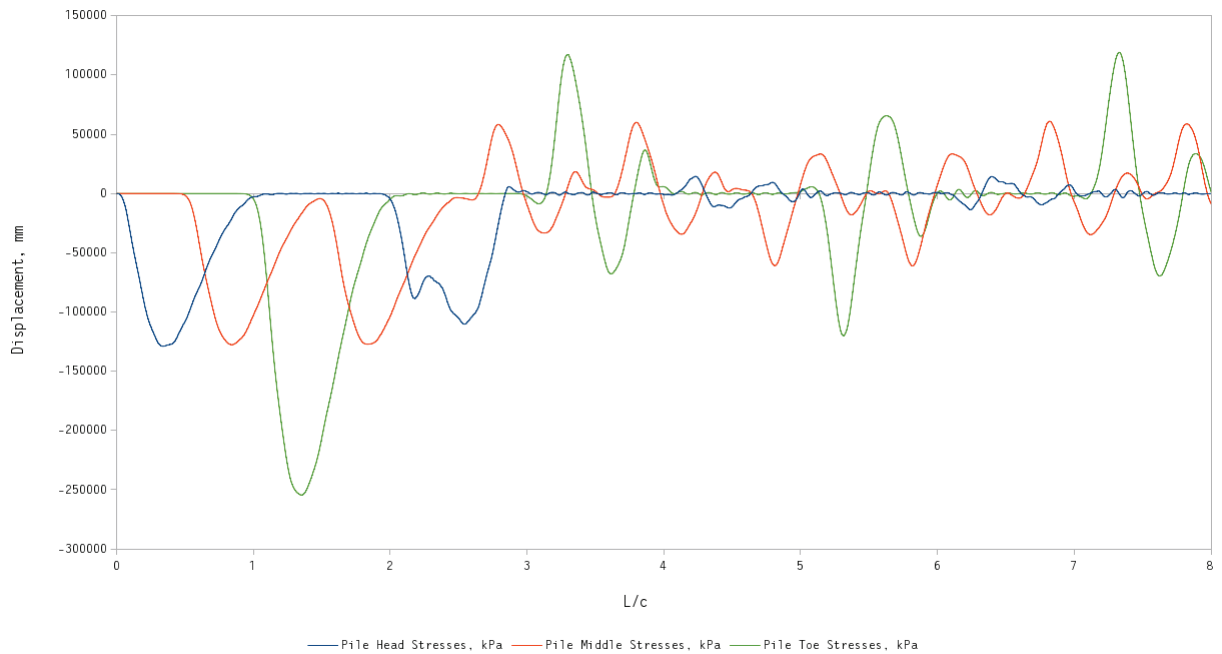


Figure 44 Pile Stresses, ITR = 1

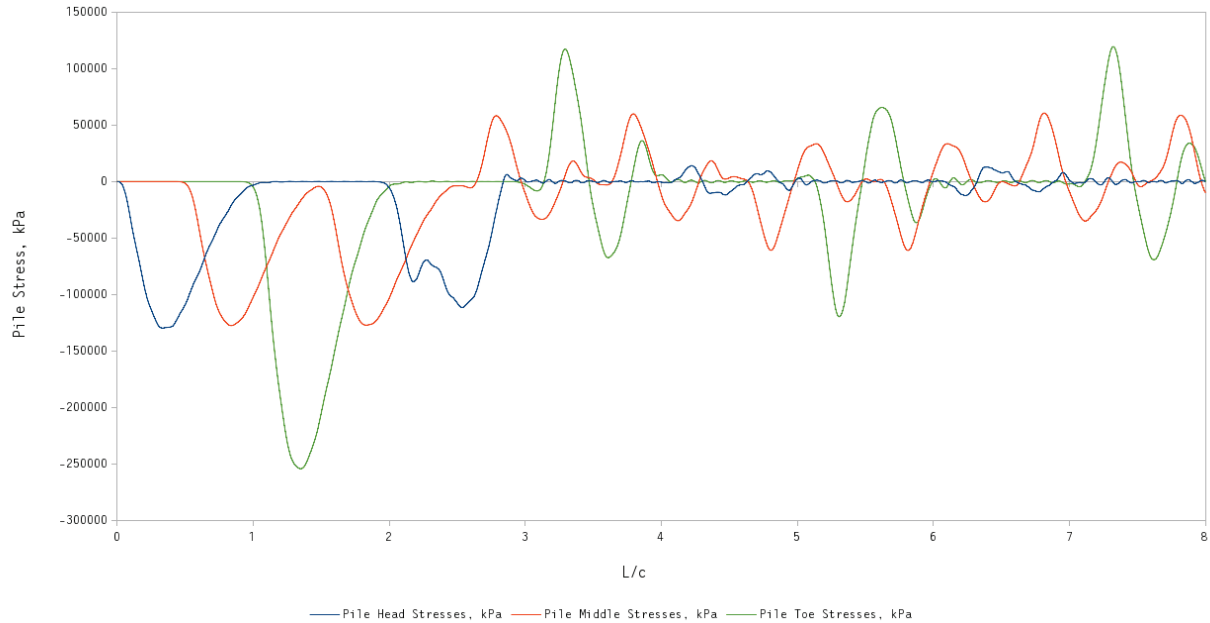


Figure 45 Pile Stresses, ITR = 0.25

The intensity of the parasite oscillations—especially at the pile head—was greater than is seen in Figure 28. To some extent, this was to be expected, given the rebound force of the pile head in addition to the initial impulse. However, even here some noise was being injected into the system by replacing a smooth force-time curve with a modeled hammer. The stresses in the pile were considerably diminished in the later times than they were for the purely analytical force-time relationship.

Generally, use of cushion materials in impact pile drivers is to lessen the stresses in both the ram and frame of the hammer. Looked at another way, the cushion material prevents the generation of high frequency (and high intensity) vibrations that come from “steel on steel” impact. This is helpful both for the physical reality and for the finite element model; with a cushioned hammer, modeling the hammer produces a relatively smooth force-time curve. If a pile

cushion is added as is done with concrete piles, more decrease in high frequency vibrations can be expected.

The effect of varying the effective thickness of the pile head-driving accessory interface was minimal. It should be noted, however, that the relatively low cushion material stiffness might be dominant and mask those variations. Thus, it is necessary to examine this with cushionless hammers, where two stiff interfaces are encountered.

Fixed End Results, Cushionless Hammer

When the hammer cushion was removed, both interfaces were subject to changes in their implicit thickness, which was varied in the same way as it was with the cushioned hammer. Figures 46, 47 and 48 show the displacement and force results when this was done.

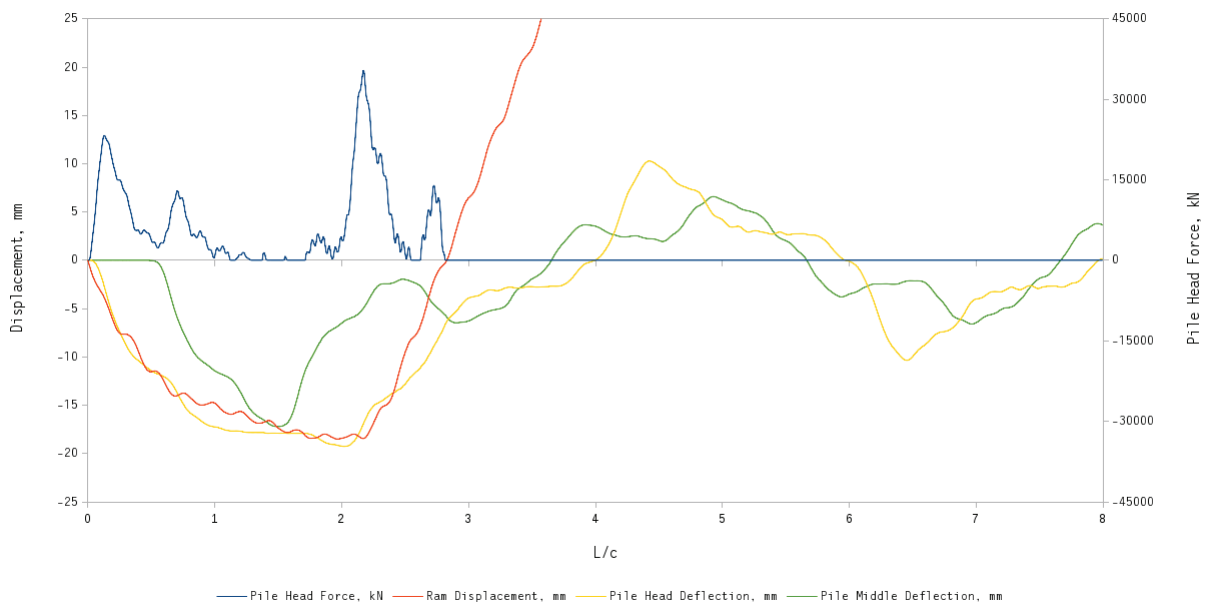


Figure 46 Force-and Displacement-Time Relationships, ITR = 4

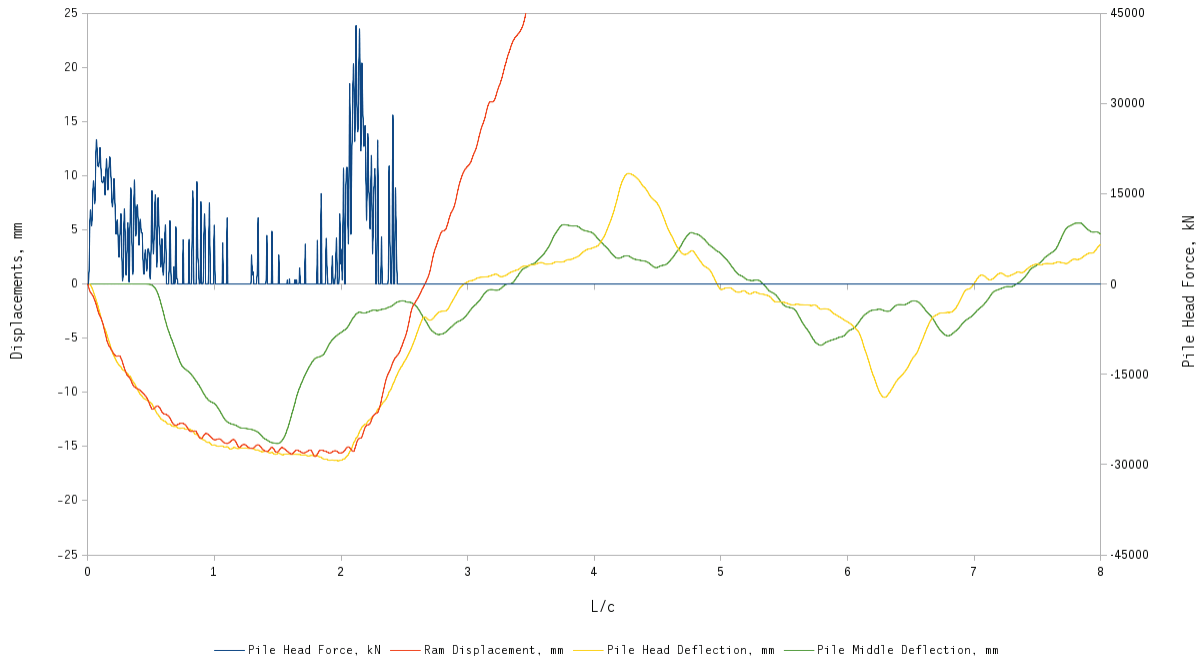


Figure 47 Force-and Displacement-Time Relationships, ITR = 1

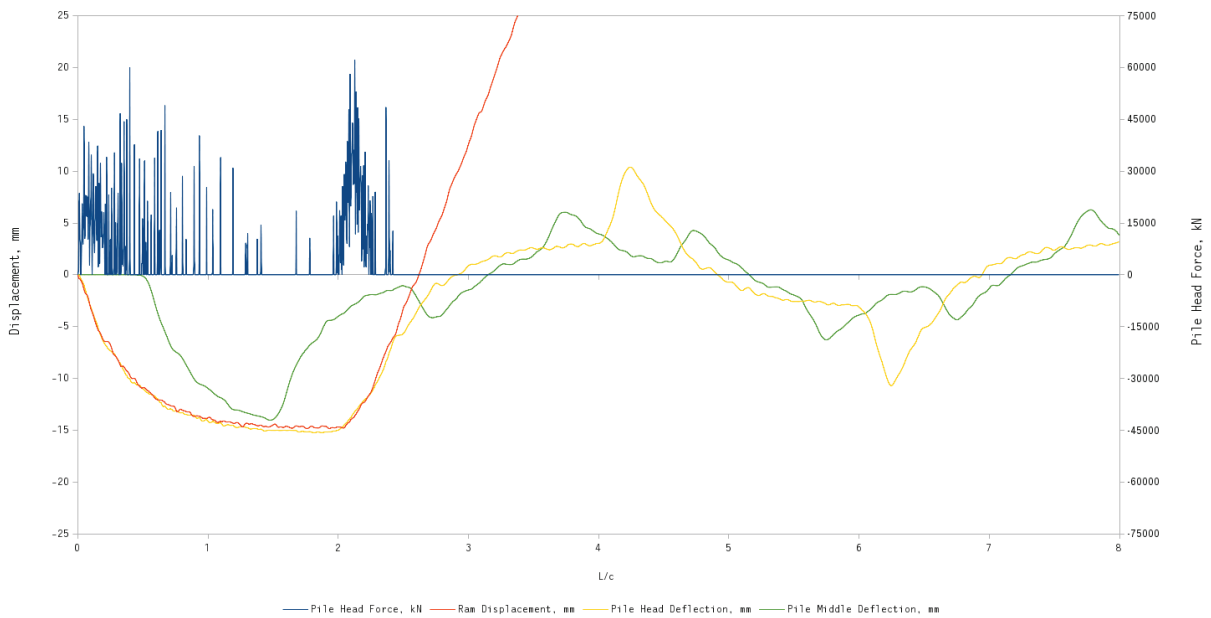


Figure 48 Force-and Displacement-Time Relationships, ITR = 0.25

Figures 46, 47 and 48 document two different parameters—force and displacement—and the trends in both need to be discussed.

With the ITR values of 0.25 and 1, the force-time relationship shows considerable instability, which indicates a great deal of “chattering” at that part of the model. Increasing the ITR to 4 significantly attenuates those instabilities.

Turning to the displacements, the instabilities of the force-time curves are not replicated to the same degree in the ram point or pile head displacements. It is interesting to note that the ripple in the ram point displacement is most pronounced at ITR=4; this is most likely because the softer springs and higher masses at the interface tend to result in lower frequency, higher displacement oscillations. All three of the curves show an increase in displacement until approximately $2L/c$; however, the peak displacement is larger with ITR=4. This is again most likely because of the relatively soft spring and higher mass nature of the interface; the mass is acting as a temporary energy storage “device,” the energy to be released on rebound. The subsequent track of the pile head velocity indicates that this modulation of the impact energy by the interface elements does not have a deleterious effect on the results, which was one objective with the configuration of the interface elements. One of the advantages of using Rayleigh type damping for model stabilization is that smoothing effects can be introduced without energy dissipation (unless, of course, the damping is at the boundaries of the model.) Using a dissipative type of damping at an interface, be that velocity based or the bi-linear “coefficient of restitution” approach common in wave equation code, always runs the risk of misrepresenting the energy transfer between the hammer and the pile.

Comparing the ram point and pile head displacements between each other, in all three cases the two tracked each other until the ram point and driving accessory separated from each other and the ram achieved uniform upward or rebound

velocity. This indicated that the effects of driving accessory flexibility, either axial or plate/beam, were minimal.

The effect on the stress-time relationships is shown in Figures 49, 50 and 51.

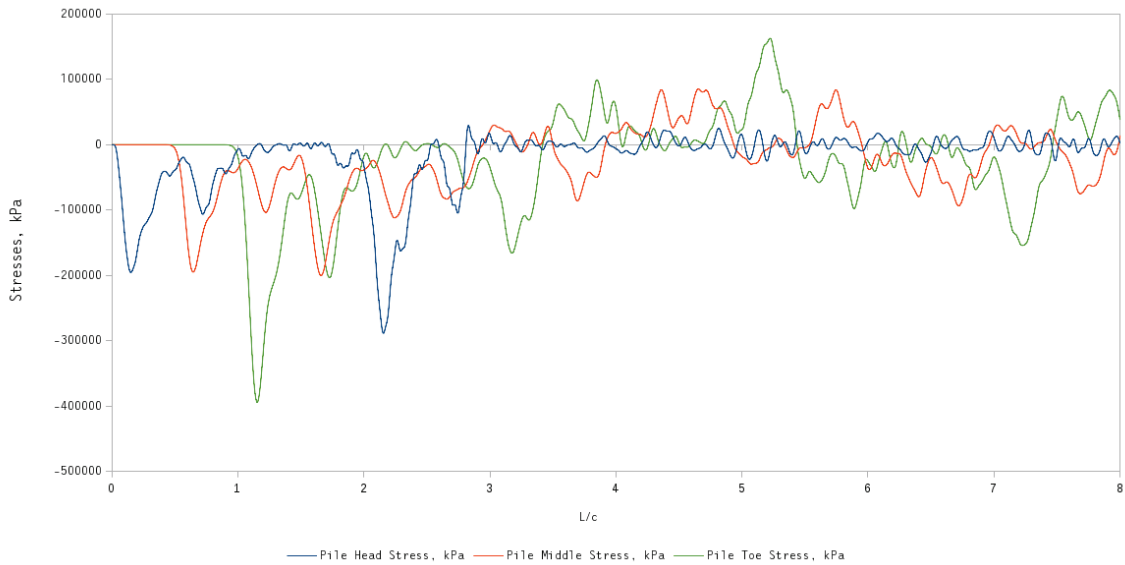


Figure 49 Pile Stresses, ITR = 4

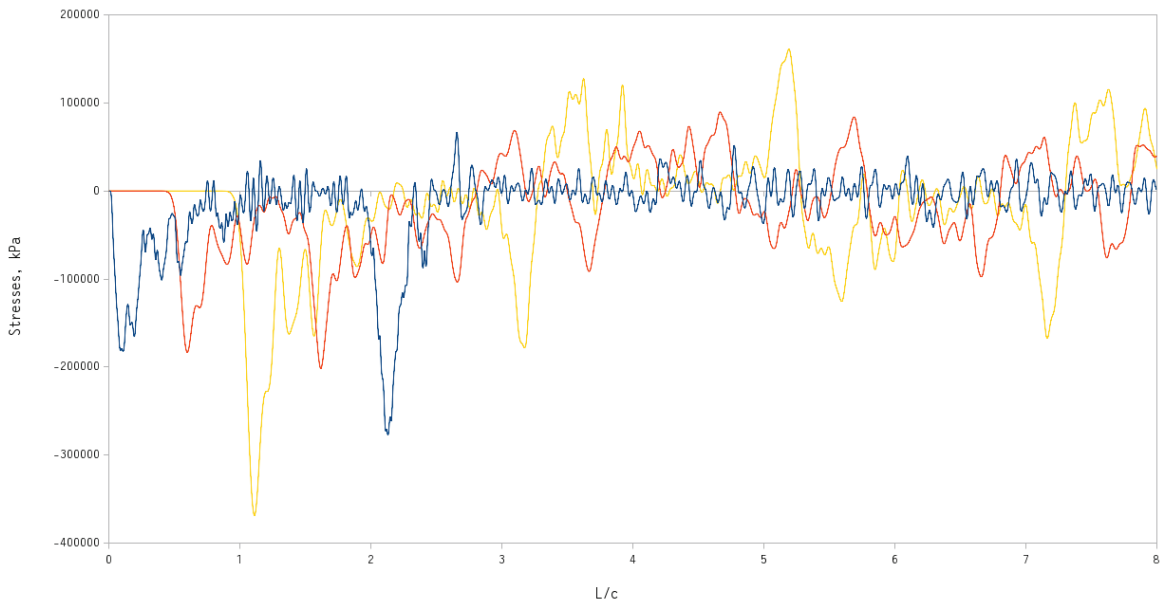


Figure 50 Pile Stresses, ITR = 1

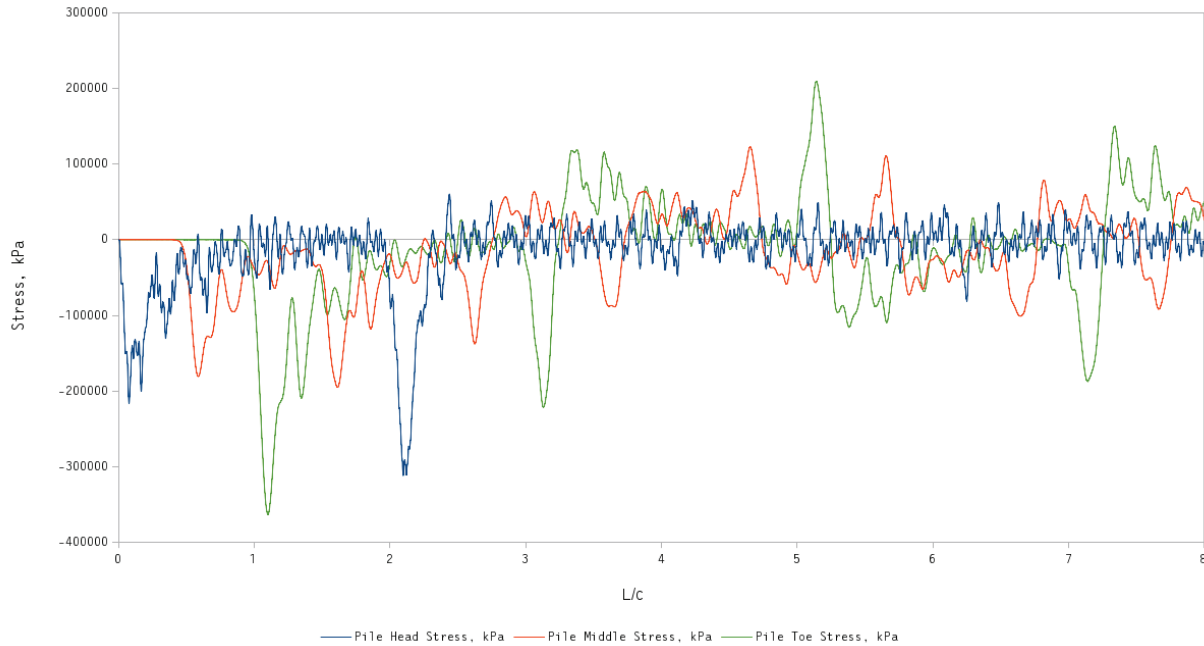


Figure 51 Pile Stresses, ITR = 0.25

The results for the stresses paralleled those for the displacements. The parasite oscillations were definitely attenuated with higher values of ITR, and some variations took place both in peak stresses and in the timing of those peak stresses.

Given the results in this portion of the study, it was decided that, for subsequent work, ITR=1. This seems to be a reasonable balance of the desire for stability and accuracy in the model.

Bearing Graph Study

One common use of wave equation analysis is the so-called “bearing graph” study (Hannigan et. al. (2006)). In this type of study the resistance of the soil is varied with a common hammer-pile system to determine the blow counts and stresses during driving, thus constructing a “bearing graph.” A typical bearing graph is shown in Figure 52.

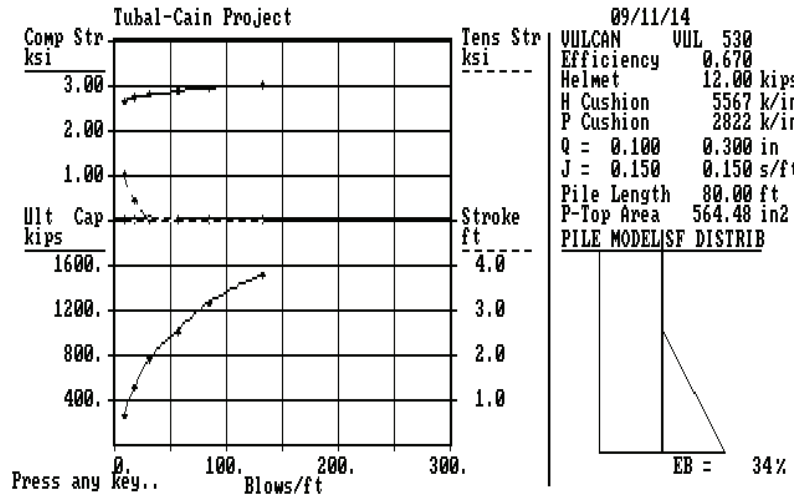


Figure 52 Bearing Graph for Air-Steam Hammer

In this study, the R_{ult} vs. blow count will be emphasized. The simple way of varying the static capacity of the pile is to vary ξ and η using Soil Model 2(b).

First the relationship was established between the parameters ξ and η and the capacity that results using Davisson's method, and this is shown in Figure 53.

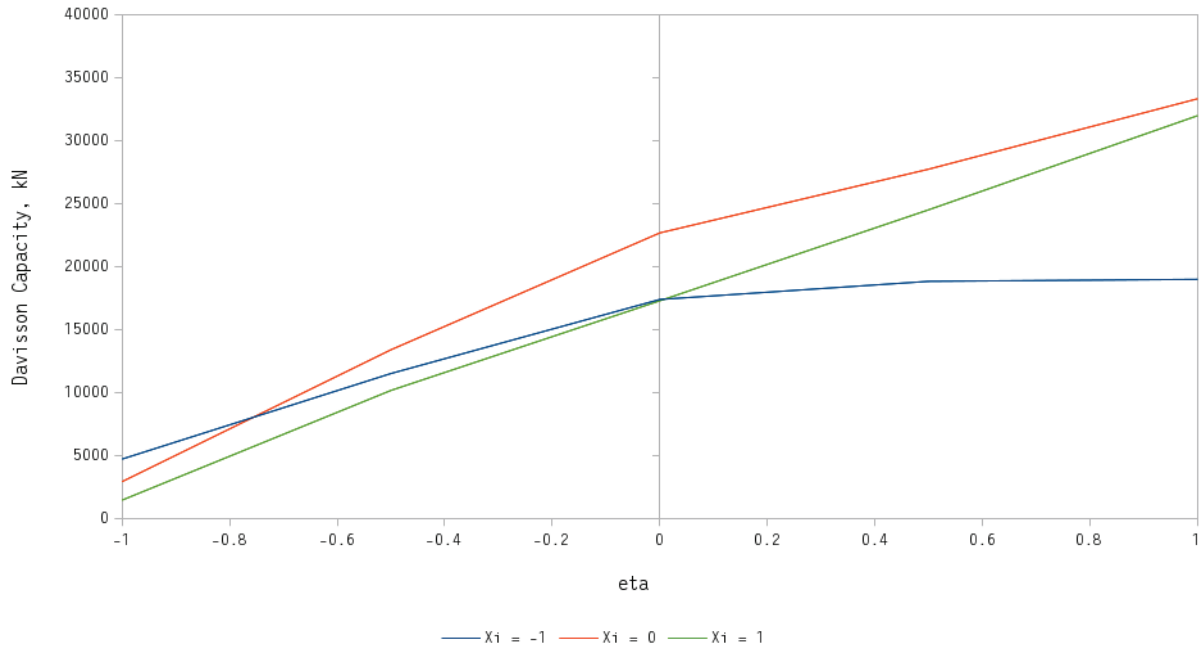


Figure 53 ξ and η vs. Ultimate Davisson Capacity

As anticipated, the increase in η for a given ξ results in an increase in the capacity/resistance of the pile. This is more pronounced in the purely cohesive soil ($\xi = 1$) and the mixed soil ($\xi = 0$) than in the purely cohesionless soil ($\xi = -1$.)

The blow count vs. Davisson capacity is shown in Figure 54.

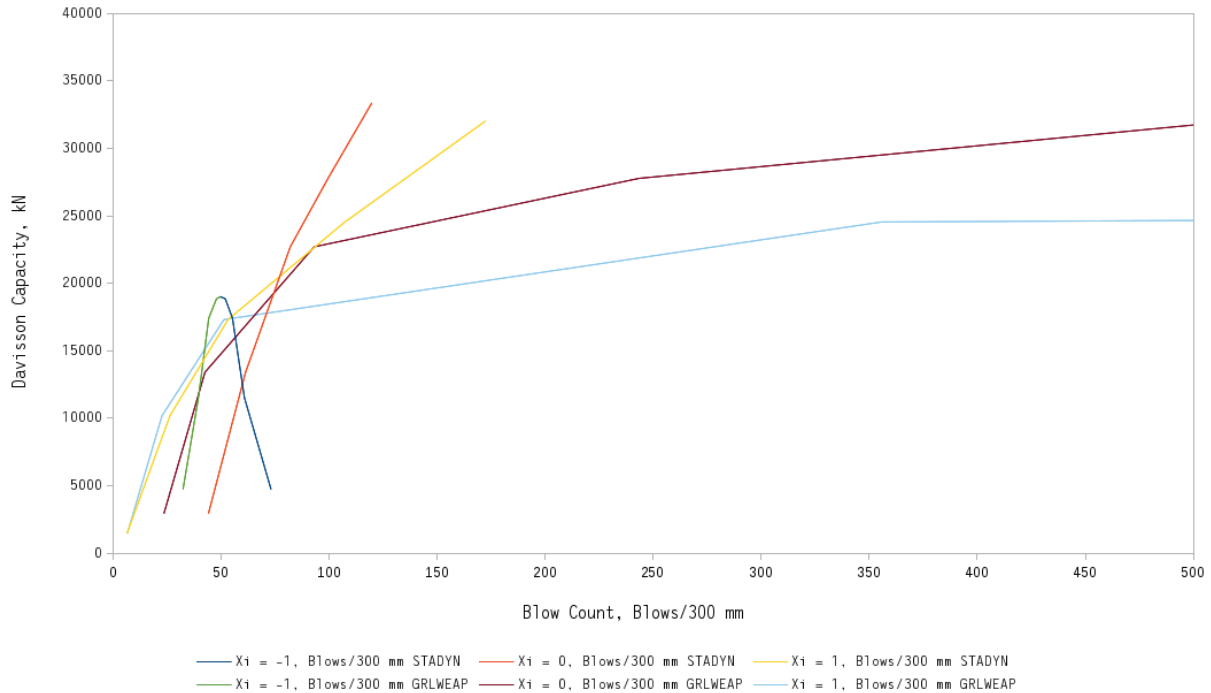


Figure 54 Blow Count vs. Davison Capacity

There were two methods used to determine the blow count. The first was the standard method used in STADYN, i.e., the average of the pile middle displacement for the last half of the analysis, in this case times between $^{8L}/_c$ and $^{16L}/_c$. The second used the method of GRLWEAP, which is to subtract a quake value from the maximum pile toe displacement (Goble and Rausche (1986)). The pile toe used quake, appropriate for an open ended pipe pile, is 2.54 mm.

With the STADYN method, the blow count trended for the mixed and cohesive soils, as one would expect. The purely cohesionless soil, however, actually saw a decrease in blow count with an increase in capacity, although there was little real variation in that blow count.

With the GRLWEAP criterion, for the purely cohesionless soil both criteria are in near agreement until a blow count of about 50 blows/300 mm, after which the

GRLWEAP criterion predicted a higher blow count for a given capacity. With the mixed soil, the GRLWEAP method produced an even flatter blow count curve. The purely cohesionless soil saw a mirror-image reversal of the trend from the STADYN method, which was an improvement; however, the capacity did not increase enough to see how the trend follows through.

Possible reasons for these phenomena include deficiencies in the blow count criterion and residual effects not modeled, even when the runs were taken to $^{16}L/c$. This suggested that the pile set criterion requires further refinement. For this study, however, and especially with the optimization study, the pile set per blow was not of primary interest, although the displacement-time history is certainly important. It is interesting to note that McVay et.al. (2002) state that the implementation of their instrumentation system “would allow the elimination of the current driving criterion based on blow count, which does not handle changing driving conditions (soil, rock hammer, etc.)”

CHAPTER VII

CASE WITH STATIC LOAD TEST

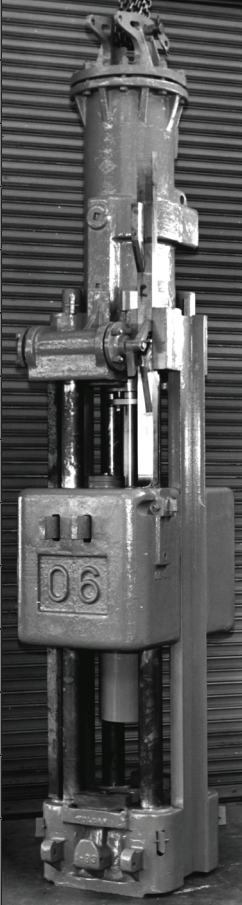
One of the most extensive comparisons performed between static analytic methods and static load tests for driven and bored piles is that of Finno (1989). It is an excellent case to study and compare with the results from STADYN, especially the static ones.

Although four (4) different piles and drilled shafts were analyzed, for this study the pipe pile will be considered. The pile outside diameter is 457.2 mm with a wall thickness of 9.52 mm. The pile was driven closed ended with a bottom plate 19.1 mm thick. The pile penetrated 15.24 m into the soil. The soil was divided into two layers as follows:

1. Loose Siliceous Sand, $\varphi = 30.5^\circ$, $\gamma_{dry} = 1610 \text{ kg/m}^3$, $\gamma_{sat} = 2002.5 \text{ kg/m}^3$, $c = 0$. The layer was 7.315 m thick and the water table was 5.182 m below the surface. For STADYN, $\xi = -1$, $\eta = -0.56$.
2. Soft Clay, $c = 24 \text{ kPa}$. For STADYN, $\xi = 0$, $\eta = -0.6$.

The piles were driven with a Vulcan 06 hammer, properties are given in Table 4.

Table 4 Properties of Vulcan 06 Hammer

Property	Value	Hammer Photo
Ram Mass	2948 kg	
Hammer Equivalent Stroke	914 mm	
Hammer Efficiency	67%	
Ram Velocity at Impact	3.46 $\frac{m}{sec}$	
Ram O.D.	285.8 mm	
Ram I.D.	0 mm	
Cross-Sectional Area of Ram	0.0642 m^2	
Ram Length	5831 mm	
Mass of Cap	464.94 kg	
Cap O.D.	482.6 mm	
Cap I.D.	0 mm	
Cap Body Thickness	322.5 mm	
Cushion Thickness	127 mm	
Cushion Material	Micarta & Aluminum	

Some important notes about Table 6 are as follows:

1. The hammer efficiency used was the “standard” GRLWEAP efficiency. Air/steam hammers have widely variable efficiencies based upon the condition of the equipment, its lubrication and the batter angle (if any) of the piles being driven. The last was not an issue here as the piles were driven plumb.
2. The “Ram O.D.,” “Ram Length” and “Cross-Sectional Area of Ram” were based on a cylindrical ram the same diameter as the cushion material. With conventional Vulcan hammers, this is not the case, as is evident from the photo in Table 6. The effect of ram shape with cushioned hammers (cushionless

hammers are another matter altogether) has been a matter of dispute for a long time; for this study, the effects of ram shape for cushioned hammers were neglected.

3. The “Cap O.D.,” “Cap I.D.,” and “Mass of Cap” were based on factory data. The “Cap Body Thickness” is derived from those data and may be different for the actual cap being used.
4. The “Cushion Thickness” and “Cushion Material” were from Finno (1989). STADYN did not model cushion plasticity/bilinearity.

The static load tests are considered first. For this case, these were performed at two (2) weeks, five (5) weeks, and forty-three (43) weeks after installation. The first and last static load tests were compared with STADYN static results and are shown in Figure 55.

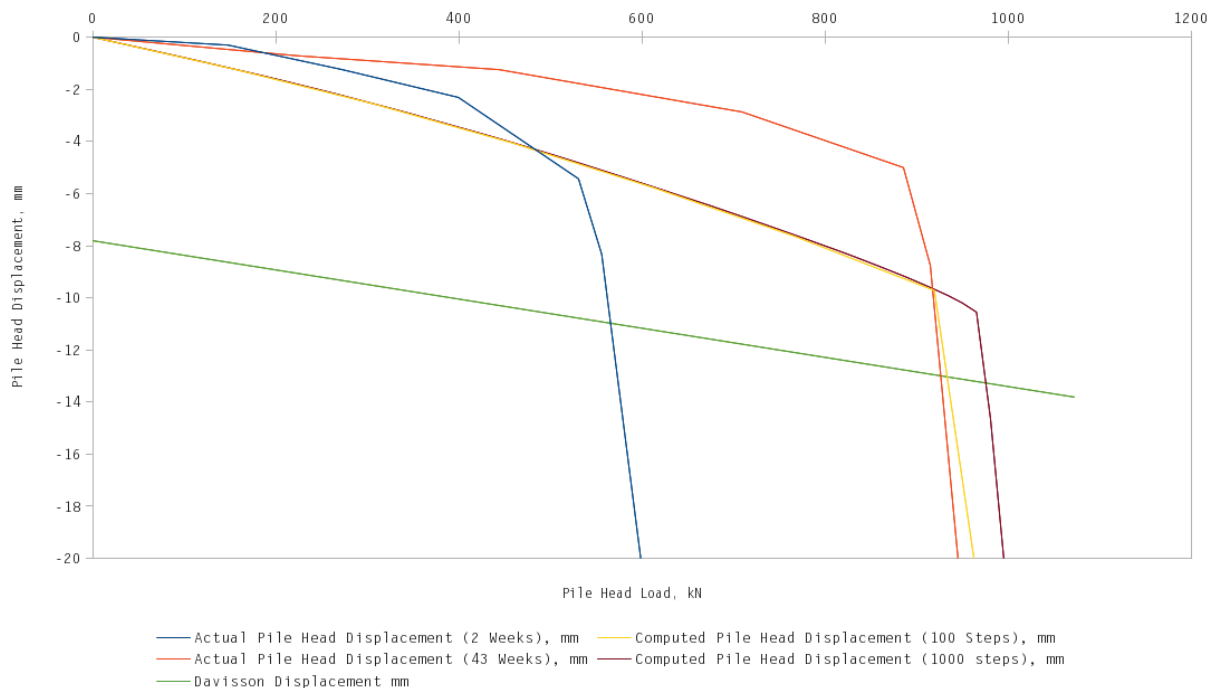


Figure 55 Comparison of STADYN results with Static Load Test Results from Finno (1989)

There were two STADYN results: one with one hundred load steps to the Meyerhof load and one with one thousand. This was done in order to output two-dimensional plots; with the larger load steps, the static load point immediately after the Davisson line is crossed showed collapse, giving results with excessive deflection. The two simulated static load test sequences resulted in virtually identical results until the “knee” in the static load curve, at which point the smaller steps extended the knee outward. The result was that, while the one hundred step static load curve had a Davisson capacity of 933 kN (very close to the original static load test) the one thousand step test increased the Davisson capacity to 976 kN.

The STADYN results showed good agreement with the longer-term result. STADYN did not have the capability to estimate either the effects of thixotropy or the elevation of pore water pressures during driving. The most significant difference between STADYN and the static load tests was that the former had a lower deflection in the lower load range. This indicates that STADYN’s estimate of the modulus of elasticity may have been too low in this case. The value of the modulus of elasticity, as discussed earlier, was the most problematic soil property in this application.

It is interesting to note that, with twenty-four static predictions, the mean for these predictions for the pipe pile was 956 kN and the standard deviation was 294 kN. It is also interesting to note that Finno (1989) does not explicitly calculate the Davisson static failure load.

For the load step just beyond the Davisson failure criterion, the pile head load was 981 kN and the toe load 10 kN. Although this did not represent a great deal of toe loading—although the pile has technically failed by this time—a look at

the results around the toe is in order. The first principal stresses around the toe are shown in Figure 56.

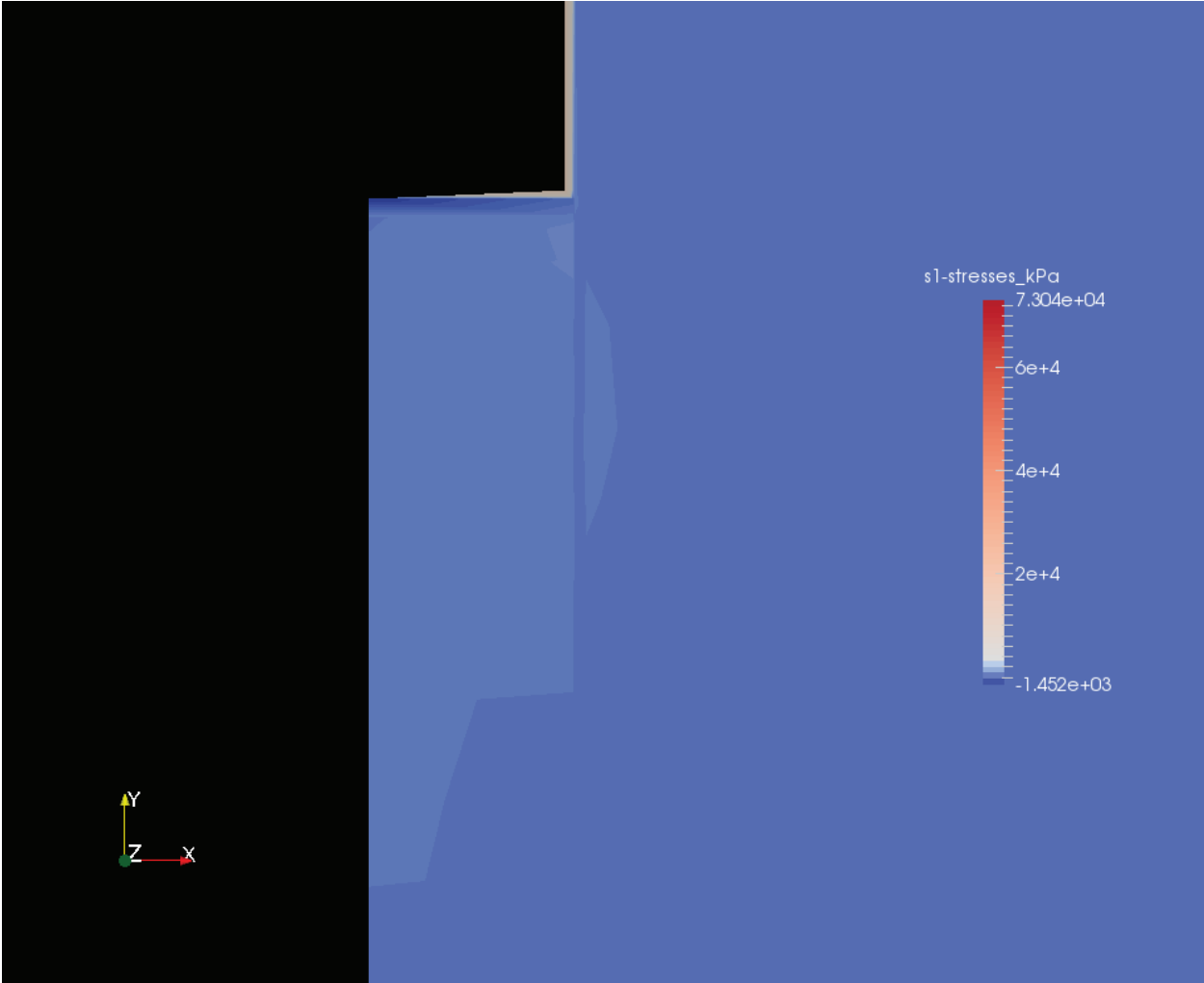


Figure 56 First Principal Stresses at Pile Toe, Simulation of Finno (1989)

The angled pile toe plate was due to STADYN’s requirement for “smooth” transitions between pile sections. The results showed elevated stresses directly under the pile toe but not far away from that. This is confirmed if the y- and x-stresses are examined in Figures 57 and 58 respectively. The x-displacements in

particular indicated that the area under the pile toe is attempting to expand, only to be resisted by the soil mass.

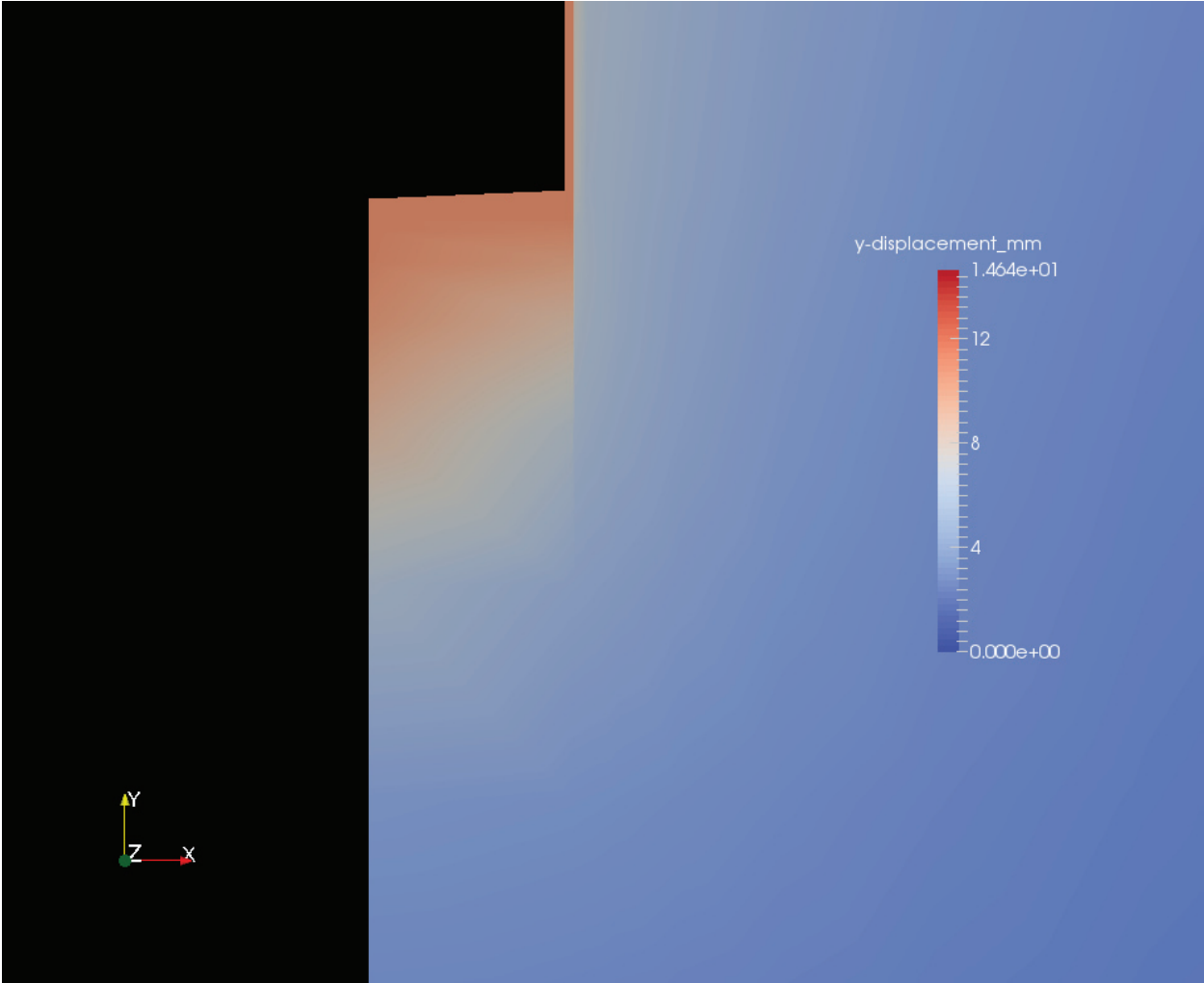


Figure 57 y-direction Displacements at Pile Toe, Simulation of Finno (1989)

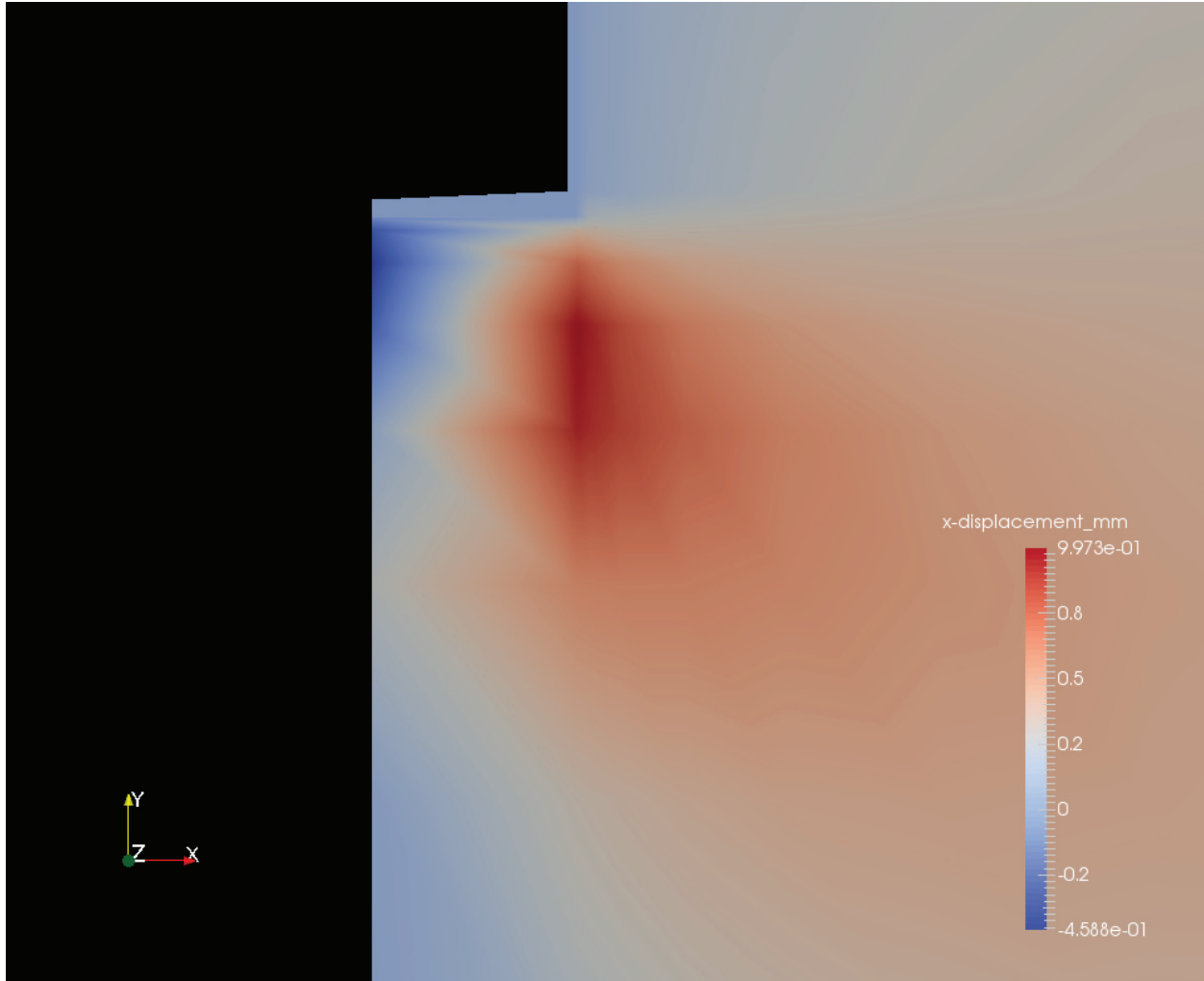


Figure 58 x-direction Displacement at Pile Toe, Simulation of Finno (1989)

Turning to the dynamic analysis, STADYN predicted the final blow count at around 18 blows/300 mm. Driving logs from the installation of the pile indicate a blow count of around 10 blows/300 mm at the end of driving. This differential was sensible since, as is evident from Figure 55, the resistance of the pile at the time of driving was considerably lower (due to set-up effects) than the long-term resistance. STADYN’s result was more of a “restrike” type of result, and a restrike was not performed in the course of this study. The low blow counts also made comparison difficult; low blow counts will also play an important part in the optimization study.

The y-displacement-time history is shown in Figure 59 and the y-stress-time history is shown in Figure 60. As before, with these plots the x-axis is a time axis.



Figure 59 y-displacement-time History, Simulation of Finno (1989)

Focusing first on the pile head, the pile displaced in two steps. Ultimately the differences between the displacements of the various points along the pile (the cross-section is uniform except for the pile toe) began to fade as the hammer energy is dissipated into the soil.

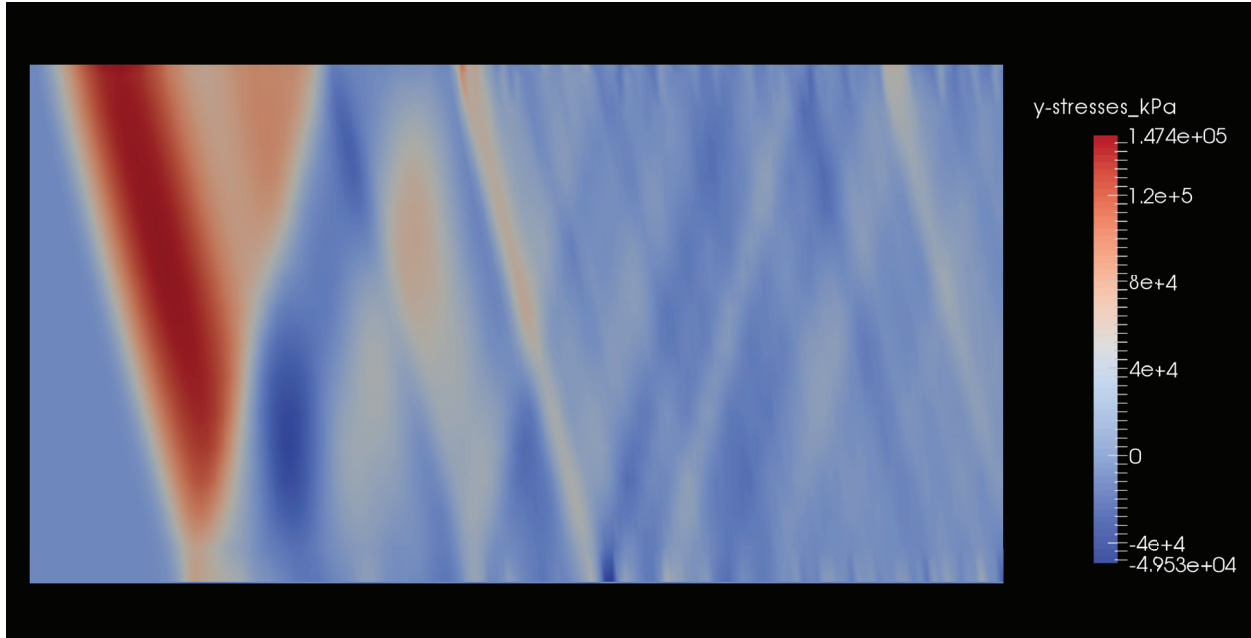


Figure 60 y-stress-time History, Simulation of Finno (1989)

For this case, the toe showed less of the “free-end” characteristics than the earlier case, with substantial compressive stresses extending to the pile toe itself. This reflected the difference between the closed toe of this simulation and the open toe of the earlier case. The reflection was likewise not as strongly tensile and was more affected by the intermediate reflections of the shaft. Examination of both pile head (top edge of the graph) and pile toe (bottom edge of the graph) show more local variations in time than the regions between the two. This is because the parasite oscillations were for the most part generated at the boundaries of the pile.

Visible in both figures but especially Figure 60 is an additional stress wave in the middle of the diagram. This was probably due to an additional striking of the pile head by the driving accessory. This also added to the parasite oscillations.

CHAPTER VIII

COMPARISON WITH GRLWEAP

Another interesting comparison to make was with GRLWEAP, a widely used one-dimensional wave equation program. The test case was a notional soil profile from Southeast Asia, into which a 150 m long pile was driven 70 m into the sea bed for a conventional offshore oil platform. The pile was a 1372 mm O.D. \times 51 mm wall thickness open ended pipe pile. Neither plugging nor set-up effects were considered for this analysis.

The soil profile is given in Table 5.

Table 5 Soil Profile for GRLWEAP Comparison

Soil Characterization	Layer Thickness, m	Submerged Unit Weight, $\frac{\text{kN}}{\text{m}^3}$	Cohesion, kPa	ξ	η	Saturated Unit Mass, $\frac{\text{kg}}{\text{m}^3}$
Very Soft Clay	3	5	10	1	-1	1510.2
Medium Clay	10	7	40	1	-0.65	1714.3
Very Stiff Clay	16	8	120	1	0.2	1816.3
Stiff to Very Stiff Clay	25	9	80	1	-0.25	1918.4
Hard Clay	8	8	200	1	1	1816.3
Very Stiff Clay	8+	8	160	1	0.6	1816.3

The differences between the submerged unit weight (based on the soil data) and the saturated unit mass was due to the fact that the latter are based on as close a match of ξ and η as possible. The cohesion was most closely matched, but the soil properties scheme had difficulty replicating the high void ratios of the original soil. For cohesive soils, this is not as much a difficulty as it is with those with friction

angle, as the Mohr-Coulomb failure criterion is based strictly on the cohesion when $\varphi = 0$.

In performing the two types of analyses, the differences between the GRLWEAP analysis and the STADYN analysis quickly become evident. With GRLWEAP, it was first necessary to use soil properties to perform a static analysis on the pile. From there the SRD was estimated and then additional values above and below were added to arrive at a “bearing graph” (see Figure 52) type of analysis. With STADYN, the soil properties were directly applied to the model, which used these in the dynamic and static analysis to model the dynamic performance of the system and estimated the SRD through a simulated static load test.

GRLWEAP Results

The first step in the GRLWEAP analysis was to construct the hammer, pile and soil model in the program. The pile was straightforward, being uniform in diameter and cross-section. The hammer selected was a Vulcan 5110, with properties shown in Table 6.

Table 6 Properties of Vulcan 5110 Hammer

Property	Value	Hammer View
Ram Mass	49896 kg	
Hammer Equivalent Stroke	1524 mm	
Hammer Efficiency	67%	
Ram Velocity at Impact	4.47 m/sec	
Ram O.D.	793.7 mm	
Ram I.D.	0 mm	
Cross-Sectional Area of Ram	0.495 m ²	
Ram Length	12796 mm	
Mass of Cap	17872 kg	
Cap O.D.	1905 mm	
Cap I.D.	0 mm	
Cap Body Thickness	795.6 mm	
Cushion Thickness	787.4 mm	
Cushion Material	Micarta & Aluminum	

With the soil properties, static methods were employed to estimate the SRD. Although these are not always ideal (SRD and ultimate pile capacity are not always identical) it is a reasonable start. For offshore piling, two methods were used for this purpose: the Dennis and Olson (1983) method for clay and the API RP2A method (American Petroleum Institute (2002)), which is widely used and recommended by Mukherjee and Nagarajub (2013) in the region under consideration. Applying the soil properties and pile geometry, the ultimate capacities (which are then used for the SRD) are shown in Table 7. Both methods indicated that most (~99%) of the SRD was shaft resistance, which is typical for this type of pile. All other soil properties entered into GRLWEAP followed the recommendations of the software instructions except for the shaft damping, which was set at either 0.2 sec/m or 0.3 sec/m, following the recommendations of Mukherjee and Nagarajub (2013).

The blow count results at the SRD computed for both static methods and damping parameters are shown in Table 7.

Table 7 SRD and Blow Count Results from GRLWEAP Calculations

Parameter	Dennis and Olson (1983)	American Petroleum Institute (2002)
SRD, kN	20,279	26,417
Blow Count, 0.3 $\frac{\text{sec}}{\text{m}}$ damping, $\frac{\text{blows}}{\text{m}}$	72.5	142.3
Blow Count, 0.2 $\frac{\text{sec}}{\text{m}}$ damping, $\frac{\text{blows}}{\text{m}}$	61.2	109.3
Blow Count, 0.3 $\frac{\text{sec}}{\text{m}}$ damping, $\frac{\text{blows}}{0.3 \text{ m}}$	21.8	42.7
Blow Count, 0.2 $\frac{\text{sec}}{\text{m}}$ damping, $\frac{\text{blows}}{0.3 \text{ m}}$	18.4	32.8

Decreasing the damping by a third resulted in a 20-30% change in the blow count, which illustrates the sensitivity of the results to the damping.

The bearing graph that resulted for damping of 0.3 sec/m is shown in Figure 61.

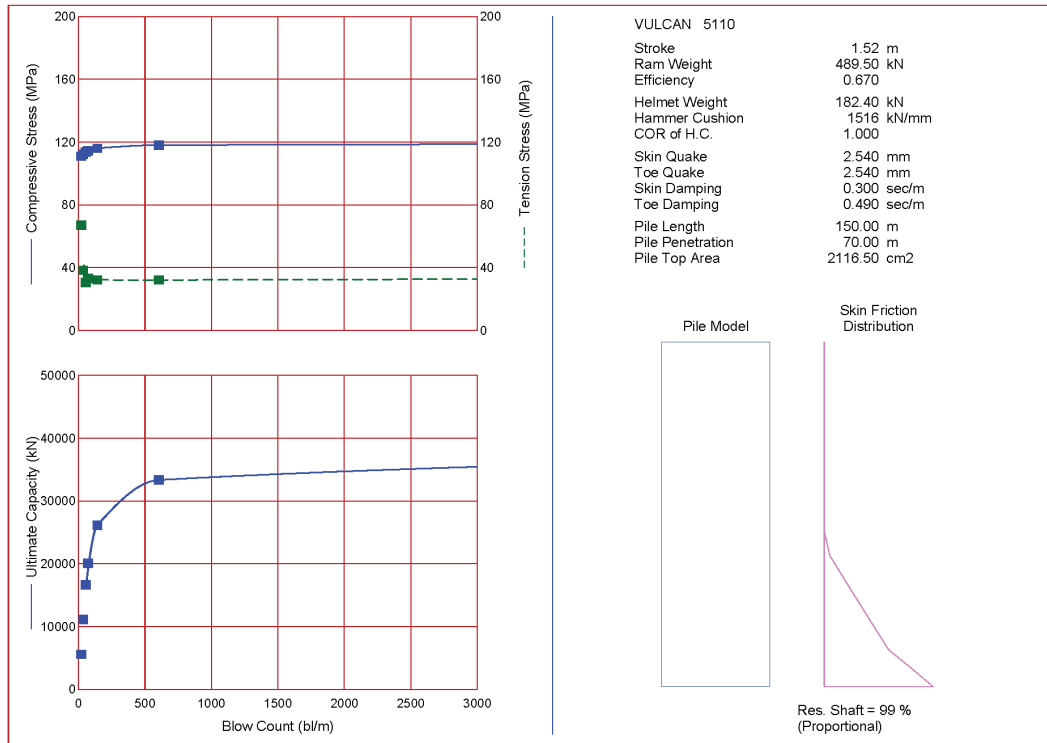


Figure 61 Bearing Graph Results for GRLWEAP Comparison

The force and velocity time curves for the same damping are given in Figure 62.

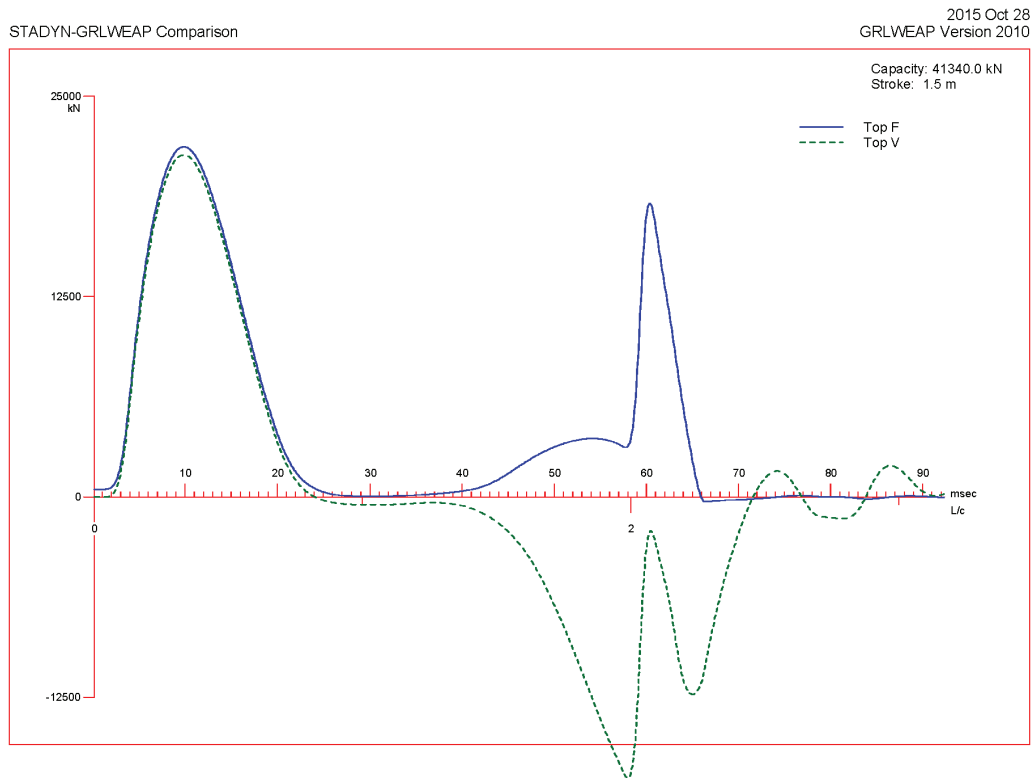


Figure 62 Force-and Velocity-Time Results for GRLWEAP Comparison

It should be noted that the pile head velocity was multiplied by the impedance of the pile to enable it to be plotted with the force, in accordance with semi-infinite pile theory (Warrington (1997)). It should also be noted that the force-time history was for an SRD higher than either of the computed estimates.

STADYN Results

The input for STADYN used the same method as before. The model is shown in Figure 63.

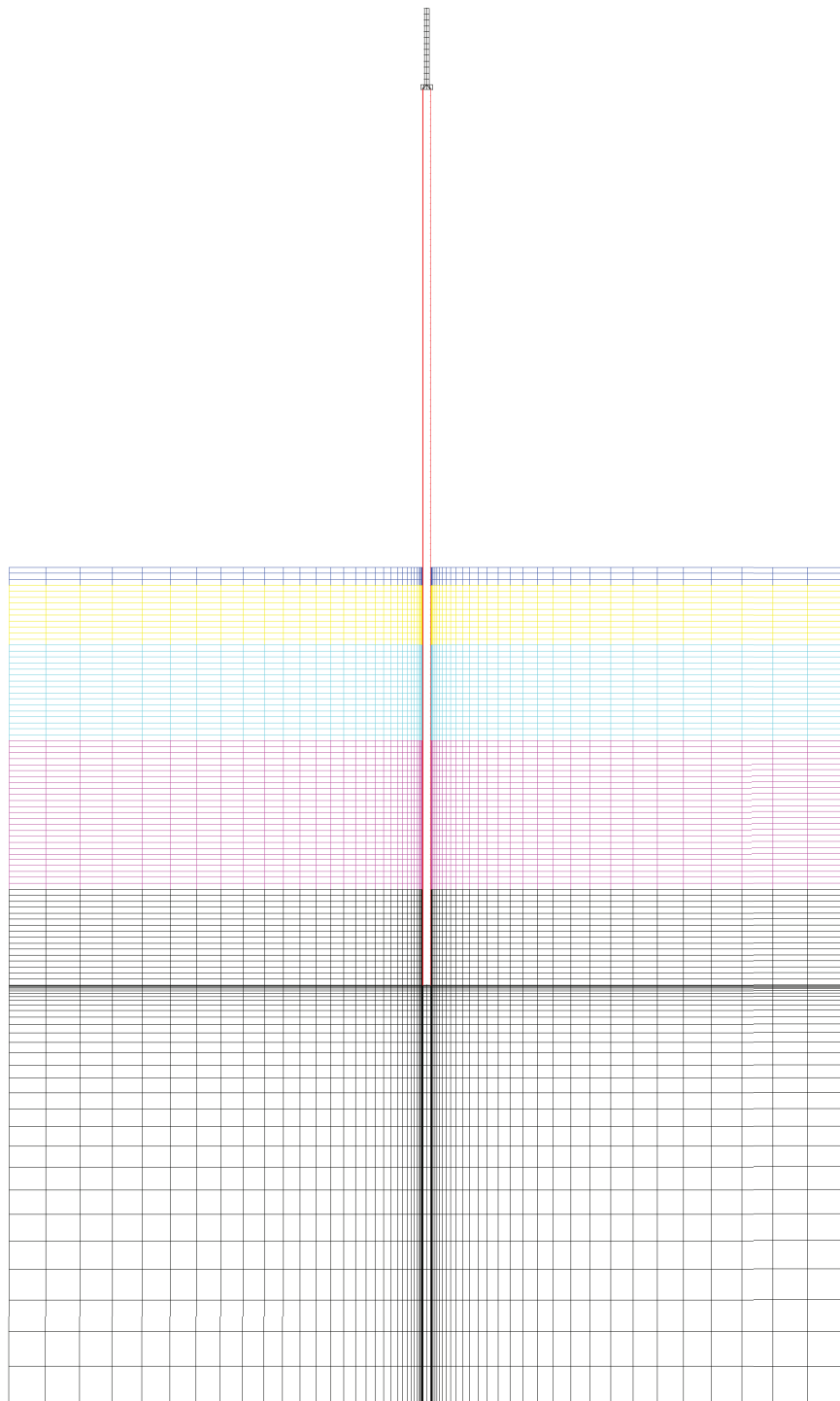


Figure 63 STADYN Model for GRLWEAP Comparison

The dynamic run was done first and the results were shown in Figure 64.

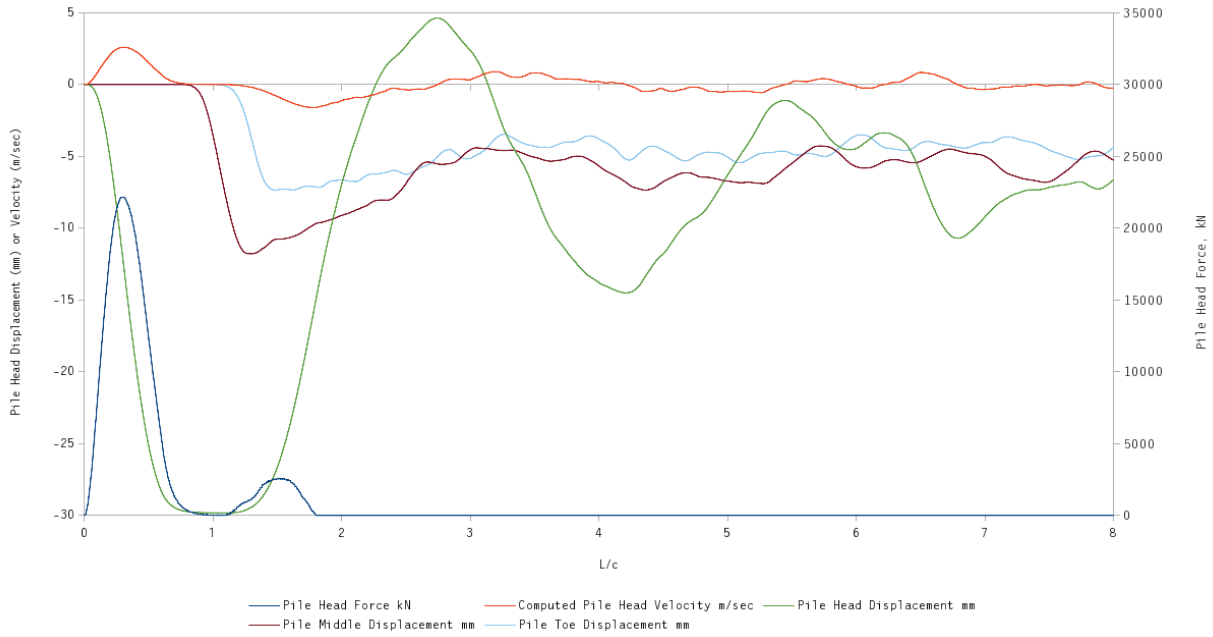


Figure 64 STADYN Force-, Velocity- and Displacement-Time Results for GRLWEAP Comparison

The pile, within internal oscillations, stabilized after about $3L/c$. Thus, a more reasonable result for the permanent set/blow count could be expected. Using the STADYN criterion developed earlier, the blow count was 51.6 blows/300 mm, or 172 blows/meter.

Static load test results are shown in Figure 65.

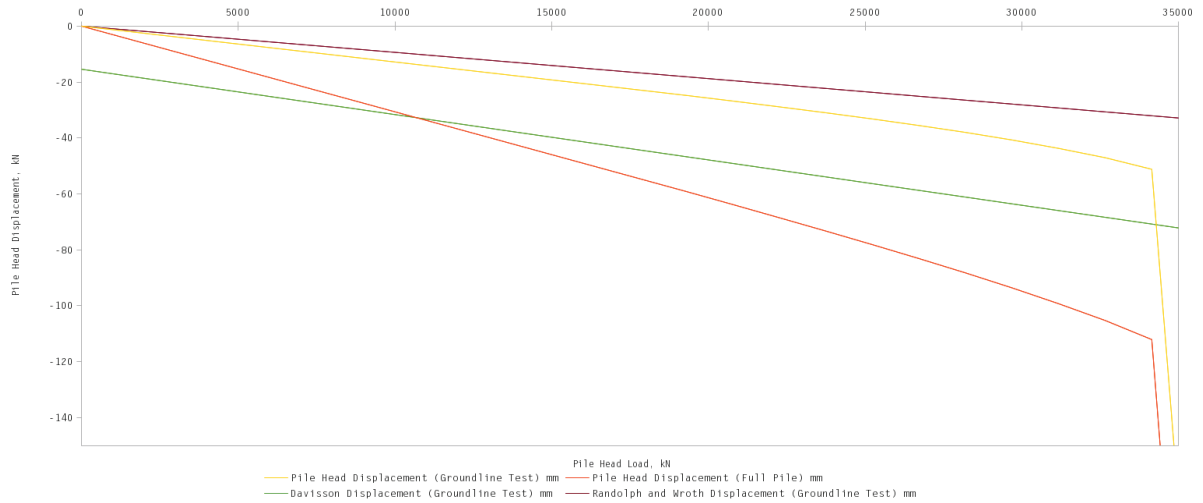


Figure 65 STADYN Static Load Results for GRLWEAP Comparison

The static load test was run two ways. One was with the load at the pile head. The other was a “mudline” test, i.e., if the pile was cut off at the mudline and statically load tested there. The latter variant, which is shown in Figure 65, was done for two reasons:

1. To have results which corresponded with the method of Randolph and Wroth (1978), which assumes a pile starting at the mudline. The Davisson line is for the mudline case.
2. To investigate the effects of the unsupported length of the pile on the static load-deflection test.

The interpretations of those static load tests are summarized in Table 8.

Table 8 Static Load Interpretations for GRLWEAP Comparison

Interpretation Method	Mudline Test, kN	Actual Pile Head Test, kN
Davisson Load	34285	34290
Brinch-Hansen 80% Load	35627	37111
Brinch-Hansen 90% Load	35627	35627
Maximum Curvature Load	35627	35627
Slope-Tangent Load	35253	35253

The results vary little between the two cases, and for that matter are consistent among themselves.

Comparison of the Results

The following observations are made in comparing the force and velocity results of the two methods:

1. The peak pile head force for GRLWEAP was 21856 kN and for STADYN 22158 kN, a difference of 1.4%.
2. The peak pile head velocity for GRLWEAP was 2.48 m/sec and for STADYN 2.59 m/sec, a difference of 4.2%.
3. One possible explanation as to why STADYN's values for force and velocity were higher than GRLWEAP's is that the latter uses a dissipative model (coefficient of restitution) model at the interfaces. Another source of difference may be beam effects in the cap, which would have increased the cap's flexibility and thus its spring constant.

The most divergent results were those of the blow count and SRD. STADYN's blow count was 21% greater than GRLWEAP's at the higher (0.3 sec/m) damping value and using the method of the American Petroleum Institute (2002). STADYN's

SRD was even more divergent, being 31% higher than the method of the American Petroleum Institute (2002). The blow count results are considered first.

Figure 61 shows a range of possible SRD's and blow counts, as is typical with bearing graphs. The whole rationale for the bearing graph approach is to allow for variations in actual SRD and to quantify those variations using the actual blow count results. If STADYN's actual predicted blow count was replicated in the field, using Figure 61 and linear interpolation the SRD would be estimated to be 26,577 kN, which is 1.7% greater than the SRD estimated by the method of the American Petroleum Institute (2002). So the significance of this blow count variation at this range of SRD's is not great.

This variation should be compared with the variations induced by changing the damping coefficient. If the damping coefficient is increased less than 10% from its upper bound value of 0.3 sec/m, then the SRD estimated by the method of the American Petroleum Institute (2002) would allow GRLWEAP to replicate STADYN's blow count estimate. This should be compared with the effects of decreasing the damping coefficient to its lower bound values, which can be seen in Table 7.

This leaves the divergence in SRD between STADYN and the method of American Petroleum Institute (2002) and even more the method of Dennis and Olson (1983). At this point, some important factors need to be considered.

First, it is admitted that Davisson's Method, for all of its virtues, is not entirely relevant for offshore piling. However, Table 8 shows that the results from the other methods—which are more intended to determine a plunging failure point—are not that different from Davisson's.

Second, static load testing is uncommon in offshore piling due to their size and the cost of testing. Most piles for offshore structures, be they driven or suction

piles, are primarily loaded laterally or in tension. The lateral capacity of piles is beyond both GRLWEAP and STADYN; the tension capacity for high frictional piles such as this one is very close to the compressive. Further complicating the comparison is, as Audibert and Banford (1989) noted about static methods of pile capacity, "...the effects of pile plugging, the time after driving, and the increase with time in the shear transfer capacity (commonly referred to as set-up), were not considered." The American Petroleum Institute (2002) method was one of those static methods explicitly discussed by Audibert and Banford (1989). In offshore piling, set-up can take years to complete, and was not included in the STADYN model.

Third, the static load tests at the mudline and when the pile's protrusion is included had virtually identical static load capacities but very different force-deflection characteristics. For the SRD's estimated by Dennis and Olson (1983) and the API RP2A methods, the deflections of the mudline case and the actual pile head case vary by approximately 40-47 mm, which is a significant difference. With a conventional offshore platform, a static load test would be run from the top (before the platform is grouted to the pile) and in service, the mudline case would be more relevant to the actual performance of the pile. Irrespective of the merits of STADYN's method for estimated static load capacity and SRD, this was another illustration of the fallacy of divorcing the load-deflection characteristics of the pile from its capacity, which traditional static load capacity methods tend to do.

Finally, for cohesive soils one thing that would bring down STADYN's SRD would be to apply an alpha factor to the soil cohesion. With this type of a method, the SRD and capacity are assumed independent of effective stress and solely dependent upon cohesion, which complies with Mohr-Coulomb theory (see Equation 19.) However, other static methods are "beta" methods, which include the effects of effective stress. The API RP2A method attempts to combine the two. One way to

model this in STADYN would be to include some friction by making $\xi < 1$, either in the entire soil mass or in the elements adjacent to the pile (interface elements.) This must be done carefully, however, because STADYN includes effects of soil elasticity and the deflection that results therefrom, and may require different adjustments than is conventionally done with static methods. This issue was discussed in Serdaroglu (2010) and needs further investigation.

An important conclusion is that the static methods used in conjunction with GRLWEAP and the static load interpretation methods used to reduce STADYN's methodology to "a number" are not always directly comparable, especially with the long offshore piles under consideration. On the other hand, using the same hammer, soil and pile data to define the system, both routines arrive at comparable blow count results within the limits of the methodology being employed.

CHAPTER IX

OPTIMIZATION RUNS AND CAPWAP COMPARISON

With the basic integrity of the model established, it is necessary to test STADYN's signal matching capabilities. For this case, actual field data were made available for meaningful comparison.

Overview of Field Data

The field data were taken from Mondello and Killingsworth (2014). The pile driven was a test pile to verify the performance of the Vulcan SC-9 hammer, which is a relatively new type of air/steam hammer. There were no soil boring logs available for this test site; however, for a location less than 500 meters from the test pile, a soil boring was available and is shown—along with the key for soil consistency—in Figure 66. The key for the Unified System of soil classification is shown in Figure 67.

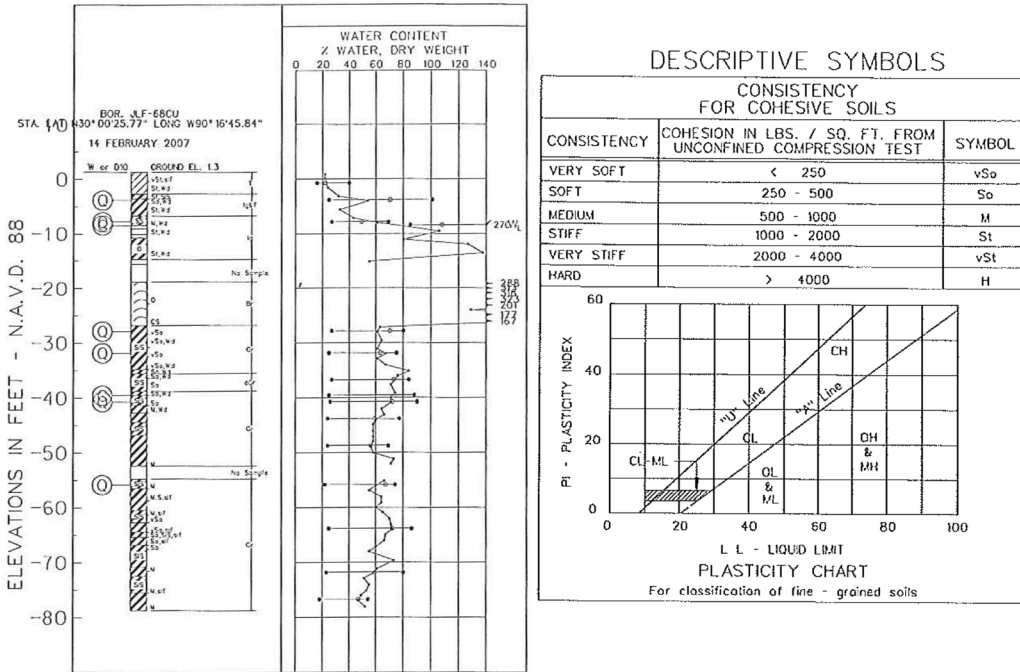


Figure 66 Soil Boring Logs for Nearby Job (from USACE Solicitation W912P8-10-R-0011)

UNIFIED SOIL CLASSIFICATION

MAJOR DIVISION	TYPE	LETTER SYMBOL	TYPICAL NAMES	
COARSE-GRAINED SOILS More than half of material is larger than No. 200 sieve size	CLEAN GRAVEL (Little or No Fines)	GW	GRAVEL, Well-Graded, gravel-sand mixtures, little or no fines	
	GRAVELS of coarse fraction is larger than No. 4 smaller than No. 4 sieve size	GP	GRAVEL, Poorly-Graded, gravel-sand mixtures, little or no fines	
	SANDS More than half of coarse fraction is smaller than No. 4 sieve size	SANDS w/ FINES (Appreciable Amount of Fines)	GM	SILTY GRAVEL, gravel-sand-silt mixtures
		CLEAN SAND (Little or No Fines)	GC	CLAYEY GRAVEL, gravel-sand-clay mixtures
	FINE-GRAINED SOILS More than half the material is smaller than No. 200 sieve size	SANDS w/ FINES (Appreciable Amount of Fines)	SW	SAND, Well-Graded, gravelly sands
		SILTS & CLAYS (Liquid Limit < 50)	SP	SAND, Poorly-Graded, gravelly sands
			SM	SILTY SAND, sand-silt mixtures
FINE-GRAINED SOILS More than half the material is smaller than No. 200 sieve size	SILTS & CLAYS (Liquid Limit > 50)	SC	CLAYEY SAND, sand-clay mixtures	
		ML	SILT & very fine sand, silty or clayey fine sand or clayey silt with slight plasticity	
		CL	LEAN CLAYS: Sandy Clays; Silty Clays; of low to medium plasticity	
		OL	ORGANIC SILTS and organic silty clays of low plasticity	
		MH	SILT, fine sandy or silty soil with high plasticity	
HIGHLY ORGANIC SOILS	SILTS & CLAYS (Liquid Limit > 50)	CH	FAT CLAY, inorganic clay of high plasticity	
		OH	ORGANIC CLAYS of medium to high plasticity, organic silts	
		PT	PEAT, and other highly organic soil	
WOOD		Wd	WOOD	
NO SAMPLE				

NOTE: Soils possessing characteristics of two groups are designated by combinations of group symbols
A comma will be used between modification symbol. Example: So, Gr, w/SS, S/S, (CH)

Figure 67 Unified Soil System Key for Figure 66 (from USACE Solicitation W912P8-10-R0011)

The actual force-and velocity-time curves are shown in Figure 68 and the estimated static load test results (based on CAPWAP data) are shown in Figure 69. A photo of the test setup, showing the hammer and pile, can be seen in Figure 70.

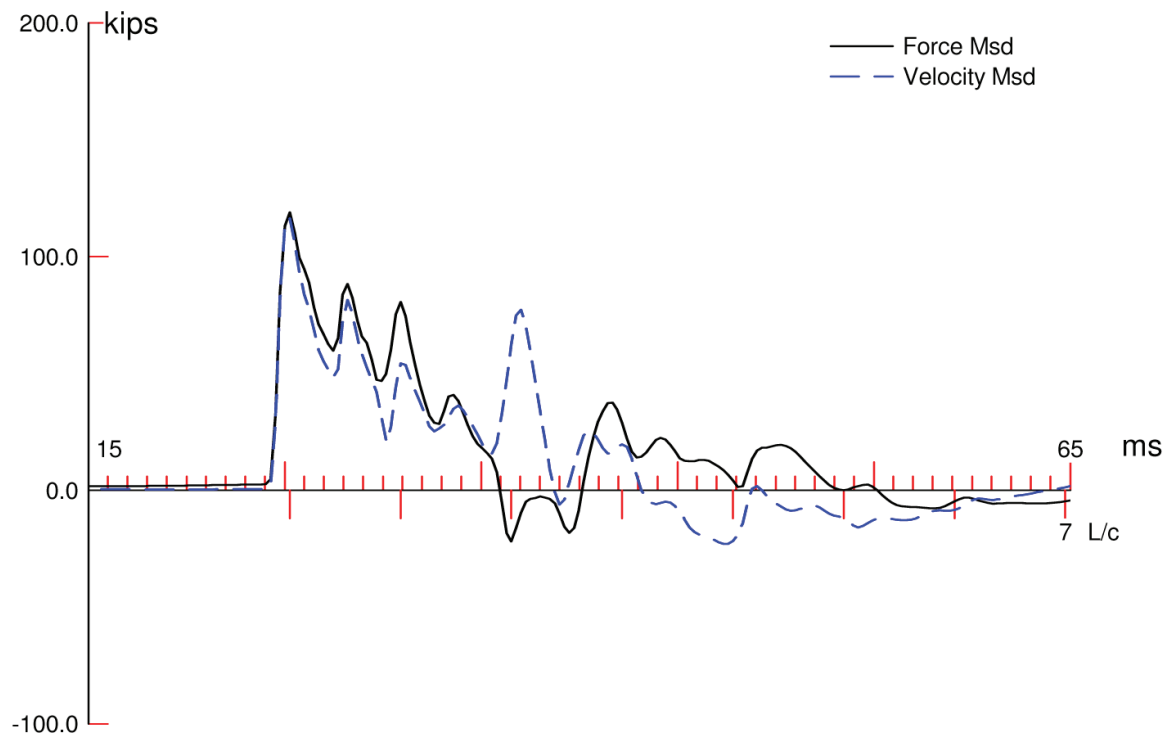


Figure 68 Force-time and Velocity-time histories for SC-9 Test (from Mondello and Killingsworth (2014))

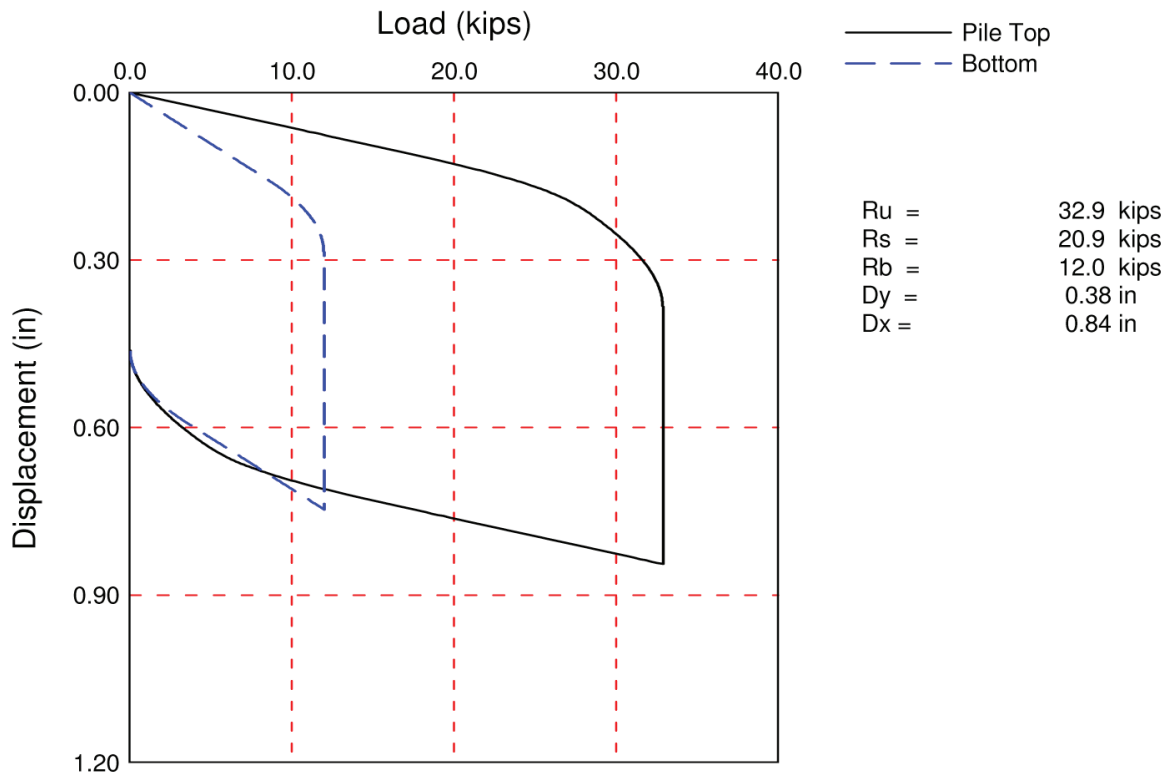


Figure 69 Estimated Static Load Test Results (from Mondello and Killingsworth (2014))



Figure 70 Test Setup for Mondello and Killingsworth (2014)

There are some things to note about this test and the data:

1. The pile is somewhat unusual in that it is a 172 mm O.D. x 13 mm wall thickness steel pipe pile, 13.72 meters long, which then has a timber pile “stinger” on the end 305 mm in diameter at the top, 254 mm at the butt, and 10.67 m long. This means that the pile is composite, with two different cross

sections and acoustic speeds. Many theoretical methods (such as Liang (2003)) and even new signal matching techniques such as iCAP® (Likins, Liang and Hyatt (2012)) only permit uniform piles. This is an additional challenge to the signal-matching algorithm. Also, since the wood pile “stinger” is larger than the pipe pile (it is unusual for a stinger to be larger than the parent pile) it is reasonable to expect that the resistance along the shaft of the steel segment will be reduced in a sort of “solid jetting” procedure.

2. The results in Figure 69 include an estimated static load. It is not explicitly stated which static load test criterion was used to arrive at this number, or the methodology employed, although traditionally CAPWAP has been correlated with the Davisson criterion (Rausche et.al. (2010)). The ultimate resistance obtained by the method used is 146.3 kN. CAPWAP achieved a Match Quality of 3.96, which is near the upper limit of typical values for this parameter.
3. The observed set for the blow being analyzed is 11.73 mm, which translates into a blow count of 26 blows/300 mm. While this is not unusual for pile driven into the stratigraphy of the New Orleans area, this is a fairly low blow count both for pile driving in general and for analysis using pile dynamics in particular. The large displacements further add to the variability of the results. It is interesting to note that the CAPWAP computed set is 8.33 mm, or a blow count of 36 blows/300 mm, which is considerably different from the observed blow count. One persistent danger in the result is that, with the soil as soft as it is, the model always operated close to the collapse load, a characteristic exacerbated by the purely plastic nature of the soil’s response beyond the elastic limit (see Figure 9.)
4. The available boring logs indicate that the soils are predominantly soft to medium fat clays with some silts and organic material. Based on these data and

experience with the soils in the area, the water table was assumed to be 1 meter below the ground surface. Static load tests were not available for this job site or pile.

5. For best results using dynamic analysis, measured data are typically taken in a “restrike” condition. This is to allow pore water pressures around the pile, which are elevated during driving, to dissipate to the state they would be in during service. Chen et.al. (2011) show that this process is a consolidation process, which involves the elevation and dissipation of pore water pressures. Unfortunately in this case the data were taken during driving; the set-up factor is unknown. Although this tends to depress the ultimate resistance during driving, the effect this has on the correlation introduces yet another uncertainty. Wang, Verma and Steward (2009) performed an extensive study on set-up factors on a South Louisiana job site; however, they note that “...the predictability of the models still needs to be improved with more dynamic and static testing data.”
6. Although Mondello and Killingsworth (2014) state that “(t)he hammer was reportedly operated at the maximum 3.0 feet ram stroke height during testing”, video taken of the hammer during operation do not indicate that this is the case. Since the SC-9 is a closed hammer, i.e., the ram is internal, it is more difficult to determine the stroke without instrumentation than it is with an open-style hammer.

While many of the aspects of this test project were less than ideal for correlation purposes, it was judged suitable because of the availability of a complete CAPWAP report on the results.

Summary of Results

The field recorded pile head force-time curve was input into STADYN and the resulting velocity-time traces were compared with field data. This was done repetitively, varying the soil parameters with the polytope method, until the tolerance of the optimization method was achieved.

To obtain a broad scope of results, the shaft layering was divided in a number of ways. A separate layer for the toe resistance was always maintained. The shaft layering was divided as follows:

1. One shaft layer for the entire length of the shaft.
2. Two shaft layers, one for the upper, steel portion of the shaft and one for the lower, wood portion of the shaft.
3. Four shaft layers, two evenly divided layers for the upper portion and two for the lower portion.
4. Eight shaft layers, four evenly divided layers for the upper portion and four for the lower portion.
5. Each finite element row as a layer, which worked out for twelve (12) layers for the upper portion and the same number for the lower.

The two-shaft layer model is shown in Figure 71. The top “layer” was in fact the upper layer above the water table and the one under it the upper layer below the water table. It should be noted, however, that values of ξ and η are maintained at the same value on both sides of the phreatic surface.

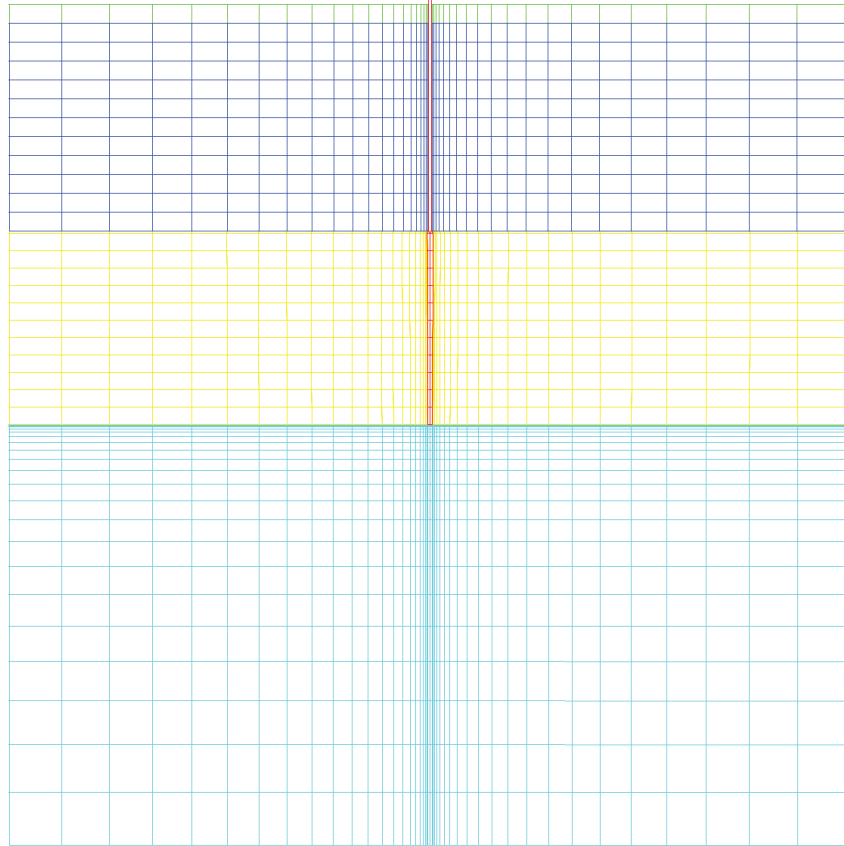


Figure 71 Two Shaft Layer Model for Mondello and Killingsworth (2014) Comparison

A summary of the results is given in Table 9. Graphical representation of the RMS differences is shown in Figure 72 and the static load test results in Figure 73.

Table 9 Overall Results of Mondello and Killingsworth (2014) Comparison

Method	Number of Shaft Layers	Davisson Ultimate Capacity, kN	Number of Optimization Steps	RMS Difference
Standard Polytope	2	269.5	3000	0.00155
Standard Polytope	4	186.2	2996	0.00192
Standard Polytope	8	118.1	3000	0.00194
Standard Polytope	24	23.0	3000	0.00207
Annealed Polytope	2	No Result	No Result	No Result
Annealed Polytope	4	187.1	2515	0.00149
Annealed Polytope	8	28.5	2493	0.00200
Annealed Polytope	24	160.7	2876	0.00175

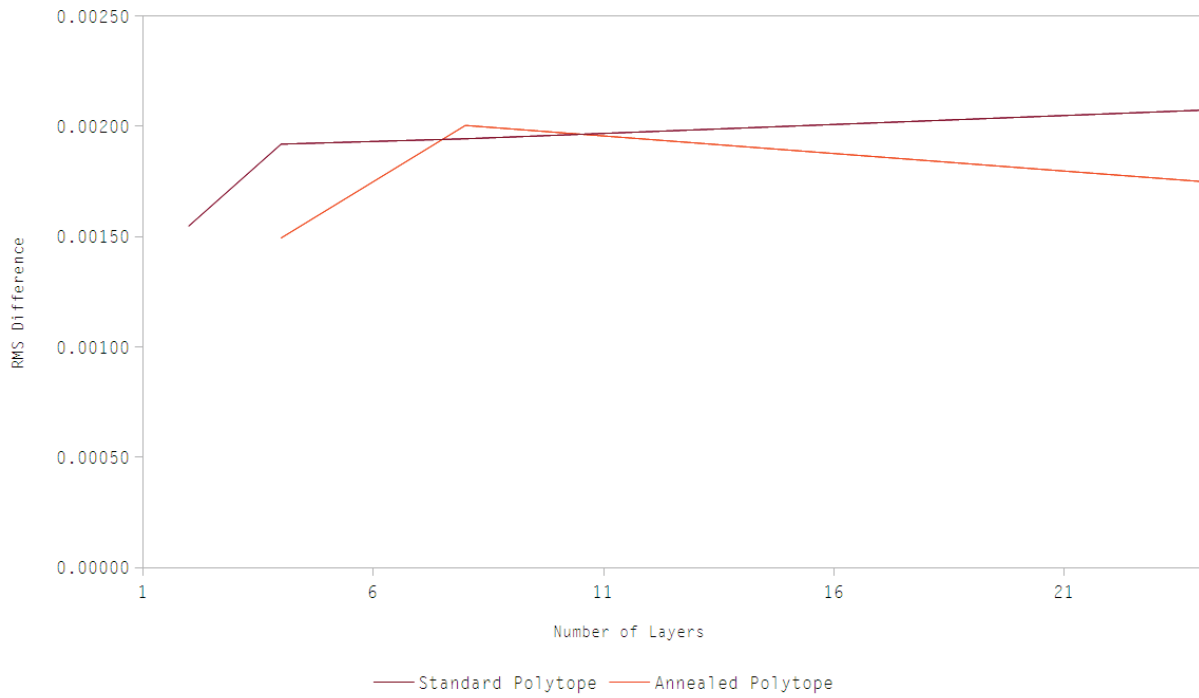


Figure 72 RMS Differences of Mondello and Killingsworth (2014) Comparison

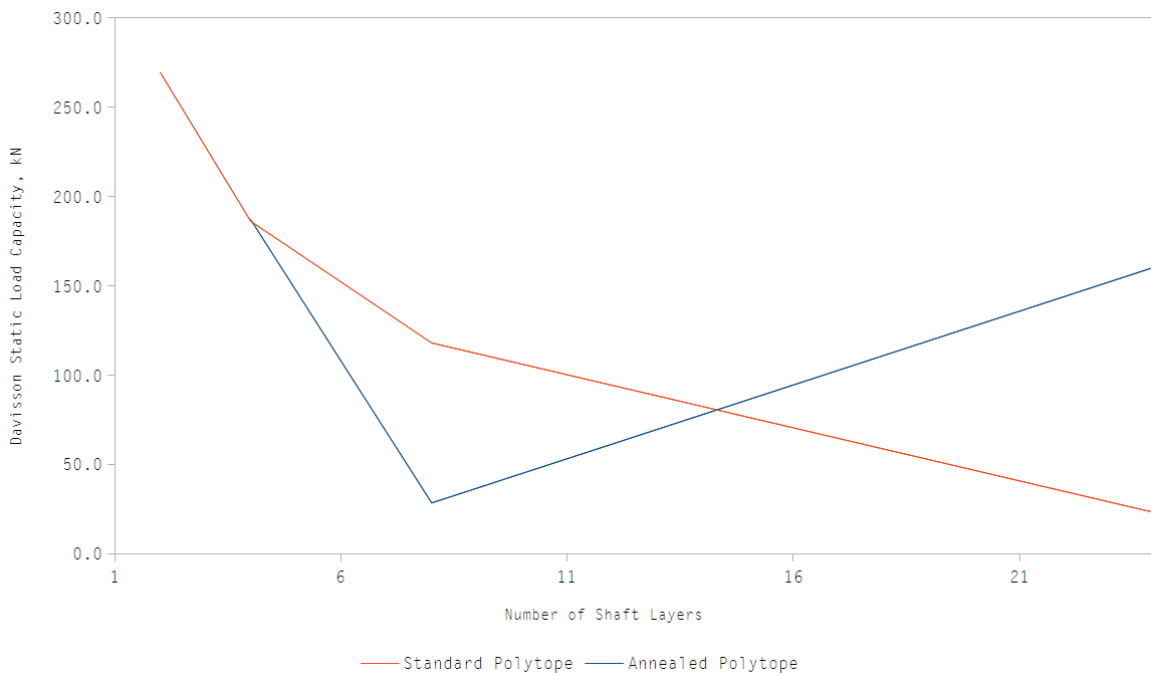


Figure 73 Static Load Test Results of Mondello and Killingsworth (2014) Comparison

The single shaft layer runs produced no meaningful result. The optimization methods drifted into unrealistic values of η , which given the soft soils was always a danger. In any case single layer runs for this particular pile configuration were not realistic; the stratigraphy may justify using it, but the vast differences in the pile profile did not. The annealed two-layer run likewise did not produce a meaningful result; the perturbations induced by the annealing method produced unrealistic soil properties from which the optimization routine could not recover.

Details of Standard Two-Layer Case

The two-layer standard (non-annealed) optimization produced the lowest RMS difference between the actual and computed velocity-time histories for the standard runs and is the simplest from the standpoint of visualizing the results. The first data produced will be the two velocity-time histories, shown in Figure 74.

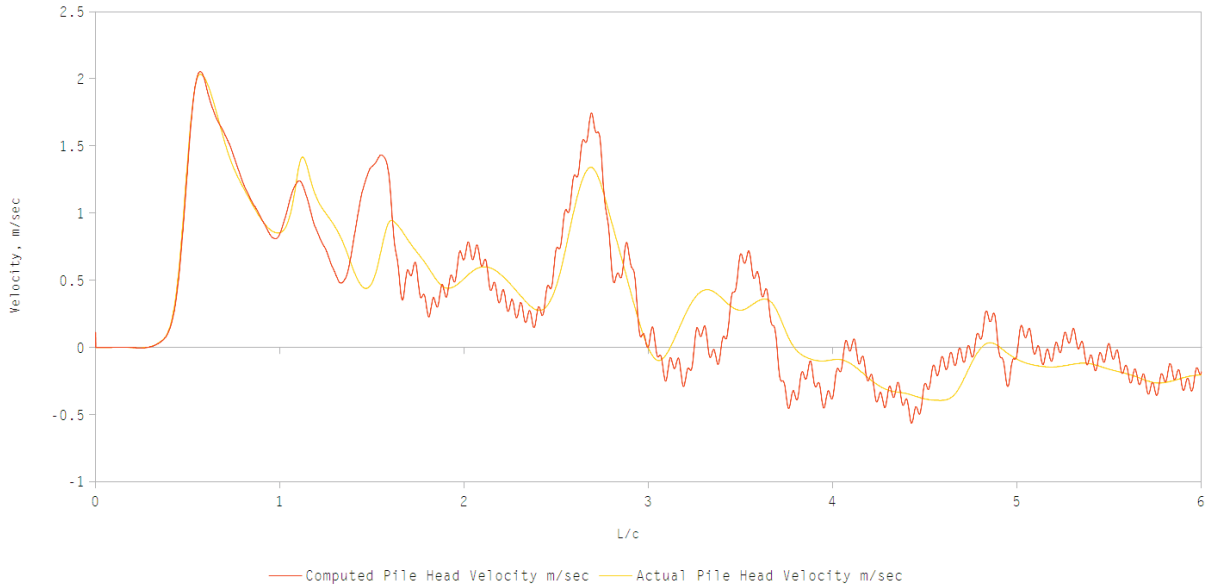


Figure 74 Velocity-Time Histories, Two-Layer Standard Polytope Case

The tracking of the computed values with the actual values was reasonable if not exact. Parasite oscillations can be seen with the computed velocity, although their effect is largely self-canceling in the computation of RMS difference. It is important to note that, as opposed to the modeled hammer runs, the parasite oscillations were not due to interface effects.

The optimization history is shown in Figure 75.

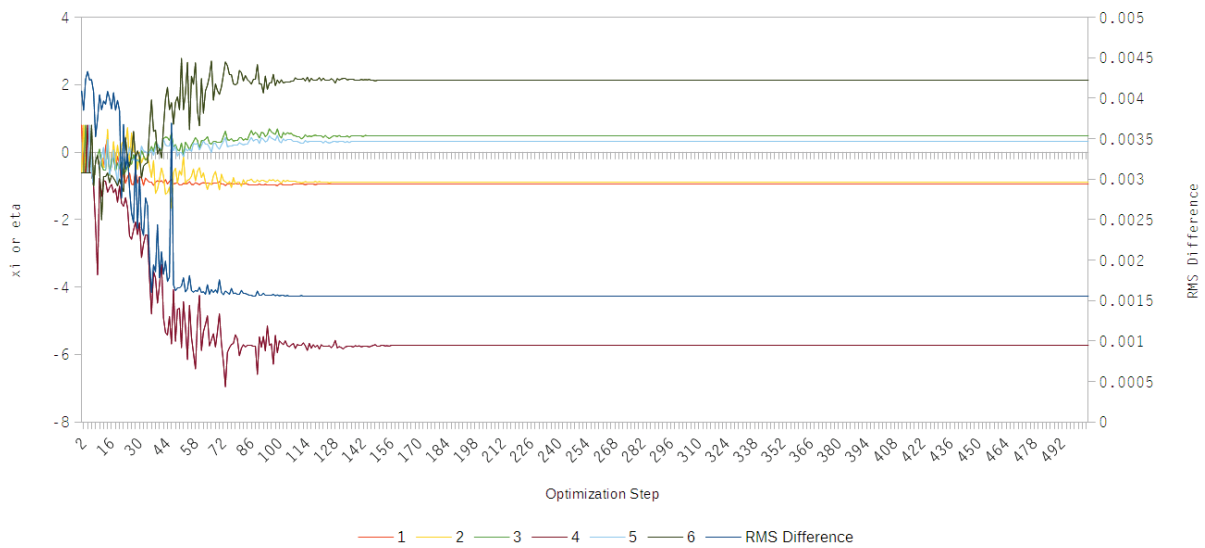


Figure 75 Optimization History, Two-Layer Standard Polytope Case

The values for ξ and η have their axis on the left. To simplify passing the parameters to the dynamic analysis routine during optimization, they were given integer indices. To translate them to actual soil parameters, ξ values are odd and η values are even; the layer number for the η value is half of the index and the corresponding ξ value is one less. Thus, parameters 1 and 2 are for the layer facing the steel portion, parameters 3 and 4 are for the wood portion, and 5 and 6 are for the toe. The RMS difference has its axis on the right. The x-axis is the number for the optimization step.

The initial steps at the left show the routine forming the initial polytope. This is essential for this type of routine, and in this case, the range of values is important, as it needs to be as broad as practicable to avoid local minima. In this case, the goal was to cover the region shown in Figure 17 as completely as possible. Once this initial polytope was formed, the routine continued until the RMS values reached the tolerance. It is important to note that the minimum case for RMS value was not necessarily the last one, but for the standard run could be any of the last six cases considered (six being the number of parameters, which can vary with other layering schemes.) The case with the lowest RMS value was chosen as the result of the optimization.

One major difficulty with the standard runs (as inspection of Table 9 indicates) is that the tolerance chosen was too tight. As is evident from Figure 75, the values for ξ , η and the RMS difference converged fairly quickly, but very small oscillations of the RMS difference kept the differences outside of the tolerance without improving the result.

The layer-by-layer results can be seen more easily in Figure 76.

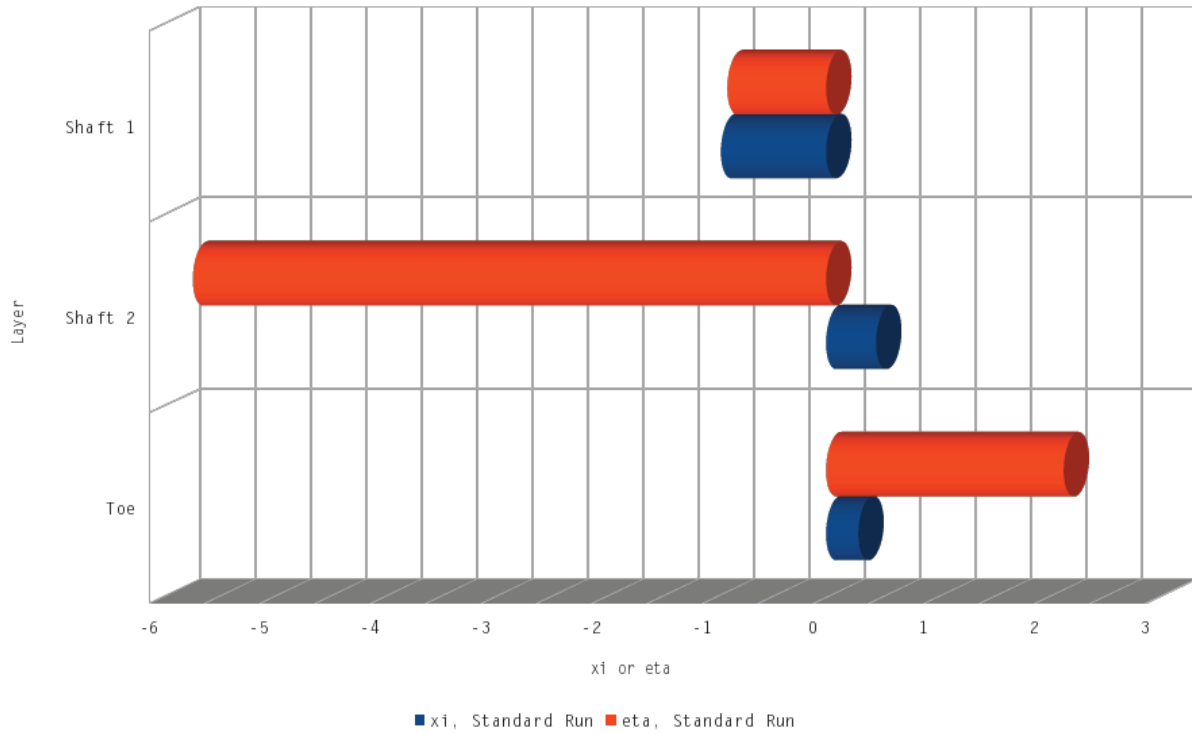


Figure 76 Layer-by-Layer Results, Two-Layer Standard Polytope Case

The static load test result is shown in Figure 77. The SRD of this case was the highest of any of the cases.

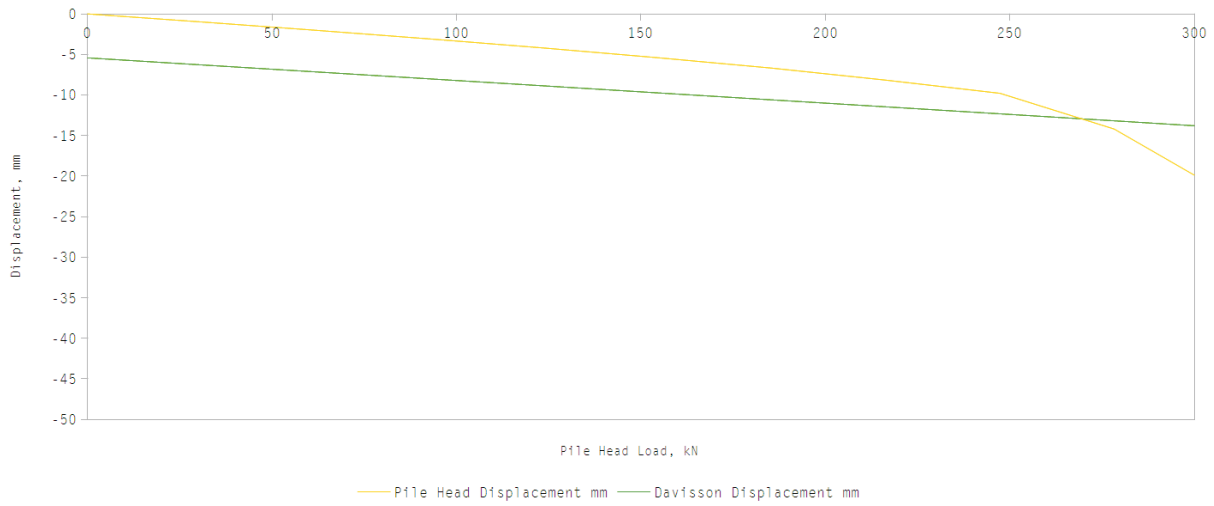


Figure 77 Static Load Test Result, Two-Layer Standard Polytope Case

Turning to the two-dimensional results, the stress-time history (similar to Figure 60) is shown in Figure 78.

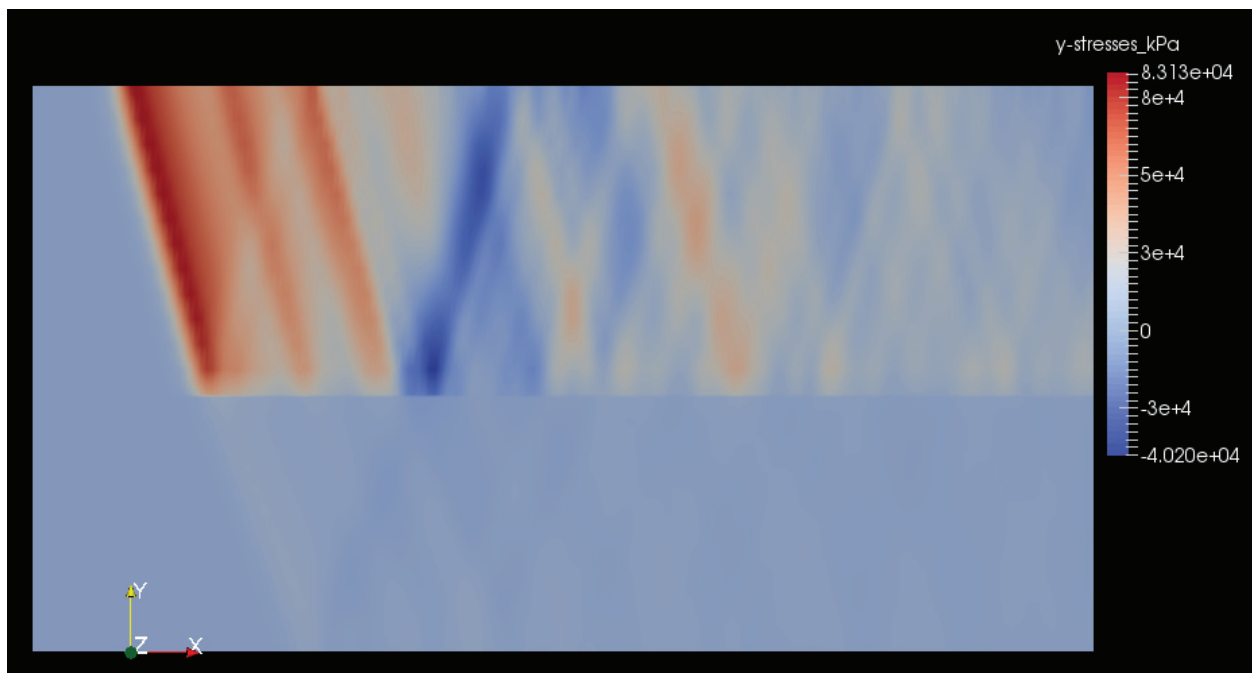


Figure 78 Stress-Time History, Two-Layer Standard Polytope Case

The effect of the cross-section and material change from steel to wood can be seen very clearly here. The stress levels in the wood were much lower than they are in the steel. The reflections from the pile toe, the interface between steel and wood and the shaft resistance made the response of this pile to impact very complex.

The displacement-time history (similar to Figure 59) is shown in Figure 79.

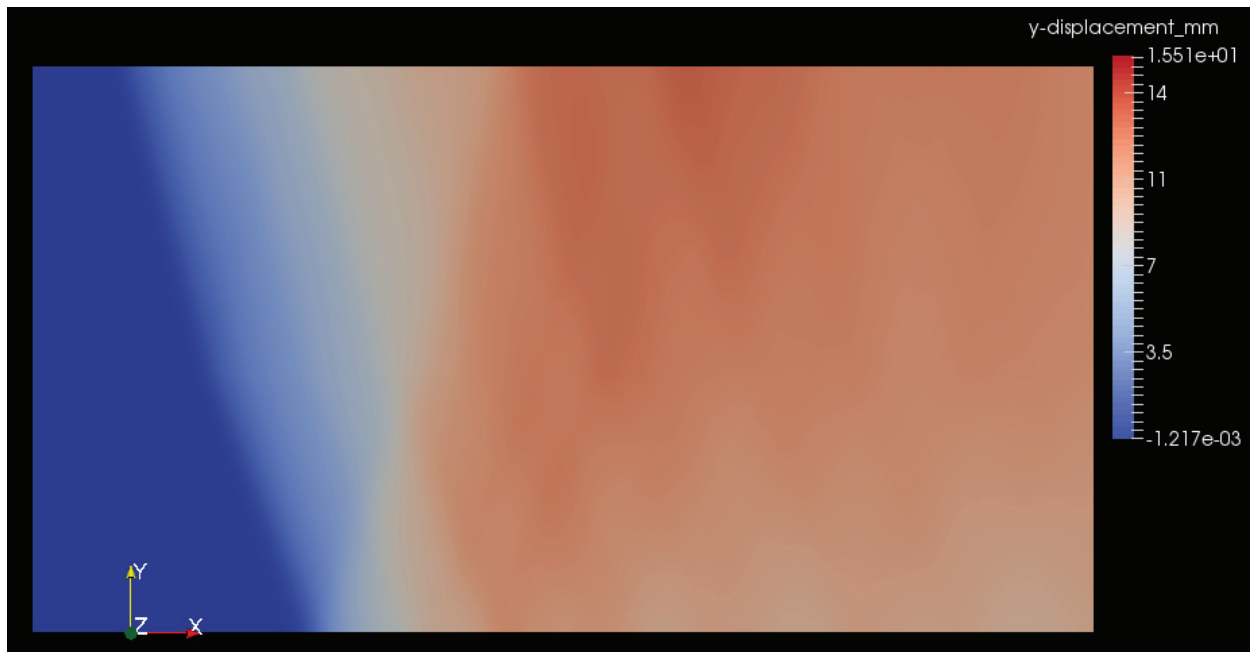


Figure 79 y-displacement-time History, Two-Layer Standard Polytope Case

The change in acoustic speed from steel to wood can be seen, along with the effects of the reflections. The change in displacement along the pile axis was not as pronounced as the pile stresses.

The first principal stresses for the static case immediately after Davisson's failure criterion are shown in Figure 80.

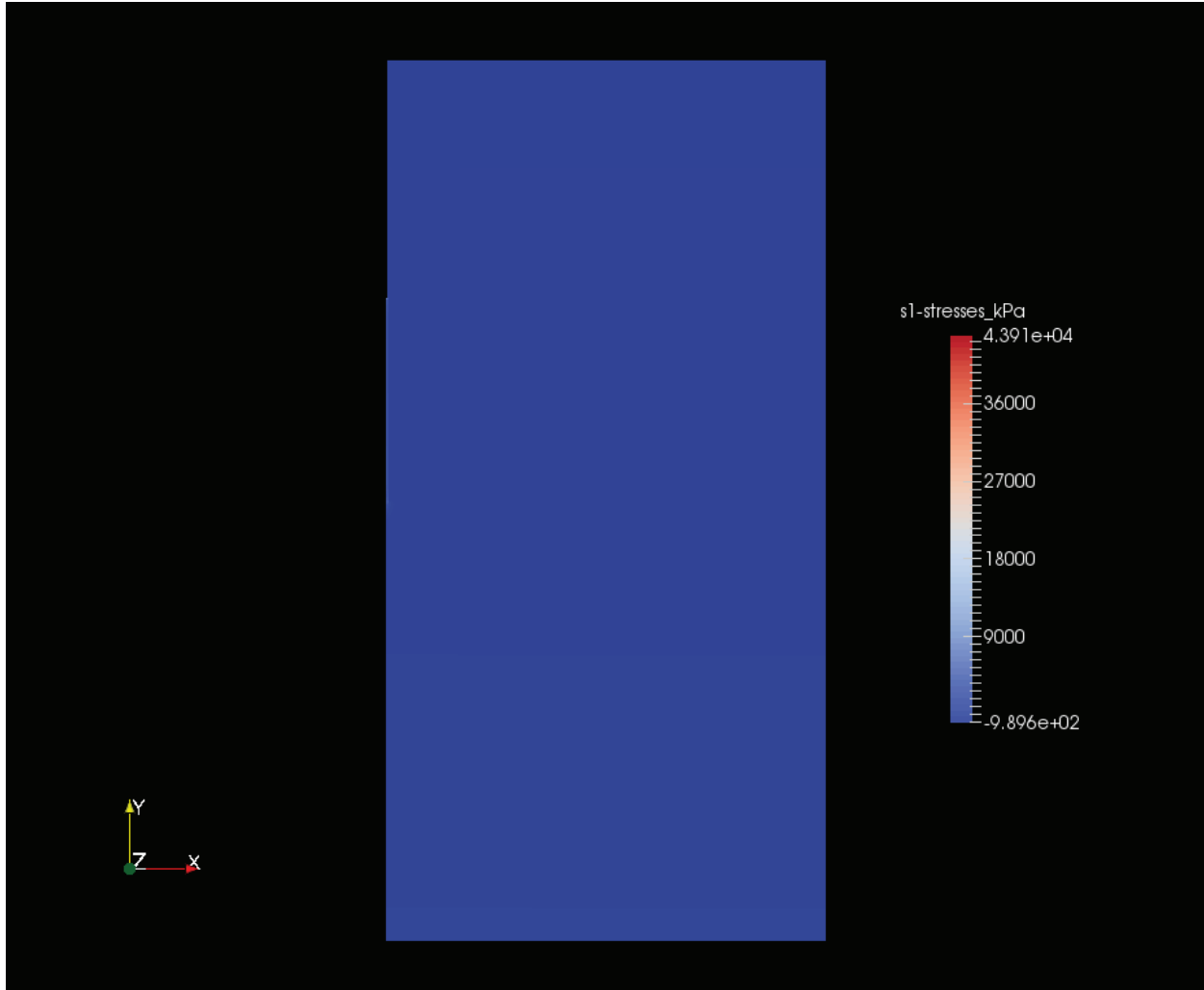


Figure 80 First Principal Stresses, Two-Layer Standard Polytope Case

The variation in the stresses was minimal. Of interest is the point at the splice between steel and wood, shown in Figure 81.

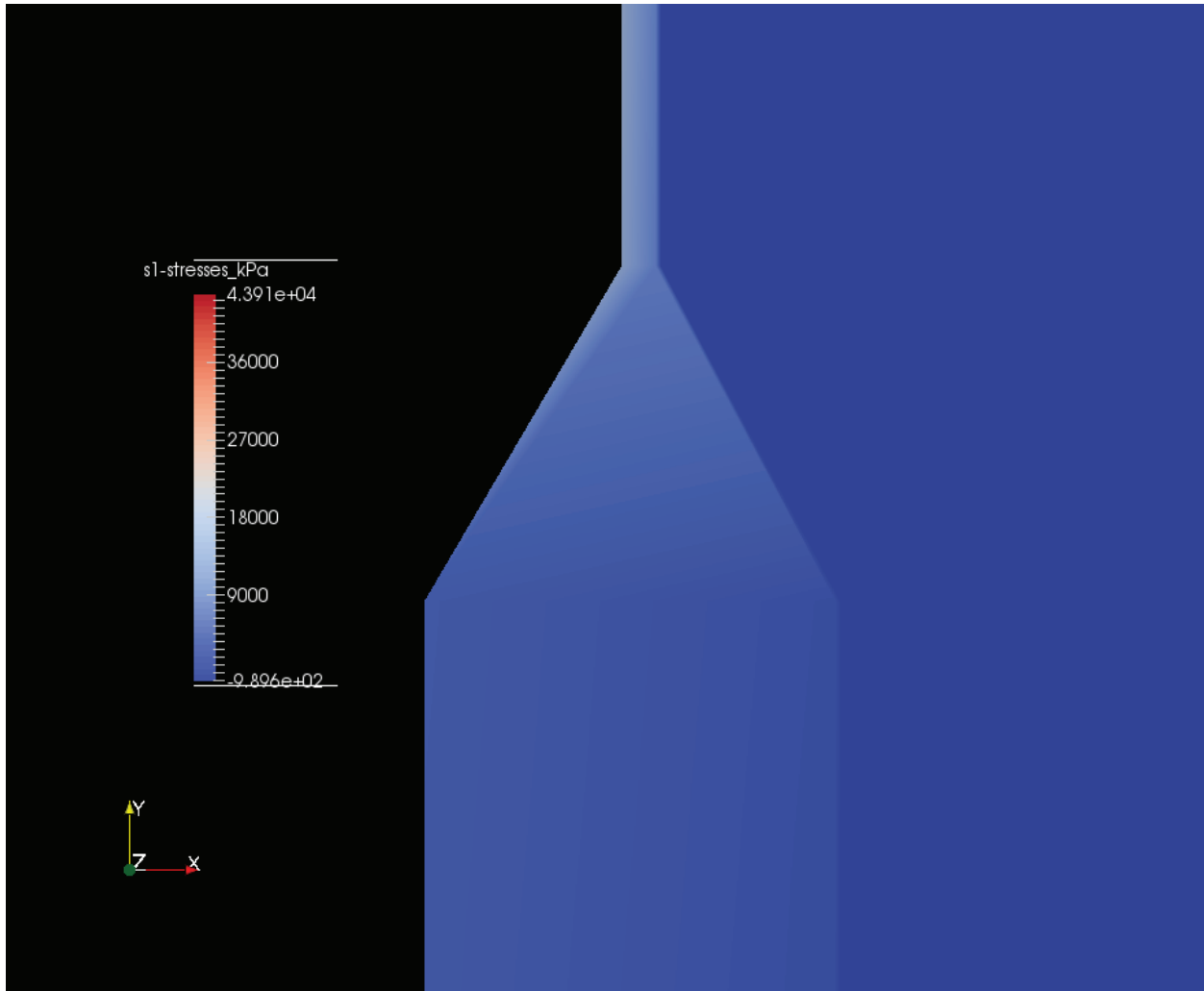


Figure 81 First Principal Stresses at Pile Splice, Two-Layer Standard Polytope Case

The change in stress and cross section—which so affected the dynamic results—was very evident here. Also evident was the way in which it is necessary to effect transitions in the pile cross-section, as was the case in Figure 58.

The vertical displacements are shown for the entire system in Figure 82.

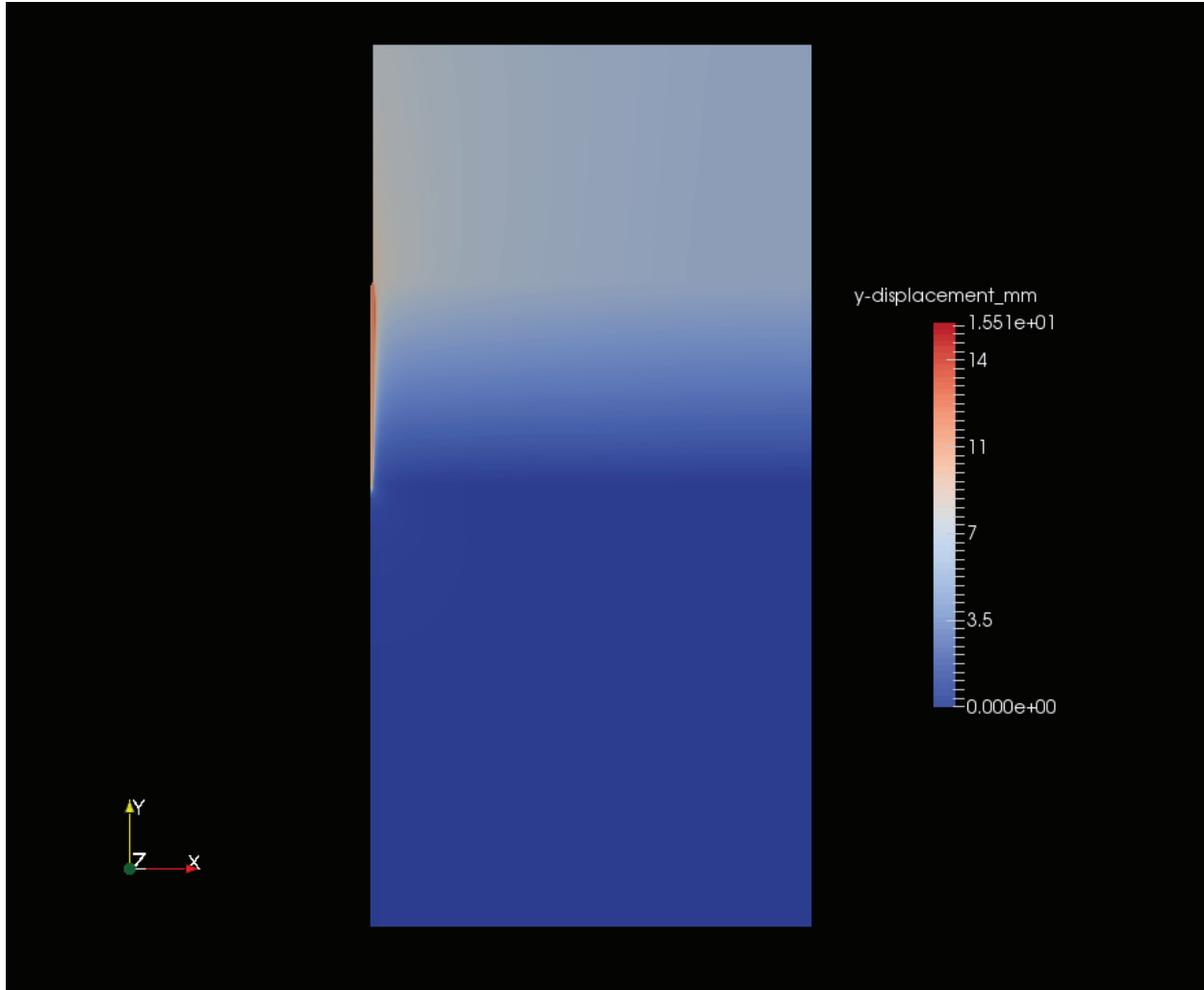


Figure 82 Vertical Displacements, Two-Layer Standard Polytope Case

The significant vertical displacements at the elevation of the steel pile were due to the fact that the optimization routine set the η value of the second layer (Parameter 4 in Figure 75) low, and thus the unit weight of the soil was low, leading to downward displacement of the upper regions. This illustrates the difficulties in analyzing such soft soils.

The vertical displacements at the pile splice are shown in Figure 83 and at the pile toe in Figure 84.

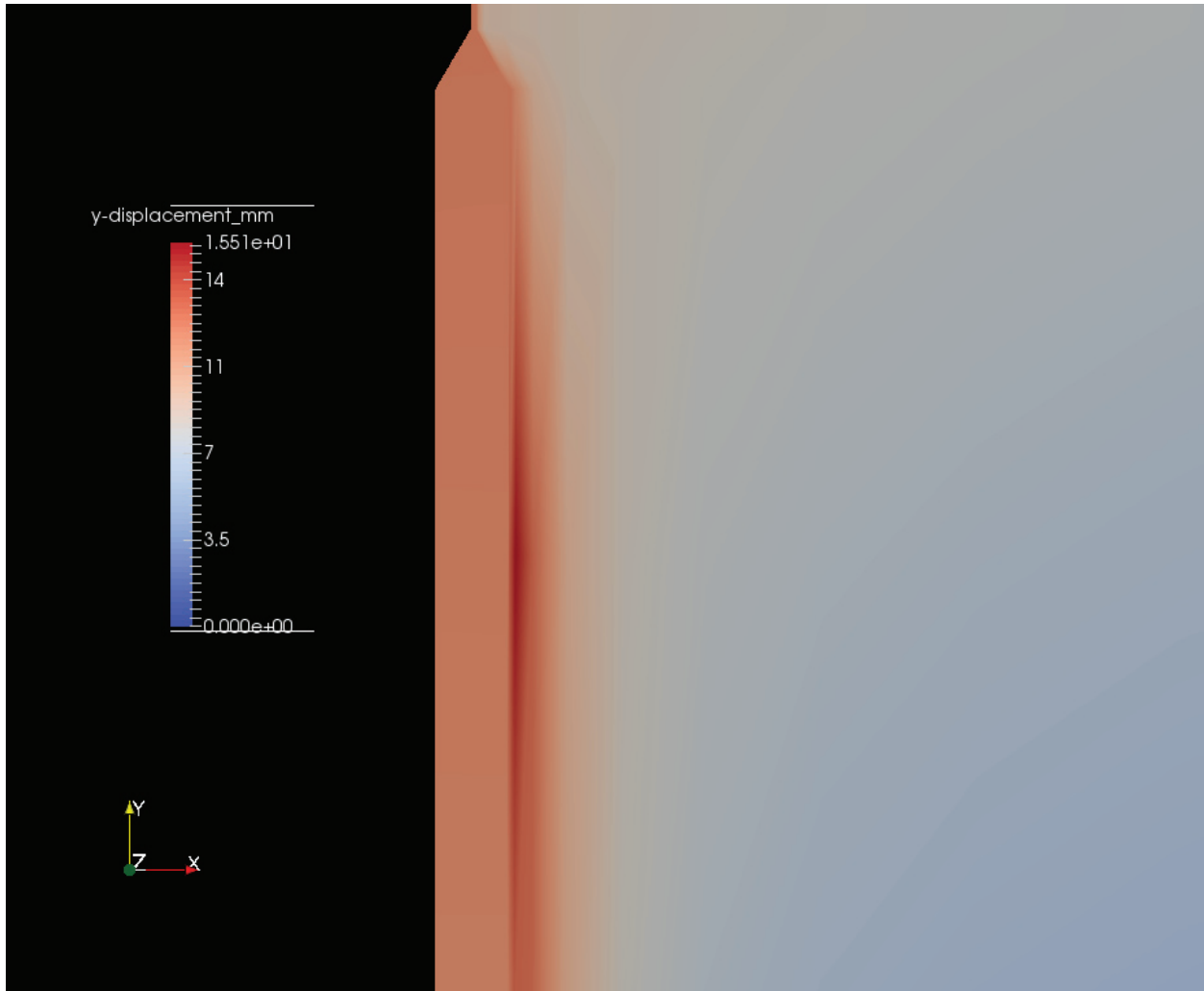


Figure 83 Vertical Displacements, Two-Layer Standard Polytope Case, Steel-Wood Interface

The soil displacements near the soil-wood pile interface were greater than those of the pile at the same elevation. This indicated a down-drag effect; whether this is actually taking place or is simply an effect of the property layering results was not clear.

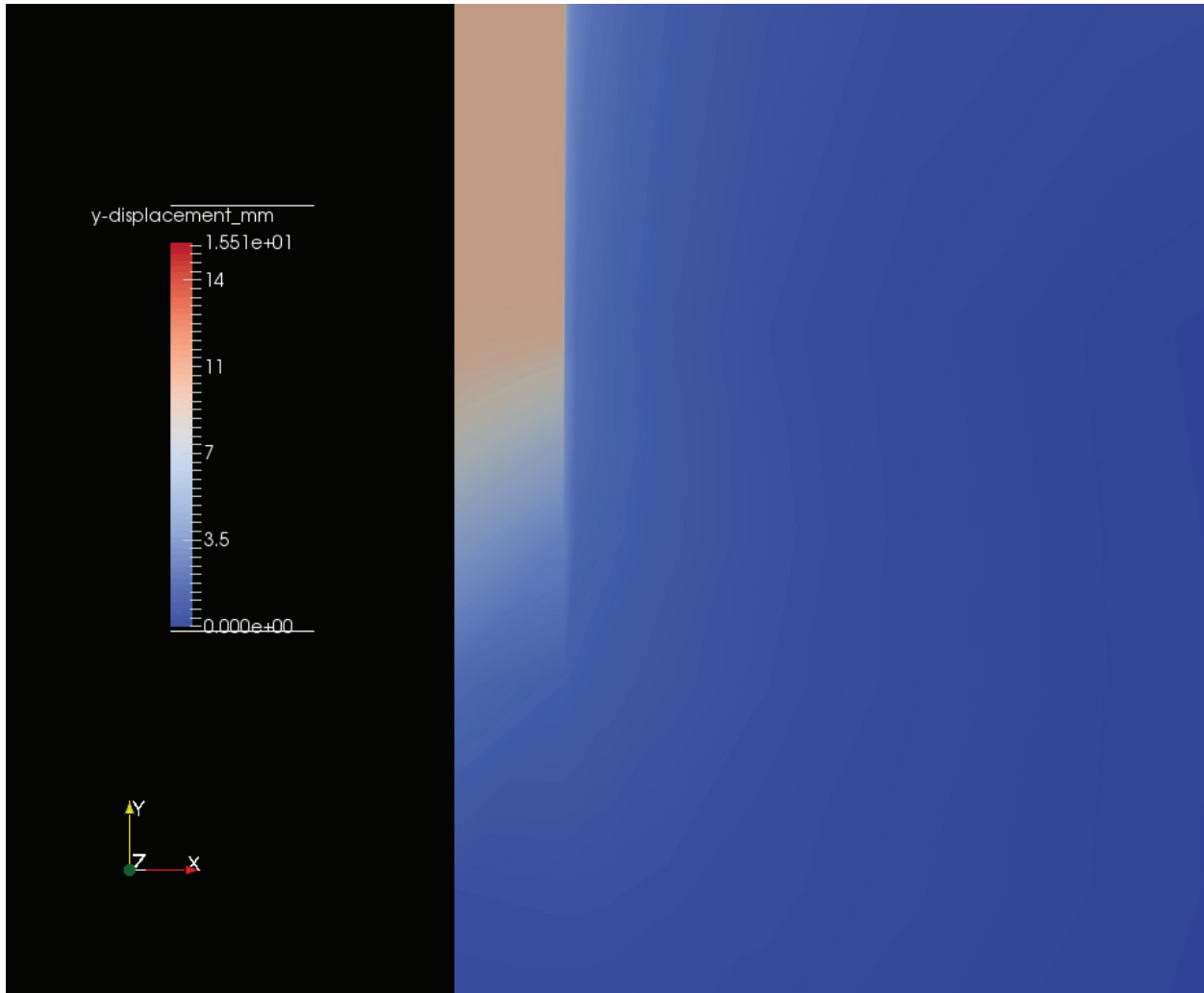


Figure 84 Vertical Displacements, Two-Layer Standard Polytope Case, Pile Toe

The pile and soil almost formed a continuum in this case. This illustrates the fact that with wood piles (and to a lesser extent concrete) the properties of the soil and the soil are not as divergent as they are with steel. This influences the way these materials interact with the soils.

Other Optimization Cases

Inspection of Figures 72 and 73 showed that, for the standard runs, the RMS difference tended to increase with the number of layers analyzed and the SRD tended to decrease. The addition of layers tended to make signal matching harder, which is not a usual result in an optimization problem.

This result, however, should be considered in view of the annealed runs, also shown in Figures 72 and 73. Two of the better matches are at both “ends” of the annealed cases, i.e., the four- and 24-layer cases. In fact, the four-layer case had the best RMS matching of all of the runs, standard or annealed. The 8-layer case was something of an outlier, having both the highest RMS result and the lowest SRD of any annealed case (only the 24-layer standard case was outside of these results.) Of greater interest is the fact that, for both of the four-layer cases, the SRD was virtually identical, although the RMS matching was not.

To examine this further, first the velocity-time history for the four-layer annealed case is shown in Figure 85.

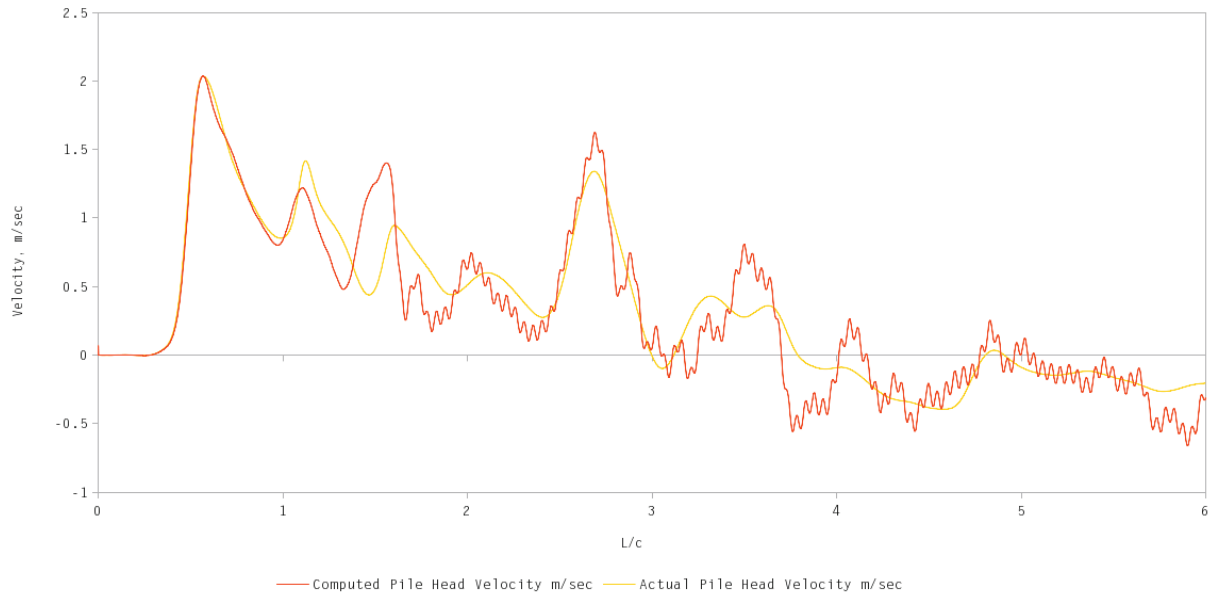


Figure 85 Velocity-Time Histories, Four-Layer Annealed Polytope Case

The results are similar to those in Figure 74. Again the largest divergence came in the region between L/c and $2L/c$, which may indicate spurious shifting of the accelerometers during rebound. Poskitt and Yip-Wong (1991) discuss the possible effects of accelerometer mounting and resonance effects in pile instrumentation.

The optimization history of the four-layer annealed case is shown in Figure 86. The layer numbering is similar to that in Figure 75.

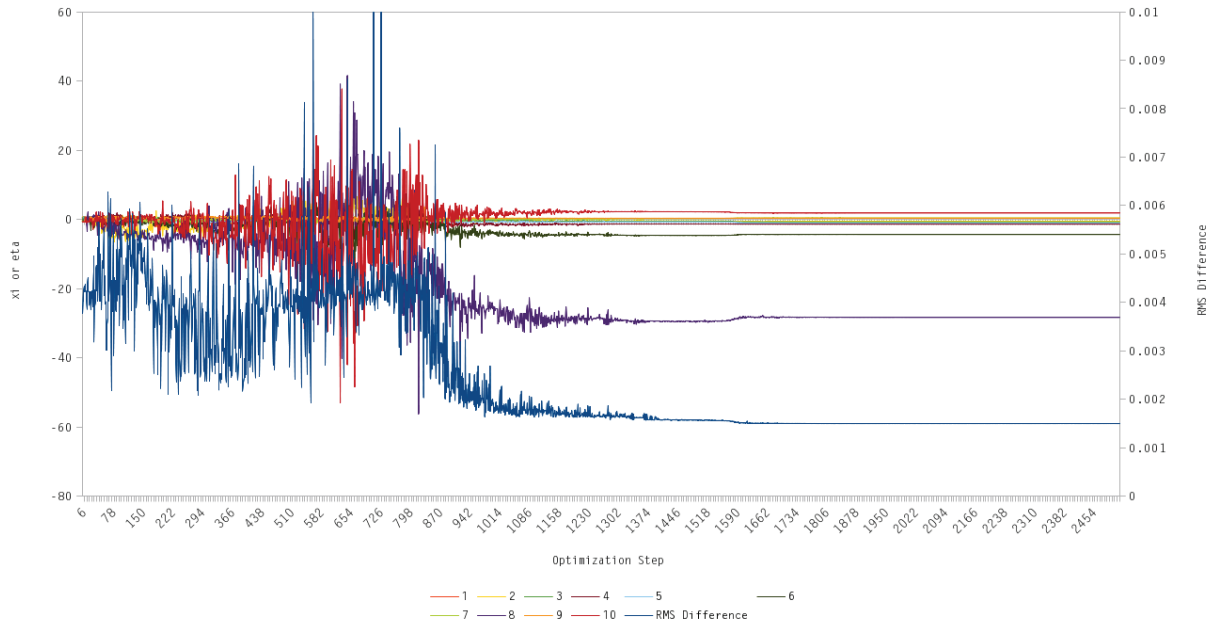


Figure 86 Optimization History, Four-Layer Annealed Polytope Case

Comparison of Figure 75 with Figure 86 shows the much broader range of values of η (and thus the RMS difference) which the annealing technique explored. However, one of the major challenges (especially for the annealed cases) was to select an appropriate stopping tolerance. As is evident, the stopping tolerance was too small for this and the other annealed cases.

The values of ξ and η for both the standard and polytope four-layer cases are shown in Figure 87.

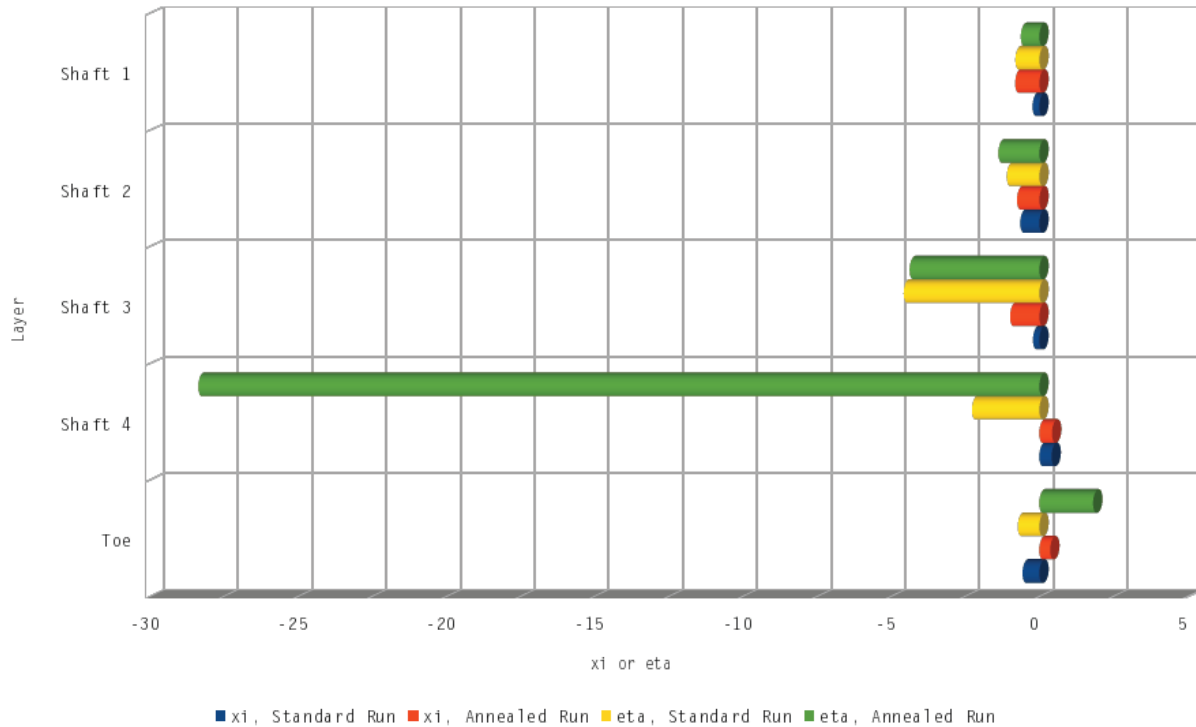


Figure 87 Layer-by-Layer Results, Four-Layer Standard and Annealed Polytope Cases

There is considerable divergence for the ξ results for the odd-numbered layers and the toe. The η results were similar until the last shaft layer and the toe. It seems that the model varied in its assignment of pile end resistance between shaft layer four and the toe. With the standard run, the difference between the two was not as pronounced as with the annealed model; this shifted the resistance almost entirely to the toe. This was also the case with the standard two-layer model, as can be seen in Figure 76. It should be noted that the lower layer(s) faced a tapered wood pile; as noted earlier, tapered pile sections are not true shaft or toe interfaces but are somewhere between the two.

In spite of this difference, the SRD for both four-layer cases were very close, and this related to the uniqueness issue.

CHAPTER X

DISCUSSION

Revisiting the Uniqueness Issue

As discussed earlier, the issue of uniqueness has been a contentious one since Rausche et.al. (1972) and Screwvala (1973). Using a methodology that is as significantly different as STADYN's is from CAPWAP can, perhaps, put a new perspective on this problem.

In a sense, finite element models such as STADYN only add to the uniqueness problem because of their multiple iterations. This takes place in STADYN at several levels; it iterates to find the stress state at the failure surface if the failure criterion exceeds zero, and for the static runs it iterates the incremental displacements until they too reach a certain tolerance. Such iterations are unavoidable with plasticity models such as this, and are common with finite element analyses. They raise uniqueness issues of their own, but the objective is to find the most likely set of elastic and plastic stress states in the system. This allows the analysis of the soil as a continuum with distributed mass and elasticity rather than as a simplified rheology.

Once the method of analyzing plasticity is determined, the issue of arriving at a pile capacity given the data from dynamic testing can be addressed. Here, in spite of the considerable differences between STADYN and CAPWAP, the similarities can be highlighted. A reasonable approach to understanding is to consider both methods as linear transformations (Bowen and Wang (1976)) of dimension

$$\mathbb{R}_n \rightarrow \mathbb{R}_1, n > 1 \quad (118)$$

Here n represents the number of parameters being varied in the system, be they quakes, dampings and resistances (CAPWAP) or ξ and η (STADYN.) On the right hand side is the signal matching parameter. For CAPWAP, this is the Match Quality; for STADYN, it is the least squares result of Equation 115.

Now consider the inverse of this transformation,

$$\mathbb{R}_n \leftarrow \mathbb{R}_1, n > 1 \quad (119)$$

In both cases, the number of system parameters (a vector) exceeds the number of signal matching parameters (a scalar.) Without a lengthy discussion of linear transformations, neither transformation is isomorphic, and thus the transformation shown in Equation 118 is not invertible. The system parameters can be taken and (with a given model) obtain a specific signal matching parameter, but a signal matching parameter cannot be taken to generate a unique set of system parameters as shown in Equation 119. The same difficulty occurs if the right hand side of Equations 118 and 119 is the SRD of the pile. The issue is further complicated by the fact that there is no relationship that can be established between a signal matching parameter and a static pile capacity or resistance. Thus, it is likely that, with a given signal matching, more than one possible pile capacity can be determined. This is essentially the conclusion of Danzinger et.al. (1996), albeit they came to this conclusion through a different process.

At first glance, this makes the solution impossible. In reality, a great deal of optimization relies on the satisfaction of one output parameter with multiple input parameters. In solving for an SRD, what is being sought is not the unique solution to the problem, but the most likely solution to the problem. On the other hand, construction of a unique soil profile along the pile shaft and at the toe is impossible

because of the difficulties of Equation 119. This is illustrated in Figure 87, where two different soil profiles generate nearly identical values for SRD.

As far as the problems surrounding Equation 9 are concerned, there are a number of ways this can be dealt with. As discussed earlier, the parameters are dependent of one another. It is also possible to eliminate the first derivative term with Rayleigh damping, although this must be done in the context of the frequency range of the impulse from the pile. In a sense, STADYN did this on a number of levels. It models the soil with only mass and elasticity, and it models the interfaces in the same way. STADYN also has the advantage of being capable of matching the velocity-time history given a force-time one rather than the other way around, as CAPWAP does. Matching the velocity-time history, and thus through integration the displacement-time history, eliminates the blow count discrepancies that Danzinger et.al. (1996) noted. This advantage was not achieved through conscious decision but through the nature of the finite element model itself.

If the physical modeling of the system replicates its physical reality, then the force-time and velocity-time histories of both at the pile head should be the same. The object of signal matching is to achieve this goal. The method used for signal matching does not have to involve the mathematics of the modeling, but it does need to arrive at its objective with as little intervention as possible. The best way to achieve this goal is to have the physical modeling of the system accurately represent the behavior in actual driving and loading. If the limitations and uncertainties of the method relative to the results obtained are understood, then the issue of uniqueness is less significant.

There are two other issues that need mention here: the issue of initial conditions and the use of data collection from the pile head only.

Variations in results from optimization or matching schemes due to different initial conditions is a persistent problem in a problem such as this one where multiple local minima are present. The use of the polytope method, annealed and non-annealed, was an attempt to cast as wide of a net as possible and avoid being trapped in these local minima. Investigation of alternate starting points was very limited in this study, and requires further research. With the expanded computational power available, problems such as this can be investigated more readily than in the past. This also touches on another issue that was not investigated in this study: residual stresses. With residual stresses, the initial conditions are determined by means other than only effective stresses. This will obviously have an effect on the results, although convergence with multiple runs should be expected.

All of the modeling and results for both systems are based on pile head data collection. As was the case many years ago with Glanville et.al. (1938), monitoring dynamic parameters at points along the pile other than the head produces useful results that make it possible to better quantify the performance of the system. Fellenius (2014) advocates this for static testing, and dynamic testing would benefit from it as well. McVay et.al. (2002) and Alvarez, Zuckerman and Lemke (2006) made significant progress in demonstrating the viability of this concept with field testing.

Rheology

The rheology of soils is a complex subject which has led to a variety of models (Šuklje (1969); Tuma and Abdel-Hady (1973)). One-dimensional pile dynamics has further complicated matters by introducing soil models that are specific to the application, such as that of Smith (1960). Progress in the field will be hindered without applying improved rheologies to the problem.

The Smith (1960) model has been used for many years in both forward and inverse applications; however, it has shortcomings, some of which are as follows:

1. At this point, there is no definite connection between the Smith properties of the soil and the more conventional properties which geotechnical engineers are familiar with and which are tested for during site investigation. McVay and Kuo (1999) attempted to improve this situation but obtaining a definitive result ran into several significant barriers, not the least of which was the uniqueness issue based on Equations 118 and 119. No where is this more apparent than the damping property, whose variations are well documented (Mukherjee and Nagarajub (2013)) and whose importance is well understood (Meseck (1985)).
2. The nature of the “damping” that is modeled is not entirely clear. Much of the damping that takes place during driving is in fact radiation of the stress wave from the pile into the distributed mass and elasticity/plasticity of the surrounding soil. This is explicitly stated for models such as Randolph and Simons (1986) and Corté and Lepert (1986), but radiation damping is an additional option for CAPWAP (Rausche et.al. (2010)).
3. The use of a fixed soil quake for most shaft cases and many toe cases implies an invariant failure strain, which is counterintuitive.

One advantage of any 1D model is the lowered cost of computation. This is especially advantageous with a signal matching routine such as CAPWAP. This advantage becomes less of a factor with rising computational resources.

In including the soil mass, STADYN (along with any other 3D FEA method) addressed these problems with a more comprehensive modeling of the soil response. But the elasto-plastic Mohr-Coulomb model used in STADYN had difficulties of its own, some of which were as follows:

1. It was difficult to accurately evaluate the modulus of elasticity of the soil. The soil is not elastic to start with; the elasto-plastic model is a crude attempt (Massarsch (1983)) to replicate what is in reality closer to a hyperbolic model. Because of this and other factors, including the issue of matching strains between static and dynamic loading, the modulus of elasticity remained the single largest source of error in the soil model.
2. Lateral stresses due to effective stresses do not have a consistent method of evaluation. In principle, a theory of elasticity approach is the best, but in practice, other approaches (such as Jaky's Equation) obtain better results. Since the soil exerts a lateral pressure on the pile and that lateral pressure influences both shaft and toe resistance, it makes sense that an accurate evaluation of these stresses is important.
3. The properties of the soil mass and the properties of the soil at the pile interface are not the same. For the forward method, an expedient method to deal with this is the use of interface elements (Serdaroglu (2010)). With the inverse method, when the interface properties are assumed, so is the solution, which defeats the whole purpose of the inverse method. As the analysis of the Mondello and Killingsworth (2014) results shows, even in stratigraphies that are "obviously" cohesive, the inverse method returned soils with a degree of friction. The alternative to interface elements is to project the interface properties back into the soil mass for the purpose of pile dynamics; how much this would influence the results is not clear.

The use of the " $\xi - \eta$ " system to define soil properties introduces another potential inaccuracy into the system. Although the properties that result may be "typical," they may not be the actual soil properties in the field. It is a simplification to reduce the number of variables for optimization and to head off results that are

physically unlikely if not impossible. How significant the variations from actual soil properties are depends upon the property. For some (specific gravity, Poisson's Ratio) the difference may not be great; for others (cohesion, modulus of elasticity) the difference may be very important.

One possible improvement to STADYN would have been to include other soil models (Potts and Zdravkovic (1999)). As mentioned earlier, the applicability issue would come into play; many of these models are designed for specific soil types, and with driven piles, the presence of soils of widely varying cohesion and friction is not unusual. The lack of common testing methodology has also hindered the advance of these models in other applications.

Numerical Method

The selection of appropriate numerical methods has been a significant one since Smith (1955). The use of finite-difference methods with the mass concentrated at the bottom of each segment is common for wave equation routines; others use the method of characteristics or a method more closely related to Equation 7. Given the variations possible in the hammer-pile portion of the system, for modeling flexibility the requirement that L/c be constant for each pile segment should be unnecessary. The main requirement for a successful finite difference method is that it be consistent and stable, which by the Lax equivalence theorem guarantees its convergence, at least for linear equations. Runge-Kutta methods such as those employed by Bossard and Corté (1983) would satisfy this requirement without excessive discretization constraints, although segments that produce excessively small time steps should be avoided.

The use of explicit methods in finite difference techniques carried over into the finite element realm. This was due to two factors: the efficiency of the

computation and the issue of “plasticity overrun” discussed earlier. The largest departure in STADYN, however, was the use of four-node quadrilaterals in the analysis, as opposed to the eight-node serendipity elements common in geotechnical engineering. This eliminated some but not all of the numerical noise in the solution.

One of the goals in configuring STADYN was to avoid the application of “material damping” which is based primarily on numerical considerations and not on material properties. Although more work needs to be done to improve the parasite oscillations, the basic configuration of the program is a reasonable platform from which to progress.

Optimization Techniques

Mondello and Killingsworth (2014) was not the ideal case for either CAPWAP or STADYN for two principal reasons: the low blow count/high set/low SRD of the pile, and the lack of either “restrike” data or static load testing, which left elevated pore pressures not adequately considered. Nevertheless, some results could be obtained from the data, both actual and simulated.

The use of signal-matching techniques that operate according to Equation 118 have been used for a long time and the discussion on uniqueness applies here. In a sense, the use of the word “optimization” was a misnomer in this application; the objective was not as much to optimize the design of the pile as to match the actual velocity-time history to the simulated one. In both cases, however, a parameter was being minimized. Since the search techniques common to this problem are referred to as optimization techniques, this usage was retained for this study.

In many presentations of pile dynamics, the goal is stated to be the separation of the dynamic resistance from the static one. This is explicit in the Case

Method (Fellenius (2014)). However, optimization techniques ignore the physics of the problem; the match is purely a mathematical construct. This shifts the accuracy issue to the modeling of the system. The physics of the problem must be modeled realistically and the solution technique must converge properly.

Having chosen to perform signal matching in this way, generally the first option to consider was a gradient method of some kind. Problems such as this, however, are not well suited for gradient methods because of the presence of numerous local minima, to say nothing of the problematic differentiability of the function in question. In this respect, the polytope method, simplistic as it is, proved a major benefit in searching for the optimum signal match. This was because it could “cast a wide net” initially in the construct of the initial polytope, thus reducing the dependence of the solution on the selection of the starting point. Being a derivative-free method also addressed the nature of the function more reasonably than a gradient-based method.

Ultimately, however, the polytope method by itself was not completely effective in finding the minimum. By adding annealing, a still wider variety of cases could be considered in the search for the best signal matching. The four- and 24-layer annealed cases produced similar results to each other, and the two four-layer cases matched each other well. This suggests that, in the interim of finding the “best” method for search, more than one method be applied to the problem to insure that the optimum matching has taken place.

Varying the methodology also brings up two other parameters: the discretization (layering) of the pile and the aggregation of the soil properties. Optimization techniques work best with fewer parameters to optimize. In the case of the soil properties, the “ $\xi - \eta$ ” system has been discussed; further refinement of this is needed. Layering soils, however, by assuming that the properties in certain

regions of the stratum are uniform, is a well-established practice in soil mechanics and foundation design. Too few layers result in an oversimplified soil profile that does not properly represent the soils at hand; too many layers risk overloading the optimization technique. Part of any search for an optimum signal match should include varying the way the soils are layered in the model. Here some help from the soil borings would be a legitimate form of intervention.

One major disadvantage of the polytope method (especially in its annealed form) was the slowness of the convergence. It is possible that a gradient method coupled with annealing, would speed up the search while at the same time avoid local minima through the annealing process. This was not tried in this study. The major source of the slowness, however, was the costly nature of the 3D FEA. These techniques could be just as easily be applied to a Smith (1960) model, although the limitations of that model would still apply.

CHAPTER XI

CONCLUSION AND RECOMMENDATIONS FOR FURTHER STUDY

1. The finite element method is a well-established method for the analysis of piles under high rate strain analysis. In spite of the numerical difficulties, the method has been successfully applied to the problem since the early 1980's, and STADYN is yet another code for this purpose.
2. The addition of features to STADYN specific to the application, such as soil layering and hammer modeling, were very useful for proper running of the model, especially in the inverse method. Also, the use of four-node quadrilateral elements, while unusual for geotechnical applications, proved to be effective for high-strain dynamic methods. These improvements illustrate that the use of packaged, general purpose codes, while very much the norm in this application for the last twenty years, may not be the best way to implement the finite element method in pile dynamics.
3. Explicit methods for dynamic analysis gave the most satisfactory results due to plasticity considerations. An invariant stiffness matrix also performed satisfactorily for the static analysis; this is especially true if the "load test" is stopped after the Davisson criterion is reached.
4. In spite of its limitations, the Mohr-Coulomb model is arguably the best for this application. This is due to the variations in soils into which piles are driven. The greatest weakness shown in STADYN was with purely cohesionless soils. Cohesive soils generally have received the most attention; however, from a finite element analysis standpoint their behavior is closest to conventional Tresca type

failure and their elasto-plastic matrix is, in the purely cohesive state, symmetric. More study is necessary on this topic.

5. The use of the “same” model for both static and dynamic analysis in the forward mode was successfully developed and demonstrated. Good results were obtained when compared with actual static load test data. The largest discrepancy between STADYN and GRLWEAP came in the definition of the static load of the pile.
6. Although the case under consideration was not ideal, the polytope method–standard and annealed–showed potential as a signal-matching technique for the inverse method, although much work needs to be done using cases with both static load test results and higher blow counts.
7. There are many issues which were not resolved in this study but which need to be addressed for STADYN to be used in actual practice. They include residual stress analysis, pile set-up and the effect (and estimation) of elevated pore water pressures and thixotropic effects, a better method of final set estimation, plasticity in hammer and pile cushions, and studies using concrete piles.

REFERENCES

- Abbo, A.J., Lyamin, A.V., Sloan, S.W. and Hambleton, J.P. (2011). "A C2 continuous approximation to the Mohr-Coulomb yield surface." *International Journal of Solids and Structures*, 48(21), 3001-3010.
- Abbott, M.B. (1966) *An Introduction to the Method of Characteristics*, American Elsevier, New York, NY.
- Alvarez, C., Zuckerman, B., and Lemke, J. (2006) "Dynamic Pile Analysis Using CAPWAP and Multiple Sensors." *GeoCongress 2006*, American Society of Civil Engineers, Reston, VA, 1-5.
- American Petroleum Institute. (2002). "Recommended Practice for Planning, Designing and Constructing Fixed Offshore Platforms—Working Stress Design," *API RP2A-WSD*, Twenty-First Edition w/Errata and Supplement, Washington, DC.
- Department of the Army. (1986). "Laboratory Soils Testing," *EM 1110-2-1906*, Washington, DC.
- Department of the Army. (1990). "Settlement Analysis," *EM 1110-1-1904*, Washington, DC.
- Audibert, J. M., and Bamford, S. R. (1989). "TLP foundation design and analysis." *Tension Leg Platform: a State of the Art Review*. American Society of Civil Engineers, New York, NY, 77-117.
- Balthaus, H. (1988). "Numerical Modelling of Pile Driving Based on an Automatic CAPWAP Search Procedure." *Proceedings of the Third International Conference on the Application of Stress-Wave Theory to Piles*, Bi-Tech Publishers, Vancouver, BC, 219-230.
- Bolton, M.D. (1986) "The strength and dilatancy of sands." *Geotechnique*, 36(1), 65-78.
- Bossard, A., and Corté, J-F. (1983). *Battage des pieux programme de calcul Batlab* [Pile Driving Calculation Program Batlab,] Laboratoire Central des Ponts et Chaussées, Paris, France. (in French)
- Bowen, R.M., and Wang, C.-C. (1976). *Introduction to Vectors and Tensors*, Springer, New York, NY.
- Bowman, F. (1958). *Introduction to Bessel Functions*, Dover Publications, New York, NY.

- Builes, M., García, E. and Riveros, C.A. (2008). “Dynamic and static measurements of small strain moduli of toyoura sand,” *Rev. Fac. Ing. Univ. Antioquia*, 43, 86-101.
- Carnahan, B., Luther, H.A. and Wilkes, J.O. (1969). *Applied Numerical Methods*, John Wiley & Sons, Inc., New York, NY
- Chapra, Steven C., and Canale, Raymond P. (1985). *Numerical Methods for Engineers with Personal Computer Applications*, McGraw-Hill, New York, NY.
- Chellis, R.D. (1961). *Pile Foundations*, Second Edition, McGraw-Hill, New York, NY.
- Chen, Z.L., Tang, L.L., Niu, S.B., and Yu, C. (2011) “Three-Dimensional Consolidation of Visco-Elastic Soil Around a Driven Pile.” *Applied Mechanics and Materials*, 66-68, 1291-1295.
- Chow, Y. K., Chan, W. T., Liu, L. F. and Lee, S. L. (1995). “Prediction of pile capacity from stress-wave measurements: A neural network approach.” *International Journal for Numerical and Analytical Methods in Geomechanics*, 19(2), 107–126.
- Cook, R.D., Malkus, D.S. and Plesha, M.E. (1989). *Concepts and Applications of Finite Element Analysis*, John Wiley & Sons, Inc., New York, NY
- Corté, J.-F., and Lepert, P. (1986). “Lateral Resistance During Driving and Dynamic Pile Testing.” *Numerical Methods in Offshore Piling*, Éditions Technip, Paris, France, 19-34.
- Coutinho, A.L.G.A, Costa, A.M., Alves, J.L.D., Landau, L., and Ebecken, N.F.F. (1988). “Pile Driving Simulation and Analysis by the Finite Element Method.” *Proceedings of the Third International Conference on the Application of Stress-Wave Theory to Piles*, Bi-Tech Publishers, Vancouver, BC, 197-207.
- Cuthill, E., and McKee, J. (1969). “Reducing the bandwidth of sparse symmetric matrices.” *Proceedings of the 1969 24th National Conference of the Association for Computing Machinery*, Association of Computing Machinery, New York, NY, 157-172.
- Danzinger, B.R., de Rezende Lopes, F., da Costa, A.M. and Pacheco, M.P. (1996). “A Discussion on the Uniqueness of CAPWAP-type Analyses.” *Proceedings of the Fifth International Conference on the Application of Stress-Wave Theory to Piles*, University of Florida, Gainesville, FL, 394-408.
- Das, B.M. (1985). *Advanced Soil Mechanics*, McGraw-Hill Book Company, Singapore.

- Deeks, A.J. (1992). *Numerical Analysis of Pile Driving Dynamics*, PhD Dissertation, University of Western Australia, Perth, Western Australia.
- Dennis, N.D., and Olson, R.E. (1983). "Axial Capacity of Steel Pipe Piles in Clay" *Proceedings of the Conference on Geotechnical Practice in Offshore Engineering*, American Society of Civil Engineers, New York, NY, 376-388.
- Desai, C.S., Zaman, M., Lightner, J.G. and Siriwardane, H.J. (1984). "Thin-Layer Element for Interfaces and Joints." *International Journal for Numerical and Analytical Methods in Geomechanics*, 8(1), 19-43.
- Dolwin, J., and Poskitt, T.J. (1982). "An Optimisation Method for Pile Driving Analysis." *Proceedings of the Second Conference on Numerical Methods in Offshore Piling*, Austin, TX, 91-106.
- Duncan, J.M., and Chang, C.Y. (1970). "Nonlinear Analysis of Stress and Strain in Soils." *Journal of the Soil Mechanics and Foundations Division, American Society of Civil Engineers*, 96(5), 1629-1653.
- Federal Highway Administration (2001) "Load and Resistance Factor Design (LRFD) for Highway Bridge Substructures." *FHWA HI-98-032, NHI Course No. 132068*, Federal Highway Administration, Washington, DC.
- Fellenius, B.H. (2011) "Capacity versus Deformation Analysis for Design of Footings and Piled Foundations." *Journal of the Southeast Asian Geotechnical Society*, 42(2), 70-77.
- Fellenius, B.H. (2014) *Basics of Foundation Design*. <<http://www.fellenius.net>> (March 13, 2015)
- Finno, R.J, Editor (1989). *Predicted and Observed Axial Behavior of Piles: Results of a Pile Prediction Symposium*, American Society of Civil Engineers, New York, NY.
- Fischer, H.C. (1960). "On Longitudinal Impact IV: New Graphodynamical Pulse Method of Computing Pile-Driving Processes" *Applied Scientific Research* 9(1), 93 -138.
- Fried, I., and Malkus, D.S. (1975). "Finite Element Mass Matrix Lumping by Numerical Integration with no Convergence Rate Loss." *International Journal of Solids and Structures*, 11(4), 461-466.
- Gelfand, I.M., and Levitan, B.M. (1951). "On the determination of a differential equation from its spectral function." *Izv. Akad. Nauk. SSSR*, 15, 309-360. (in Russian)

- Gill, P.E., Murray, W. and Wright, M.H. (1981). *Practical Optimization*, Academic Press, Inc., London, England.
- Glanville, W.H., Grime, G., Fox, E.N, and Davies, W.W (1938). *An Investigation of the Stresses in Reinforced Concrete Piles During Driving*, Department of Scientific and Industrial Research, British Building Research Board, London, England.
- Goble, G.G., Rausche, F., and Likins, G. (1975). "Bearing Capacity of Piles from Dynamic Measurements." *Ohio DOT-05-75*, Ohio Department of Transportation, Columbus, OH.
- Goble, G.G. (1983). "Analysis of Offshore Pile Driving—A Review." *Proceedings of the Conference on Geotechnical Practice in Offshore Engineering*, American Society of Civil Engineers, New York, NY, 596-603.
- Goble, G.G., and Rausche, F. (1976). "Wave Equation Analysis of Pile Driving, WEAP Program." *FHWA-IP-76-14*, Federal Highway Administration, Washington, DC.
- Goble, G.G., and Rausche, F. (1986). *Wave Equation Analysis of Pile Foundations, WEAP86 Program*, Federal Highway Administration, Washington, DC.
- Griffiths, D.V., and Lane, P.A. (1999). "Slope stability analysis by finite elements." *Geotechnique* 49(3) 387-403.
- Griffiths, D.V., and Willson, S.M. (1986). "An explicit form of the plastic matrix for a Mohr-Coulomb material." *Communications in Applied Numerical Methods*, 2(5), 523-529.
- Gumenskii, B.M., and Komarov, N.S. (1961) *Soil Drilling by Vibration*. Consultants Bureau, New York, NY.
- Hannigan, P.J., Goble, G.G., Thendean, G., Likins, G.E., and Rausche, F. (1997). "Design and Construction of Driven Pile Foundations." *FHWA-HI-97-013*, Federal Highway Administration, Washington, DC.
- Hannigan, P.J., Goble, G.G., Likins, G.E. and Rausche, F. (2006). "Design and Construction of Driven Pile Foundations." *FHWA-NHI-05-042 and FHWA-NHI-05-043*, Federal Highway Administration, Washington, DC.
- Healy, B.E., Pecknold, D.A, and Dodds, Jr., R.H. (1992). "Applications of Parallel and Vector Algorithms in Nonlinear Structural Dynamics Using the Finite Element Method." *UILU-ENG-92-2011*, University of Illinois at Urbana-Champaign, Urbana, IL.

- Héritier, B., and Paquet, J. (1986). “Battage d’un pieu en milieu pulvérant: acquisition des données et simulation.” [Pile driving into a granular medium: data collection and simulation.] *Annales de l’Institut Technique du Bâtiment et des Travaux Publics*, 198(450) 2-23. (in French)
- Hirsch, T.J., Carr, L. and Lowery, L.L., Jr. (1976). “Pile Driving Analysis—Wave Equation Users’ Manual, TTI Program.” *FHWA-IP-76-13*, Federal Highway Administration, Washington, DC.
- Holeyman, A. (1986). “Static Versus Dynamic Pile Bearing Capacity (Discussion to Session 4).” *Proceedings of the International Symposium on Penetrability and Drivability of Piles*, Volume 2, Japanese Society of Soil Mechanics and Foundation Engineering, 80-82.
- Horvath, R.G., and Killeavy, M. (1988). “Variation of “CAPWAP” Results With Blows Selected for Analysis.” *Proceedings of the Third International Conference on the Application of Stress-Wave Theory to Piles*, Bi-Tech Publishers, Vancouver, BC, pp. 735-748.
- Hughes, T.J.R. (2000). *The Finite Element Method: Linear Static and Dynamic Finite Element Analysis*. Dover Publications, Mineola, NY.
- Hughes, T.J.R. and Liu W.K. (1978). “Implicit-Explicit Finite Elements in Transient Analysis: Implementation and Numerical Analysis”. *Journal of Applied Mechanics*, 45(2), 375-378.
- Isaacs, D.V. (1931). “Reinforced Concrete Pile Formulae.” *Journal of the Institution of Engineers Australia*, 3(9), 305-323.
- Isenberg, J. (1972) “Analytic Modeling of Rock-Structure Interaction.” *R-7215-2299*, U.S. Bureau of Mines, Washington, DC.
- King, J.T. (1984). *Introduction to Numerical Computation*. McGraw-Hill Book Company, New York, NY.
- Kyfor, Z.G., Schnore, A.R., Carlo, T.A. and Baily, P.F. (1992). “Static Testing of Deep Foundations.” *FHWA-SA-91-042*, Federal Highway Administration, Washington, DC.
- LeVeque, R.J. (1992). *Numerical Methods for Conservation Laws*. Birkhäuser Verlag, Basel, Switzerland.
- Lewis, R.M., Torczon, V. and Trosset, M.W. (2000). “Direct Search Techniques: Then and Now.” *NASA/CR-2000-210125*. NASA Langley Research Center, Hampton, VA.

- Liang, R. Y. (2003). "New Wave Equation Technique for High Strain Impact Testing of Driven Piles." *Journal of Geotechnical Testing*, 26(1), 111-117.
- Likins, G., Fellenius, B.H., and Holtz, R.D. (2012). "Pile Driving Formulas" *Pile Driver*, 9(2), 60-67.
- Likins, G. E., Liang, L., and Hyatt, T. (2012). "Development of Automatic Signal Matching Procedure -iCAP®." *Proceedings from Testing and Design Methods for Deep Foundations*; IS-Kanazawa, Kanazawa, Japan, 97-104.
- Lomax, H., Pulliam, T.H. and Zingg, D.W. (2003). *Fundamentals of Computational Fluid Dynamics*. Springer-Verlag, Berlin, Germany.
- Long, M. (2001). "Assessment of SIMBAT® Dynamic Pile Tests" *Foundations and ground improvement; proceedings of a specialty conference*, Blacksburg, Virginia, 539-553.
- Mabsout, M.E, and Tassoulas, J.L. (1994). "A finite element method for the simulation of pile driving." *International Journal for Numerical Methods in Engineering*, 37, 257-278.
- Manley, R.G. (1945). *Waveform Analysis*. John Wiley and Sons, New York, NY.
- Masouleh, S.F., and Fakharian, K. (2008). "Verification of Signal Matching Analysis of Pile Driving Using a Finite Difference Based Continuum Numerical Method." *International Journal of Civil Engineerng*. 6(3), 174-183.
- Massarsch, K. R. (1983). "Vibration Problems in Soft Soils." *Proceedings of the Symposium on Recent Developments in Laboratory and Field Tests and Analysis of Geotechnical Problems*, Asian Institute of Technology, A. A. Balkema, Rotterdam, 539-549.
- McCarron, W.O. (2013). "Numerical Modeling Applications in Offshore Petroleum Developments." *Geo-Strata*, 17(3), 34-39.
- McNamara, J.F. (1974). "Solution Schemes for Problems of Nonlinear Structural Dynamics." *Journal of Pressure Vessel Technology*, 96(2), 96-102.
- McVay, M.C., Alvarez, V., Zhang, L.M., Perez, A. and Gibsen, A. (2002) "Estimating Driven Pile Capacities During Construction." *Florida DOT 99700-3600-119*. University of Florida, Gainesville, FL.
- McVay, M.C. and Kuo, C.L. (1999) "Estimate Damping and Quake by Using Traditional Soil Testings." *Report WPI0510838*, Florida Department of Transportation, Tallahassee, FL.

- Meseck, H. (1985). "Application of a Wave Equation Programme to Establish the Bearing Capacity of Driven Piles." *Proceedings of the International Symposium on Penetrability and Drivability of Piles*, Volume 2, Japanese Society of Soil Mechanics and Foundation Engineering, 84-90.
- Middendorp, P., and Verbeek (2006). "30 years of experience with the wave equation solution based on the method of characteristics." *GeoCongress 2006*, American Society of Civil Engineers, Reston, VA, 1-6.
- Mitwally, H., and Novak, M. (1988). "Pile Driving Analysis Using Shaft Models and FEM." *Proceedings of the Third International Conference on the Application of Stress-Wave Theory to Piles*, Bi-Tech Publishers, Vancouver, BC, 455-466.
- Mondello, B., and Killingsworth, S. (2014). "Dynamic Pile Testing Results, Crescent Foundation Demonstration Test Pile – Vulcan SC9 Hammer, Kenner, Louisiana." *GRL Job. No. 1432012-1*. GRL Engineers, Inc, Hammond, LA.
- Mosher, R.L., and Dawkins, W.P. (2000). "Theoretical Manual for Pile Foundations." *ERDC/ITL TR-00-5*, U.S. Army Corps of Engineers, Washington, DC.
- Mukherjee, K. and Nagarajub, N. (2013). "Installation of Offshore Driven Piles– Regional Experience." *Proceedings of the Second Marine Operations Specialty Symposium (MOSS 2012)*, Research Publishing Services, Singapore, 245-290.
- Nath, B. (1990). "A Continuum Method of Pile Driving Analysis: Comparison with the Wave Equation Method." *Computers and Geotechnics*, 10(4), 265-285.
- Naval Facilities Engineering Command (1986). "Foundations and Earth Structures." *DM 7.02*. Naval Facilities Engineering Command, Alexandria, VA.
- Nayak, G.C., and Zienkiewicz, O.C. (1972). "Elasto/plastic stress analysis. An generalisation for various constitutive relationships." *International Journal of Numerical Methods in Engineering*, 5,(1), 113-135.
- Naylor, D.J., Pande, G.N., Simpson, B. and Tabb, R. (1981). *Finite Elements in Geotechnical Engineering*. Pineridge Press, Swansea, Wales.
- Newmark, N.M., and Rosenbleuth, E. (1971). *Fundamentals of Earthquake Engineering*. Prentice-Hall, Englewood Cliffs, NJ.
- Ning, W.Q., and Yamamoto, N. (2008). "The Gel'fand-Levitan theory for one-dimensional hyperbolic systems with impulsive inputs." *Inverse Problems* (24)2, 25-29.

- Ortiz, M., and Simo, J.C. (1986). "An Analysis of a New Class of Integration Algorithms for Elastoplastic Constitutive Relations." *International Journal for Numerical Methods in Engineering*, 23(3), 353-366.
- Osman, M.A., Ahmed, E.M.A., and Ahmed, O.B.E.M. (2013). "Comparison Between Dynamic and Static Pile Load Testing." *Electronic Journal of Geotechnical Engineering*, 18(Q), 3615-3624.
- Owen, D.R.J., and Hinton, E. (1980). *Finite Elements in Plasticity: Theory and Practice*. Pineridge Press, Swansea, Wales.
- Pande, G.N., and Sharma, K.G. (1979). "On joint/interface elements and associated problems of numerical ill-conditioning" *International Journal for Numerical and Analytical Methods in Geomechanics*, 3(3), 293-300.
- Pao, Y.H., and Yu, Y.Y. (2011). "Attenuation and Damping of Multireflected Transient Elastic Wave in a Pile." *Journal of Engineering Mechanics, ASCE*, 137(8), 571-579.
- Parker, F., and Radhakrishnan, N. (1975). "Background Theory and Documentation of Five University of Texas Soil-Structure Interaction Computer Programs." *Miscellaneous Paper K-75-2*, U.S. Army Corps of Engineers, Vicksburg, MS.
- Parola, J.F. (1970). *Mechanics of Impact Pile Driving*. PhD Dissertation, University Of Illinois At Urbana-Champaign, Urbana, IL.
- Pinto, P.L., Grazina, J.C., and Lourenço, J.C. (2008). "Evaluation of 1D and 2D numerical modelling techniques of dynamic pile testing." *Science, Technology and Practice: Proceedings of the 8th International Conference on the Application of Stress-Wave Theory to Piles*, IOS Press, Amsterdam, the Netherlands, 353-357.
- Poskitt, T.J., and Yip-Wong, K.L. (1991) "Frequency response problems to instrumented pile tests." *Ground Engineering*, 24(4), 28-39.
- Potts, D.M., and Martins, J.P. (1982) "The shaft resistance of axially loaded piles in clay." *Geotechnique*, 32(4), 369-386.
- Potts, D.M., and Zdravkovic, L.(1999) *Finite Element Analysis in Geotechnical Engineering: Theory*. Thomas Telford Publishing, London, England.
- Potts, D.M., and Zdravkovic, L.(2001) *Finite Element Analysis in Geotechnical Engineering: Application*. Thomas Telford Publishing, London, England.
- Powrie, W. (2014) *Soil Mechanics: Concepts and Applications*. Taylor & Francis, Boca Raton, FL.

- Press, W.H., Teukolsky, S.A., Vetterling, W.T., and Flannery, B.P. (1992) *Numerical Recipes in Fortran 77*. Second Edition. Cambridge University Press, Cambridge, England.
- Randolph, M.F. (1983). “Design Considerations for Offshore Piles.” *Proceedings of the Conference on Geotechnical Practice in Offshore Engineering*. American Society of Civil Engineers, New York, NY, 422-439.
- Randolph, M.F., and Simons, H.A. (1986). “An Improved Soil Model for One-Dimensional Pile Driving Analysis.” *Numerical Method in Offshore Piling*, Éditions Technip, Paris, 3-18.
- Randolph, M.F. and Wroth, C.P. (1978). “Analysis of Deformation of Vertically Loaded Piles.” *Journal of the Geotechnical Engineering Division of the American Society of Civil Engineers*, 104(12), 1465-1488.
- Rausche, F. (1970). *Soil Response from Dynamic Analysis and Measurements on Piles*. PhD Dissertation, Case Western Reserve University, Cleveland, OH.
- Rausche, F., Moses, F., and Goble, G.G. (1972). “Soil Resistance Predictions from Pile Dynamics.” *Journal of the Soil Mechanics and Foundations Division, ASCE*, 98(9), 917-937.
- Rausche, F., Goble, G.G., and Likins, G. (1985). “Dynamic Determination of Pile Capacity.” *Journal of Geotechnical Engineering*, 111(3), 367-383.
- Rausche, F., Nagy, M., and Webster, S. (2009). “CAPWAP and Refined Wave Equation Analyses for Driveability Predictions and Capacity Assessment of Offshore Pile Installations.” *ASME 2009 28th International Conference on Ocean, Offshore and Arctic Engineering (OMAE2009)*, American Society of Mechanical Engineers, New York, NY, 375-383.
- Rausche, F., Likins, G. E., Liang, L., and Hussein, M.H. (2010). “Static and Dynamic Models for CAPWAP Signal Matching.” *The Art of Foundation Engineering Practice*, American Society of Civil Engineers, Reston, VA, 534-553.
- Reid, J.D., Coon, B.A., Lewis, B.A., Sutherland, S.H. and Murray, Y.D. (2004). “Evaluation of LS-DYNA Soil Material Model 147.” *FHWA-HRT-04-094*, Federal Highway Administration, Washington, DC.
- Samtani, N.C., and Nowatski, E.A. (2006). “Soils and Foundations Reference Manual.” *FHWA NHI-06-088 and NHI-06-089*. National Highway Institute, Washington, DC.

- Schnabel, R.B., Koontz, J.E., and Weiss, B.E. (1985). "A Modular System of Algorithms for Unconstrained Minimization." *CU-CS-240-82* (revised,) University of Colorado at Boulder, Boulder, CO.
- Schümann, B., and Grabe, J. (2011) "FE-based modelling of pile driving in saturated soils." *Proceedings of the 8th International Conference on Structural Dynamics, EURO-DYN 2011*, Leuven, Belgium, 894-900.
- Screwvala, F.N. (1973), discussion of Rausche et.al. (1972) "Soil Resistance Predictions from Pile Dynamics." *Journal of the Soil Mechanics and Foundations Division, ASCE*, 99(5), 412-413.
- Serdaroglu, M.S. (2010) *Nonlinear Analysis of Pile Driving and Ground Vibrations in Saturated Cohesive Soils Using the Finite Element Method*. PhD Thesis, University of Iowa, Iowa City, IA.
- Sewell, G. (1985) *Analysis of a Finite Element Method: PDE/PROTRAN*. Springer Verlag, New York, NY.
- Shahin, M.A., Jaksa, M.B., and Maier, H.R. (2001) "Artificial neural network applications in geotechnical engineering." *Australian Geomechanics*, 36(1), 49-62.
- Sloan, S. (1987). "Substepping Schemes for the Numerical Integration of Elastoplastic Stress-Strain Relations." *International Journal for Numerical Methods in Engineering*, 24(5), 893-911.
- Smith, E.A.L. (1955). "Impact and Longitudinal Wave Transmission." *Transactions of the American Society of Mechanical Engineers*, August, 963-973.
- Smith, E.A.L. (1960). "Pile-Driving Analysis by the Wave Equation." *Journal of the Soil Mechanics and Foundations Division*, 127(1) 35-61.
- Smith, I.M. and Chow, Y.K. (1982). "Three-dimensional analysis of pile drivability." *Proceedings of the Second Conference on Numerical Methods in Offshore Piling*, Austin, TX, 1-19.
- Smith, I.M., and Griffiths, D.V. (1988). *Programming the Finite Element Method*. Second Edition. John Wiley & Sons, Chichester, England.
- Sobolev, S.L. (1964). *Partial Differential Equations of Mathematical Physics*. Pergamon Press, Oxford, England.
- Šuklje, L. (1969). *Rheological Aspects of Soil Mechanics*. Wiley-Interscience, London, England.

- Svinkin, M. (2011). "Engineering Aspects in Evaluation of Pile Capacity by Dynamic Testing." *Structures Congress 2011*, American Society of Civil Engineers, Reston, VA, 1686-1697.
- To, P. (1985). *Dynamic Response of Footings and Piles*. PhD Dissertation, University of Manchester, Manchester, England.
- Townsend, F.C., Anderson, J.B. and Rahelison, L. (2001). "Evaluation of FEM Engineering Parameters from Insitu Tests." *RPWO-14*, Florida Department of Transportation, Tallahassee, FL.
- Tuma, J.J. and Abdel-Hady, M. (1973). *Engineering Soil Mechanics*. Prentice-Hall, Englewood Cliffs, NJ.
- Verruijt, A., and van Bars, S. (2007). *Soil Mechanics*. VSSD, Delft, the Netherlands.
- Voitus van Hamme, G.E.J.S.L., Jansz, J.W., Bomer, H. and Arentsen, D. (1974). "Hydroblok and improved piledriving analysis." *De Ingenieur*, 86(18), 345-353.
- Wang, J., Verma, N. and Steward, E. (2009). "Estimating Setup of Driven Piles into Louisiana Clayey Soils." *FHWA/LA.09/463*, Louisiana Department of Transportation, Baton Rouge, LA.
- Warrington, D.C. (1987). "A Proposal for a Simplified Model for the Determination of Dynamic Loads and Stresses During Pile Driving." *Proceedings of the Nineteenth Annual Offshore Technology Conference*, Offshore Technology Conference, Dallas, TX, 329-338.
- Warrington, D.C. (1997). *Closed Form Solution of the Wave Equation for Piles*. MS Thesis, University of Tennessee at Chattanooga, Chattanooga, TN.
- Warrington, D.C., Editor (2007). *Pile Driving by Pile Buck*. Pile Buck International, Vero Beach, FL.
- Webster, A.G., and Plimpton, S.J. (1966). *Partial Differential Equations of Mathematical Physics*. Dover Publications, New York, NY.
- Wellington, A.M. (1893). *Piles and Pile Driving*. Engineering News Publishing Company, New York, NY.
- Winterkorn, H.F. and Fang, H.-Y. (1975). *Foundation Engineering Handbook*. Van Nostrand Reinhold Company, New York, NY.
- Woods, R., and Rahim, A. (2008). *CRISP Technical Reference Manual*. CRISP Consortium Ltd., Guildford, England.

Zeevaert, A.E. (1980). *Finite Element Formulation for the Analysis of Interfaces, Nonlinear and Large Displacement Problems in Geotechnical Engineering*. PhD Dissertation, Georgia Institute of Technology, Atlanta, GA.

Zienkiewicz, O.C., and Taylor, R.L. (2000a). *The Finite Element Method. Volume 1: The Basis*. Fifth Edition, Butterworth-Heinemann, Oxford, England.

Zienkiewicz, O.C., and Taylor, R.L. (2000b). *The Finite Element Method. Volume 2: Solid Mechanics*. Fifth Edition, Butterworth-Heinemann, Oxford, England

Zienkiewicz, O.C., Valliappan, S., and King, I.P. (1969). "Elasto-plastic solutions of associated visco-plasticity in soil mechanics." *International Journal of Numerical Methods in Engineering*, 1(1), 75-100.

VITA

A South Floridian, Don C. Warrington graduated from the St. Andrew's School in Boca Raton, Florida. After this he attended and graduated magna cum laude from Texas A&M University in 1976 with a Bachelor of Science Degree in Mechanical Engineering. He received his Master of Science Degree with a concentration in Civil Engineering from the University of Tennessee at Chattanooga in 1997, during which pursuit he was selected twice to Who's Who Among Students in American Universities and Colleges. He received his Doctor of Philosophy Degree in Computational Engineering from the University of Tennessee at Chattanooga in August 2016.

After a brief stint in the aerospace industry at Texas Instruments, he was a principal and held various management and technical positions at the Vulcan Iron Works Inc. in Chattanooga from 1978 to 1996. After this he worked as a consultant to various companies which owned the product line, and is currently an engineering consultant to Pile Hammer Equipment in Ft. Payne, Alabama. He was also an editor of *Pile Buck* from 2000 to 2007, and edited two books, *Sheet Pile Design by Pile Buck* and *Pile Driving by Pile Buck*. He is a co-author of *Soils in Construction*, published by Pearson Education.

From 1996 to 2010 he worked at the Church of God Department of Lay Ministries; his last position was Ministries Coordinator, and he authored numerous books and coordinated several programs. In 2001 he began teaching as an Adjunct Professor at the University of Tennessee at Chattanooga, where he teaches Soil Mechanics and Foundations. A registered Professional Engineer, he is a member of the American Society of Civil Engineers and was elected to the Order of the Engineer in 2011. He was selected for Best Adjunct Teaching for the academic year 2014-5. He lives in Chattanooga with his wife Judy.